ABSTRACT

Title of Document:

MULTI-SCALE INVERSE MODELING IN BIOLOGICAL MASS TRANSPORT PROCESSES

Kouroush Sadegh Zadeh, Ph.D., 2006

Directed By:

Dr. Hubert J. Montas, Associate professor,
Fischell Department of Bioengineering

A state-of-the-art inverse modeling strategy was developed, analyzed, and applied in two different biological mass transport processes. The strategy was developed in the framework of the nonlinear optimization problem in which model parameters were estimated by minimizing an appropriate objective function which represents the discrepancy between the observed and predicted responses of the biological systems. The *forward problems* were solved numerically using the mass conservative Galerkin based linear finite element and finite difference methods. Before incorporating in the framework of the inverse code, the numerical simulators were validated with either analytical or reference solutions.

In the inverse code, the Osborne- Moré extended version of the Levenberg-Marquardt algorithm was used to determine the search direction. The Jacobian matrix was constructed using partial derivatives of the state variables with respect to model parameters by one and two-sided finite difference approximations. A mixed termination criterion was used to end the optimization.

The strategy was applied to parameter identification problem in Fluorescence Recovery after Photobleaching (FRAP) protocol to estimate the optimized values of the mass transport and binding rate parameters for GFP-tagged glucocorticoid receptor. Results indicate that the protocol provides enough information to uniquely estimate one parameter. It also provides enough information to uniquely estimate the individual values of the binding rate coefficients given the value of the molecular diffusion coefficient is known. However, the protocol provides insufficient information for unique simultaneous estimation of three parameters (diffusion coefficient and binding rate parameters) owing to the high intercorrelation between the molecular diffusion coefficient and pseudo-association rate parameter. Attempts to estimate macromolecule mass transport and binding rate parameters simultaneously from FRAP data result in misleading conclusions regarding concentrations of free macromolecule and bound complex inside the cell, average binding time per vacant site, average time for diffusion of macromolecules from one site to the next, and slow or rapid mobility of biomolecules in cells. To obtain unique values for molecular diffusion coefficient and binding rate parameters of biomolecule, two FRAP experiments should be conducted on the same class of macromolecule and cell. One experiment should be used to measure the molecular diffusion coefficient independently of binding in an effective diffusion regime and the other should be conducted in a reaction dominant or reaction-diffusion regime to quantify the binding rate parameters.

The inverse modeling strategy was also successfully used to identify hydraulic parameters for both single and multi-objective optimization problems in

homogeneous and heterogeneous variably saturated soils. Incorporating both soil water content information and soil water pressure head data in the framework of the multi-objective parameter optimization, produced excellent result for both soil water content and pressure head profiles.

MULTI-SCALE INVERSE MODELING IN BIOLOGICAL MASS TRANSPORT PROCESSES

By

KOUROUSH SADEGH ZADEH, Ph.D., 2006

Dissertation submitted to the Faculty of the Graduate School of the
University of Maryland, College Park, in partial fulfillment
of the requirements for the degree of
Doctor of Philosophy
2006

Advisory Committee:
Dr. Hubert J. Montas, Associate Professor, Chair/Bioengineering
Dr. Adel Shirmohammadi, Professor, Co-advisor/Bioengineering
Dr. Howard C. Elman, Professor/Computer Science
Dr. Marco Colombini, Professor/Biology
Dr. Yang Tao, Professor/Bioengineering

Knowledge is power

<div align="right">*Ferdowsi (940-1020)*</div>

The sea of Being has emerged from hidden depths
But how, that's a pearl of scholarship no one has pierced
Each scholar had conjecture idly on the subject
But none can describe how the matter actually rests

<div align="right">*Khayyam*</div>

Dedication

To the memory of my parents
and
In honor of their dedication to my education

Acknowledgements

Several people have been instrumental in successful completion of this study over the course of the past few years. I would like to take this opportunity to express my sincere appreciation and gratitude to them.

First and foremost I would like to acknowledge and appreciate the continuous support, guidance, and encouragement of my advisor Dr. Hubert J. Montas. His charming personality, friendship, everlasting patience, and confidence on my work were essential in successful completion of this project. I greatly appreciate the long weekly hours he spent discussing technical issues and his brain storming suggestions. My debt to him cannot be acknowledged here in full.

I would also like to express my sincerest and deepest gratitude to my co-advisor Dr. Adel Shirmohammadi and his wonderful family, Minoo, Shaida, and Bobak. This endeavor would not have started if it was not for his help, friendship, and guidance. Dr. Shirmohammadi and his family have given me peace and comfort in their home throughout my PhD study. My debt to him is beyond evaluation.

I would also like to thank Dr. Howard Elman, Dr. Marco Colombini, and Dr. Yang Tao for accepting to serve on the final examination committee.

I also like to express my appreciation to Dr. James McNally, head of the Receptor Biology and Gene Expression Laboratory at NCI-NIH, for providing experimental data on Fluorescence Recovery after Photobleaching to validate mathematical modeling of in vivo protein transport.

Finally, I would like to thank Dr. Richard McCuen for his indulgence to discuss the statistical assessment of the inverse problem.

Table of Contents

List of Tables

xii

List of Figures

xv

xvii

xviii

NOMENCLATURE

$a_{i,j}$ = Elements of the tri-diagonal matrix $[A]$

$[A]$ = Global matrix in finite element approximation of flow equation

$b_{i,j}$ = Elements of the tri-diagonal matrix $[B]$

$[B]$ = Stiffness mass matrix in finite element approximation of flow equation

C = Total concentration of the bound complex $(C = FS)$

C = Parameter covariance matrix

$\hat{C}$ = Approximation for soil water capacity function (C) in finite element solution of

Richards' equation

C_{eq} = Total concentration of bound complex at equilibrium (before photobleaching)

C_{ii} = Parameter variances in covariance matrix

$COR(P)_{ij}$ = Parameter correlation matrix or variance-covariance matrix

$C(\theta)$ = Specific soil moisture capacity function (L^{-1})

dt = Time increment in the numerical solution

dt_{max} = Maximum of time increment in adaptive time loop

dt_{min} = Minimum of time increment in adaptive time loop

D = Positive definite scaling symmetric matrix in Osborne- Moré algorithm

D_C = Diffusion coefficient ($L^2 T^{-1}$) of bound complex

D_F = Diffusion coefficient ($L^2 T^{-1}$) of free biomolecule

D_S = Diffusion coefficient ($L^2 T^{-1}$) of vacant binding site(s)

$D(\theta)$ = Soil water diffusivity function (L^2T^{-1})

e_i = Expected error frequencies in χ^2 distribution

$eigs(H)$ = Eigenvalues of Hessian

E = Statistical expectation.

f = Weighing factor in Crank-Nicolson approximation of flow equation

$\overline{frap}$ = Average of the Laplace transform of the fluorescent intensity within the bleach

     spot

$\overline{\hat{frap}}$ = Model predicted average of the fluorescent intensity within the bleach spot

F = Total concentration of free biomolecule

$\{F\}$ = Driving force vector in finite element approximation of flow equation

F_{eq} = Total concentration of free biomolecule at equilibrium (before photobleaching)

h = Soil water pressure head (L)

$\hat{h}(z,t)$ = Approximate solution of state variable $h(z,t)$ for weak formulation in finite

element method

h_i = Measured soil water pressure head

$\hat{h}_i$ = Predicted soil water pressure head

H = Hessian matrix

H_A = Alternative hypothesis

H_0 = Null hypothesis

$H_j(t)$ = Unknown and time dependent coefficients that represent the solution of state

variable $h(z,t)$ at nodes within the domain in finite element solution of flow equation

i = Iteration level in inverse algorithm

i = Position in the finite difference mesh

I_1 = Modified Bessel function of the first kind

$I(t_i)$ = Experimental FRAP recovery

$I(b,t_i)$ = Numerically estimated values of the $I(t_i)$ for any time step

$J = N \times P$ Jacobian (sensitivity) matrix

k = Number of cells in χ^2 test

k = Number of subgroups in Bartlett's test

$\hat{K}$ = Approximation for K in finite element solution of Richards' equation

K_1 = Modified Bessel function of the second kind

K_a = Free biomolecule-vacant binding site association rate constant (T^{-1})

$K_a^* = K_a S$ = Pseudo-association rate constant

K_d = Free biomolecule-vacant binding site dissociation rate coefficient (T^{-1}).

$K(h)$ = Unsaturated hydraulic conductivity function (LT^{-1})

$K_{i\pm1/2}$ = Inter-block unsaturated hydraulic conductivity function in finite difference approximation of the h-based form and mixed form Richards' equations

$L(\beta)$ = Likelihood function

$L(\hat{h})$ = Operator

m = Curve fitting parameters in van Genuchten's model

m = Iteration level in numerical simulator of forward problem

M = Number of observations for soil water pressure head

n = Time step in numerical simulator of forward problem

n = Curve fitting parameters in van Genuchten's model

N = Number of observations (sample size in statistical tests)

N = Normal probability distribution function

N_e = Number of elements in finite element mesh

o_i = Observed error frequencies in χ^2 distribution

$OF(\beta)$ = Objective function in nonlinear optimization

P = Size of the parameter vector being optimized

q = Darcian flux ($L^3 L^{-2} s^{-1}$)

r = Radial coordinate in cylindrical system

r = Residual vector

$RMSE$ = Root Mean Squared Error

R^2 = Coefficient of determination

s = Laplace transform variable

s = Estimated error variance

s = Standard deviation of the random variable

s_i^2 = Variance of subgroups in Bartlett's test

s_p^2 = The pooled variance in Bartlett's test (weighted average of the variances of the

   subgroups)

S = Total concentration of vacant binding sites inside cell

S_e = Effective saturation ($0 \le S_e \le 1$)

t = Time (T)

t = Critical t-statistic

$t_{v,1-\alpha/2}$ = Tabled value of the *Student's t* distribution

t_i = time step

T = The Bartlett's test statistic

U = Observed state variable

$\hat{U}_i$ = Predicted state variable

U = Vector and/or matrix of model predictions

U^* = Vector and/or matrix of observations

v = Degree of freedom

V = Error covariance matrix

V_β = Covariance matrix for parameter vector

w = Radius of the bleached area

w_i = Weighting function in formulation of the objective function

W = The Levene test statistic

$\bar{x}$ = Mean of the random variable

z = Vertical coordinate (L) in Cartesian coordinate system

$\bar{Z}_{i.}$ = Subgroups means in the Levene test

$\bar{Z}_{..}$ = Overall mean of the residuals (Z_{ij}) in the Levene test

α = Air entry value in van Genuchten's model (L^{-1})

α = Level of significance

α^i = Search length or step size in inverse algorithm

β = Vector of the optimized parameters

$\hat{\beta}$ = Estimated value of the parameter vector

β^* = Parameter vector containing the prior information

γ = Level of confidence

δ = Convergence criterion in Picard loop in the numerical solution

δ^i = Parameter vector increment in each iteration in the Levenberg-Marquardt algorithm

δ_1 and δ_2 = User defined small values in stopping criterion in the Marquardt-Levenberg algorithm

$\Delta\beta$ = Search direction or step direction

Δr = Node spacing in cylindrical coordinate system

Δt = Time increment in finite element and finite difference methods

Δz = Node spacing

∇OF = Gradient vector of the objective function

$\nabla^2 OF$ = Second derivative of the objective function

ι = Pore connectivity index in Mualem's model

λ = Lagrange multiplier or the Marquardt parameter

$\phi_i(z)$ = Weight function in finite element method

$\phi_j(z)$ = Selected basis function in finite element approximation

$\Phi(\overline{frap})$ = Objective function on FRAP experiment data

$\Phi(\theta + h)$ = Objective function on soil water pressure head and soil water content information

$\Phi(\theta)$ = Objective function on soil water content information

μ_0 = Mean of random variable in population

μ_0 = Mean of errors in population (in hypothesis test on the mean of errors)

σ_θ^2 = Variance of the measured soil water pressure head

σ_h^2 = Variance of the measured soil water pressure head

τ = Dummy variable of integration

θ = Volumetric soil moisture content ($L^3 L^{-3}$)

θ_i = Measured soil moisture content ($L^3 L^{-3}$)

$\hat{\theta}_i$ = Predicted soil moisture content ($L^3 L^{-3}$)

θ_r = Residual soil moisture content ($L^3 L^{-3}$)

θ_s = Saturated soil moisture content ($L^3 L^{-3}$)

$\hat{\theta}(z,t)$ = Approximations for $\theta(z,t)$ in finite element solution of mixed form Richards' equation

χ^2 = Chi-square test statistic

$\chi^2_{(\alpha,k-1)}$ = Tabled upper critical value of the *chi-square distribution* with $k-1$ degree of freedom at the level of significance α.

CHAPTER 1: INTRODUCTION

One knows so much, comprehends so little.
Einstein

Transport of mass, energy, and momentum has crucial role in many branches of science and engineering. In biological systems, transport phenomena are central to the biological processes that take place in different units of organisms. They determine the behavior and function of cells, tissues, and organs, and regulate interactions between synthetic agents (e.g. drugs) and recipient targets. In bioenvironmental systems, transport processes are important to understand, simulate, predict, analyze, and prevent point and non-point source pollution. They regulate the delivery of nutrients and water to plants and the movement of pesticides, viral and bacterial agents (causes of waterborne diseases) through the landscape. Theses phenomena are crucial elements in the design and use of biosensors, high density cell culture, filtration units for kidney dialysis, heart-lung bypass machine, and membrane oxygenators in human health related arena (Truskey *et al.,* 2004) and ion selective electrodes, neutron probe, pH-meter, Electrical conductivity meter, and time domain reflectometery used in bioenvironmental systems analysis. Transport processes are critical in the removal of toxins from blood, remediation of impaired water bodies, bioremediation of contaminated lands, and reclamation of saline and sodic soils.

In recent decades public concern has increased over various terminal diseases (such as many forms of cancer) and the fate and potential carcinogenic nature of agrochemicals and land disposed industrial compounds. This has accelerated the need for both drug and bioenvironmental research on i) more advanced and clinically relevant

drug and therapeutic agents delivery systems, ii) more accurate predictions of carcinogenic chemical transport toward surface and subsurface water resources, iii) evaluating the effects of current pharmaceuticals in curing environmentally- induced and waterborne diseases, iv) management strategies to decrease the uploads of contaminants to environment, v) developing novel therapeutic agents and innovative methods to predict, prevent and control the diseases, and vi) finding strategies to remediate the impaired water bodies and contaminated lands.

In this context, several sophisticated mathematical models have been developed to predict and simulate the behavior, effects, and fate of drugs and contaminants in biological systems (from cells to landscapes). However, the use of these models is not an easy task since they contain numerous parameters that need to be determined before the model(s) can be used for the considered situation. The success of model predictions depends largely on the proper representation of relevant processes, uncertainty in model parameters (Alley et al., 2002), and parameter identification which is a critical step in modeling process. Difficulties in model calibration and parameter identification are quite common in modeling mass transport problems in biological systems.

There are several in vivo, in vitro, laboratory and large scale methods to measure fluid flow, mass transport, and reaction rate parameters. However, in vitro and laboratory scale results may not be representative of in vivo and large scales transport processes. In-vivo and large scale measurements, on the other hand, are tedious, time consuming, expensive, and often impose unrealistic and simplified initial and boundary conditions on transport processes in biological systems. Finally, information regarding parameter uncertainty is not readily obtained from these methods unless a very large number of

samples and measurements are taken at significant additional cost (Bouwer and Jackson 1974; Green *et al.,* 1986; Klute and Dirksen1986; Kool *et al.,* 1987; Kaufman and Jain, 1990; Simunek and van Genuchten, 1996; Finsterle, 2004; Polisetty *et al.,* 2006). To overcome these limitations indirect methods, such as parameter optimization by inverse modeling, can be used to identify model parameters.

Inverse modeling is usually defined as estimation of model parameters by matching a numerical or analytical model to observed data representing the system response at discrete times and spatial locations (Finsterle, 2004). In other words, "inverse problems are those where a set of measured results is analyzed in order to get as much information as possible on a "model" which is proposed to represent a system in the real world" (Sabatier, 2000). Inverse techniques usually combine a numerical or analytical model with a parameter optimization algorithm and experimental data set(s) to estimate the optimum values of model parameters, imposed initial and boundary condition and other properties of the excitation-response relationship of the system. The technique searches for the best combination of parameter values in an iterative way, by varying the unknown coefficients and comparing the measured response of the system with the predicted simulation given by the forward model. The search continues until a global or local minimum of the objective function, defined by the differences between the measured and simulated values of state variable(s), is obtained. Several optimization algorithms have been proposed to numerically solve the inverse problem. They include the conjugate gradient method, Newton's algorithm, global optimization technique, Simplex method, quasi-Newton methods, genetic algorithm (Sabatier, 2000), and Monte Carlo-Markov Chain (MCMC) method. Among these algorithms, the Newton based

optimization approach (especially the Levenberg-Marquardt algorithm) and the quasi-Newton methods (especially *the Hessian update method* by *DFP* (Davidon, 1959; Fletcher and Powell, 1963) and *BFGS algorithms* (Broyden, 1970; Fletcher 1970; Goldfarb, 1970; Shanno, 1970)) are the most widely used optimization methods.

The task seems straightforward, just a matter of selecting a proper mathematical model and estimating its parameters via parameter optimization algorithms, but as Polisetty *et al.,* (2006) noticed several conceptual and computational difficulties have made the implementation of the inverse modeling more challenging: 1) judicious choice of a mathematical model (forward model) which is representative enough to simulate the behavior of the biological systems, with sufficient accuracy, and at the same time allows interpretation of the results beyond pure parameter estimation, 2) the type and quality of input data is a crucial prerequisite for successful parameter optimization by inverse modeling. The data should provide enough information regarding the excitation-response relationship of the system and have reasonable scattering, 3) well-posedness of the inverse problem which depends on the model structure, the quality and quantity of the input data, and the type of imposed initial and boundary conditions (Russo *et al.,* 1991).

1.1. Overall Goal of the Study

The overall goal of this study is to develop, apply, validate, and analyze an efficient and state-of-the-art inverse modeling strategy for mass transport problems in different biological systems. The optimization strategy will be developed by adapting and extending methods from the literature. The strategy will be applied to two transport processes including mobility and binding of biomolecules in living cells, and water flow in partially saturated porous media. The possible ill-posedness of the inverse problem

will be analyzed by different techniques. The strategy will be evaluated against experimental data and previous optimization techniques.

1.2. Organization

The organization of this manuscript follows the above objectives. Chapter two reviews recent and pertinent literature on estimation of model parameters by optimization (minimization/maximization) algorithms, simulation of biomolecule transport in living cells, water flow in partially saturated porous media, and analytical and numerical solutions of flow equations. Chapter three presents the specific objectives of the study. Chapter four describes methods and materials used in the development and application of the inverse modeling strategy in different biological mass transport problems. The results of the study are presented in chapter five, and this is followed by the summary and conclusions (chapter six) and recommendations for future research in chapter seven.

CHAPTER 2: REVIEW OF LITERATURE

Science is a cemetery of dead ideas.
Miguel de Unamuno

The literature review below covers optimization problem, simulation models of biomolecule transport in living cells, water flow and pollutant transport in the environment, the increasing demand for developing and calibrating sophisticated models, advances and challenges in numerical solution of partial differential equations governing transport phenomena in different biological systems, and problems associated with model calibration and parameter identification. Parameter estimations by direct and indirect methods, as well as their limitations, are also reviewed. A detailed review is presented on parameter optimization using laboratory and large scale data by inverse modeling.

2.1. Parameter Optimization by Inverse Modeling

The inverse problem is usually treated as a nonlinear optimization problem in which model parameters are estimated by minimizing an appropriate objective function which represents the discrepancy between the observed and predicted responses of a system. When the measurement errors asymptotically follow a multivariate normal distribution with zero mean and covariance matrix, V, the likelihood function can be formulated as (Bard, 1974):

$$L(\beta) = (2\pi)^{-N/2} \det[V]^{-1/2} \exp[-\frac{1}{2}(U^* - U(\beta))^T V^{-1} (U^* - U(\beta))] \qquad [2.1]$$

where $L(\beta)$ is the likelihood function, N is number of observations, β is vector of the parameters being optimized, U^* is a vector and/or matrix of observations, and U is a corresponding vector and/or matrix of model predictions as a function of the parameters being optimized which is obtained by solving the forward problem. In this approach, the likelihood function is defined as the joint probability density function of the observations and is considered a function of the unknown parameters. The maximum likelihood estimator is those values of the unknown parameters that maximize the magnitude of the same likelihood function (Bard, 1974). Since logarithm is a monotonic increasing function of its argument (the value of β that maximizes $L(\beta)$ also maximizes $\ln L(\beta)$), and since $\ln L(\beta)$ is simpler and much easier to use than $L(\beta)$ itself, $\ln L(\beta)$ is often used in optimization:

$$\ln L(\beta) = -\frac{N}{2}\ln(2\pi) - \frac{1}{2}\det[V] - \frac{1}{2}(U^* - U(\beta))^T V^{-1}(U^* - U(\beta))] \qquad [2.2]$$

In equations [2.1] and [2.2] the error covariance matrix is defined as:

$$V = E[(U^* - U(\beta))^T (U^* - U(\beta))] \qquad [2.3]$$

where E is statistical expectation.

The maximum of the likelihood function must satisfy the set of equations:

$$\frac{\partial \ln L(\beta)}{\partial \beta} = 0 \qquad [2.4]$$

When the error covariance matrix is known, maximization of equation [2.2] is equivalent to the minimization of the following weighted least square problem (i.e. values of β that maximize equation [2.2] also minimize the equation below):

$$\phi(\beta) = [(U^* - U(\beta))^T V^{-1}(U^* - U(\beta))] \qquad [2.5]$$

where $\phi(\beta)$ is the objective or penalty function.

If there is information about the values and distributions of parameters, it can be incorporated in the objective function (Simunek and van Genuchten, 1996) as:

$$\phi(\beta) = [(U^* - U(\beta))^T V^{-1}(U^* - U(\beta))] + [(\beta^* - \hat{\beta})^T V_\beta^{-1}(\beta^* - \hat{\beta})] \qquad [2.6]$$

in which β^* is parameter vector containing the prior information, $\hat{\beta}$ is the corresponding predicted parameter vector, and V_β is covariance matrix for parameter vector . This kind of optimization is known as *Bayesian estimation*. The second term in equation [2.6], which is sometimes called the *plausibility criterion* (Carrera and Neuman, 1986) insures that the optimized values of the parameters remain in some feasible region around β^*. Matrices V and V_β, which are sometimes called weighting matrices, provide information about the measurement accuracy as well as any possible correlation between measurement errors and between parameters (Kool *et al.*, 1987).

An obvious limitation of equation [2.6] is that the error covariance matrix generally is not known. A common approach to overcoming this problem is to make some a priori assumptions about the structure of the error covariance matrix (Kool and Parker, 1988). In the absence of any additional information regarding the accuracy of input data, the simplest and most recommended way is to assume observation errors are uncorrelated which implies setting V equal to the identity matrix and V_β to zero. In this case the optimization problem collapses to the well known ordinary least squares formulation (Beck and Arnold, 1977):

$$\phi(\beta) = \frac{1}{2} \sum_{i=1}^{N} [U^* - U(\beta)]^2 = \frac{1}{2} r^T r \qquad [2.7]$$

where r is the residual (difference between observed and predicted state variable) column vector.

Many techniques have been developed in the past to solve the nonlinear optimization problems (Bard, 1974; Beck and Arnold, 1977; Seber and Wild, 2004). These techniques carry out solution of equation [2.7] iteratively by first starting with an initial guess of parameter vector (β^i) and updating it in each iteration;

$$\beta^{i+1} = \beta^i + \delta^i \tag{2.8}$$

where $\delta^i = \alpha^i \Delta \beta^i$ is the parameter vector increment in each iteration, i is the iteration level, $\Delta \beta$ is the search direction (or step direction), and α^i is the search length (or step size), until some termination criteria are met:

$$\left| \phi(\beta^{i+1}) - \phi(\beta^i) \right| \leq \delta_1 \tag{2.9}$$

and:

$$\Delta \beta^i \leq \delta_2 \tag{2.10}$$

Where δ_1 and δ_2 are set to user defined small values.

Several optimization algorithms have been proposed to numerically solve the optimization problem. They include the steepest descent scheme, conjugate gradient method, Newton's algorithm, Gauss-Newton method, global optimization technique, Simplex method, Levenberg-Marquardt algorithm, quasi-Newton methods, genetic algorithm (Sabatier, 2000), and Monte Carlo-Markov Chain (MCMC) method. Among the optimization algorithms, the Newton method is quadratically convergent and quickly converges for most problems (Kool *et al.,* 1987). The problem, however, with this method is the evaluation of the Hessian matrix which is usually not available analytically. Consequently, this method is not commonly used for optimization problems. Among the

alternatives, the quasi-Newton algorithm approximates the Hessian from the available information about the value and the first derivative of the objective function using secant update method. Another alternative is using the Levenberg-Marquardt (Levenberg, 1943; Marquardt, 1961) algorithm:

$$\Delta\beta^{(k)} = -(J(\beta^{(k)})^T J(\beta^{(k)}) + \lambda D(\beta^{(k)})^T D(\beta^{(k)}))^{-1} J(\beta^{(k)})^T r(\beta^{(k)})$$

[2.11]

in which λ is the Lagrange multiplier or the Marquardt parameter (a Positive scalar) which controls both the magnitude and direction of $\Delta\beta$ and $D = diag(d_1, d_2, ..., d_p)$ is a positive definite scaling symmetric matrix. For non-zero values of λ, the Hessian approximation is always a positive definite matrix which ensures the descent property of the algorithm even if the initial guess is not so "smart" (Kool *et al.,* 1987).

If D is the identity matrix, the Levenberg-Marquardt algorithm interpolates between the steepest descent ($\lambda \to +\infty$) and the Gauss-Newton ($\lambda \to 0$) methods. The steepest descent scheme is often too inefficient, requiring a large number of iterations which tend to zigzag in a hemstitching pattern and is not recommended for optimization (Bard, 1974; Seber and Wild, 2004). Nevertheless, recently some investigators have used this algorithm to quantify transmisivity and pollutant transport in groundwater systems (Knowles and Lee, 2004; Knowles *et al.,* 2004). The Gauss-Newton formula assumes that $J^T J$ is a sufficient approximation for the Hessian.

The Levenberg-Marquardt algorithm has been widely used to estimate model parameters in optimization problems (Russo *et al.,* 1990; Simunek and van Genuchten, 1996; Malengier, 2004, among many others). In modern optimization codes, however, equation [2.11] is not usually used. Instead the Osborne-Moré adapted version of the

Levenberg-Marquardt method (Osborne, 1976; Moré, 1977) which avoids the computation of possibly ill-conditioned $J^T J$ is implemented in the optimization algorithm:

$$\min_{\Delta\beta} \left\| \begin{pmatrix} r^i \\ 0 \end{pmatrix} + \begin{pmatrix} J^i \\ (\lambda^i D^i)^{\frac{1}{2}} \end{pmatrix} \Delta\beta \right\|^2 \qquad [2.12]$$

Note that [2.11] are the normal equations for [2.12].

Equation [2.12] can be easily solved by introducing orthogonal householder matrix and applying series of orthogonal Givens rotations. The solution procedure can be found in standard optimization textbooks (Golub and van Loan, 1983, among others) and will not be covered in this study.

In minimization problem, the goal is to minimize $\phi(\beta)$ over $\Box^\beta$. Most optimization problems require a global minimum of $\phi(\beta)$ such that $\phi(\beta) \leq \phi(\hat{\beta})$ for all β in $\Box^\beta$ (where $\hat{\beta}$ is the minimum). However, a global minimum is only possible for a restricted class of functions such as convex functions (Dixon and Szego, 1975 and 1978). In most optimization problems the best we can hope is a robust and efficient numerical algorithm that will converge to a local minimum (Seber and Wild, 2004). There are two types of local minimum:

1. If for a infinitesimal scalar δ ($\delta > 0$) and $\beta \neq \hat{\beta}$:

$$\left\| \hat{\beta} - \beta \right\| < \delta \Rightarrow \phi(\hat{\beta}) < \phi(\beta)$$

then $\hat{\beta}$ is a *strong local minimum.*

2. If $\left\| \hat{\beta} - \beta \right\| < \delta \Rightarrow \phi(\hat{\beta}) \leq \phi(\beta)$, then $\hat{\beta}$ is a *weak local minimum*.

Assuming that the objective function has continuous first and second derivatives, the following criteria can be used to verify the strength of the locality of the minimum:

1. $\nabla \phi(\hat{\beta}) = 0$

2. $H(\hat{\beta})$ is positive definite.

These conditions are *necessary* and *sufficient* for $\hat{\beta}$ to become a strong local minimum (Seber and Wild, 2004).

2.2. Biomolecule Transport in Living Cells

The ultimate goal of molecular biology is to understand the biological processes that take place in living cells, tissues, and organs. Mathematical modeling of the biological processes and innovative experimental techniques are substantial tools to study the dynamics of cells. One of the most widely used experimental protocol to understand the biological processes and to study transport of biomolecules in small systems such as living cells is the Fluorescence Recovery after Photobleaching (FRAP). It is a useful technique to study dynamics of living cells and biological processes such as diffusion and binding reactions. FRAP is actually a simple and straightforward technique used to monitor the movement of the fluorescence molecules. These molecules can absorb light of one wavelength (blue for instance) and emit light of other kind (e.g. green). However, if exposed to repeated cycles of excitation-emission, they lose their ability to emit fluorescence. This phenomenon is called *"photobleaching"* or *"photochemical bleaching"* (Carrero *et al.,* 2003). In this technique a small region of living cell

12

containing GFP-tagged protein is exposed to a brief but intense laser beam, produced by a laser scanning confocal microscope, to irreversibly inactivate fluorescence emission in that region. Before exposure to the light, the living cell is in an equilibrium state with uniform fluorescents. Photobleaching creates two different populations of the fluorescence molecules which are spatially separated in the beginning of the experiment. Unbleached molecules from the undisturbed area move toward the bleached region and the rate of fluorescent recovery is measured as a function of time. The result is a noisy graph as shown in Figure 2.1 which is known as FRAP recovery curve. However, because of noisy signals the original graph by itself is not suitable for quantitative study of the dynamics of living cells. The FRAP community generally uses a normalized average fluorescence recovery curve as represented in Figure 2.2.

By analyzing the FRAP curve one can quantify how many photons return to the bleached area in comparison to the amount of light that was there before the photobleaching. This is known as *percent recovery*. The other question that can be addressed is that of how fast do the fluorophores move toward the bleached area. This is a measure of *free molecular diffusion coefficient* of the biomolecule.

The FRAP technique was developed in the 1970's and initially used to study lateral diffusion of lipids through cell membrane (Poo and Cone, 1974; Liebman and Entine, 1974; Bretscher and Rafe, 1975; Axelrod *et al*., 1976; Schlessinger *et al*., 1976; Edidin *et al.*, 1976). At the time biophysicists did not pay much attention to the protocol but since late 1990 invention of the Green Fluorescent Protein (GFP) technique, also known as GFP fusion protein technology, and development of commercially available confocal-microscope-based photobleaching methods, its applications skyrocketed.
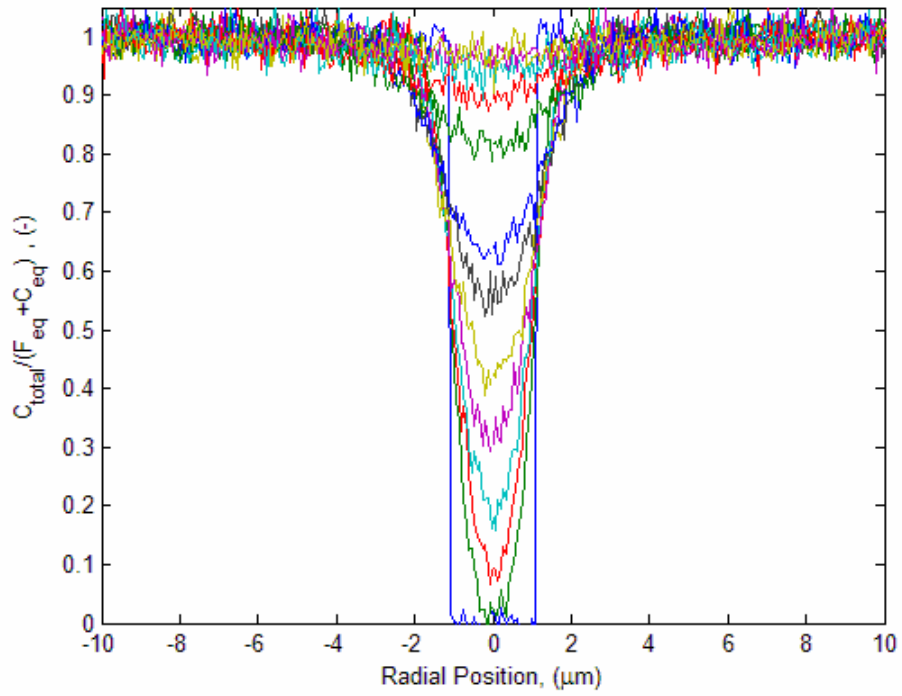
Figure 2.1. Original FRAP recovery curve
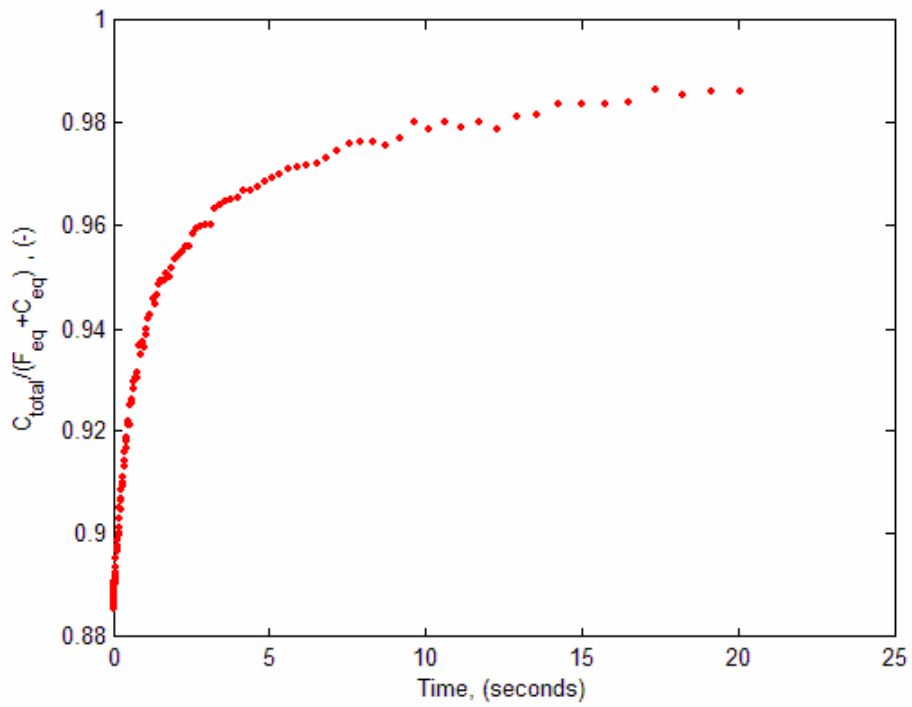
Figure 2.2. Normalized FRAP recovery curve

14

So far most of the FRAP analyses have been qualitative. Some investigators studied the interaction of GFP-tagged proteins with binding sites inside living cells (McNally *et al.,* 2000; Phair and Misteli, 2000). Some considered faster and slower recovery as measures of weaker and tighter binding, respectively. By analyzing the shape of a single FRAP curve, others tried to draw conclusion about the underlying biological process (Dundre *et al.,* 2002; Kimura *et al.,* 2002; Carrero *et al.,* 2003). Ignoring diffusion and presuming a full reaction regime, some researchers performed quantitative analyses to identify rate constants for binding (Thompson *et al.,* 1981; Kaufman and Jain, 1990; Berk *et al.,* 1997; Bulinski *et al.,* 2001; Coscoy *et al.,* 2002; Dundre *et al.,* 2002).

One of the first attempts to estimate biomolecule mass transport and binding rate parameters using in vivo information was carried out by Kaufmann and Jain (1990 and 1991). Using eight data points, they tried to estimate four parameters. Then they simplified the forward model to diffusion dominant or reaction dominant and tried to estimate lumped model parameters.

One of the most thorough analyses of the protocol was performed by Sprague *et al.,* (2004) who identified under what circumstances one can determine the individual rate constants, and where pure diffusion, pure reaction, and diffusion-reaction regimes are dominant. Using the biochemical reaction below, they described the binding reactions between free biomolecule and binding sites inside living cell during the course of a FRAP experiment:

$$\text{F} + \text{S} \underset{K_d}{\overset{K_a}{\rightleftharpoons}} \text{C} \qquad\qquad [2.13]$$

where F is total concentration of free proteins, S is total concentration of vacant bindingsites on the nuclear matrix, C is concentration of the bound complex $(C = FS)$,

K_a is free protein-vacant binding site association rate constant (T^{-1}), and K_d is dissociation rate coefficient (T^{-1}). The equation only describes the binding process. To fully describe the reaction-diffusion process inside cell during the course of the FRAP, they incorporated diffusion process by writing a set of three coupled nonlinear partial differential equations:

$$\frac{\partial F}{\partial t} = D_F \nabla^2 F - K_a FS + K_d C$$

$$\frac{\partial S}{\partial t} = D_F \nabla^2 S - K_a FS + K_d C \qquad [2.14]$$

$$\frac{\partial C}{\partial t} = D_C \nabla^2 C + K_a FS - K_d C$$

in which D_F, D_S, and D_C are the diffusion coefficients ($L^2 T^{-1}$) of free macro-molecule, vacant binding sites, and bound complex, respectively.

To simplify and solve equation [2.14], they made the following assumptions:

1. Two-dimensional diffusion takes place in the plane of focus. This is a legitimate assumption when the bleaching area creates a cylindrical path through the cell which is the case in circular bleach spot with reasonable spot size (Kaufman and Jain, 1990; Sprague *et al.*, 2004). The assumption eliminates the azimuthal and vertical components of the equation.

2. On the time and length scales of the FRAP experiments of DNA binding biomolecules, the binding sites are assumed to be part of a relatively immobile and large complex (Kaufman and Jain, 1990; Bulinski *et al.*, 2001; Coscoy 2002; Sprague *et al.*, 2004). This means that the diffusion of bound complex is negligible ($D_C = 0$).

3. The biological system is at the state of equilibrium before photobleaching and it

16

remains so over the time course of the FRAP experiment. This is a reasonable assumption because most biological FRAP experiments take about several seconds to several minutes whereas the GFP-fusion expression changes over a time course of hours (Sprague *et al.*, 2004). This eliminates the second equation in the system of three coupled nonlinear partial differential equations and hence Eq. [2.14] collapses to one-site-mobile-immobile model (in cylindrical coordinate system):

$$\frac{\partial F}{\partial t} = D_F \frac{\partial^2 F}{\partial r^2} + D_F \frac{1}{r} \frac{\partial F}{\partial r} - K_a^* F + K_d C$$

$$\frac{\partial C}{\partial t} = K_a^* F - K_d C$$

[2.15]

where $K_a^* = K_a S$ is the pseudo-association rate coefficient.

There have been no analytical solutions for equation [2.14], but for heat conduction problem between two concentric cylinders, Carslaw and Jaeger (1959) presented an analytical solution involving Bessel functions. Sprague *et al.,* (2002) extended the strategy for equation [2.15] and developed a semi-analytical solution in Laplace space:

$$\overline{frap} = \frac{1}{s} - \frac{F_{eq}}{s}[1 - 2K_1(qr)I_1(qr)][1 + \frac{K_a^*}{s + K_d}] - \frac{C_{eq}}{s + K_d}$$

[2.16]

where:

$$q^2 = \frac{s}{D_f}[1 + \frac{K_a^*}{s + K_d}]$$

[2.17]

$$C_{eq} = \frac{K_a^*}{K_a^* + K_d}$$

[2.18]

$$F_{eq} = \frac{K_d}{K_a^* + K_d}$$

[2.19]

$$C_{eq} + F_{eq} = 1$$

[2.20]

in which s is the Laplace transform variable that inverts to yield time. $\overline{frap}$ is the average of the Laplace transform of the fluorescent intensity within the bleach spot and I_1 and K_1 are the modified Bessel functions of the first and second kind.

Sprague *et al.,* (2004) used equations [2.16] to [2.20] to simulate the mobility of GFP-tagged glucocorticoid receptor (GFP-GR) in nuclei of both normal and ATP depleted cells. Using the mass of GFP-GR, they assumed an estimated value for the free diffusion coefficient and fitted two binding rate constants by a curve fitting procedure. Based on these results they concluded that 14 percent of GFP-GR is free and 86 percent is bound to DNA or other unknown binding sites. Their strategy, however, failed to simultaneously estimate the optimum values of all parameters. They also didn't report if the parameter values were unique.

Beaudouin *et al.,* (2006) used the full diffusion-reaction models in FRAP experiment to study mobility of five chromatin-interacting proteins inside living cells. They found that transient interactions are common for chromatin proteins. Individual proteins locally sample chromatin for binding sites rather than diffusing globally followed by binding at random nuclear positions. They also concluded that complementary procedures are needed to measure transient biochemical interactions in living cells.

What is missing from these comprehensive FRAP analyses is a robust and systematic method to extract as much physiochemical information from the protocol as possible and to quantify the related in vivo mass transport and reaction rate parameters.

2.3. Water Flow through Partially Saturated Porous Media

Historically Richards' equation (Richards, 1931) has been used to simulate fluid flow in variably saturated porous media. Assuming no sink or source terms, for a rigid, isotropic, and homogeneous porous material, the "mixed form" of this equation, for single phase, non-hysteretic, and transient water flow can be written as:

$$\frac{\partial \theta}{\partial t} - \nabla \cdot K(h)\nabla h + \frac{\partial K}{\partial z} = 0 \qquad [2.21]$$

Where θ is the volumetric soil moisture content ($L^3 L^{-3}$), h is the soil water pressure head (L), $K(h)$ is the unsaturated hydraulic conductivity function (LT^{-1}), z is vertical coordinate (L), assumed positive downward, and t denotes time (T). Using the chain rule of differentiation two other forms of the equation have been developed (Bear, 1972, 1979; Celia *et al.,* 1990):

θ-based form:

$$\frac{\partial \theta}{\partial t} - \nabla \cdot D(\theta)\nabla \theta + \frac{\partial K}{\partial z} = 0 \qquad [2.22]$$

h-based form:

$$C(h)\frac{\partial h}{\partial t} - \nabla \cdot K(h)\nabla h + \frac{\partial K}{\partial z} = 0 \qquad [2.23]$$

in which $D(\theta) = K(\theta)\partial h / \partial \theta = K(\theta)/C(\theta)$ is the soil water diffusivity function ($L^2 T^{-1}$) and $C(\theta) = d\theta / dh$ is the specific soil moisture capacity function (L^{-1}).

Solution of Richards' equation and simulation of water flow in partially saturated porous media require knowledge of the soil hydraulic conductivity and water content versus soil water pressure head. These relationships are known as hydraulic properties of

the media. In the present study, van Genuchten's (1980) closed form equation for soil water retention curve and Mualem's (1976) unsaturated hydraulic conductivity function were used to describe the soil hydraulic properties. The equations are:

$$\theta = \theta_r + (\theta_s - \theta_r)[1 + (\alpha h)^n]^{-m} \qquad [2.24]$$

$$K(S_e) = K_s S_e^l [\frac{f(S_e)}{f(1)}]^2 \qquad [2.25]$$

where;

$$S_e = \frac{\theta - \theta_r}{\theta_s - \theta_r} \qquad [2.26]$$

$$f(S_e) = \int_0^{S_e} \frac{1}{h(x)} dx \qquad [2.27]$$

Substituting equations [2.24], [2.26], and [2.27] into equation [2.25] and doing some mathematical operations yields:

$$K(S_e) = K_s S_e^l [1 - (1 - S_e^{1/m})^m]^2 \qquad [2.28]$$

$$K(h) = \frac{K_s \{1 - (\alpha h)^{mn}[1 + (\alpha h)^n]^{-m}\}^2}{[1 + (\alpha h)^n]^{ml}} \qquad [2.29]$$

$$D(S_e) = \frac{(1 - m)K_s S_e^{l-1/m}[(1 - S_e^{1/m})^{-m} + (1 - S_e^{1/m})^m - 2]}{m\alpha(\theta_s - \theta_r)} \qquad [2.30]$$

which are known as *soil hydraulic functions*. In these expressions θ_s is the saturated soil moisture content ($L^3 L^{-3}$), θ_r is the residual soil moisture content ($L^3 L^{-3}$), S_e is effective saturation ($0 \leq S_e \leq 1$), α is air entry value (L^{-1}) which is a measure of the first moment of the pore size density function, n is an inverse measure of the second moment of the pore size density function (as α increases, so does the first moment and as n increases the pore size density function becomes narrower (Wise, 1991; Clement *et al.*, 1994)), ι is

pore connectivity index, and $m = 1 - 1/n$ is a curve fitting parameter.

Due to the changes in fluid pressure in partially saturated porous media, the solution of equation [2.21], [2.22], and [2.23] is not an easy task. Two main reasons for this difficulty are: 1) the highly nonlinear nature of the partial differential equations, and 2) the heterogeneity of the flow domain in the unsaturated region (Bouloutas, 1989). Consequently, several investigators, considering simplifying assumptions about initial and boundary conditions and soil properties, have developed analytical solutions to Richards' equation. Philip (1957a, 1957b, 1969), in a landmark contribution to the theoretical treatment of the unsaturated flow, developed analytical solutions for the $\theta - based$ Richards equation. Using Kirchhoff transformation (Carslaw and Jaeger, 1959) to linearize Richards equation and assuming that unsaturated hydraulic conductivity is an exponential function of pressure head, Warrick (1975) and Lomen and Warrick (1974) obtained analytical solutions for one, two, and three-dimensional infiltration from point, line, and disk sources. Several other useful analytical solutions have been presented by Youngs (1957), Gardner (1958), Smith and Parlange (1978), Parlange *et al.* (1985), Sander *et al.* (1988), Broadbridge and White (1988), and Philip (1987; 1992), among others.

2.3.1. Numerical Solution of Flow Equations

While analytical solutions are useful for a number of applications such as verification of numerical models and approximate determination of hydraulic properties, their over-simplified nature reduces their predictive ability (Bouloutas, 1989). Also, the unsaturated flow equation is highly nonlinear, therefore numerical solutions are usually the only viable procedures to treat flow and transport phenomena in partially saturated porous

21

media. The standard numerical schemes are the finite element and finite difference methods which are usually coupled with a backward Euler time discretization. Except for the fully explicit forward method, any other Euler time-marching algorithm generates nonlinear algebraic equations which should be solved using iterative procedures such as Newton (Newton-Raphson) or Picard algorithms.

2.3.1.1. Finite Element Methods

The finite element method was first proposed by Courant (1943) although the term "finite element" was not used at the time. The method received its name from the work of Turner *et al.* (1956) in analyzing structural problems where a continuous structure is approximated by a series of sub-domains called "finite elements". Later it was rediscovered that the method is associated with the calculus of variation (Remson *et al.,* 1971). For regular mesh networks, the finite difference and finite element methods produce identical difference equations. However, the ability of finite element methods to treat irregular geometries, complex boundary conditions, and heterogeneous and anisotropic media attracted significant interest in porous media studies. Zienkiewicz (1966, 1967) contributed significantly in extending the method in structural analysis and indicated that the method can be used to analyze problems in subsurface hydrology. Javandel *et al.* (1968, 1969) played a significant role in application of the procedure to transient hydrological problems. Neuman (1973), and Duguid and Reeves (1976) developed algorithms to solve two-dimensional problems using pressure head based form of the Richards equation. In most of these research works linear triangular or linear quadrilateral elements were used to discretize the spatial domain while the standard fixed point Picard iteration scheme was used to handle the nonlinearities.

Neuman (1975) was first to observe that the consistent mass matrix produced by finite element discretization of the time derivative of the Richards' equation results in oscillatory solution that often prevents it from converging to a stable and smooth solution. The reason was the highly nonlinear nature of the relationships among soil water content, soil water pressure head, unsaturated hydraulic conductivity, and specific soil water capacity. Because of these nonlinearities and because of the high sensitivity of the Newton-Raphson linearization scheme to initial estimates of pressure head, the algorithm failed to converge. To improve the convergence rate and increase computational efficiency he proposed a "mass lumping" procedure which significantly enhanced the rate of convergence and CPU performance.

Bruch and Zyvloski (1974) were the first investigators to formulate a finite element algorithm to solve the water content based form of the Richards equation. They used triangular and rectangular elements in both space and time. By performing regression analysis on experimental data, they found that the unsaturated hydraulic conductivity and diffusivity are quadratic functions of soil water content. They compared the results with other numerical works and found a good agreement. They also, for the first time in porous media studies, used the quasi-Newton method to handle the nonlinearities of the system of discretized equations.

Yeh and Ward (1980) developed a finite element solution of the pressure-based form of the Richards equation. Using linear basis functions and the Picard iteration scheme, Hromadka and Guymon (1980) solved the horizontal, one-dimensional water content based form of the Richards equation. They claimed that the best results, in terms of accuracy, were obtained by using the consistent mass matrix.

In a series of reports and papers van Genuchten (1978, 1982, and 1983) compared the performance and computational efficiency of finite difference and finite element methods in solving Richards' and the convective-dispersive-reactive equations in multi-dimensions simultaneously. He used different basis functions and concluded that the Galerkin scheme with Hermitian basis function, which produces solutions for both the pressure head and its gradient, and with two point Gaussian integration procedure lagged considerably behind the correct solution and showed oscillatory behavior. Using the five point Gauss-Lobatto integration generated more accurate solutions. However, even with higher quadrature rule the Hermitian basis function showed spatial oscillations of the same order of magnitude as those of the linear basis function. He also reported that the Hermitian based Galerkin scheme was more accurate than the usual linear basis function but at the expense of 2.5 times more computational time.

To improve the efficiency of finite element methods and by considering an idea like block centered values of unsaturated hydraulic conductivity functions in finite differences, Huyakorn and Thomas (1984) presented a Galerkin scheme on rectangular and triangular elements in conjunction with the use of average value of nonlinear terms over an element. Using this method- which they called "*influence coefficient matrices*"- all elemental matrices were calculated as a weighted sum of predefined matrices and hence the expensive numerical integration operations were avoided. This method, although efficient in comparison to the usual integration over deformed quadrilaterals, isn't accurate. The Newton-Raphson and Picard one point iteration methods were used to treat the nonlinearities. They noticed that the former needs greater cost per iteration, but because of its quadratic convergence can be comparable in overall cost with the Picard

method. They also concluded that when convergence is difficult to obtain using the Picard method, the Newton-Raphson method may successfully be used. The surprising conclusion of this study is that they obtained these results using a consistent mass matrix.

In a significant work, Milly (1985) investigated the poor mass balance behavior of the $h-based$ Richards equation with Picard linearization method, and suggested a mass conservative algorithm using a new definition of the soil water capacity term. In comparison with the standard $h-based$ form, using this algorithm significantly reduced the global mass balance error but didn't totally eliminate it. He also reported that the distributed mass matrices did not converge at all or the rate of convergence was painfully slow which is in contrast with the results observed by Huyakorn and Thomas (1984).

In another study, Huyakorn *et al.* (1986) used the influence coefficient matrices method to solve a three-dimensional problem. The standard Picard method and the symmetric successive over-relaxation (SSOR) scheme were used to handle the nonlinearities and solve the system of linear equations, respectively. They concluded that the symmetric successive over-relaxation method with a relaxation factor of one converged very quickly (less than ten iterations).

In a landmark study, Celia *et al.* (1990) pointed out that the mass balance problems of the $h-based$ Richards' equation come from the fact that the time derivative, $\partial\theta/\partial t$, and its equivalent $C(h)\partial h/\partial t$ (where $C(h)=\partial\theta/\partial h$ is the specific soil moisture capacity) are mathematically equivalent in a continuous partial differential equation, their discrete analogs are not. This inequality is amplified because of the highly nonlinear nature of the soil water capacity term. To eliminate the problem they developed a "mixed form" Richards equation and modified Picard linearization technique which

uses a Taylor series expansion of θ in the iteration space in order to relate θ and h. This led to perfectly conserved mass and significant numerical solution performance, while requiring no additional computer efforts. Since then, this approach has been a standard procedure in solving water flow problems in unsaturated porous media in both finite difference and finite element methods. They also showed that finite difference is superior to the finite element without lumping the mass matrix and in case of mass lumping they produce the same results. Celia and Binning (1992) later extended this technique to two-phase flow problems. A similar method was employed by Allen and Murphy (1986) in the context of finite element collocation method and by Celia *et al.* (1987) in the context of an alternating version of the collocation approximation of space.

Rathfelder and Abriola (1994) noticed that the standard Picard method in conjunction with the h-based form of the Richards' equation could be equally good as the modified Picard scheme for the mixed form equation, if the soil water capacity term was evaluated using a chord-slope method.

Forsyth *et al.* (1995) developed a numerical method to simulate two-phase saturated-unsaturated flow problems using monotone finite element and finite volume space discretization and variable substitution. The algorithm uses the water content based form of the Richards' equation in unsaturated regions and switched to the standard h-based form in and near saturated zones. For very dry initial condition, where there's a steep moisture and/or salt front, the proposed algorithm required an order of magnitude less Newton iterations compared to the standard pressure-based form. In problems, where the initial state is not very dry, the algorithm was 30 per cent more efficient than the h-based form and in saturated porous media they were the same. They argued that the

26

method was mass-conservative, strictly monotone for any time step and mesh size (if upstream weighting is used), required no special treatments of discontinuities in heterogeneous porous media, and could be easily implemented in the context of finite element and finite volume methods.

Lehmann and Ackerer (1998) compared Picard, Modified Picard, and Newton-Raphson algorithms in solving the pressure-head based and mixed forms of the Richards' equations. They concluded that modified Picard method produces better results in terms of CPU time than the Newton-Raphson method when the Jacobian matrix is calculated using a perturbation approach. Having used an analytically calculated Jacobian matrix they noticed that the later form is more efficient than the modified Picard method. Nevertheless, when they used the modified Picard method at the beginning of the iteration procedure and switched to the Newton method as iteration proceeded, they obtain good results in terms of accuracy and CPU time.

A "primary variable substitution" technique similar to that of Forsyth *et al.* (1995) was used by Diersch and Perrochet (1999) in which the water content based form of the Richards' equation was applied in unsaturated regions and the standard h-based form in and near saturated zones. Gui *et al.* (2000) and Hao *et al.* (2005) reported large mass balance error when the mixed form was used to simulate different irrigation operations with free drainage boundary condition at the outlet.

2.3.1.2. Finite Difference Methods

The first attempt to solve unsaturated flow problems by numerical means appeared in the 1960's. Hanks and Bowers (1962) used a finite difference method with Crank-Nicolson time discretization scheme to study one-dimensional flow in a layered soil. Whisler and

Klute (1965) applied the finite difference method with Picard linearization to a one-dimensional flow problem. Liakopolous (1966) and Molz and Remson (1970) considered a non-conservative form of Richards equation in which both the gravity and diffusivity terms were expanded using the chain rule of differentiation. Rubin (1968) employed alternating direction implicit (ADI) finite difference method to solve the two-dimensional $h-based$ Richards equation. The predictive ability of the $h-based$ form of the Richards equation for coupled saturated-unsaturated one-dimensional flow was first studied by Freeze (1969) and Hornberger *et al.* (1969). In a significant study Freeze (1971a, 1971b) developed a finite difference model for three-dimensional saturated-unsaturated flow using Crank-Nicolson time discretization, Picard iteration, and the line successive over-relaxation (LSOR) method for solution of the resulting system of algebraic equations. Cooley (1971) developed a finite difference model to solve transient unsaturated flow problem. The finite difference solution of Freeze (1971) and Cooley (1971), however, were not robust and suffered from numerical instability and convergence difficulties. These problems stemmed from the inefficiencies of the line successive over-relaxation and alternating direction implicit (ADI) methods used to solve the two-dimensional $h-based$ form of the Richards equation and the resulting system of algebraic equations (Clement *et al.,* 1994).

Haverkamp *et al.* (1977) compared three finite difference schemes for solution of the one-dimensional $\theta-based$ and $h-based$ Richards equation for two sets of soil parameters. The time discretization was carried out by: 1) explicit Euler method, 2) fully implicit method with explicit linearization, and 3) fully implicit method with implicit linearization. They concluded that explicit methods needed to meet severe time step

restrictions to ensure stability and also needed 5 to 10 times more computer time than implicit methods. The fully implicit method with implicit linearization was superior to the fully implicit method with explicit linearization. In another study, Haverkamp and Vauclin (1981) compared the performance of the finite difference solution of three forms of Richards' equation: Kirchhoff transformed form, $h-based$ form, and the non-conservative form. The three models were compared with the semi-analytical solution of Philip. They noticed that the Kirchhoff transformed form was the most accurate. They also observed a significant decrease in its efficiency (in terms of CPU time and number of iterations) in comparison with the $h-based$ form. On the other hand the non-conservative form produced the worst results.

Ababou (1988) developed a finite difference model for three-dimensional flow in heterogeneous porous media. Hills *et al.* (1989) showed that finite difference solution of the water content-based form of the Richards equation can result in significantly improved performance compared to the standard pressure-based form when modeling infiltration into a very dry and heterogeneous soil.

Kirkland *et al.* (1992) presented a finite difference solution for two-dimensional partially saturated flow problems. The goal was to develop an efficient model to simulate infiltration into a heterogeneous and very dry soil. They used a "transformed" Richards' equation which had the characteristic of water content-based formula in the unsaturated region and that of the pressure-based form in or near the saturated zone. The resulting system of linear algebraic equations was solved by the preconditioned conjugate gradient method (PCG). This model, however, did not include the effect of specific storage and therefore could not be used to accurately simulate a wide variety of flow problems such

as transient drainage and seepage face in large domains (Clement *et al.,* 1994). To overcome this limitation, Clement *et al.* (1994) developed a finite difference code that can be used to simulate different flow scenarios in partially saturated media. They used mixed form of the Richards equation with modified Picard linearization technique proposed by Celia *et al.* (1990). The resulting system of linear algebraic equations was solved by preconditioned conjugate gradient method. They concluded that this algorithm was computationally efficient, highly stable, and required minimum computer storage and time.

Since the mass-lumped linear finite element method leads to the standard finite difference approximation of flow equation, Simunek *et al.* (2005) used finite difference method to solve partially saturated flow problem in their HYDRUS1D code.

2.3.2. Parameter Identification in Water Flow through Porous Media

Despite remarkable efforts to solve partial differential equations governing water flow and pollutant transport phenomena in variably saturated soils, there have been relatively few attempts to calibrate and validate them against large scale data. The reason is the large number of model parameters which requires intensive datasets that are not readily available. To calibrate these models one approach is to impose rather restrictive initial and boundary conditions on transport properties of the system that allow direct computation of the parameters (Kool *et al.* 1987). Another approach is parameter estimation by inverse methods which will be reviewed in the following sections.

2.3.2.1. Direct Methods

There are several laboratory and field scale methods to measure hydraulic and transport parameters in water flow and contaminant transport through variably saturated soils (Bouwer and Jackson 1974; Green *et al.,* 1986; Klute and Dirksen1986). However, laboratory scale results may not be representative of field scale transport parameters. Field scale measurements, on the other hand, are tedious, time consuming, expensive, and often impose unrealistic and simplified initial and boundary conditions on transport processes in biological systems. Finally, information regarding parameter uncertainty is not readily obtained from these methods unless a very large number of samples and measurements are taken at significant additional cost (Kool *et al.,* 1987; Simunek and van Genuchten, 1996; Finsterle, 2004). To overcome these limitations indirect methods, such as parameter optimization by inverse modeling, can be used to identify mass transport and reaction parameters.

2.3.2.2. Indirect Methods: Inverse Modeling

A promising approach for parameter estimation is the use of inverse modeling. Model calibration, history matching, nonlinear regression, and optimization are equivalent terms for inverse modeling (Finsterle, 2004). In this procedure, laboratory and/or field measurements of system variables such as discharge, fluid pressure, and concentrations are used to find optimum values for model parameters such as parameters of characteristics curve, and contaminant transport. Inverse modeling may be viewed as a procedure for converting more easily measured data such as water content and pressure head into harder to obtain transport parameters such as kinetic rate constants, saturated hydraulic conductivity, dispersion coefficient, retardation factor, degradation and production coefficients, and pore water velocity.

Unlike direct inversion methods, inverse modeling does not impose any constraints on the form or complexity of the forward model, on the choice of initial and boundary conditions, on the constitutive relationships, or on the treatment of heterogeneities via deterministic or stochastic formulations. Therefore, experimental conditions can be chosen based on convenience rather than by a need to simplify the mathematics of the process (Kool *et al.,* 1987). Additionally, if information regarding parameter uncertainty and model accuracy is needed, it can be obtained from the parameter optimization procedure (Yeh *et al.,* 1986; Kool *et al.,* 1987; Ewing and Lin, 1991; Sun, 1994; McLaughlin and Townly, 1996; Simunek and van Genuchten, 1996; Durner *et al.,* 1997; Zimmerman *et al.,* 1998; Hopmans *et al.,* 2002).

On the other hand, a general problem of parameter optimization via inverse modeling is ill-posedness. A problem is ill-posed when it either has no solution at all, no unique solution, or the solution is not stable (Tyn Myint-u, 1980). Generally, ill-posedness arises from non-uniqueness and instability. Instability occurs when the estimated parameters are excessively sensitive to the input data. Any small errors in measurements will then lead to significant error in estimated values of parameters. If boundary conditions are improperly formulated, appreciable errors in parameter optimization may arise for the inverse modeling (Yeh, 1986; Kool *et al.,* 1987). Non-uniqueness occurs when there are multiple parameter vectors that can produce almost the same values of the objective function (Yeh, 1986; Kool *et al.,* 1987) thus making it impossible to determine the correct and unique solution. This problem is closely related to parameter identifiability. In other words, is it possible to obtain accurate values for the parameters in a given mathematical model from the available experimental data?

Parameter identifiability depends on both the structure of the mathematical model and the experimental data used. A common cause for non-identifiability of model parameters is high intercorrelation among parameters. In these situations a change in one parameter generates a corresponding change in the correlated parameter making it impossible to obtain accurate estimate for either of them. Furthermore, even when parameters in a mathematical model are independent of each other, the experimental data may produce an objective function that is not sensitive enough to one or more parameters. The characteristics of the second situation are wide confidence regions on the estimated parameters and large estimation variances (Kool *et al.,* 1987). Where the only solution for the first case is fixing one of the parameters and estimating the other one, in the second case performing multi-objective optimization by coupling different kinds of experimental data may lead to unique solution (Kool *et al.,* 1987).

2.3.2.2.1. Laboratory Scale

One of the first attempts to estimate soil hydraulic properties from transient column drainage experiment in laboratory scale was that of Zachmann *et al.* (1981, 1982) who used cumulative drainage outflow data to estimate two unknown parameters in a four-parameter flow model using Ordinary Least Squares (OLS) formulation. They solved the pressure head based form of the Richards' equation (as direct problem) by finite differences and used an OLS approach for their parameter estimation procedure. In another study carried out by Hornung (1983), an initially saturated soil column was subjected to constant infiltration flux at the surface and gravity drainage at the bottom. The final pressure head at some fixed positions inside the column and the outflow rate

from the column were measured. Soil hydraulic properties were represented by van Genuchten's model. Hornung assumed that $K_s, \theta_r,$ and θ_s were known and estimated α and n by inverse modeling.

Using column drainage experiment Kool *et al.* (1985) estimated $n, \theta_r,$ and α in van Genuchten's model. Unlike the gravity drainage experiment of Zachmann *et al.* (1981, 1982) and Hornung (1983), soil drainage in this study was initiated by one-step change in air pressure at the upper boundary of the soil sample. Kool *et al.* (1985) claimed that except for very coarse material the gravity drainage experiment must be carried out in unrealistically long columns in order to get the desired solution.

Parker *et al.* (1985) used the one-step outflow experiment to determine soil hydraulic properties. Soil cores were assembled in a pressure plate apparatus. After increasing pneumatic pressure on the soil samples the cumulative outflow rates were measured as a function of time. The parameters $n, \theta_r,$ and α were then estimated by inverse modeling. Predicted $\theta(h)$ and $K(h)$ were compared to independently determined soil hydraulic properties for the same soil cores and good agreement was found for all of them within the measurement domain. Extrapolation to lower pressure heads, however, proved to be less reliable (Parker *et al.* 1985). van Dame *et al.* (1990) modified the one-step outflow method of Parker *et al.* (1985) into a multi-step procedure for estimating soil hydraulic functions. By analyzing parameter response surface, Toorman *et al.* (1992) showed that the one-step method doesn't provide enough information to uniquely estimate the parameters of the characteristic curve.

Additional studies include Yeh and Yoon (1981) who studied the parameter identifiability problem for an aquifer. Cooley (1982 and 1983) who incorporated prior

information about the parameters into a nonlinear groundwater flow model. Parker and van Genuchten (1984) who applied an inverse technique to laboratory and field scale displacement experiment. Carrera and Neuman (1984) who used a maximum likelihood method and incorporated the prior information in their parameter optimization procedure assuming both steady and transient flow conditions. Yeh (1986) and Kool *et al.* (1987) reviewed general aspects of parameter optimization procedures. Kool and Parker (1988) applied an inverse modeling scheme to a flow experiment consisting of infiltration, gravity drainage and evaporation at the soil surface. Using transient outflow and soil water matric potential head data, Eching and Hopmans (1993) studied optimization of the soil hydraulic functions. In another study, Eching *et al.* (1994) discussed how laboratory determined parameters are related to the field scale parameters.

Some studies introduced geostatistics considerations in the inverse modeling procedures (Clifton and Neuman, 1982; Kitanidis and Vomvoris, 1983; Kitanidis, 1995; Yeh *et al.,* 1996; Zimmerman *et al.,* 1998), while others combined parameter optimization techniques with scaling capabilities (Shouse *et al.,* 1992; Eching *et al.,* 1994). Also, some research works coupled numerical inverse problems, such as heat transport, with unsaturated or saturated flow (Carrera, 1987; Mishra and Parker, 1989; Sun and Yeh, 1990). Laboratory scale inverse modeling analyses have also been carried out by Hudson *et al.* (1996), Gariner *et al.* (1997), Finsterle *et al.* (1998), Hwang and Powers (2002), Bitterlich and Knabner (2002), and Bohne and Salzmann (2002), among many others.

Analyzing infiltration data and parameter response surfaces, Russo *et al.* (1991) concluded that the use of prior information (e.g. regularization) of the model parameters

reduces the degree of ill-posedness and might lead to a stable and unique solution even when the input data are associated with considerable measurement errors. Carrera and Neuman (1986c), Toorman and Wierenga (1992), and Simunek and van Genuchten (1996) studied the uniqueness of the inverse problem using generated data.

2.3.2.2.2. Field Scale

While most of the studies on inverse problems in biological systems have been carried out on laboratory scale and numerically generated data, the most promising aspect of the technique is its potential application to large scale situations (Abbaspour *et al.,* 1999 and 2000; Jhorar *et al.,* 2002). Dane and Hruska (1983) developed a parameter optimization method to simultaneously determine characteristic curve parameters and hydraulic conductivity functions from a transient field experiment. A gravity drainage experiment was conducted in a clay loam soil trough. Water contents were measured by neutron probe after 7 and 25 days of initiation of drainage. To prevent evaporation, zero flux boundary condition was imposed at the top of the soil. By measuring pressure head at the depth of 90cm, Dirichlet type boundary condition was applied at the bottom of the lysimeter. Before initiation of drainage, the saturated hydraulic conductivity and saturated water content were measured by neutron probe. By inspection of the available $\theta(h)$ data a "smart guess" was assumed for θ_r. They could estimate α and n by coupling an optimization algorithm with the finite difference solution of the pressure head form of the Richards' equation. They found reasonable agreement between simulated and independently measured $\theta(h)$ but observed that the predicted $K(h)$ overestimated measured conductivities by approximately one order of magnitude. Significantly better results were obtained, with only small changes in the resulting optimum values of α and

n, when they used K_S values arbitrarily 10 times lower than the measured value. They suggested that, in measuring K_S by ponded infiltration, macropore flow caused an inflated value for saturated hydraulic conductivity.

A more general approach would be to take α, θ_s, θ_r, K_s, and n as unknown vector and determine their values by inverse modeling. The reason is that obtaining reliable value for K_S is very difficult, especially in structured media. On the other hand, one can obtain a value for θ_r by determining water content at $h = 15$ atmosphere, which is the arbitrary definition of the residual water content. Numerous studies, however, have shown that the parameter estimation process is not very sensitive to the value of θ_r (Kool *et al.*, 1987). Consequently, one may fix its value and thereby help the convergence of the inverse procedure by removing one parameter from the problem.

A detailed field experiment was conducted at the Los Alamos National laboratory (Abeele, 1984) and the results were used by Kool *et al.*, (1987) to identify the unknown parameters K_S, θ_r, n, and α. Solving the one-dimensional Richards' equation by a fully implicit and mass-lumped Galerkin-type linear finite element code with variable time step and constant node spacing of 5 cm, they successfully estimated the unknown parameter vector. The estimated $\theta(h)$ and $K(h)$ were compared with independently measured data and excellent agreement was found. The observed $K(h)$ was calculated from the lysimeter drainage experiment using the instantaneous profile method. Among four unknowns the estimated saturated hydraulic conductivity was the least accurate parameter with wider confidence interval suggesting that obtaining a good value for in-situ saturated hydraulic conductivity is quite difficult. This confirms the

results of Dane and Hruska (1983). These studies show that in order to get a good estimate for in-situ saturated hydraulic conductivity one must have several data points at early observation times in drainage experiment and assign them more weight in the objective function. They claimed that in order to obtain a unique solution for the inverse problem, it is necessary to use water content and pressure head profiles simultaneously in the objective function. Mishra and Parker (1989) used synthetic data to simultaneously estimate the hydraulic and transport parameters.

Using flow rate and pressure head data, Gribb (1996) estimated the saturated hydraulic conductivity and the soil water matric potential head at air entry point. Using water content data, monitored during an infiltration-redistribution event, Zijlstra and Dane (1996) estimated the saturated hydraulic conductivity and parameters of soil water characteristics curve for both homogeneous and layered systems. Generating synthetic data for pressure head and water content during infiltration experiment and coupling them with prior information and geostatistical inverse methodology, Yeh and Zhang (1996), Zhang and Yeh (1997), and Hughson and Yeh (2000) identified saturated hydraulic conductivity and air entry value.

Abbaspour *et al.* (1997) developed a sequential uncertainty domain parameter optimization procedure. They claimed that the method is general, forward, sequential, iterative, and Bayesian in nature. They also reported that the procedure is stable, convergent, and proper for global minimization. Abbaspour *et al.* (1999, 2000) applied the technique to estimate the soil water retention curve parameters of a layered field soil. However, their experiment imposed artificial conditions such as constant irrigation rate and gravel on top of the soil surface to prevent sealing and reduce evaporation. Pan and

Wu (1998) measured pressure head during an infiltration experiment and estimated the optimized values of saturated hydraulic conductivity and the parameters of soil water retention curve. Monitoring water content and pressure in a watershed scale infiltration-percolation-redistribution event at Yucca mountain and coupling them with prior information, Badurraga and Bodvarsson (1999) identified parameters of soil water characteristic curve and the saturated hydraulic conductivity. Finsterle (2000), Finsterle *et al.* (2003), and Ghezzehei *et al.* (2004) identified capillary strength by using seepage rate data. Monitoring concentration of nitrate and water pressure, Schmied *et al.* (2000) estimated parameters of the soil water characteristic curve, the saturated hydraulic conductivity of the soil, plant water uptake, and nitrogen turnover parameters in a large scale agricultural field.

Using evaporation and evapotranspiration data, Jhorar *et al.* (2002) investigated the use of inverse modeling for determining soil hydraulic properties of irrigated lands with deep groundwater Table. The experiment was repeated for three different soil types. The PEST optimization code was used to solve the inverse problem. The results indicated that when ET fluxes data are accurate α, θ_s, and n can be optimized precisely. Inverse estimating of these parameters results in effective soil hydraulic properties that reliably predict different water balance components for different soil types.

To estimate transport coefficients Ritter *et al.* (2003 and 2005) applied WAVE (water and agrochemicals in soil, crop and vadose environment) software to a sprinkler fertigated banana plantation field data in the north of Tenerife (Canary Islands). Inverse modeling in this study suffered from ill-posedness, because nine parameters were estimated simultaneously. The algorithm they used could only estimate four unknowns

and they could not find the global minimum. To optimize further coefficients more measurements were needed. They concluded that when input data are subjected to measurements errors, the convergence of the minimization method at several points in the parameter space may be very slow due to instability. In these cases, especially when over-parameterized models are used, inverse techniques should be complemented with prior information obtained by direct measurement methods or other available data.

In a less restrictive approach, Olyphant (2003) applied inverse modeling to field measurements of pressure head and water contents profiles of a field soil and net surface flux (infiltration/evaporation). The optimization results indicated that consistent set of parameters can be achieved. Wang *et al.* (2003) and Kowalsky *et al.* (2004) used water content information as input data, obtained through infiltration experiment, and coupled them with prior information to estimate hydraulic parameters. The former evaluated different conceptual models while the later employed geostatistics and pilot point method.

Recently, Knowles *et al.* (2004) and Knowles and Yan (2004) used the steepest descent scheme to estimate groundwater flow parameters. Using the Levenberg-Marquardt algorithm, Malengier (2004) estimated the groundwater hydraulic parameters in a drainage basin.

Some investigators extended the use of inverse techniques to parameter identification in multiphase flow. Finsterle and Pruess (1995) measured water potential, gas pressure, and cumulative evaporation during two-phase flow ventilation experiment and coupled the data with a priori information to identify the parameters of soil water retention curve and the saturated hydraulic conductivity. Conducting multi-step outflow

experiment and measuring cumulative outflow and pressure, Chen *et al.* (1999) estimated the capillary pressure-saturation relationship parameters for two fluids (oil and water). Vasco and Datta-Gupta (1997) and Wu *et al.* (1999) coupled regularization with water cut data and water/oil ratio, pressure, and a geostatistical model to determine hydraulic conductivity in the oil reservoir experiment. Engelhardt *et al.* (2003) measured temperature and cumulative outflow during non-isothermal two-phase flow experiment (e.g. gas injection into heated column) to inversely estimate thermal conductivity, heat capacity, hydraulic conductivity, and matric potential head at air entry value.

Unlike the laboratory scale experiments, large scale experiments face the problem of heterogeneity and over-parameterization. The heterogeneous (e.g. stratified and layered) nature of geological deposits has led some researchers to estimate separate parameters for each layer.

2.4. Summary of the Literature Review

The review of literature on inverse modeling can be summarized as follows:

1. Several techniques have been developed to identify the parameters of sophisticated models. Direct inversion methods have been proven inefficient. A promising approach is estimation of model parameters using inverse modeling that has been increasingly researched during recent years.

2. The optimization algorithms to solve the inverse problems and find the minimum of the objective function have been continually improved and refined but the basic idea and difficulties associated with solving the inverse problems remain the same.

3. The task of parameter estimation in FRAP protocol is the topic of ongoing research. So far most of the parameter estimation in FRAP studies have been qualitative and merely curve fitting. There have been no ill-posedness analysis of the inverse problem in FRAP procedure.

4. While the use of inverse modeling in saturated flow and transport problems has been extensive, its application to unsaturated and transient flow and transport problems has been far less extensive with most studies carried out at the laboratory scale (especially the one-step and multi-step outflow methods) and using the Mualem-van Genuchten water characteristic model parameters. A few studies have employed more sophisticated water retention functions such as bimodal (Zurmuhl and Durner, 1998) and hysteretic models.

5. Stochastic inverse modeling approaches, such as those presented by Zimmerman *et al.* (1998), have not been extensively used in unsaturated flow and transport problems (except for Daghan, 1985: Yeh and Zhang (1996); Zhang and Yeh (1997); Kowalsky *et al.,* 2004).

6. Only a few studies have used inverse modeling approaches in multi-phase flow systems.

7. A large number of computer codes have been developed to solve optimization problems (Moré and Wright, 1993). In geohydrology all of these codes deal with the flow and transport problems in the saturated region. A few computer codes have been developed to solve inverse problems in unsaturated flow and transport problems: ONE-STEP program (Kool *et al.,* 1985; Eching and Hopmans, 1993) which determines hydraulic parameters from outflow

experiment, HYDRUS software (Simunak *et al.,* 2005), and iTOUGH2 code (Finsterle, 2004). These codes don't guarantee unique and stable solution for inverse problems. Any numerical solutions of partial differential equations governing flow and transport processes in unsaturated porous media can be used in conjunction with the parameter optimization packages such as PEST (Doherty, 1994) and UCODE (Poeter and Hill, 1998) or any other commercial optimization software.

8. A potential problem with inverse modeling is ill-posedness, particularly non-uniqueness. None of the developed codes analyze the posedness of the inverse problem.

Overall, inverse modeling appears to offer the characteristics needed for parameter identification in sophisticated models of biological systems. It however remains to: 1) evaluate the strategy in systems of coupled nonlinear partial differential equations governing mass transport and reaction kinetics across complex biological systems, 2) investigate whether judicious selection of calibration data and forward model can eliminate potential ill-posedness problems, and 3) evaluate possible ill-posedness of the inverse problem with innovative techniques.

Success in these activities will further permit the evaluation of the uncertainty of the identified model parameters.

CHAPTER 3: SPECIFIC OBJECTIVES OF THE RESEARCH

> *Basic research is what I am doing when*
> *I don't know what I am doing.*
> *Wernher von Braun*

The goal of this study is to develop, apply, and analyze a state of the art inverse modeling strategy to optimize model parameters of mass transport processes in biological systems. The specific objectives are as follows:

1. To develop an inverse modeling strategy by coupling numerical solution of a system of coupled nonlinear partial differential equations governing species transport in different biological systems with optimization algorithm and set(s) of experimental/synthetic data to inversely estimate model parameters.

2. To apply the strategy to parameter identification problems in biomolecule transport in living cells.

3. To apply the strategy to parameter optimization problems in fluid flow in variably saturated porous media.

4. To analyze and distinguish possible ill-posedness of the inverse problems by innovative techniques.

The inverse problem will be treated as a nonlinear optimization problem in which model parameters are estimated by minimizing an appropriate objective function which represents the discrepancies between the observed and predicted responses of the biological systems. Several finite element and finite difference

approximations will be compared for their ability to efficiently solve the forward problem and the best method will be selected for coupling with the optimization algorithm. Several Newton based optimization methods will be compared to find the one that is most suitable for solving optimization problems in biological systems, which will form the core of the proposed inverse modeling strategy. The numerical solution of the forward problem will be validated by either analytical or reference solutions. The inverse problem will be validated with synthetic and experimental data sets. The solution for forward models will be provided in one-dimension. Extension to higher dimensions will be left for future research. Also, regularization and incorporation of a priori information regarding the parameters will be left for future studies.

The validated inverse modeling strategy will be used to optimization problems in different biological systems. The scale of application will range from biomolecule transport in living cells to fluid flow in lysimeter. Both homogeneous and heterogeneous porous media will be considered. Application of the inverse modeling strategy to regional and watershed scales will be left for future research. Validation of the strategy with the genetic algorithm and Monte Carlo–Markov Chain (MCMC) method will be left for future research.

The posedness of the inverse problems will be studied by performing stability and uniqueness analysis. An input data perturbation approach will be used to study the stability of the inverse problem. Parameter hyper-space will be constructed and analyzed to investigate the uniqueness of the inverse problem. The commonly used parameter response surfaces analysis will be thoroughly and

critically studied. Multi-objective parameter optimization approach and residual analysis will be used to distinguish the problem. The use of Liapunov series analysis will be left for future research. The use of information theory and the Generalized Likelihood Uncertainty Estimation (GLUE) methodology will be left for future research.

CHAPTER 4: METHODS AND MATERIALS

> *As far as the laws of mathematics refer to reality,*
> *they are not certain; and as far as they are certain,*
> *they do not refer to reality.*
>
> *Einstein*

This chapter presents the methodology used to develop, apply, and analyze a state-of-the-art inverse modeling strategy which is applicable to diverse optimization problems in biological systems. The solution of the *forward problem* by means of numerical methods and formulation of the *inverse problem,* in the framework of nonlinear optimization, are discussed in detail. Both the finite difference and finite element approximations of partial differential equations governing transport phenomena are presented. The application of the developed strategy in two different transport problems, in molecular biology and fluid flow in partially saturated porous materials, is also described. Both homogeneous and heterogeneous porous media are considered. Methods for analyzing the inverse modeling technique are then presented.

4.1. Development of the Inverse Modeling Strategy

The inverse modeling strategy will be developed by identifying the best optimization algorithm for its three main components: 1) robustness of the method in finding the search direction, 2) controlling the size of the search step, and 3) an efficient stopping criterion. The methods used to identify the best techniques for these components are described below.

4.1.1. Optimization Algorithm

To obtain the search direction in each iteration, $\phi(\beta)$ in equation [2.7] is expanded with respect to $\Delta\beta$ around β^i by Taylor series expansion (Kool *et al.,* 1987):

$$\phi(\beta^i + \Delta\beta) = \phi(\beta^i) + \nabla\phi(\beta^i)^T \Delta\beta + \frac{\Delta\beta^T}{2}\nabla^2\phi(\beta^i)\Delta\beta + ... \qquad [4.1]$$

If the derivative of equation [4.1] with respect to $\Delta\beta$ is set to zero, then $\Delta\beta$ is a minimizer of the objective function:

$$\nabla\phi + \nabla^2\phi\Delta\beta = 0 \qquad [4.2]$$

or:

$$\Delta\beta = -\nabla\phi(\nabla^2\phi)^{-1} \qquad [4.3]$$

To get straightforward expressions for $\Delta\beta$, one needs to differentiate Eq. [2.7] twice with respect to β. Assuming $\phi(p)$ is twice-continuously differentiable, the gradient vector, $\nabla\phi(\beta)$, and the Hessian matrix, $\nabla^2\phi(p)$, can be calculated as:

$$\nabla\phi(\beta) = \sum_{i=1}^{N} r_i(\beta)\frac{\partial r_i(\beta)}{\partial\beta_i} = -J(\beta)^T r(\beta) \qquad [4.4]$$

and the second derivative:

$$\nabla^2\phi(\beta) = \sum_{i=1}^{N}\left[\frac{\partial r_i(\beta)}{\partial\beta_j}\frac{\partial r_i(\beta)}{\partial\beta_i} + \frac{\partial r_i^2(\beta)}{\partial\beta_i\partial\beta_j}r_i(\beta)\right] = J(\beta)^T J(\beta) + \sum_{i=1}^{N}\frac{\partial r_i^2(\beta)}{\partial\beta_i\partial\beta_j}r_i(\beta)$$

$$[4.5]$$

where J is the $N \times \beta$ Jacobian (sensitivity) matrix.

Inserting equations [4.4] and [4.5] into Eq. [4.3], one finds the well known Newton's algorithm for updating the unknown vector in each iteration:

$$\Delta \beta^{(k)} = -(J(\beta^{(k)})^T J(\beta^{(k)}) + \sum_{i=1}^{N} \frac{\partial r_i^2(\beta)}{\partial \beta_i \partial \beta_j} r_i(\beta))^{-1} J(\beta^{(k)})^T r(\beta^{(k)})$$

[4.6]

As discussed in chapter 2, equation [4.6] is not usually used in nonlinear optimization. Alternatively, the general purpose Levenberg-Marquardt algorithm:

$$\Delta \beta^{(k)} = -(J(\beta^{(k)})^T J(\beta^{(k)}) + \lambda D(\beta^{(k)})^T D(\beta^{(k)}))^{-1} J(\beta^{(k)})^T r(\beta^{(k)})$$

[2.11]

is generally used in nonlinear optimization problems.

To avoid the computation of possibly ill-conditioned $J^T J$ in equation [2.11], the Osborne-Moré modified version of the LM algorithm (Osborne, 1976; Moré, 1977):

$$\min \left\| \begin{pmatrix} r(\beta^k) \\ 0 \end{pmatrix} + \begin{pmatrix} J(\beta)^k \\ (\lambda^k D^k)^{\frac{1}{2}} \end{pmatrix} \Delta \beta^k \right\|^2$$

[2.12]

will be implemented in the inverse algorithm. The QR decomposition will be used to solve Eq. [2.12].

Owing to the nonlinear nature of Eq. [2.7], its minimization was carried out iteratively by first starting with an initial guess of parameter vector, $\{\beta^{(k)}\}$ and updating it at each iteration until the termination criteria were met:

$$\beta^{(k+1)} = \beta^{(k)} + \alpha^{(k)} \Delta \beta^{(k)}$$

where $\alpha^{(k)}$ is a scalar step length and $\Delta p^{(k)}$ is the direction of search (step direction).

All Newton based optimization algorithm require computation of the Jacobian matrix:

$$J = \frac{\partial r_i(\beta)}{\partial \beta_i} = -\frac{\partial U(\beta)}{\partial \beta_i}$$ [4.7]

where $U(\beta)$ is obtained by solving the forward problem which is a or a set of coupled nonlinear partial differential equation(s) governing the transport phenomena in the biological system of interest. The derivatives of $U(\beta)$ with respect to model parameters are not available analytically. A combination of "one-sided" and "two-sided" finite differences methods will be used to calculate the partial derivatives of the state variable(s) with respect to model parameters. At the beginning of the optimization, where the search is far from the minimum, the "one-sided" finite difference scheme is used;

$$J_i = -\frac{U(\beta_1, \beta_2, \dots \beta_i + \Delta\beta_i, \dots \beta_p) - U(\beta_1, \beta_2, \dots \beta_i, \dots \beta_p)}{\Delta\beta_i}$$ [4.8]

As optimization proceeds in descent direction, the algorithm switches to more accurate but computationally expensive approach in which the partial derivatives are calculated using a central finite difference scheme;

$$J_i = -\frac{U(\beta_1, \beta_2, \dots \beta_i + \Delta\beta_i, \dots \beta_p) - U(\beta_1, \beta_2, \dots \beta_i - \Delta\beta_i, \dots \beta_p)}{2\Delta\beta_i}$$ [4.9]

The truncation error of equation [4.9] is $\frac{\Delta\beta_i^3 \partial^4 OF(\beta_i)/\partial\beta_i^4}{24}$ (Bard, 1974) but in comparison to equation [4.8] it requires solving the forward problem, by means of finite element or finite difference approximations, twice for each partial derivative in each iteration of the inverse code.

The scaling matrix and the Lagrange multiplier, in Eq. [2.12], are updated in each iteration. Given λ is a positive scalar, the Hessian matrix must be positive definite in order to insure the descent property of the algorithm. To achieve this, the value of D is

initialized using a $\beta \times \beta$ unit matrix before the beginning of the optimization loop in the

inverse code. Then the diagonal elements of D is updated in every iteration;

$$d_j^0 = \left\| J_j^0 \right\|$$
$$d_j^i = \max(d_j^{i-1}, \left\| J_j^i \right\|)$$

where j is the jth column of the Jacobian matrix and i is the iteration level in inverse

code. The algorithm below updates D in each iteration:

for $i = 1 : p$

$$D(i,i) = \max(norm(J(:,i), D(i,i)))$$

end

4.1.2. Selection of the Efficient Optimization Algorithm

In order to choose the best and the most efficient algorithm, the steepest descent method

(Eq. [2.11] with $\lambda \rightarrow +\infty$ and $D = I_p$), the Gauss-Newton scheme (Eq. [2.11] with

$\lambda = 0$), equation [2.11], and the developed optimization algorithm (using Eq.[2.12]) will

be used to identify model parameters in the Convective-Dispersive-Reactive equation,

which is used here as a simple optimization problem (Toride *et al,* 1995):

$$\frac{\partial}{\partial t}(\theta C + \rho_b S) = \frac{\partial}{\partial z}(\theta D \frac{\partial C}{\partial z} - J_w C) - \theta \mu_l C - \mu_s \rho_b S + \theta \gamma_l + \rho_b \gamma_s$$

[4.10]

where C is concentration of the pollutant in the liquid phase (ML^{-3}), S is concentration

of the pollutant in the adsorbed phase (MM^{-1}), J_w is the volumetric water flux density

(LT^{-1}), D is the dispersion coefficient ($L^2 T^{-1}$), θ is the volumetric water content

($L^3 L^{-3}$), ρ_b is the soil bulk density (ML^{-3}), $\gamma_l (ML^{-3}T^{-1})$ and $\gamma_s (MM^{-1}T^{-1})$ are zero-

order source terms for the liquid and adsorbed phases, respectively, μ_l and μ_s are first-order decay coefficients for degradation of the pollutant in the liquid and adsorbed phases, respectively (T^{-1}), z is vertical distance from the soil surface downward (L), and t is time (T).

Assuming contaminant adsorption by the solid phase is described by a linear isotherm:

$$S = K_d C \qquad [4.11]$$

where K_d is an empirical distribution coefficient ($M^{-1}L^{-3}$), inserting equation [4.11] into equation [4.10], and assuming steady state and saturated flow in a homogeneous soil yields:

$$R\frac{\partial C}{\partial t} = D\frac{\partial^2 C}{\partial z^2} - v\frac{\partial C}{\partial z} - \mu C + \gamma \qquad [4.12]$$

Where $v = J_w / \theta$ is mean pore water velocity and R is the retardation factor defined by:

$$R = 1 + \rho_b K_d / \theta \qquad [4.13]$$

and μ and γ are combined first and zero-order rate coefficients (Toride *et al*, 1995):

$$\mu = \mu_l + \frac{\rho_b K_d \mu_s}{\theta}$$
$$\gamma = \gamma_l + \rho_b \gamma_s / \theta \qquad [4.14]$$

Inspection of equation [4.12] shows that when the first-order degradation coefficients in liquid and solid phases are identical, it reduces to:

$$\mu = \mu_l R$$
$$\gamma = \gamma_l + \rho_b \gamma_s / \theta \qquad [4.15]$$

A backward in time and central in space finite difference discretization of equation [4.12] yields:

$$R\frac{C_i^{n+1}-C_i^n}{\Delta t}=Df[\frac{C_{i+1}^{n+1}-2C_i^{n+1}+C_{i-1}^{n+1}}{(\Delta z)^2}]-vf[\frac{C_{i+1}^{n+1}-C_{i-1}^{n+1}}{2\Delta z}]+$$

$$D(1-f)[\frac{C_{i+1}^n-2C_i^n+C_{i-1}^n}{(\Delta z)^2}]-v(1-f)[\frac{C_{i+1}^n-C_{i-1}^n}{2\Delta z}]-\frac{\mu}{2}[C_i^{n+1}+C_i^n]+\gamma$$

[4.16]

where f is the time-weighting factor ($f=1$ for fully implicit scheme, $f=1/2$ for Crank-Nicolson algorithm, and $f=0$ for explicit method). Rearranging equation [4.16] one can obtain the following tridiagonal matrix equation:

$$[-\frac{Df\Delta t}{R(\Delta z)^2}-\frac{vf\Delta t}{2\Delta zR}]C_{i-1}^{n+1}+[1+\frac{2Df\Delta t}{R(\Delta z)^2}+\frac{\mu\Delta t}{2R}]C_i^{n+1}+[-\frac{Df\Delta t}{R(\Delta z)^2}+\frac{vf\Delta t}{2\Delta zR}]C_{i+1}^{n+1}=$$

$$[\frac{D(1-f)\Delta t}{R(\Delta z)^2}+\frac{v(1-f)\Delta t}{2\Delta zR}]C_{i-1}^n+[1-\frac{2D(1-f)\Delta t}{R(\Delta z)^2}-\frac{\mu\Delta t}{2R}]C_i^n+[\frac{Df\Delta t}{R(\Delta z)^2}-\frac{vf\Delta t}{2\Delta zR}]C_{i+1}^n+\gamma$$

[4.17]

which produces a system of linear algebraic equations that can easily be programmed and solved.

The numerical simulator of the Convective-Dispersive-Reactive equation will be validated with the analytical solution of Kreft and Zuber (1978):

$$C=\frac{C_0}{2}erfc\left[\frac{Rx-vt}{\sqrt{4DRt}}\right]+\frac{1}{2}\exp[\frac{vx}{D}]erfc\left[\frac{Rx+vt}{\sqrt{4DRt}}\right]$$

[4.18]

where C_0 is the concentration of tracer (ML^{-3}).

The numerical simulator will then be coupled with the inverse modeling strategy and a synthetic data set to estimate the optimized value of the parameter vector $\beta=[D,v,\mu,\gamma]$. The retardation factor will be kept constant. The synthetic data set will

be produced by solving Eq. [4.17] for a hypothetical breakthrough experiment with uniform initial condition and first type boundary condition at the inlet and second type boundary condition at the outlet using the parameter values: $D = 3.4290 cm/\min^2$, $v = 0.1345 cm/\min$, $\mu = 1.0917 \times 10^{-4} \min^{-1}$, $\gamma = 4.0914 \times 10^{-4}$, and $R = 1$. The predicted pollutant concentration values will then be sampled at discrete times for $x = L$. The data set will then be corrupted by adding $N(0, 0.05)$ error term to each "measurement". The noisy synthetic data will then be used as input for parameter optimization purpose in the context of the aforementioned optimization algorithms. The method producing the best replication of the parameters will then be incorporated in the proposed inverse modeling strategy.

4.1.3. Challenges of the Levenberg-Marquardt Algorithm

The Main challenge in the implementation of the Levenberg-Marquardt algorithm is a robust and effective strategy for controlling the size of λ at each iteration so that it is efficient for a broad range of optimization problems. To overcome the challenge, three approaches will be tested.

In the first approach, two indices will be calculated and compared with each other to estimate the relative nonlinearity of the objective function. The first index is the linear predicted sum of squares (Mathworks, 2006):

$$f_{NR} = (J * \Delta\beta^T + r)^T * (J * \Delta\beta^T + r) \qquad [4.19]$$

The second index is obtained by cubic spline interpolation of the magnitudes of the objective function and their slopes (i.e. $\nabla\phi$) in two consecutive iterations and is called f_{sp}. From the spline interpolation, the search length (α), which is the estimated length to

the minimum, will be calculated. The magnitude of these indices will then be compared

to choose how λ should be updated. If f_{NR} is greater than f_{sp}, then λ is reduced by;

$$\lambda = \frac{\lambda}{1+\alpha} \qquad [4.20]$$

otherwise it is increased by;

$$\lambda = \lambda + \frac{f_{sp} - f_{NR}}{\alpha} \qquad [4.21]$$

The philosophy behind this is that the difference between f_{sp} and f_{NR} is a measure of the

effectiveness of the Gauss-Newton algorithm and the linearity of the problem. These

operations determine whether to use a direction approaching to the steepest descent

direction or the Gauss-Newton direction.

The second approach is starting with a large λ and decreasing it as the magnitude

of the objective function decreases. If in an iteration the function value is greater than in

the previous iteration, then λ is increased and the algorithm repeats the iteration with the

new λ until a considerable reduction in the magnitude of the objective function is

achieved. The algorithm below will be incorporated in the inverse code:

$$\lambda = 1$$
$$if \ \phi(\beta)^{i+1} < \phi(\beta)^{i}$$
$$\lambda = \xi_1 * \lambda$$
$$else$$
$$\lambda = \xi_2 * \lambda$$
$$end \qquad [4.22]$$

where $\xi_1 < 1$ and $\xi_2 > 1$.

The third approach is the *Hessian update method* using the *BFGS algorithm*

(Broyden, 1970; Fletcher 1970; Goldfarb, 1970; Shanno, 1970) to estimate the Hessian in

each iteration. In this algorithm, the optimization starts by choosing a $p \times p$ identity matrix as an initial approximation for the Hessian. The search direction is calculated as follows:

$$A\Delta\beta = -\nabla\phi \qquad \text{[4.23]}$$

where $A = \hat{H}$ is an estimator of the Hessian. Then using line search along $\Delta\beta$ the step length, α, is estimated. Finally using:

$$\beta^{i+1} = \beta^i + \Delta\beta^i \qquad \text{[4.24]}$$

the parameter increment is calculated.

To approximate the Hessian matrix at the next iteration, the BFGS update method will be used:

$$A_{i+1} = A_i + \frac{\gamma_i \gamma_i^T}{\gamma_i \Delta\beta_i^T} - \frac{A_i^T \Delta\beta_i \Delta\beta_i^T A_i}{\Delta\beta_i^T A_i \Delta\beta_i} \qquad \text{[4.25]}$$

where;

$$\begin{aligned} \gamma_i &= \nabla\phi_{i+1} - \nabla\phi_i \\ \Delta\beta_i &= \Delta\beta_{i+1} - \Delta\beta_i \end{aligned} \qquad \text{[4.26]}$$

The iteration process is continued until the termination rule is met.

4.1.4. Termination Criteria for Inverse Code

One of the crucial steps in optimization algorithm is stopping criterion. In this study, several rules will be critically evaluated in order to determine the best termination criteria. The following stopping rules will be tested:

1. Sorooshian *et al.,* (1983) suggested a stopping rule based on the changes in the parameter values at each iteration:

$$if \ \Delta\beta < \delta_1$$
$$\qquad Stop$$
$$else$$
$$\qquad Continue \ Optimization \ Loop$$
$$end \qquad\qquad\qquad\qquad\qquad\qquad\qquad\qquad\qquad [4.27]$$

2. Another criterion is the relative and absolute changes in the magnitude of the objective function in every iteration:

$$if \ \Delta\phi(\beta^{i+1})/\phi(\beta^i) < \delta_2 \ \ \& \ \ \Delta\phi(\beta^i) < \delta_1$$
$$\qquad Stop$$
$$else$$
$$\qquad Continue \ Optimization \ Loop$$
$$end \qquad\qquad\qquad\qquad\qquad\qquad\qquad\qquad\qquad [4.28]$$

3. A third measure of the closeness of the solution to the real minimum is the norm of the gradient of the objective function with respect to the parameters at the solution ($\left\|\nabla\phi(\beta)\right\|_{\beta=\hat{\beta}}$) which should be zero:

$$if \ \left\|\nabla\phi(\beta)\right\|_{\beta=\hat{\beta}} < \delta_1$$
$$\qquad Stop$$
$$else$$
$$\qquad Continue \ Optimization \ Loop$$
$$end \qquad\qquad\qquad\qquad\qquad\qquad\qquad\qquad\qquad [4.29]$$

These criteria will be implemented in the inverse code and will be critically evaluated to select the most efficient stopping rule for the inverse code.

4.2. Parameter Optimization in Biomolecule Transport in Living Cells

Having tested the efficiency of the algorithm, the first application of the strategy will be in the field of molecular biology where the transport of nuclear proteins in the nucleoplasm will be investigated.

4.2.1. Formulation of the Forward Problem

The first optimization problem considered in this study is protein transport in living cells. To fully describe diffusion-reaction inside cell during the course of the FRAP protocol, a system of three coupled non-linear partial differential equations is selected as *forward problem*:

$$\frac{\partial F}{\partial t} = D_{Frr}\frac{\partial^2 F}{\partial r^2} + D_{Frr}\frac{1}{r}\frac{\partial F}{\partial r} + D_{F\theta\theta}\frac{1}{r^2}\frac{\partial^2 F}{\partial \theta^2} + D_{Fzz}\frac{\partial^2 F}{\partial z^2} - K_a FS + K_d C$$

$$\frac{\partial S}{\partial t} = D_{Srr}\frac{\partial^2 S}{\partial r^2} + D_{Srr}\frac{1}{r}\frac{\partial S}{\partial r} + D_{S\theta\theta}\frac{1}{r^2}\frac{\partial^2 S}{\partial \theta^2} + D_{Szz}\frac{\partial^2 S}{\partial z^2} - K_a FS + K_d C \qquad [4.30]$$

$$\frac{\partial C}{\partial t} = D_{Crr}\frac{\partial^2 C}{\partial r^2} + D_{Crr}\frac{1}{r}\frac{\partial C}{\partial r} + D_{C\theta\theta}\frac{1}{r^2}\frac{\partial^2 C}{\partial \theta^2} + D_{Czz}\frac{\partial^2 C}{\partial z^2} + K_a FS - K_d C$$

To develop and solve equation [4.30] the following assumption are made:

1. The medium is isotropic and homogeneous and the axes of the diffusion tensors D_F, D_S, and D_C are parallel to those of the coordinate system. By these assumptions the second-order diffusion tensors collapse to the diffusion coefficients D_F, D_S, and D_C.

2. Two-dimensional diffusion takes place in the plane of focus. This is a legitimate assumption when the bleaching area creates a cylindrical path through the cell which is the case in circular bleach spot with reasonable spot size (Kaufman and Jain, 1990; Sprague et al., 2004). The assumption eliminates the azimuthal and vertical components of the equation.

3. There are no advective velocity fields in the bleached area. Ignoring the convective flux will lead to the overestimation of the diffusion coefficient but in the presence of binding reaction this overestimation is negligible (in other words,

we assume that the Peclet number is less than unity and advection is not dominant).

4. The effects of temperature rise, caused by the absorption of laser by sample and fluorophore, on the macromolecule mass transport and binding parameters are negligible. In other words, we assume isothermal flow of macromolecules toward bleached area form undisturbed regions.

An efficient and accurate solution of the forward problem is crucial to the success of inverse modeling effort. In this study a fully implicit backward in time and central in space finite difference discretization of equation [4.30] in radial direction will be used:

$$
\frac{F_i^{n+1,m+1} - F_i^n}{\Delta t} = D_F \frac{F_{i+1}^{n+1,m+1} - 2F_i^{n+1,m+1} + F_{i-1}^{n+1,m+1}}{(\Delta r)^2} +
$$

$$
\frac{D_F}{r} \frac{F_{i+1}^{n+1,m+1} - F_{i-1}^{n+1,m+1}}{2\Delta r} - K_{asoc} F_i^{n+1,m+1} S_i^{n+1,m+1} + K_{disoc} C_i^{n+1,m+1}
$$

$$
\frac{S_i^{n+1,m+1} - S_i^n}{\Delta t} = D_S \frac{S_{i+1}^{n+1,m+1} - 2S_i^{n+1,m+1} + S_{i-1}^{n+1,m+1}}{(\Delta r)^2} +
$$

$$
\frac{D_S}{r} \frac{S_{i+1}^{n+1,m+1} - S_{i-1}^{n+1,m+1}}{2\Delta r} - K_{asoc} F_i^{n+1,m+1} S_i^{n+1,m+1} + K_{disoc} C_i^{n+1,m+1}
$$

$$
\frac{C_i^{n+1,m+1} - C_i^n}{\Delta t} = D_C \frac{C_{i+1}^{n+1,m+1} - 2C_i^{n+1,m+1} + C_{i-1}^{n+1,m+1}}{(\Delta r)^2} +
$$

$$
\frac{D_C}{r} \frac{C_{i+1}^{n+1,m+1} - C_{i-1}^{n+1,m+1}}{2\Delta r} - K_{asoc} F_i^{n+1,m+1} S_i^{n+1,m+1} + K_{disoc} C_i^{n+1,m+1}
$$

[4.31]

where Δr is node spacing in the cylindrical coordinate system and n and m are the time step and iteration level, respectively. Rearranging equation [4.31] one can obtain the following block tri-diagonal matrix equation:

$$[\frac{D_F\Delta t}{\Delta r}(\frac{1}{2r}-\frac{1}{\Delta r})]F_{i-1}^{n+1,m+1} + [1+\frac{2D_F\Delta t}{(\Delta r)^2}+K_{asoc}\Delta tS_i^*]F_i^{n+1,m+1} -$$

$$[\frac{D_F\Delta t}{\Delta r}(\frac{1}{2r}+\frac{1}{\Delta r})]F_{i+1}^{n+1,m+1} - K_{disoc}C_i^{n+1,m+1} = F_i^n$$

$$[\frac{D_S\Delta t}{\Delta r}(\frac{1}{2r}-\frac{1}{\Delta r})]S_{i-1}^{n+1,m+1} + [1+\frac{2D_S\Delta t}{(\Delta r)^2}]S_i^{n+1,m+1} -$$

$$[\frac{D_S\Delta t}{\Delta r}(\frac{1}{2r}+\frac{1}{\Delta r})]S_{i+1}^{n+1,m+1} + K_{asoc}\Delta tF_i^{n+1,m+1}S^* - K_{disoc}\Delta tC_i^{n+1,m+1} = S_i^n$$

$$[\frac{D_C\Delta t}{\Delta r}(\frac{1}{2r}-\frac{1}{\Delta r})]C_{i-1}^{n+1,m+1} + [1+\frac{2D_C\Delta t}{(\Delta r)^2}+K_{disoc}\Delta t]C_i^{n+1,m+1} -$$

$$[\frac{D_C\Delta t}{\Delta r}(\frac{1}{2r}+\frac{1}{\Delta r})]C_{i+1}^{n+1,m+1} - K_{asoc}\Delta tS_i^*F_i^{n+1,m+1} = C_i^n$$

$$[4.32]$$

By setting coefficients of D_s and D_C in equation [4.32] to zero, one can obtain a solution for the one-site-mobile-immobile model (equation [2.15]) as well. To solve equation [4.32] the following initial and boundary condition will be used:

I.C.:

$$F(0,r) = \begin{cases} 0, 0 < r \le w \\ F_{eq}, w < r \le R \end{cases}$$

$$S(0,r) = S_{eq}$$

$$C(0,r) = \begin{cases} 0, 0 < r \le w \\ C_{eq}, w < r \le R \end{cases}$$

where w is the radius of the bleached area. The initial condition implies that the act of bleaching does not changes the concentrations of free protein, bound complex, and vacant binding sites in the bleached area of the cell, but it only affects the fluorescence tags on the biomolecules by making them invisible to the experiment.

The boundary conditions will be formulated as:

B.C.:

$$\frac{\partial F}{\partial r}\bigg|_{r=0} = \frac{\partial F}{\partial r}\bigg|_{r=R} = 0$$

$$\frac{\partial S}{\partial r}\bigg|_{r=0} = \frac{\partial S}{\partial r}\bigg|_{r=R} = 0$$

$$\frac{\partial C}{\partial r}\bigg|_{r=0} = \frac{\partial C}{\partial r}\bigg|_{r=R} = 0$$

which imply that the diffusive biomolecule flux is zero at the center of the bleach spot and far beyond the bleached area throughout the course of the FRAP experiment. Obviously, for lateral diffusion of lipids, proteins, ions, salt, and water through cell membrane or from cytoplasm to nucleus and vice versa these boundary conditions are not applicable.

The matrix equation of system [4.32] is presented in Figure 4.1. The system of algebraic equations produced by [4.32] is nonlinear because of the interaction term ($K_a FS$). Therefore, the equations must be linearized and solved iteratively. In the present study, the Picard fixed point iteration method will be used to linearize and solve the matrix equation. To decrease the CPU time and maintain small truncation error, an adaptive time step procedure will be used. The iterative procedure and adaptive time step approach will be discussed in 4.3.1.3 and 4.3.1.4.

The solution of equation [4.32] for a parameter vector $\beta = [D_F, D_S, D_C, K_a, K_d]$ and the prescribed initial and boundary conditions, produces spatio-temporal distribution of free protein ($F(\beta,r,t)$), vacant binding sites ($S(\beta,r,t)$), and bound complex ($C(\beta,r,t)$) inside bleached area. In the numerical code, the average of the fluorescent intensity within the bleach spot is calculated by:

$$\overline{\widehat{frap}} = \frac{2}{w^2}\int_0^w r[F(\beta,r,t) + C(\beta,r,t)]dr \qquad [4.33]$$

$$
\begin{bmatrix}
\alpha_1 & 0 & 0 & \beta_1 & 0 & -Koff\,\Delta t & \gamma_1 & 0 & 0 & 0 & 0 & 0 & 0 & 0 & 0 \\
0 & \alpha_2 & 0 & KonS^*\Delta t & \beta_2 & -Koff\,\Delta t & 0 & \gamma_2 & 0 & 0 & 0 & 0 & 0 & 0 & 0 \\
0 & 0 & \alpha_3 & -KonS^*\Delta t & 0 & \beta_3 & 0 & 0 & \gamma_3 & 0 & 0 & 0 & 0 & 0 & 0 \\
0 & 0 & 0 & \alpha_1 & 0 & 0 & \beta_1 & 0 & -Koff\,\Delta t & \gamma_1 & 0 & 0 & 0 & 0 & 0 \\
0 & 0 & 0 & 0 & \alpha_2 & 0 & KonS^*\Delta t & \beta_2 & -Koff\,\Delta t & 0 & \gamma_2 & 0 & 0 & 0 & 0 \\
0 & 0 & 0 & 0 & 0 & \alpha_3 & -KonS^*\Delta t & 0 & \beta_3 & 0 & 0 & \gamma_3 & 0 & 0 & 0 \\
0 & 0 & 0 & 0 & 0 & 0 & \alpha_1 & 0 & 0 & \beta_1 & 0 & -Koff\,\Delta t & \gamma_1 & 0 & 0 \\
0 & 0 & 0 & 0 & 0 & 0 & 0 & \alpha_2 & 0 & KonS^*\Delta t & \beta_2 & -Koff\,\Delta t & 0 & \gamma_2 & 0 \\
0 & 0 & 0 & 0 & 0 & 0 & 0 & 0 & \alpha_3 & -KonS^*\Delta t & 0 & \beta_3 & 0 & 0 & \gamma_3 \\
0 & 0 & 0 & 0 & 0 & 0 & 0 & 0 & 0 & \alpha_1 & 0 & 0 & \beta_1 & 0 & -Koff\,\Delta t \\
0 & 0 & 0 & 0 & 0 & 0 & 0 & 0 & 0 & 0 & \alpha_2 & 0 & KonS^*\Delta t & \beta_2 & -Koff\,\Delta t \\
0 & 0 & 0 & 0 & 0 & 0 & 0 & 0 & 0 & 0 & 0 & \alpha_3 & -KonS^*\Delta t & 0 & \beta_3 \\
0 & 0 & 0 & 0 & 0 & 0 & 0 & 0 & 0 & 0 & 0 & 0 & \alpha_1 & 0 & 0 \\
0 & 0 & 0 & 0 & 0 & 0 & 0 & 0 & 0 & 0 & 0 & 0 & 0 & \alpha_2 & 0 \\
0 & 0 & 0 & 0 & 0 & 0 & 0 & 0 & 0 & 0 & 0 & 0 & 0 & 0 & \alpha_3
\end{bmatrix}
\begin{bmatrix}
F_1 \\ S_1 \\ C_1 \\ F_2 \\ S_2 \\ C_2 \\ . \\ . \\ . \\ F_{N-1} \\ S_{N-1} \\ C_{N-1} \\ F_N \\ S_N \\ C_N
\end{bmatrix}^{n+1}
=
\begin{bmatrix}
F_1 \\ S_1 \\ C_1 \\ F_2 \\ S_2 \\ C_2 \\ . \\ . \\ . \\ F_{N-1} \\ S_{N-1} \\ C_{N-1} \\ F_N \\ S_N \\ C_N
\end{bmatrix}^{n}
$$

$$\alpha_1 = \frac{D_F \Delta t}{\Delta r}\left(\frac{1}{2r} - \frac{1}{\Delta r}\right) \qquad\qquad \alpha_2 = \frac{D_S \Delta t}{\Delta r}\left(\frac{1}{2r} - \frac{1}{\Delta r}\right) \qquad\qquad \alpha_3 = \frac{D_C \Delta t}{\Delta r}\left(\frac{1}{2r} - \frac{1}{\Delta r}\right)$$

$$\beta_1 = 1 + \frac{2D_F \Delta t}{(\Delta r)^2} + K_{asoc}\Delta t\,S_i^* \qquad\qquad \beta_2 = 1 + \frac{2D_S \Delta t}{(\Delta r)^2} \qquad\qquad \beta_3 = 1 + \frac{2D_C \Delta t}{(\Delta r)^2} + K_{off}\Delta t$$

$$\gamma_1 = -\frac{D_F \Delta t}{\Delta r}\left(\frac{1}{2r} + \frac{1}{\Delta r}\right) \qquad\qquad \gamma_2 = -\frac{D_S \Delta t}{\Delta r}\left(\frac{1}{2r} + \frac{1}{\Delta r}\right) \qquad\qquad \gamma_3 = -\frac{D_C \Delta t}{\Delta r}\left(\frac{1}{2r} + \frac{1}{\Delta r}\right)$$

Figure 4.1. Matrix equation of system [4.30] discretized by finite difference method.

where $\overline{\hat{frap}}$ is the model predicted average of the fluorescent intensity within the bleach spot.

The accuracy of the numerical simulator will be validated with analytical solution. To validate the numerical model with the analytical solution, the values of $D_c = 0$, $D_s = 0$ will be used, which deletes the second partial differential equation from equation [4.32] and reduces it to the one-site-mobile-immobile equation. To obtain $\overline{frap}$ in semi-analytical solution of Sprague *et al.,* (2004), the MATLAB routine *invlap.m* (Hollenbeck, 1998) will be used to calculate the inverse Laplace transform numerically.

4.2.2. Formulation of the Inverse Problem: Optimization Scenarios

The developed optimization algorithm along with the verified numerical simulator of the forward problem, in the framework of the inverse modeling strategy, will be used to simulate transport of GFP-tagged protein inside nucleus of living cell for five optimization scenarios described below. Assuming that experimental FRAP, $I(t_i)$, can be obtained independently for any time step, t_i, the FRAP data will be used for the nonlinear optimization procedure. Let $I(\beta, t_i)$ be the numerically estimated values of $I(t_i)$ for any time step (i.e. values obtained by solution of Eq. [4.32]) corresponding to a trial vector of parameter values $\beta = [D_f, K_a, K_d, D_s, D_c]$. The inverse problem then is to find an optimum combination of parameters that minimizes the objective function:

$$\phi(\beta) = \sum_{i=1}^{N}[I(t_i) - I(t_i, \beta)]^2 \qquad [4.34]$$

where w_i is a weighting function typically given a value other than unity only if prior

63

information suggests giving unequal relative importance to each experimental data point.

To determine the mass transport and binding rate parameters of the GFP-tagged glucocorticoid receptor (which is a transcription factor), three data sets will be used:

1. A FRAP experiment data which was conducted on the mouse adenocarcinoma cell line 3617 by Sprague *et al.*, (2004) and presented in Table 4.1. This data set consists of 43 fluorescent recovery values gathered in the course of a 20-second FRAP experiment and post processed to remove noise.

2. A generated data set will be obtained by solving Eq. [4.32] for a hypothetical cell with prescribed initial and boundary conditions and parameter values: $D_f = 30 \mu m^2 s^{-1}$, $D_S = 0 \mu m^2 s^{-1}$, $D_C = 0 \mu m^2 s^{-1}$, $K_a^* = 30 s^{-1}$, $K_d = 0.1108 s^{-1}$, and $w = 0.5 \mu m$. Predicted FRAP recovery values will then be sampled at discrete times for bleach spot radius (i.e; $w = 0.5 \mu m$). The data will be corrupted by adding $N(0, 0.01)$ error term to each "measurement". They will then be used as input for parameter optimization problem and well-posedness analysis of the inverse problem.

3. The third data set is similar to the second one but without perturbation. The data will be used to determine what can and what cannot be identified using the FRAP data.

The five application scenarios are as follow. In scenario A, the developed inverse modeling strategy will be used to identify five unknown parameters $[D_f, K_a, K_d, D_s, D_c]$ for GFP-GR using the real FRAP data. Statistical assessment of the estimation will be carried out by analyzing the goodness-of-fit indices. In scenario B the real FRAP data will be used to identify mass transport (D_f) and reaction rate parameters

Table 4.1. Experimental data for GFP-tagged glucocorticoid receptor (GFP-GR) in the nucleoplasm of mouse adenocarcinoma cell line 3617 (data from Sprague *et al.* 2004).

Time (second)	Recovery (%)	Time (second)	Recovery (%)	Time (second)	Recovery (%)
0.0090	0.0574	0.6000	0.7438	9.4280	0.9724
0.0490	0.2230	0.6400	0.6946	10.2160	0.9748
0.0880	0.2988	0.6790	0.7363	11.0050	0.9845
0.1280	0.4216	0.7190	0.7055	11.7930	0.9696
0.1670	0.4536	0.7580	0.7750	12.5810	0.9799
0.2060	0.4970	1.5460	0.8423	13.3690	0.9804
0.2460	0.4989	2.3350	0.8988	14.1570	0.9802
0.2850	0.5300	3.1230	0.9226	14.9460	0.9907
0.3250	0.5977	3.9110	0.9365	15.7340	0.9635
0.3640	0.6850	4.6990	0.9471	16.5220	0.9800
0.4030	0.5796	5.4870	0.9347	17.3100	0.9843
0.4430	0.6828	6.2750	0.9460	18.0980	0.9768
0.4820	0.6568	7.0640	0.9526	18.8870	0.9878
0.5220	0.6715	7.8520	0.9538		
0.5610	0.7314	8.6400	0.9540		

(K_a^* and K_a) for GFP-GR in one-site-mobile-immobile model (Eq. [2.15]). To test the well-posedness of the inverse problem, the optimization will be carried out using different initial guesses for the parameter vector ($\beta = [D_f, K_a^*, K_d]$). In scenario C, two of the three parameters in one-site-mobile-immobile model will be kept constant and the third parameter will be estimated using the strategy. The goal is to determine whether or not the FRAP protocol produce enough information to uniquely estimate one parameter. The optimization algorithm will be used to estimate a single parameter for both noise free and noisy data. In scenario D, pairs of model parameters, under the assumption that the value of the third parameter is known, will be estimated. In the first attempt, the

optimized values of the individual binding rate coefficients will be determined given a known value of the free molecular diffusion coefficient of the GFP-GR. Again the optimization algorithm will be used for both noise free and noisy data. Then, given the value of the pseudo-association rate, the optimized values of the molecular diffusion coefficient and dissociation rate constant will be estimated. Finally, we'll assume that the "true" value of the dissociation coefficient is known and will try to estimate the optimized values of the free molecular diffusion coefficient and the pseudo-association rate parameter. Again, the goal is to determine which pairs of parameters, if any, can be uniquely estimated using the FRAP data. Finally, in scenario E, three parameters of the one-site-mobile-immobile model will be identified for noise free FRAP data.

4.3. Parameter Optimization in Water Flow through Partially Saturated Porous Media

The second optimization problem considered in this study is water flow through porous media. Since developing robust and efficient algorithm to solve the flow equations is crucial in the parameter identification in flow and transport phenomena in saturated-unsaturated porous media, therefore, all forms of the Richards' equations will be solved using both the finite element and finite differences methods and their performances will be compared with each other and with the "exact solution". The most efficient, accurate, and mass-conservative formulation will be implemented in the inverse code to perform parameter optimization in two field scale drainage experiments.

4.3.1. Formulation of the Forward Problem

The h-based form and the mixed form Richards' equation will be selected as the direct problem in parameter identification in water flow through variably saturated porous

media:

The h-based form:

$$C(h)\frac{\partial h}{\partial t} - \nabla.K(h)\nabla h + \frac{\partial K}{\partial z} = 0 \qquad\qquad [2.3]$$

The mixed form:

$$\frac{\partial \theta}{\partial t} - \nabla.K(h)\nabla h + \frac{\partial K}{\partial z} = 0 \qquad\qquad [2.1]$$

These partial differential equations will be solved using the finite element and finite difference approximations which are discussed next. The mass conservation properties of the numerical simulators, nodal fluxes, adaptive time step, and iterative procedures are also presented below.

4.3.1.1. Finite Element Approximation of Flow Equations

4.3.1.1.1. h-based Richards' Equation

The first step in solving the h-based form flow equation by finite element method is to divide the domain into number of sub-domains called "elements". Then the weak formulation of the dependent variable, h, is developed using an interpolating polynomial (with global numbering of nodes):

$$h(z,t) \cong \hat{h}(z,t) = \sum_{j=1}^{N_e} H_j(t)\phi_j(z) \qquad\qquad [4.35]$$

where N_e is number of elements, $\phi_j(z)$ is the selected basis function, and $H_j(t)$ is the associated and time-dependent unknown coefficients that represent the solution of flow equation at nodes within the domain. Substituting Eq. [4.35] into the weak formulation of Eq. [2.3] will not satisfy the partial differential equation and hence will produce a

residual (when N_e approaches infinity the approximate solution, $\hat{h}(z,t)$, converges to the exact solution). The goal in finite element approximation is to minimize this error. This can be accomplished by introducing the weight function, $\phi_i(z)$, and setting the integral of the weighted residuals to zero. In other words, the residuals can be minimized by requiring that $L(\hat{h})$ (See Eq. [4.36]) be orthogonal to the weighting functions. In Galerkin method, which is used in this study, the weighting functions are chosen to be identical to the basis function (Pinder and Gray, 1977; Huyakorn and Pinder, 1983). The piecewise linear Lagrange polynomial (depicted in Figure 4.2) is chosen as the basis and weight functions:

$$\int_\Omega L(\hat{h})d\Omega = \int_0^{\Delta z} [\hat{C}\frac{\partial \hat{h}}{\partial t} - \frac{\partial}{\partial z}[\hat{K}\frac{\partial \hat{h}}{\partial z}] + \frac{\partial \hat{K}}{\partial z}]\phi_i(z)dz = 0 \qquad [4.36]$$

where Δz is node spacing, and $\hat{h}$, $\hat{K}$, and $\hat{C}$ are approximations for h, K, and C, respectively. Since there are two nodes in every element, one may develop the following approximations within every element (with local numbering of nodes):

$$\hat{h}(z) = \sum_{l=1}^{2} h_l \phi_l(z)$$

$$\hat{K}(z) = \sum_{l=1}^{2} K_l \phi_l(z) \qquad [4.37]$$

$$\hat{C}(z) = \sum_{l=1}^{2} C_l \phi_l(z)$$

Performing integration by parts (Green's theorem), one can reduce the second order derivative in Eq. [2.36]:

$$\int_0^{\Delta z} \hat{C}\frac{\partial \hat{h}}{\partial t}\phi_i(z)dz - \hat{K}\phi_i(z)\frac{\partial \hat{h}}{\partial z}\Big|_0^{\Delta z} + \int_0^{\Delta z} \frac{\partial \hat{h}}{\partial z}\hat{K}\frac{\partial \phi_i(z)}{\partial z}dz + \int_0^{\Delta z} \frac{\partial \hat{K}}{\partial z}\phi_i(z)dz = 0 \quad [4.38]$$

68
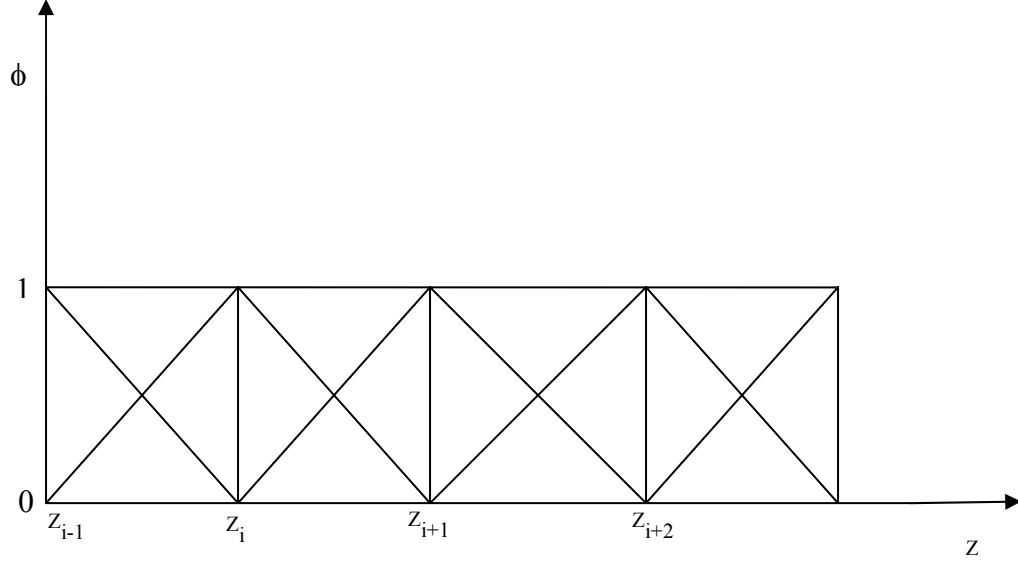
Figure 4.2. Schematic representation of the piecewise linear Lagrange polynomials.

The second term in the equation is only evaluated for the boundaries and therefore is eliminated for the internal nodes. Treatment of the boundary conditions in finite element will be discussed later in this section. The following derivations are only for the internal nodes. Eliminating the second term and substituting Eq. [4.37] into Eq. [4.38] yields:

$$\int_0^{\Delta z} \hat{C} \frac{\partial}{\partial t} [\sum_{j=1}^{N_e} H_j(t)\phi_j(z)]\phi_i(z)dz + \int_0^{\Delta z} \frac{\partial}{\partial z}[\sum_{j=1}^{N_e} H_j(t)\phi_j(z)]\hat{K}\frac{\partial \phi_i(z)}{\partial z}dz + \int_0^{\Delta z} \frac{\partial \hat{K}}{\partial z}\phi_i(z)dz = 0$$

[4.39]

Since we integrate over z, terms that are a function of time only come out of the integral:

$$\sum_{j=1}^{N_e} \frac{\partial H_j(t)}{\partial t}\int_0^{\Delta z} \hat{C}\phi_i(z)\phi_j(z)dz + \sum_{j=1}^{N_e} H_j(t)\int_0^{\Delta z} \hat{K}\frac{\partial \phi_i(z)}{\partial z}\frac{\partial \phi_j(z)}{\partial z}dz + \int_0^{\Delta z} \frac{\partial \hat{K}}{\partial z}\phi_i(z)dz = 0$$

[4.40]

69

Equation [4.40] is generally written in matrix form:

$$[A]\{H\}+[B]\{\frac{dH}{dt}\}=\{F\}$$ [4.41]

Where:

$$[A]=\int_0^L \hat{K}\frac{\partial \phi_i(z)}{\partial z}\frac{\partial \phi_j(z)}{\partial z}dz$$

$$[B]=\int_0^L [\hat{C}\phi_i(z)\phi_j(z)dz$$

$$\{F\}=-\int_0^L \frac{\partial \hat{K}}{\partial z}\phi_i(z)dz$$ [4.42]

Using fully implicit backward Euler time-marching algorithm, one can discretize the time derivative in equation [4.41] as:

$$[A]\{H_j\}^{n+1,m}+[B]\{\frac{H_j^{n+1,m}-H_j^n}{\Delta t}\}=\{F\}$$ [4.43]

where j represents location in space and n and m denote time and iteration levels, respectively. This equation generates system of N nonlinear algebraic equations which should be solved iteratively. Detailed evaluation of the integrals in Eq. [4.42] and assembly of the stiffness mass and global matrices are given in appendix A.

Upon substituting these matrices in Eq. [4.43] the resulting finite element approximation for $h-$ based Richards' equation is:

$$[(C_{i-1}^{n+1,m}+C_i^{n+1,m})\frac{\Delta z}{12\Delta t}+\frac{(K_{i-1}^{n+1,m}+K_i^{n+1,m})}{2\Delta z}]h_{i-1}^{n+1,m+1}$$

$$+[(C_{i-1}^{n+1,m}+6C_i^{n+1,m}+C_{i+1}^{n+1,m})\frac{\Delta z}{12\Delta t}+\frac{(K_{i-1}^{n+1,m}+2K_i^{n+1,m}+K_{i+1}^{n+1,m})}{2\Delta z}]h_i^{n+1,m+1}$$

$$+[(C_i^{n+1,m}+C_{i+1}^{n+1,m})\frac{\Delta z}{12\Delta t}+\frac{(K_i^{n+1,m}+K_{i+1}^{n+1,m})}{2\Delta z}]h_{i+1}^{n+1,m+1}=$$

$$[(C_{i-1}^{n+1,m}+6C_i^{n+1,m}+C_{i+1}^{n+1,m})\frac{\Delta z}{12\Delta t}]h_i^n-\frac{K_{i+1}^{n+1,m}-K_{i-1}^{n+1,m}}{2}$$

[4.44]

4.3.1.1.2. Mixed-form Richards' Equation

To develop finite element approximation of the "mixed form" Richards' equation one needs to discretize the time derivative of equation [2.1] by finite difference scheme:

$$\frac{\theta_i^{n+1,m+1} - \theta_i^n}{\Delta t} = \frac{\partial}{\partial z}[K_i^{n+1,m} \frac{\partial h_i^{n+1,m+1}}{\partial z}] - \frac{\partial K_i^{n+1,m}}{\partial z} \qquad [4.45]$$

The moisture content at the new time and iteration level can be substituted by the following Taylor series expansions in which $\theta_i^{n+1,m+1}$ is expanded with respect to h about the expansion point $h_i^{n+1,m}$ (Celia *et al.,* 1990):

$$\theta_i^{n+1,m+1} = \theta_i^{n+1,m} + \frac{d\theta_i^{n+1,m}}{dh}(h_i^{n+1,m+1} - h_i^{n+1,m}) + ... \qquad [4.46]$$

Ignoring the higher order terms and substituting equation [4.46] into Eq. [4.45] yields:

$$\frac{\theta_i^{n+1,m} + \frac{d\theta_i^{n+1,m}}{dh}(h_i^{n+1,m+1} - h_i^{n+1,m}) - \theta_i^n}{\Delta t} = \frac{\partial}{\partial z}[K_i^{n+1,m} \frac{\partial h_i^{n+1,m+1}}{\partial z}] - \frac{\partial K_i^{n+1,m}}{\partial z} \qquad [4.47]$$

Inserting the interpolating polynomial:

$$\theta(z,t) \square \hat{\theta}(z,t) = \sum_{j=1}^{N_e} \theta_j(t)\phi_j(z) \qquad [4.48]$$

and Eqs. [4.37] into Eq. [4.47] and performing integration by parts to reduce the second derivative yields:

$$\sum_{j=1}^{N_e} \frac{\theta_j^{n+1,m} - \theta_j^n}{\Delta t}\int_0^L \phi_i(z)\phi_j(z)dz + \sum_{j=1}^{N_e} \frac{h_j^{n+1,m+1}}{\Delta t}\int_0^L \hat{C}\phi_i(z)\phi_j(z)dz + \int_0^L \frac{\partial \hat{K}}{\partial z}\phi_i(z)dz$$

$$+\sum_{j=1}^{N_e} h_j^{n+1,m}\int_0^L \hat{K}\frac{\partial \phi_i(z)}{\partial z}\frac{\partial \phi_j(z)}{\partial z}dz + \sum_{j=1}^{N_e} \frac{h_j^{n+1,m}}{\Delta t}\int_0^L \hat{C}\phi_i(z)\phi_j(z)dz + \hat{K}\phi_i(z)\frac{\partial \hat{h}}{\partial z}\Big|_0^L = 0$$

$$[4.49]$$

For Dirichlet boundary condition the last term in equation [4.49] can be neglected but it must be included in the equation for Neumann condition. Finally, inserting Eq. [4.42] into equation [4.49] and assembling the global matrices, the finite element approximation of the mixed form Richards' equation can be developed as:

$$[(C_{i-1}^{n+1,m} + C_i^{n+1,m})\frac{\Delta z}{12\Delta t} + \frac{(K_{i-1}^{n+1,m} + K_i^{n+1,m})}{2\Delta z}]h_{i-1}^{n+1,m+1}$$

$$+[(C_{i-1}^{n+1,m} + 6C_i^{n+1,m} + C_{i+1}^{n+1,m})\frac{\Delta z}{12\Delta t} + \frac{(K_{i-1}^{n+1,m} + 2K_i^{n+1,m} + K_{i+1}^{n+1,m})}{2\Delta z}]h_i^{n+1,m+1}$$

$$+[(C_i^{n+1,m} + C_{i+1}^{n+1,m})\frac{\Delta z}{12\Delta t} + \frac{(K_i^{n+1,m} + K_{i+1}^{n+1,m})}{2\Delta z}]h_{i+1}^{n+1,m+1} =$$

$$[(C_{i-1}^{n+1,m} + 6C_i^{n+1,m} + C_{i+1}^{n+1,m})\frac{\Delta z}{12\Delta t}]h_i^{n,m} - [(\theta_{i-1}^{n+1,m} + 4\theta_i^{n+1,m} + \theta_{i+1}^{n+1,m})\frac{\Delta z}{6\Delta t}]$$

$$+[(\theta_{i-1}^n + 4\theta_i^n + \theta_{i+1}^n)\frac{\Delta z}{6\Delta t}] - \frac{K_{i+1}^{n+1,m} - K_{i-1}^{n+1,m}}{2}$$

[4.50]

where the pressure head, h, is the primary variable not the soil moisture content, θ. Comparing equations [4.44] and [4.50] reveals that the second and third terms in the right hand side of equation [4.50], which treat time derivative term of the Richards' equation, are the only differences between the h-based form and the mixed form Richards' equations.

4.3.1.1.3. Implementation of Boundary Conditions

Two types of boundary conditions will be studied in modeling water flow in saturated-unsaturated soils. The first kind is the Dirichlet boundary condition which is constant pressure head or water content at the inlet. Because we take z direction being positive downward, the nodes are numbered from top of the soil ground to the bottom, where node N is located. One notes that any one-dimensional finite element or finite difference

discretization of flow equations (using fully implicit Euler backward time discretization) generate the following matrix equation:

$$\begin{pmatrix} a_{1,1} & a_{1,2} & 0 & \cdots & & 0 \\ a_{2,1} & a_{2,2} & a_{2,3} & & & \cdot \\ \cdot & \cdot & \cdot & \cdot & & \cdot \\ \cdot & \cdot & a_{N-1,N-2} & a_{N-1,N-1} & a_{N-1,N} & \cdot \\ 0 & 0 & \cdots\cdots & & a_{N,N-1} & a_{N,N} \end{pmatrix} \begin{bmatrix} h_1 \\ \cdot \\ \cdot \\ \cdot \\ h_N \end{bmatrix}^{n+1,m+1} = \begin{bmatrix} b_1 \\ \cdot \\ b_i \\ \cdot \\ b_N \end{bmatrix} \begin{bmatrix} h_1 \\ \cdot \\ \cdot \\ \cdot \\ h_N \end{bmatrix}^{n,m}$$ [4.51]

Where $a_{i,j}$ and b_i represent any element of the tridiagonal matrix $[A]$ and known vector of coefficient $\{B\}$.

If Dirichlet boundary condition is applied at the top of the domain:

$$h(0,t) = h_0$$ [4.52]

Then the entries of the matrices will be:

$a_{1,1} = 1$
$a_{1,2} = 0$
$b_1 = h_0$

If it is applied at the bottom of the soil, the entries will be:

$a_{N,N} = 1$
$a_{N,N-1} = 0$
$b_{N-1} = 0$
$b_N = h_L$

For flux boundary condition at the soil surface:

$$\left[-K(h)\frac{\partial h}{\partial z} + K(h)\right]\Bigg|_{z=0} = q_0(t)$$ [4.53a]

or in term of pressure head gradient:

$$\frac{\partial h}{\partial z}\Bigg|_{z=0} = 1 - \frac{q_0(t)}{K(h)}$$ [4.53b]

for h-based equation one may write:

$$a_{1,1} = \frac{\Delta z}{12\Delta t}(3C_1 + C_2) - \frac{1}{2\Delta z}(K_1 + K_2)$$

$$a_{1,2} = \frac{\Delta z}{12\Delta t}(C_1 + C_2) + \frac{1}{2\Delta z}(K_1 + K_2)$$

$$b_1 = -[(C_1 + C_2)\frac{\Delta z}{12\Delta t} + \frac{K_1 + K_2}{2\Delta z}] * h_2^{n+1,m} - [(3C_1 + C_2)\frac{\Delta z}{12\Delta t} - \frac{K_1 + K_2}{2\Delta z}] * h_1^{n+1,m}$$

$$+[(C_1 + C_2)\frac{\Delta z}{12\Delta t}] * h_2^n + [(3C_1 + C_2)\frac{\Delta z}{12\Delta t}] * h_1^n + \frac{K_1 + K_2}{2} - \frac{q_0(t)}{\Delta z}$$

For the mixed form equation, the entries $a_{1,1}$ and $a_{1,2}$ are the same as the h-based

form but b is different:

$$b_1 = -[\frac{K_1 + K_2}{2\Delta z}] * h_2^{n+1,m} + [\frac{K_1 + K_2}{2\Delta z}] * h_1^{n+1,m} + (\theta_2^n - \theta_2^{n+1,m} + 1)\frac{\Delta z}{6\Delta t}$$

$$+(\theta_1^n - \theta_1^{n+1,m})\frac{\Delta z}{3\Delta t} + \frac{K_1 + K_2}{2} - \frac{q_0(t)}{\Delta z}$$

If flux boundary condition is applied at the bottom of the soil:

$$[-K(h)\frac{\partial h}{\partial z} + K(h)]\Big|_{z=L} = q_L(t) \tag{4.53c}$$

or in term of pressure gradient:

$$\frac{\partial h}{\partial z}\Big|_{z=L} = 1 - \frac{q_L(t)}{K(h)} \tag{4.53d}$$

the entries of the matrices will be:

$$a_{N,N} = \frac{\Delta z}{12\Delta t}(3C_N + C_{N-1}) - \frac{1}{2\Delta z}(K_{N-1} + K_N)$$

$$a_{N,N-1} = \frac{\Delta z}{12\Delta t}(C_{N-1} + C_N) + \frac{1}{2\Delta z}(K_{N-1} + K_N)$$

$$b_1 = -[(C_{N-1} + C_N)\frac{\Delta z}{12\Delta t} + \frac{K_{N-1} + K_N}{2\Delta z}] * h_{N-1}^{n+1,m} - [(3C_N + C_{N-1})\frac{\Delta z}{12\Delta t} - \frac{K_{N-1} + K_N}{2\Delta z}] * h_N^{n+1,m}$$

$$+[(C_{N-1} + C_N)\frac{\Delta z}{12\Delta t}] * h_{N-1}^n + [(3C_N + C_{N-1})\frac{\Delta z}{12\Delta t}] * h_N^n - \frac{1}{2}(K_{N-1} + K_N) - \frac{q_L(t)}{\Delta z}$$

74

Again for mixed form the entries $a_{1,1}$ and $a_{1,2}$ are the same as the h-based form but b is different:

$$b_1 = -[\frac{K_{N-1}+K_N}{2\Delta z}]*h_{N-1}^{n+1,m} +[\frac{K_{N-1}+K_N}{2\Delta z}]*h_N^{n+1,m} + (\theta_{N-1}^n - \theta_{N-1}^{n+1,m}+1)\frac{\Delta z}{6\Delta t}$$

$$+(\theta_N^n - \theta_N^{n+1,m})\frac{\Delta z}{3\Delta t} + \frac{K_{N+1}+K_N}{2} - \frac{q_L(t)}{\Delta z}$$

If free drainage boundary condition imposed at the bottom of the domain, the

boundary condition is:

$$\left.\frac{\partial h}{\partial z}\right|_{z=L} = 0 \tag{4.53e}$$

where $q_0(t)$ and $q_L(t)$ are the imposed upper and lower fluid fluxes.

4.3.1.1.4. Mass Lumping in Finite Element Method

To overcome possible oscillatory behavior and convergence problem in equations [4.44]

and [4.50], the "mass lumping" approach will be used. The matrix obtained by mass

lumping is called the "lumped mass matrix". Mass-lumping can be performed by defining

the nodal values of the time derivative as weighted averages over the entire flow region

(van Genuchten, 1978):

$$\int_0^L C\frac{\partial h}{\partial t}\phi_i(z)dz = \frac{\partial H_i}{\partial t}\int_0^L C\phi_i(z)dz \tag{4.54}$$

Application of this expression will generate another mass matrix. For linear basis

function the matrix is:

$$[B] = \frac{\Delta z}{6}\begin{pmatrix} 2C_1 & 0 & 0 & ... & 0 \\ 0 & C_1+4C_2+C_3 & 0 & & . \\ . & . & . & . & . \\ . & . & . & C_{N-2}+4C_{N-1}+C_N & 0 \\ 0 & 0 & .... & .... & C_{N-1}+2C_N \end{pmatrix}$$

Comparing this matrix with the distributed mass matrix, shows that the diagonal elements of the "lumped" matrix are identical to the row sums of the entries of the distributed matrix. The linear finite element may be further simplified by redefining the lumped mass matrix to yield (van Genuchten, 1978):

$$[B] = \Delta z \begin{pmatrix} \dfrac{C_1}{2} & 0 & \text{....} & \text{...} & 0 \\ 0 & C_2 & \text{....} & \text{......} & . \\ . & . & . & . & . \\ . & . & . & C_{N-1} & 0 \\ 0 & 0 & \text{.....} & . & \dfrac{C_N}{2} \end{pmatrix}$$

which is a finite difference scheme.

4.3.1.2. Finite Difference Approximation of Flow Equations

The first step in solution of any differential equations by finite difference scheme is discretization of the time and space domains as well as equations. There are several differences between finite element and finite difference approximations, the most noticeable being that in finite difference methods domains and equation are discretized over points and the solution is defined only at these points where in finite element methods patches or contiguous regions are used to discretize the spatial domain and solution is obtained over the entire flow domain. The other difference is that the finite difference is based on the Taylor series expansion while finite element emanates from localized polynomial expansions and error minimization principles.

4.3.1.2.1. h-based Richards' Equation

Using Taylor series expansion one may discretize equation [2.3] as:

$$\left[\frac{C_i^{n+1,m} - C_i^n}{2}\right]\frac{h_i^{n+1,m+1} - h_i^n}{\Delta t} = \frac{f}{\Delta z}\left[K_{i+1/2}^{n+1,m}\left(\frac{h_{i+1}^{n+1,m+1} - h_i^{n+1,m+1}}{\Delta z}\right) - \right.$$
$$\left. K_{i-1/2}^{n+1,m}\left(\frac{h_i^{n+1,m+1} - h_{i-1}^{n+1,m+1}}{\Delta z}\right)\right] - f\left(\frac{K_{i+1}^{n+1,m} - K_{i-1}^{n+1,m}}{2\Delta z}\right) +$$
$$\frac{(1-f)}{\Delta z}\left[K_{i+1/2}^n\left(\frac{h_{i+1}^n - h_i^n}{\Delta z}\right) - K_{i-1/2}^n\left(\frac{h_i^n - h_{i-1}^n}{\Delta z}\right)\right] - (1-f)\left(\frac{K_{i+1}^n - K_{i-1}^n}{2\Delta z}\right)$$

[4.55]

where f is weighing factor and subscript i indicates the position in the finite difference mesh and like the finite element approximations, superscripts n and m represent time step and iteration level, respectively. $f = 0$ produces the explicit approximation, $f = 1$ yields the fully implicit approximation, $f = 0.5$ results in time centered or semi-implicit or Crank-Nicolson approximation. Values in-between produce intermediate forms, particularly $f = 2/3$ is equivalent to using linear finite element to approximate time domain and is quite well studied in solving diffusion problems.

Rearranging equation [4.55] yields the following tridiagonal matrix equation:

$$\left[\frac{-f}{(\Delta z)^2} K_{i-1/2}^{n+1,m}\right]h_{i-1}^{n+1,m+1} + \left[\frac{C_i^{n+1,m} - C_i^n}{2\Delta t} + \frac{f}{(\Delta z)^2}(K_{i-1/2}^{n+1,m} + K_{i+1/2}^{n+1,m}\right]h_i^{n+1,m+1}$$
$$+\left[\frac{-f}{(\Delta z)^2} K_{i+1/2}^{n+1,m}\right]h_{i+1}^{n+1,m+1} + f\left(\frac{K_{i+1}^{n+1,m} - K_{i-1}^{n+1,m}}{2\Delta z}\right) = \left[\frac{(1-f)}{(\Delta z)^2} K_{i-1/2}^{n,m}\right]h_{i-1}^{n,m} +$$
$$\left[\frac{C_i^{n+1,m} - C_i^n}{2\Delta t} - \frac{(1-f)}{(\Delta z)^2}(K_{i-1/2}^{n,m} + K_{i+1/2}^{n,m}\right]h_i^{n,m} + \left[\frac{(1-f)}{(\Delta z)^2} K_{i+1/2}^{n,m}\right]h_{i+1}^{n,m} - (1-f)\left(\frac{K_{i+1}^{n,m} - K_{i-1}^{n,m}}{2\Delta z}\right)$$

[4.56]

Node spacing, Δz, is assumed to be constant. Since adaptive time step will be used, the time domain discretization will not be $t^n = n\Delta t$, instead it will be $t^n = \Delta t_1 + \Delta t_2 + ... + \Delta t_n$.

The hydraulic conductivity function will be evaluated half way between adjacent node points, in other words the block centered approach will be used. This can be

accomplished in one of two ways:

$$K_{i\pm1/2} = K(\frac{h_i + h_{i\pm1}}{2})$$

[4.57a]

or;

$$K_{i\pm1/2} = \frac{K(h_i) + K(h_{i\pm1})}{2}$$

[4.57b]

Zarba (1989) has shown that the later form produces more accurate approximation of $K_{i\pm1/2}$. Therefore, in this study the later form is used.

4.3.1.2.2. Mixed-form Richards' Equation

Similar to the finite element approximation of the mixed form Richards' equation, using Taylor series expansion and the modified Picard approach one can discretize equation [2.1] in one-dimension as follow:

$$\frac{\theta_i^{n+1,m} + \frac{d\theta_i^{n+1,m}}{dh}(h_i^{n+1,m+1} - h_i^{n+1,m}) - \theta_i^n}{\Delta t} = \frac{f}{\Delta z}\{K_{i+1/2}^{n+1,m}(\frac{h_{i+1}^{n+1,m+1} - h_i^{n+1,m+1}}{\Delta z}) -$$

$$K_{i-1/2}^{n+1,m}(\frac{h_i^{n+1,m+1} - h_{i-1}^{n+1,m+1}}{\Delta z})\} + \frac{(1-f)}{\Delta z}\{K_{i+1/2}^n(\frac{h_{i+1}^{n,m} - h_i^{n,m}}{\Delta z}) - K_{i-1/2}^n(\frac{h_i^{n,m} - h_{i-1}^{n,m}}{\Delta z})\}$$

$$-f(\frac{K_{i+1}^{n+1,m} - K_{i-1}^{n+1,m}}{2\Delta z}) - (1-f)(\frac{K_{i+1}^{n,m} - K_{i-1}^{n,m}}{2\Delta z})$$

[4.58]

Rearranging Eq. [4.58] leads to the following symmetrical tridiagonal matrix equation:

$$[\frac{-f\Delta t}{(\Delta z)^2} K_{i-1/2}^{n+1,m}]h_{i-1}^{n+1,m+1} + [C_i^{n+1,m} + \frac{f\Delta t}{(\Delta z)^2}(K_{i-1/2}^{n+1,m} + K_{i+1/2}^{n+1,m}]h_i^{n+1,m+1}$$

$$+[\frac{-f\Delta t}{(\Delta z)^2} K_{i+1/2}^{n+1,m}]h_{i+1}^{n+1,m+1} + f\Delta t(\frac{K_{i+1}^{n+1,m} - K_{i-1}^{n+1,m}}{2\Delta z}) =$$

$$[\frac{(1-f)\Delta t}{(\Delta z)^2} K_{i-1/2}^{n,m}]h_{i-1}^{n,m} + [-\frac{(1-f)\Delta t}{(\Delta z)^2}(K_{i-1/2}^{n,m} + K_{i+1/2}^{n,m}]h_i^{n,m} +$$

$$[\frac{(1-f)\Delta t}{(\Delta z)^2} K_{i+1/2}^{n,m}] - (1-f)\Delta t(\frac{K_{i+1}^{n,m} - K_{i-1}^{n,m}}{2\Delta z}) + (\theta_i^n - \theta_i^{n+1,m}) + C_i^{n+1,m}h_i^{n+1,m}$$

78

Where $C_i^{n+1,m} = \dfrac{d\theta_i^{n+1,m}}{dh}$ indicates the nodal values of the soil water capacity function.

Note that $(\theta_i^n - \theta_i^{n+1,m})$ is known prior to the current iteration and $(h_i^{n+1,m+1} - h_i^{n+1,m})$ in the left hand side of equation [4.58] should vanish at the end of the iteration process if the numerical solution in convergent.

4.3.1.2.3. Implementation of Boundary Conditions

Dirichlet boundary condition is treated in the same manner as in the finite element method. A zero flux Neumann boundary condition will be applied at the top of the space domain. To simulate this kind of boundary condition, Darcy's law (Eq. [4.63]) is discretized. Defining a virtual node at the top of the spatial domain, discretizing the pressure gradient, and writing equation [4.56] for node one, results in the following entries for the h-based Richards' equation (for Crank-Nicolson scheme):

$$
\begin{pmatrix}
a_{1,1} & a_{1,2} & 0 & \dots & & 0 \\
a_{2,1} & a_{2,2} & a_{2,3} & & & . \\
. & . & . & . & & . \\
. & . & a_{N-1,N-2} & a_{N-1,N-1} & a_{N-1,N} & . \\
0 & 0 & \dots & & a_{N,N-1} & a_{N,N}
\end{pmatrix}
\begin{bmatrix} h_1 \\ . \\ . \\ . \\ h_N \end{bmatrix}^{n+1,m+1}
=
\begin{pmatrix}
b_{1,1} & b_{1,2} & 0 & \dots & & 0 \\
b_{2,1} & b_{2,2} & b_{2,3} & & & . \\
. & . & . & . & & . \\
. & . & b_{N-1,N-2} & b_{N-1,N-1} & b_{N-1,N} & . \\
0 & 0 & \dots & & b_{N,N-1} & b_{N,N}
\end{pmatrix}
\begin{bmatrix} h_1 \\ . \\ . \\ . \\ h_N \end{bmatrix}^{n,m}
$$

$$[4.60]$$

$$ h_0 = h_2 - 2\Delta z $$

$$ a_{1,1} = [\frac{C_1^{n+1,m} - C_1^n}{2\Delta t} + \frac{f}{(\Delta z)^2}(K_{1-1/2}^{n+1,m} + K_{1+1/2}^{n+1,m}] $$

$$ a_{1,2} = [\frac{-f}{(\Delta z)^2}(K_{1-1/2}^{n+1,m} + K_{1+1/2}^{n+1,m})] $$

$$ b_{1,1} = -f(\frac{K_2^{n+1,m} - K_0^{n+1,m}}{2\Delta z}) - \frac{2fK_{1-1/2}^{n,m}}{\Delta z} + [\frac{C_1^{n+1,m} - C_1^n}{2\Delta t} - \frac{(1-f)}{(\Delta z)^2}(K_{1-1/2}^{n,m} + K_{1+1/2}^{n,m})] $$

$$-\frac{2(1-f)}{\Delta z}K_{1-1/2}^{n,m} - (1-f)(\frac{K_2^{n,m} - K_0^{n,m}}{2\Delta z})$$

$$b_{1,2} = \frac{(1-f)}{(\Delta z)^2}[K_{1-1/2}^{n,m} + K_{1+1/2}^{n,m}]$$

Using the same procedure, the entries for the fully implicit mixed form Richards'
equation will be:

$$a_{1,1} = \frac{C_1^{n+1,m}}{\Delta t} + \frac{K_{1-1/2}^{n+1,m} + K_{1+1/2}^{n+1,m}}{(\Delta z)^2}$$

$$a_{1,2} = \frac{-K_{1-1/2}^{n+1,m} + K_{1+1/2}^{n+1,m}}{(\Delta z)^2}$$

$$b_1 = \frac{C_1^{n,m}}{\Delta t} - \frac{K_2^{n+1,m} - K_0^{n+1,m}}{2\Delta z} - \frac{2K_{1-1/2}^{n,m}}{\Delta z} + \frac{\theta_1^{n,m} - \theta_1^{n+1,m}}{\Delta t}$$

4.3.1.3. Iterative Procedure

The system of algebraic equations produced by equations [4.32], [4.44], [4.50], [4.56],
and [4.59] are nonlinear because of the interaction term ($K_a FS$) in Eq. [4.32] and
dependence of the hydraulic functions K and C upon the solution, $h^{n+1,m+1}$ in other matrix
equations. Therefore, the equations must be linearized and solved iteratively. The
iteration methods that are generally used are the Picard and Newton (known as Newton-
Raphson method also) algorithms. Theoretically, the Newton-Raphson method converges
one order of magnitude faster than the Picard scheme, but several studies have shown that
this method is inferior to the Picard iteration method (Kuiper, 1987; Paniconi *et al.,* 1991;
Paniconi and Putti, 1994; Zhang *et al.,* 2002 among others). The Newton method
converges quadratically only in the vicinity of the solution. When the estimated values
are far from the solution, the method produces severe non-physical oscillation in the
iteration process and diverges as a consequence of neglecting higher order terms in the

Taylor series expansion (which contribute to the right hand side vector of the system of linear equations) that are still significant and result in a Jacobian matrix devoid of diagonal dominance. In contrast, the Picard method has a diagonally dominant matrix and preserves symmetry in the matrix. Furthermore, evaluation of the Jacobian matrix is often time consuming especially for highly nonlinear partial differential equations such as Richards' equation and hyperbolic convective-dispersive-reactive equations. Because of these limitations, the Newton-Raphson method will not be used in this study. Instead a modified version of the Picard method known as the Modified Picard algorithm, that makes the Picard method more robust, will be used. In this method the hydraulic functions K and C are evaluated at the current time but previous iteration level. A convergence criterion of $\delta = 1 \times 10^{-6}$ (unit of the state variable) will be used to end the Picard iteration in every time step.

Finally, it is a well known practice to use some small nonzero value for soil water capacity term at or near saturation (Rogers, 1994). The threshold value of $C = 1*10^{-5} cm^{-1}$ will be used in this study.

4.3.1.4. Adaptive Time Step

To decrease the CPU time and maintain small truncation error, an adaptive time step approach will be used to solve the matrix equations. The time step starts with a prescribed initial time increment then the time increment is increased by 5 percent if the number of Picard iteration for the previous time step is less than four and is decreased 5 percent if the number of Picard iterations is greater than eight. To avoid oscillatory behavior and maintain truncation error acceptably small, two time indices will be implemented in the adaptive time step loop. In any time step, if the time increment becomes less than dt_{min} it

81

is set to $dt = dt_{min}$ and if the time interval becomes more than dt_{max} it is set to $dt = dt_{max}$.

The time increment can not exceed these two limits ($dt_{min} \leq dt \leq dt_{max}$).

4.3.1.5. Validation of the Numerical Simulators

The numerical simulators of the forward problems will be validated with analytical and reference solutions obtained by solving the forward problem for very dense spatial grid and very fine time increment. The target problems will be drainage of a fully saturated soil and infiltration into very dry soil. The cumulative outflow and temporal and spatial distribution of soil water pressure head and soil moisture content will be compared in both solutions. The data used for the validation will be synthetic.

4.3.1.6. Mass Conservation Property of the Numerical Simulators

An accurate numerical simulator should maintain the global mass balance property over entire spatial domain for all times. The global mass conservation is a necessary but not sufficient condition for acceptability of a numerical code. The mass balance is defined as the ratio of "the total masses of fluid added to the domain" to "the total net flux into the domain". For the finite difference approximation of the Richards' equation, this will be calculated using:

$$MB(t) = \frac{\int_0^L (\theta_i^{n+1} - \theta_i^0)dz}{\int_0^t Flux_{out}d\tau - \int_0^t Flux_{in}d\tau} =$$

$$\frac{\int_0^L (\theta_i^{n+1} - \theta_i^0)dz}{\int_0^t K_{N-1/2}\left[\frac{h_N - h_{N-1}}{\Delta z} - 1\right]d\tau - \int_0^t K_{1/2}\left[\frac{h_1 - h_0}{\Delta z} - 1\right]d\tau}$$

[4.61]

where τ is dummy variable of integration.

For finite element formulation, the mass balance will be calculated as (Celia *et al.*, 1990):

$$MB(t) = \frac{\sum_{i=1}^{E-1}[(\theta_i^{n+1} - \theta_i^0)\Delta z] + (\theta_0^{n+1} - \theta_0^0)(\frac{\Delta z}{2}) + (\theta_E^{n+1} - \theta_E^0)(\frac{\Delta z}{2})}{\int_0^t K_{N-1/2}\left[\frac{h_N - h_{N-1}}{\Delta z} - 1\right]d\tau - \int_0^t K_{1/2}\left[\frac{h_1 - h_0}{\Delta z} - 1\right]d\tau} \qquad [4.62]$$

At the end of the time loop, the nodal fluxes will be calculated using Darcy-Buckingham law (Darcy, 1856; Buckingham, 1907; Hofmann and Hofmann, 1992):

$$q_i^{n+1} = K_{i+1/2}^{n+1,m}\left[\frac{h_{i+1}^{n+1,m} - h_i^{n+1,m}}{\Delta z} - 1\right] \qquad [4.63]$$

At the upper ($i = 1$) and lower ($i = N$) boundaries of the domain, the Darcian fluxes are calculated by:

$$q_1^{n+1} = -K_{1/2}^{n+1,m}\left[\frac{h_2^{n+1,m} - h_0^{n+1,m}}{\Delta z} - 1\right] \qquad [4.64]$$

$$q_N^{n+1} = -K_{N-1/2}^{n+1,m}\left[\frac{h_N^{n+1,m} - h_{N-1}^{n+1,m}}{\Delta z} - 1\right] \qquad [4.65]$$

4.3.2. Formulation of the Inverse Problem: Optimization Scenarios

The inverse problem will be formulated as a nonlinear optimization problem which involves estimating unknown hydraulic parameters from measured system attributes such as soil moisture content, soil water matric potential head, and outflow rates. The goal is to minimize some functions of the differences between the observed and model predicted responses. Both single-objective and multi-objective optimizations in homogeneous and heterogeneous partially saturated soil will be considered. Single-objective optimization

will be applied in both homogeneous and heterogeneous soils while multi-objective optimization will be carried out on the heterogeneous soil (because of the lack of additional information).

For single-objective optimization the following weighted objective function is formulated:

$$\phi(\beta) = \frac{\sum_{i=1}^{N}(U_i - \hat{U}_i)^2}{N\sigma_U^2} \qquad [4.66]$$

Where U_i and $\hat{U}_i$ are the measured and predicted soil moisture contents or soil water matric potential head and σ_U^2 is the observation variance.

For multi-objective optimization, the following complex weighted objective function is used:

$$\phi(\beta) = \frac{\sum_{i=1}^{N}(\theta_i - \hat{\theta}_i)^2}{N\sigma_\theta^2} + \frac{\sum_{j=1}^{M}(h_j - \hat{h}_j)^2}{M\sigma_h^2} \qquad [4.67]$$

Where θ_i and $\hat{\theta}_i$ are the measured and predicted soil moisture contents, h_i and $\hat{h}_i$ are the measured and predicted soil water matric potential head, σ_θ^2 and σ_h^2 are variances of the measured soil moisture content and matric potential head, and N and M are number of observations for soil moisture content and soil water pressure head, respectively.

4.3.2.1. Water Flow through Homogeneous Partially Saturated Porous Media

The data for this case were taken from the in-situ experiment conducted at the Los Alamos National Laboratory and fully described by Abeele (1984). The experiment includes free drainage from a 3m diameter by 6m deep lysimeter, filled with crushed

Bandelier Tuff, a material with silty sand texture. The lysimeter was equipped with tensiometers and neutron probe access tubes at depths 40, 116, 191, 271, 347, and 423 cm. Before the initiation of free drainage, the lysimeter was ponded by infiltration for more than one month and the mean values of the saturated water content and saturated hydraulic conductivity were measured as 0.331 and $12.44\, cmday^{-1}$. The surface of the lysimeter was covered during the drainage period yielding zero flux boundary condition at the top of the domain. The lysimeter was allowed to freely drain for 100 days during which time the temporal and spatial distributions of soil water content and soil water matric potential head were monitored.

This data set will be used to inversely estimate the optimized values of the parameter vector $[K_s, \alpha, n, \theta_r, \iota]$ through single-objective and multi-objective optimizations. In single objective optimization equation [4.66] will be used as the objective function. In multi-objective optimization equation [4.67] will be employed as the objective function.

4.3.2.2. Water Flow through Heterogeneous Partially Saturated Porous Media

A $2 \times 2 \times 1.25 m^3$ lysimeter with layered soil was equipped with five time domain reflectometry (TDR) probes (three 20cm rods of 0.3cm diameter and with 2.5cm separation) to monitor spatio-temporal distribution of soil water contents. The probes were inserted horizontally at depths of 10, 30, 50, 70, and 90cm. They were multiplexed and connected to a TRASE TDR device (Soilmoisture Inc., Santa Barbara, CA). Figure 4.3 is a schematic representation of the lysimeter. The lysimeter was saturated by providing ponding water at the top of the soil profile and allowing free drainage at the bottom for two weeks. Then, the drain tube was blocked and the surface of the lysimeter

Time Domain
Reflectometery

TDR probes
installation depths
(cm)

10 cm

30 cm

50 cm

Soil

Lysimeter

70 cm

90 cm

Sand

Drain pipe
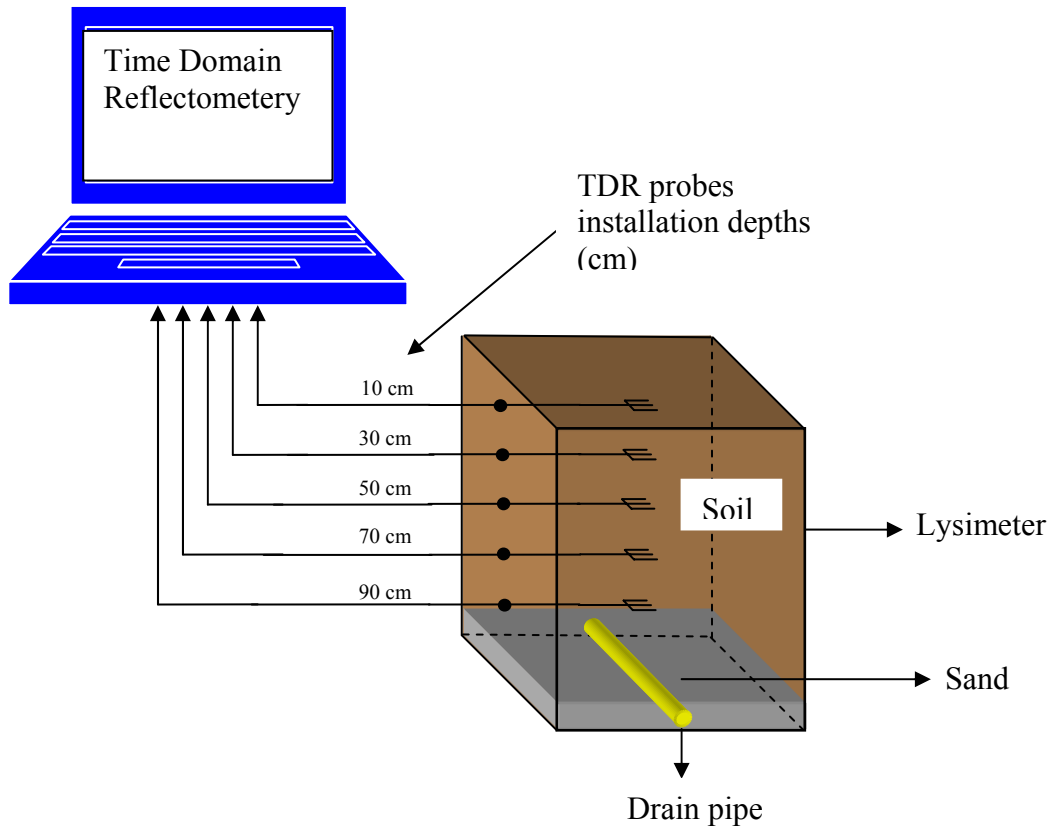
Figure 4.3. Schematic sketch of the lysimeter and TDR probes.

was covered with nylon, providing a zero flux boundary condition at the top of the domain. After two weeks, the soil moisture content was measured at five different depths, free drainage was initiated by unblocking the drain and was continued for one month. The soil moisture contents were measured at different depths frequently. The data are presented in Table 4.2. The physical properties of the soil are given in Table 4.3 in which d_g and σ_g are geometric mean and standard deviation of soil particles diameter (Shirazi and Boresma, 1984; Shirazi *et al.,* 1988).

The experimental results will be used to identify hydraulic parameters of the heterogeneous soil by single-objective optimization since there is no other additional information about other properties of the soil. Equation [4.66] will be used as objective function.

Table 4.2. The results of drainage experiment for heterogeneous soil.

Time(day) → Depth (cm) ↓	0.0000	0.7292	1.7292	2.7292	3.7292	4.7292	5.7292	6.7292	10.000	13.75	18.75	23.7917	28.8125
10	0.4126	0.3902	0.3687	0.3461	0.3334	03200	0.3102	0.3001	0.2824	0.2670	0.2606	0.2543	0.2504
30	0.4221	0.4056	0.3831	0.3634	0.3503	0.3400	0.3300	0.3215	0.3052	0.2917	0.2805	0.2700	0.2638
50	0.4293	0.4142	0.3947	0.3801	0.3669	0.3600	0.3501	0.3431	0.3312	0.3203	0.3096	0.2975	0.2891
70	0.4336	0.4216	0.4081	0.3957	0.3851	0.3765	0.3700	0.3648	0.3517	0.3400	0.3300	0.3211	0.3127
90	0.4368	0.4257	0.4158	0.4071	0.4004	0.3931	0.3872	0.3801	0.3698	0.3601	0.3509	0.3437	0.3378

Table 4.3. The physical properties of the soil at the experimental site.

Soil Depths (cm)	Clay (%)	Silt (%)	Sand (%)	Soil Texture	d_g (cm)	σ_g
0 – 20	26	44	30	L	0.034	13.6580
20– 40	29	45	26	CL	0.027	12.8880
40 – 60	28	42	30	CL	0.031	14.2780
60 – 80	21	36	43	L	0.064	14.3290
80 – 100	14	25	61	SL	0.154	12.9830
100 – 120	10	27	63	SL	0.188	10.7780

4.4. Analysis of the Inverse Modeling Strategy

Different measures will be used to analyze the results of the inverse modeling strategy. To study the closeness of the solution to the "true" minimum, the gradient of the objective function at the solution and the positive definiteness of the Hessian matrix will be analyzed. To study the stability of the inverse problem, small perturbation will be made on the input data and the inverse code will be rerun to Figure out if the optimized values of the parameters change or not. To study the uniqueness of the solution two-dimensional parameters response surfaces as well as three-dimensional parameter hyper space will be constructed and analyzed.

Absolute and relative sensitivity will be calculated and analyzed to study the sensitivity of the state variables to the changes in the parameters and to recommend a sampling strategy for data collection.

The reliability and performance of the optimization strategy will be studied using statistical goodness-of-fit indices such as variances of the optimized parameters, covariance and correlation matrices, confidence intervals on the optimized parameters, Root Mean Squared Error (RMSE), and coefficient of determination.

A residual analysis will be performed to test possible correlation, trends, and oscillations of errors. The *Student's t-test* will be used to verify if the residuals have a mean of zero. Using the *Chi-square and Kolmogorov-Smirnov* tests, hypothesis tests will be performed to test if residuals are normally distributed. Another hypothesis tests will be used to verify if the forward models are biased. *Bartlett and Levene tests* will be used to test if the variance of the residuals is constant. The t-statistic will be applied to verify if the residuals are uncorrelated.

4.4.1. Statistical Assessment

One of the advantages of the inverse modeling over the commonly used model calibration is uncertainty analysis which can be accomplished at the end of the parameter optimization procedure. The first-order approximation of the parameter covariance matrix is calculated as (Bard, 1974):

$$C = s^2 (J^T J)^{-1}$$ [4.68]

where s is the estimated error variance:

$$s = \frac{r^T r}{N - p}$$ [4.69]

The second-order approximation of the parameter covariance matrix can be obtained as (Bard, 1974):

$$C = s^2 (H)^{-1}$$ [4.70]

The diagonal elements of the parameter covariance matrix are variances which indicate the estimation uncertainties over the parameters, and the off-diagonal elements are covariance between the parameters. Using this matrix, the parameter correlation matrix (known as the variance-covariance matrix) is calculated (Bard, 1974; Beck and Arnold, 1977; Yeh, 1986; Lehmann and Ackerer, 1997):

$$COR(P)_{ij} = \frac{C_{ij}}{\sqrt{C_{ii}} \sqrt{C_{jj}}}$$ [4.71]

Equation [4.71] identifies the degree of correlation between the optimized parameters. In other words, the correlation matrix quantifies the nonorthogonality between two parameter values. A value of ±1 reflects perfect linear correlation between two parameters whereas 0 suggests no correlation at all. The matrix may be used to

identify which parameter, if any, is kept constant in the parameter optimization process because of high intercorrelation (van Genuchten, 1991).

The root mean squared error ($RMSE$) and coefficient of determination (R^2) are calculated as follows (Daniel and Wood 1976; van Genuchten, 1991):

$$RMSE = \sqrt{\frac{r^T r}{N - p}} \tag{4.72}$$

$$R^2 = \frac{[\sum \hat{U}_i U_i - \sum \hat{U}_i \sum \hat{U}_i]^2}{[\sum \hat{U}^2 - (\sum \hat{U}_i)^2][\sum U^2 - (\sum U_i)^2]} \tag{4.73}$$

where U_i and $\hat{U}_i$ are the observed and predicted state variable, respectively.

Confidence intervals on the optimized parameters are calculated using the covariance matrix (Kool and Parker, 1988):

$$pr(\hat{\beta} - t \times C_{ii}^{1/2} \leq \hat{\beta} \leq \hat{\beta} + t \times C_{ii}^{1/2}) = \gamma \tag{4.74}$$

where $\hat{\beta}$ is the estimated value of the parameter, C_{ii} is the parameter variances, obtained by the covariance matrix, and $t \equiv t_{v,1-\alpha/2}$ is the value of the student t distribution (Abramowitz and Stegun, 1964) for confidence level $\gamma = 1 - \alpha$ and degree of freedom v.

As Donaldson and Schnabel (1987) and Kool and Parker (1988) pointed out these equations are taken from linear regression and hold only approximately for nonlinear optimization problems. Furthermore, to use these equations, $\hat{\beta}$ should be the true minimum and no constraints should be imposed on the parameter space. Under these conditions, Donaldson and Schnabel (1987) showed that equations [4.68] to [4.74] show reasonable agreement with the nonlinear optimization statistics.

4.4.2. Posedness Analysis

As discussed in chapter two, inverse problems are often ill-posed. A problem is ill-posed when it either has no solution at all, no unique solution, or the solution is not stable (Tyn Myint-u, 1980; Russo *et al.,* 1998). Generally, ill-posedness arises from non-uniqueness and instability. To investigate the ill-posedness of the inverse problem, stability and uniqueness analyses will be performed.

4.4.2.1. Stability Analysis

To perform stability analysis, a generated data set will be obtained by solving the forward problems for hypothetical biological systems with prescribed initial and boundary conditions and parameter values. Normally distributed noise with zero mean and standard deviation of σ, $N(0, \sigma)$, will be added to the data. The inverse modeling strategy will then be used to identify the model parameters using these noisy generated data. The result will be compared with the original parameter vector and analyzed in terms of relative error, possible changes in the magnitudes of the parameters, estimation uncertainties, and confidence intervals on the optimized parameters.

4.4.2.2. Uniqueness Analysis

The uniqueness of the inverse problem will be evaluated by construction of two-dimensional parameter response surfaces of the objective function as a function of pairs of parameters being optimized. To further investigate possible non-uniqueness of the inverse problem, parameter hyper-spaces will be constructed and analyzed for triplets of parameters.

4.4.2.2.1. Parameter Response Surface

Response surfaces are two-dimensional plots of the objective function as a function of pairs of model parameters, used to fit a model to experimental data (Sorooshian and Gupta, 1983). They are useful in providing information about the linearity of the model and possibility of multiple minima (or maxima in case of maximization). Three pairs of response surfaces will be built to analyze possible ill-posedness of the inverse problem in biomolecule transport in living cells. The objective function, $\Phi(\overline{frap})$, will be calculated for three parameter planes: $D_f - K_a^*$, $K_a^* - K_d$, and $D_f - K_d$. The response surfaces will be constructed using a rectangular grid with parameter values $D_f = 1 - 120 \mu m^2 s^{-1}$, $K_a^* = 1 - 120 s^{-1}$, and $K_d = 0.01 - 1 s^{-1}$. The domain of each parameter will be discretized into 60 discrete points resulting in 3600 grid points for each response surface which means solving the *direct problem* (Eq.[2.32]) 10800 times to generate three plots.

Ten pairs of response surfaces will be constructed for parameter vector $[K_s, \alpha, n, \theta_r, \iota]$ in analyzing the inverse problem in water flow through homogeneous variably saturated soil. The domain of each parameter will be discretized into 50 discrete points resulting in 2500 grid points for each response surface plot implying that the Richards' equation (*direct problem*) will be solved 25000 times to generate the ten plots. Since information on both of the soil moisture content and soil water pressure head is available a complex objective function, $\Phi(\theta + h)$, will be used.

The same procedure will be followed to analyze possible non-uniqueness of the inverse problem in water flow through heterogeneous variably saturated soil. The only difference is that the objective function in this case will be $\Phi(\theta)$ since there are no

additional data sets in this case.

4.4.2.2.2. Parameter Hyper-Space

Since response surfaces are only two-dimensional cross sections of a whole $p-dimensional$ parameter domain, analysis of the behavior of the objective function in full hyper-space will reveal how the function might behave in the whole space. To gain complete perspective about the unique identifiability of the model parameters through inverse modeling of biomolecule transport in living cells, three-dimensional parameter hyper-spaces in $D_f - K_a^* - K_d$ will be constructed and analyzed. Domain of each parameter will be discretized into 100 discrete points resulting in one million grid points for the target hyper-space. This requires solving the *forward problem* (Eq.[2.32] with $D_C = 0$, $D_S = 0$) one million times which takes about two weeks run of a Pentium4 Processor550 (3.4 GHz) PC.

To analyze the behavior of the objective function in case of water flow through homogeneous variably saturated soil, five-dimensional hyper spaces should be constructed and analyzed which is not possible with state-of-the-technology. However, a three-dimensional parameter hyper space will be constructed in $\alpha - n - K_s$ directions. To achieve this goal, the domain of each parameter will be discretized into 31 discrete points resulting in 29791 grid points for the target plot. This requires solving the Richards' equation (*direct problem*) 29791 times which is very time consuming and takes about nine days using a Pentium4 Processor550 (3.4 GHz) PC. Therefore, it will be constructed and analyzed just for water flow through homogeneous variably saturated soil. The objective function will be $\Phi(\theta + h)$.

4.4.3. Sensitivity Analysis

The most accurate parameter estimation, by inverse modeling, is obtained when the state variable(s) has the highest sensitivity to the collected data and to the parameters being estimated. Parameter sensitivity analysis is an essential guideline for sampling planning, experimental data collection and for identifying the discrete points in space and time that produce the most sensitive data. To perform the parameter sensitivity analysis, columns of the last Jacobian matrix in the optimization algorithm will be used as the absolute sensitivities of the state variable(s) with respect to the parameters being optimized. The magnitudes, rather than the sign, of the absolute and relative sensitivities are of special interest. To compare the sensitivity of the state variable(s) to different parameters, the relative sensitivity, rather than absolute sensitivity, will be used. The relative sensitivity will be calculated by $(\frac{\partial U}{\partial p})(\frac{p}{\bar{U}})$, where U is the state variable. The best index to measure the magnitude of the sensitivity is the norm of the columns of the normalized Jacobian matrix at the solution ($\left\| (\frac{\partial U}{\partial p})(\frac{p}{\bar{U}}) \right\|_{\beta=\hat{\beta}}$) which will be calculated, plotted, and compared across parameters, time, and spatial locations (where applicable).

4.4.4. Residual Analysis

Residuals, or errors in parameter optimization, are defined as the difference between the observed and simulated state variable(s). An analysis of the residuals is a useful and key technique to study possible trends, oscillations, and correlation of errors. It is also important in validating the assumptions on which the inverse modeling strategy rests. The inverse methodology used in this study is based on the following assumptions:

95

1. Residuals have a mean of zero,

2. Residuals have constant variance,

3. Residuals are uncorrelated,

4. Residuals are normally distributed.

When these assumptions are met, the parameter optimization estimates poses optimal statistical properties (Bard, 1974). When these conditions are not met the parameter optimization method *may* no longer produce optimal parameter estimates.

To analyze the residuals, they will be plotted against the state variables. Since the residuals are time and/or space series, their possible correlation will be thoroughly analyzed. Error frequency analysis, normal probability plot, and hypotheses tests will be discussed. Different tests will be used to make decision about the residuals. The *Student's t-test* will be used to test if the residuals have a mean of zero. *Bartlett's test* (Snedecore and Cochran, 1983) and *Levene's test* (Levene, 1966) will be applied to determine if the residuals have constant variance. To test the normality of the residuals the Chi-square test and Kolmogorov-Smirnov one sample test will be used. Finally, the *t-statistic* will be used to test if the residuals are correlated.

4.4.4.1. Hypothesis Test on the Residuals' Mean

The basic assumption in this test is that the data come from a normally distributed population with unknown variance. In this study, the following *null and alternative hypotheses* will be formulated:

$$H_0 : \mu = \mu_0$$
$$H_A : \mu \neq \mu_0$$

[4.75]

To perform the test the following *critical t-statistic* (t) is used:

$$t = \frac{\bar{x} - \mu_0}{s / \sqrt{N}}$$

[4.76]

in which $\bar{x}$, s, and N are the mean, standard deviation, and size of the sample (errors), respectively. μ_0 is the mean of the population which is zero.

For $-t_{\alpha/2} < t < t_{\alpha/2}$ the null hypothesis (mean is zero) cannot be rejected at the significance level α. The rejection regions $t < -t_{\alpha/2}$ or $t_{\alpha/2} < t$ indicate that the null hypothesis can be rejected at the level of significance α.

4.4.4.2. Hypothesis Test on the Residuals' Variance

Bartlett's test will be used to verify if k samples, taken from the residuals, have equal variances. Equal variance across samples is called *homogeneity of variances* and is usually used in several statistical tests such as analysis of variance and nonlinear optimization which assumes that the errors have constant variance.

The following *null and alternative hypotheses* will be formulated:

$$\begin{aligned} H_0 &: \sigma_1^2 = \sigma_2^2 \\ H_A &: \sigma_1^2 \neq \sigma_2^2 \end{aligned}$$

[4.77]

Different tests will be used to determine whether the variance of the residuals is constant. The *Bartlett's test statistic* is used to verify for equality of variances across sub-groups of a sample against the alternative that variances are not constant (Snedecor and Cochran, 1983):

$$T = \frac{(N-k)\ln s_p^2 - \sum_{i=1}^{k}(N_i - 1)\ln s_i^2}{1 + \frac{1}{3(k-1)}\left[\sum_{i=1}^{k}\frac{1}{N_i - 1} - \frac{1}{N-k}\right]}$$

[4.78]

where s_i^2 is the variance of the subgroup, N_i is the sample size of the subgroup, k is the number of subgroups, and s_p^2 is the pooled variance. This variance is a weighted average of the variances:

$$s_p^2 = \sum_{i=1}^{k}(N_i - 1)\ln s_i^2 /(N-k) \qquad [4.79]$$

The rejection region is those values of $T > \chi_{(\alpha,k-1)}^2$ in which $\chi_{(\alpha,k-1)}^2$ is the *upper critical value* of the *chi-square distribution* with $k-1$ degree of freedom at the level of significance α.

The Bartlett test is sensitive to departure from normality. If residuals are known to be not normal then the Levene's test should be applied as an alternative to the Bartlett test. In the present study, the Levene's test will only be used if the chi-square and Kolmogorov-Smirnov one sample tests on the normality of the residuals (will be discussed in 4.4.4.4) verify that the errors are not normally distributed. The *Levene test statistic* is defined as (Levene, 1966):

$$W = \frac{(N-k)\sum_{i=1}^{k} N_i(\bar{Z}_{i.} - \bar{Z}..)^2}{(k-1)\sum_{i=1}^{k} \sum_{i=1}^{N_i} N_i(\bar{Z}_{ij} - \bar{Z}..)^2} \qquad [4.80]$$

where $\bar{Z}_{i.}$ are the subgroups means and $\bar{Z}_{..}$ is the overall mean of the residuals (Z_{ij}).

The Levene test rejects the null hypothesis (variances are equal or the random variable has constant variance) if:

$$W > F_{(\alpha,k-1,N-k)}$$

where $F_{(\alpha,k-1,N-k)}$ is the *upper critical value* of the *F-distribution* with $k-1$ and $N-k$

degrees of freedom at the level of significance α.

4.4.4.3. Hypothesis Test on the Correlation of the Residuals

The following *null and alternative hypotheses* will be used to test possible correlation among the residuals:

$$H_0 : \rho = 0$$
$$H_A : \rho \neq 0$$

[4.81]

where ρ is the correlation coefficient in the population. For $n > 2$ these hypotheses can be tested using the following *t-statistic* (McCuen, 1986):

$$t = \frac{R}{\sqrt{\dfrac{1 - R^2}{N - 2}}}$$

[4.82]

in which R is the correlation coefficient.

The null hypothesis (correlation coefficient is zero) is rejected when the absolute value of the *t-statistic* is greater than the *critical t-value* ($t < -t_{\alpha/2}$ or $t_{\alpha/2} < t$) at the level of significance α. If the null hypothesis is rejected, the autocorrelation will be studied by serial correlation analysis (McCuen, 2003):

$$R(\tau) = \frac{\displaystyle\sum_{i=1}^{N-\tau} U_i U_{i+\tau} - \frac{1}{N-\tau} \sum_{i=1}^{N-\tau} U_i \sum_{i=\tau+1}^{N} U_i}{\left[\displaystyle\sum_{i=1}^{N-\tau} U_i^2 - \frac{1}{N-\tau} (\sum_{i=1}^{N-\tau} U)^2 \right]^{1/2} \left[\displaystyle\sum_{i=\tau+1}^{N} U_i^2 - \frac{1}{N-\tau} (\sum_{i=\tau+1}^{N} U)^2 \right]^{1/2}}$$

[4.83]

where $R(\tau)$ is the serial correlation coefficient, τ is the separation distance or *lag*, and U_i and $\hat{U}_i$ are the observed and predicted state variable, respectively.

4.4.4.4. Hypothesis Test on the Normality of the Residuals

To test the normality of the residuals, *the chi-square goodness of fit test*, which is based on the differences between the observed (o_i) and expected (e_i) error frequencies will be used:

$$\chi^2 = \sum_{i=1}^{k} \frac{(o_i - e_i)^2}{e_i} \qquad [4.84]$$

where k is the number of intervals or cells.

To perform the test, first residuals will be grouped into different cells (histograms). The number of residuals in every cell will be counted which is e_i. Then using the upper limit of the cells, the mean, standard deviation, and the cumulative normal distribution (the expected frequencies) will be calculated. The cells will be merged when the observed error frequencies are less than 5. Then using equation [4.84], the χ^2 index will be calculated and will be compared with $\chi^2_{(1-\alpha, v)}$ (Abramowitz and Stegun, 1965). This information will be used in the hypothesis test. The null and alternative hypotheses will be formulated as:

$$\begin{aligned} H_0 &: r \sim N(\mu, \sigma) \\ H_A &: r \neq N(\mu, \sigma) \end{aligned} \qquad [4.85]$$

where μ and σ are the mean and the standard deviation of the residuals in population.

In case of small sample size and very low degrees of freedom, the Kolmogorov-Smirnov one sample test will be used to verify normality of the residuals. The results will be compared with those of the chi-square test.

CHAPTER 5: RESULTS

Science never solves a problem without creating ten more.
G. B. Shaw

5.1. Development of the Inverse Modeling Strategy

5.1.1. Optimization Algorithm

The flowchart of the code developed to solve the *inverse problem* is presented in Figure 5.1. The code was implemented in MATLAB by developing system of m-files that are presented in Appendix E. It reads the experimental data file, provides the initial guesses for parameters to be optimized, the initial condition, and space-time discretization for the numerical simulator of *the direct problem*. It then calls the numerical simulator to solve *the forward problem*. Having obtained the numerical solution of *the forward problem*, it calculates the residual vector and the magnitude of the objective function, forms the Jacobian matrix (by calling the numerical solver $p+1$ times in every iteration at the early stages of the optimization and $2p+1$ times as iteration approaches the minimum, p is number of model parameters being estimated), updates λ and D, updates the parameters, and compares the solution with the termination criteria. If the termination criteria are met it ends the optimization, otherwise it goes to the next iteration.

The flowchart of the numerical simulator used to solve the *direct problem* is presented in Figure 5.2. The numerical simulator first obtains the data file, the discretized
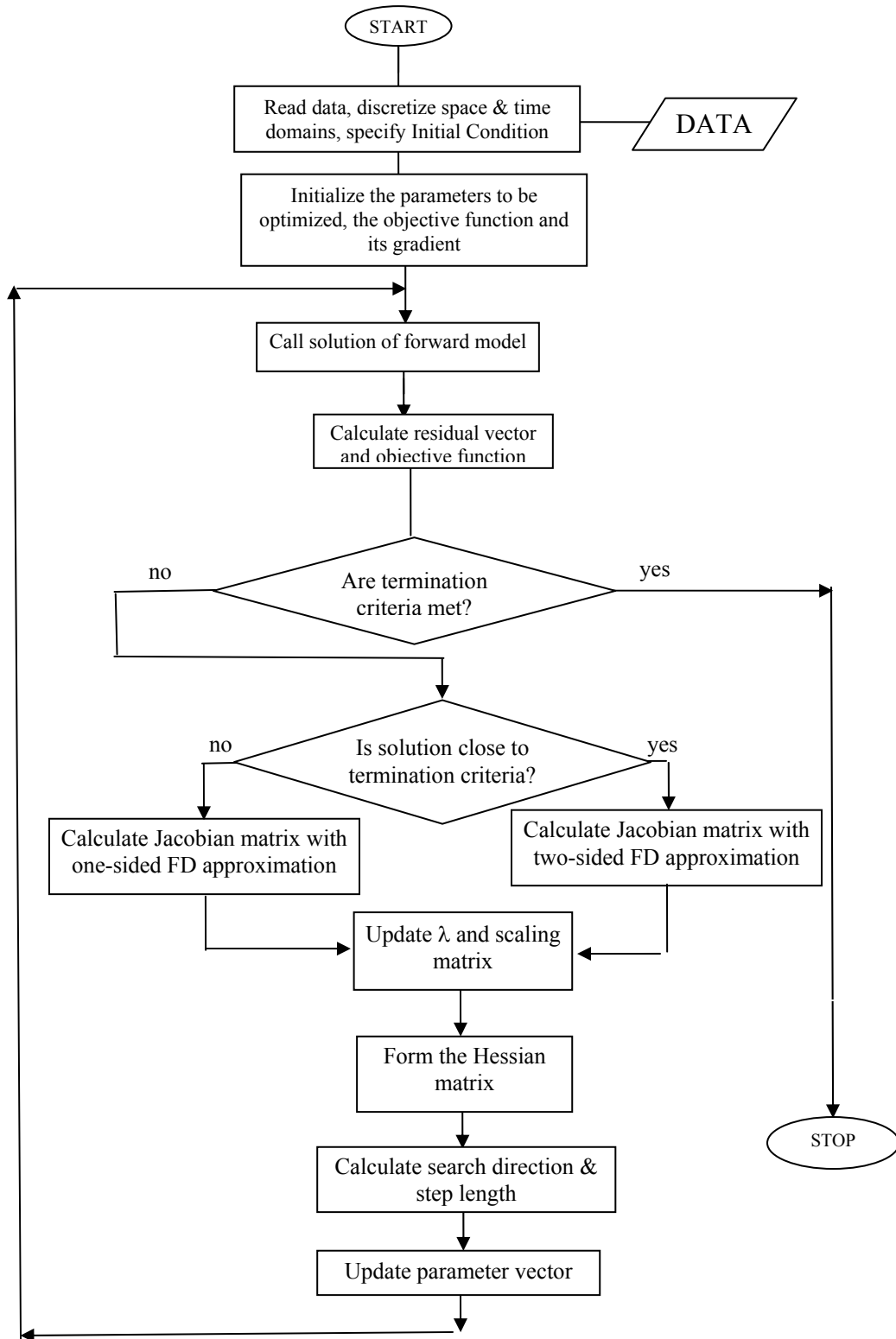
Figure 5.1. Flowchart for solution of the inverse problem.

102
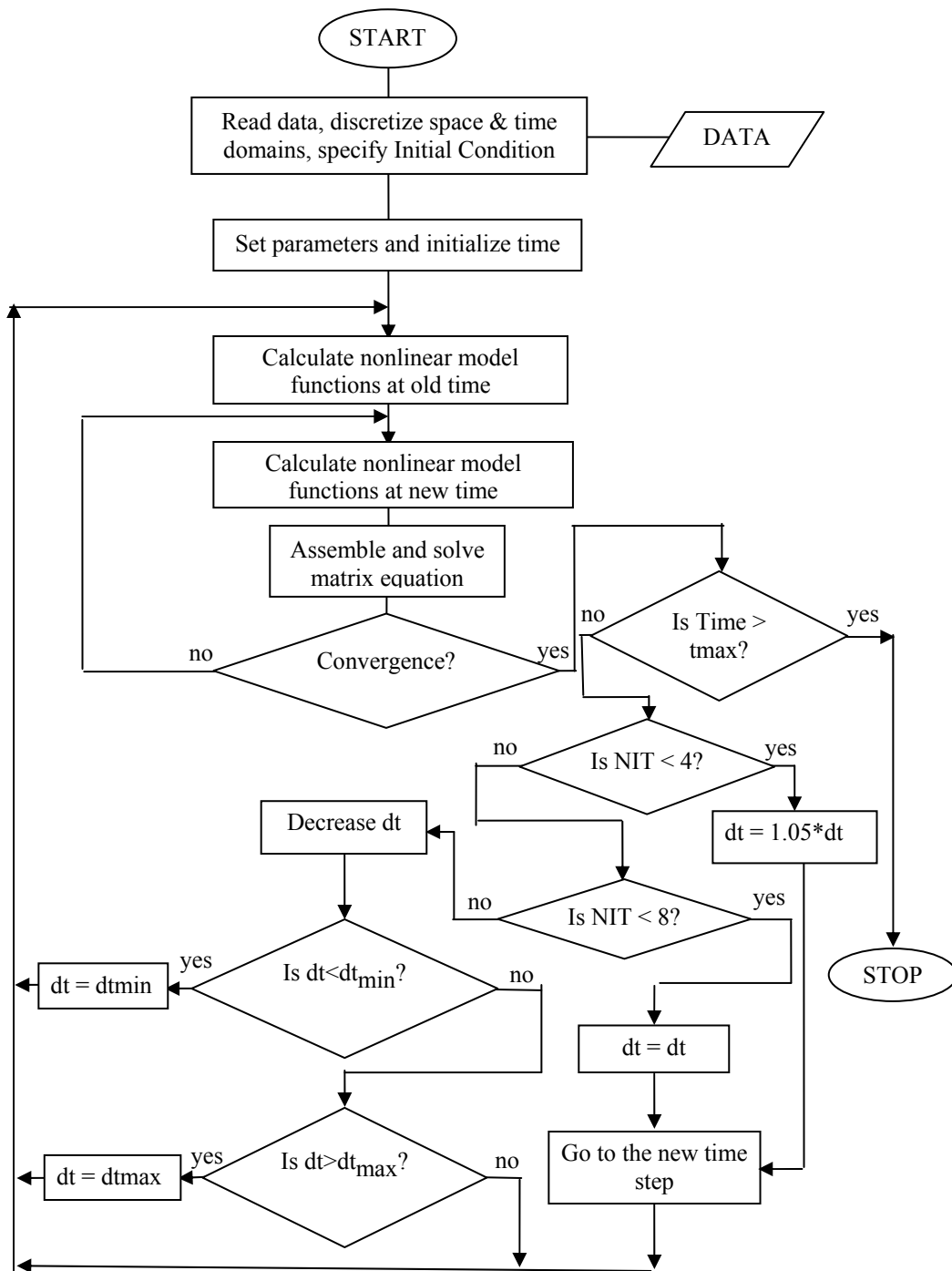
Figure 5.2. Flowchart for solution of the forward problem.

spatial and time domains, and the initial guesses for the parameters to be identified from the inverse code. It then solves the matrix equations and finds the values of the state variable(s). The simulator uses adaptive time stepping to quickly produce results when the solution doesn't change much over time. It was implemented as a system of MATLAB m-files. The m-file PROTRANS.m solves the system of three coupled nonlinear partial differential equations governing biomolecule transport and binding processes inside living cells. The m-file PROINVERSE.m identifies the mass transport and binding rate parameters of in vivo biomolecules. The m-files WATERFLOW_FUNC1.m and WATERFLOW_FUNC2.m contain the mass-lumped Galerkin based linear finite element and fully implicit finite difference solution of the flow equation, respectively. The soil hydraulic properties presented in m-files VGC_FUNC.m, VGK_FUNC.m, VGTHETA_FUNC.m, and VGD _FUNC.m. The entire code is presented in Appendix E.

5.1.2. Selection of the Efficient Optimization Algorithm

To choose the most efficient optimization algorithm for parameter identification problems considered in this study, first the numerical solution of the convective-dispersive-reactive equation (Eq. [4.17]) was validated with the analytical solution (Eq. [4.18]) of Kreft and Zuber (1978). The parameter values $D = 0.50 cm^2 \min^{-1}$, $\mu = 0$, $v = 0.5 cm/\min$, $R = 1$, and $\gamma = 0$ were used to generate both the exact and numerical solutions. The result presented in Figure 5.3. As the Figure shows there are excellent agreements between two solutions.

The numerical simulator was then coupled with the generated data (described in 4.1.2) and the steepest descent method, the Gauss-Newton scheme, equation [4.6], and
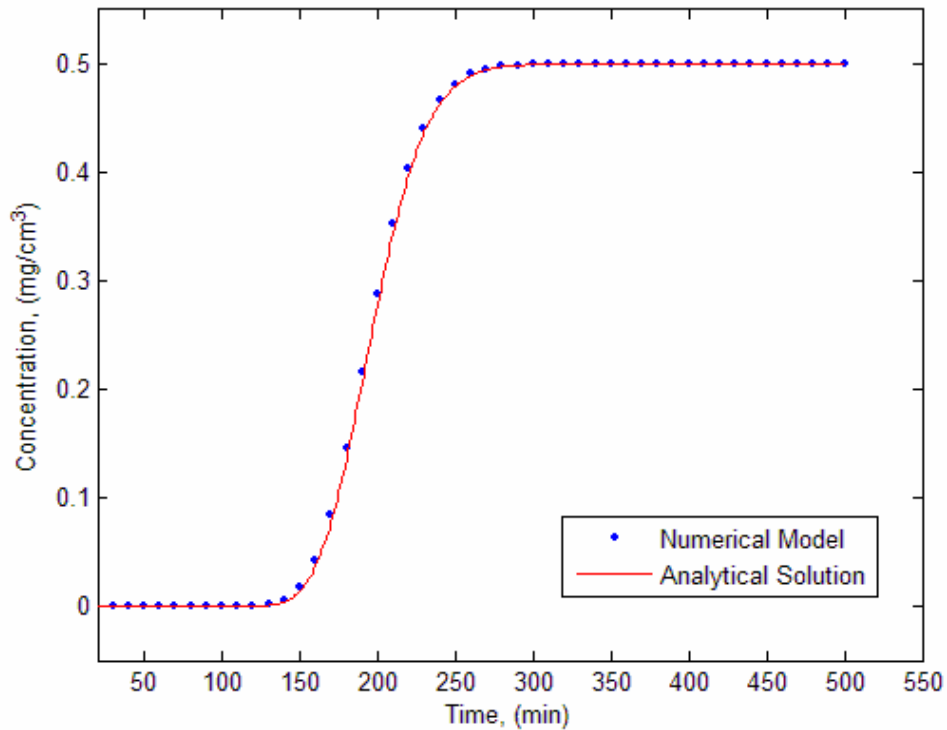
Figure 5.3. Comparison of the numerical simulator of the convective-dispersive-reactive equation with the analytical solution of Kreft and Zuber (1978).

the developed optimization algorithm, to inversely identify model parameters $\beta = [D, v, \mu, \gamma]$ for the convective-dispersive-reactive equation.

The steepest descent method was painfully slow and required a lot of iterations without significant reduction in the magnitude of the objective function. This confirms the reports of Bard (1974) and the optimization toolbox in MATLAB which reported that the steepest descent algorithm took 1000 function evaluations in order to converge to the solution in Rosenbrock's banana function (Mathworks, 2006). The Gauss-Newton failed to obtain the minimum. The reason for failure was computation of the ill-conditioned $J^T J$. In all of the optimization problems considered inthis study, the Gauss-Newton

105

algorithm did not converge to the solution. The Levenberg-Marquardt algorithm (Eq.[2.11]) suffered from the singularity of the $J^T J$ and could not find the minimum. However, the Levenberg-Marquardt algorithm could continue several iterations but the Gauss-Newton method, due to singularity and rank deficiency, failed at the early stages of optimization.

The developed algorithm was then applied to identify model parameters using the generated data. The results are presented in Figure 5.4 and Table 5.1. As Figure 5.4 shows the algorithm could successfully find the minimum and the Root Mean Square Error ($RMSE = 0.0488$) is about one per cent of the concentration of the hypothetical tracer ($C_0 = 4.4 mgcm^{-3}$).

The results of optimization in Table 5.1 indicate that the estimated values of the
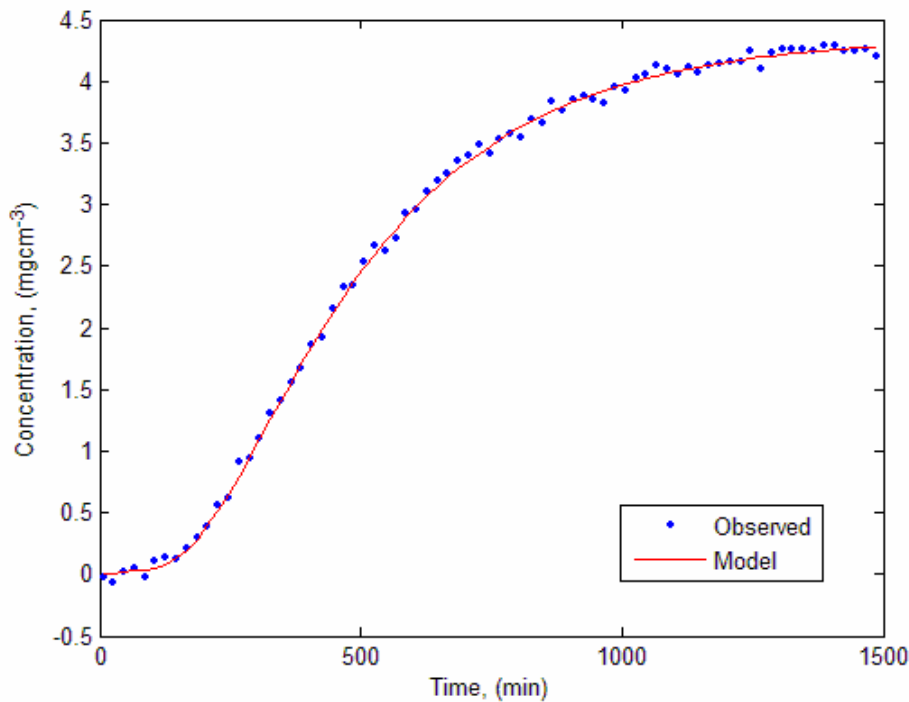
Figure 5.4. Comparison of the simulated concentration with the experimental breakthrough data for a hypothetical tracer.

Table 5.1. The results of parameter optimization for a hypothetical tracer using the developed inverse modeling strategy.

Parameters	$D(cm^2\min^{-1})$	$v(cm\min^{-1})$	$\mu(\min^{-1})$	$\gamma(-)$
True value	3.4290	0.1345	1.0917×10^{-4}	4.0914×10^{-4}
Optimized value	3.6691	0.1210	1.1627×10^{-4}	3.7641×10^{-4}

parameters are very close to the "true" values. Therefore, Eq. [2.12] was implemented in the optimization problems considered in this study.

5.1.3. Challenges of the Levenberg-Marquardt Algorithm

To determine an efficient strategy to control the step size and the Lagrange multiplier in each iteration, three approaches were compared with each other. The first approach (Eqs. [4.19], [4.20], [4.21]) was always in the descending direction but the calculation of λ and α was extremely time consuming. Furthermore, when the internal loop of the algorithm estimated the proper values of λ and α, there was no significant reduction in the magnitude of the objective function in several iterations. After several iterations with no reduction in the function value there was a sudden reduction in the magnitude of the objective function in the next iteration.

The second approach, Eq. [4.22], avoids calculation of λ and α and therefore is computationally cheap. However the judicious choice of λ and changing it as the function value changes, strongly depends on the knowledge and expertise of the user. If one chooses a large λ, the algorithm may swing around the minimum. On the other hand, if λ is given a small value at the beginning of the optimization, the algorithm takes a lot

of iterations to converge the solution.

The *Hessian update method* (Eqs. [4.23] to [4.26]) required a lot of iterations to calculate the appropriate step size in each iteration to ensure the positive definiteness of the Hessian. Since the step size is calculated by running the internal loop in this algorithm in a trial and error manner, the method is very time consuming, swings in different iterations, and is frequently not in the descent direction (because the Hessian is not always positive-definite). The result is consistent with the reports of the optimization toolbox in MATLAB in which this method took 140 function evaluations to converge to the solution in the Rosenbrock's banana function, while the Levenberg-Marquardt took 90 and the steepest descent took 1000 function evaluations (Mathworks, 2006).

Finally, critically evaluating these methods, the second approach was used in this study. In order to update λ in each iteration, the optimization started with a large λ and decreased it as the search approached the solution. The following algorithm was implemented in the inverse code to update λ:

$$\lambda = 1$$
$$if \quad \phi(\beta)^{i+1} > 1$$
$$\qquad if \quad \phi(\beta)^{i+1} < \phi(\beta)^{i}$$
$$\qquad\qquad \lambda = \xi_1 * \lambda$$
$$\qquad else$$
$$\qquad\qquad \lambda = \xi_2 * \lambda$$
$$\qquad end$$
$$elseif \quad \phi(\beta)^{i+1} > 0.1$$
$$\qquad if \quad \phi(\beta)^{i+1} < \phi(\beta)^{i}$$
$$\qquad\qquad \lambda = \xi_3 * \lambda$$
$$\qquad else$$
$$\qquad\qquad \lambda = \xi_4 * \lambda$$
$$\qquad end$$
$$elseif \quad \phi(\beta)^{i+1} > 1 \times 10^{-2}$$
$$\qquad if \quad \phi(\beta)^{i+1} < \phi(\beta)^{i}$$

$$\lambda = \xi_5 * \lambda$$

$$else$$

$$\lambda = \xi_6 * \lambda$$

$$end$$

$$elseif \quad \phi(\beta)^{i+1} > 1 \times 10^{-3}$$

$$if \quad \phi(\beta)^{i+1} < \phi(\beta)^{i}$$

$$\lambda = \xi_7 * \lambda$$

$$else$$

$$\lambda = \xi_8 * \lambda$$

$$end$$

$$else \quad \phi(\beta)^{i+1} > 1 \times 10^{-4}$$

$$if \quad \phi(\beta)^{i+1} < \phi(\beta)^{i}$$

$$\lambda = \xi_9 * \lambda$$

$$else$$

$$\lambda = \xi_{10} * \lambda$$

$$end$$

$$end$$

where $\xi_1, \xi_3, \xi_5, \xi_7$, and ξ_9 are less than unity ($\xi_1 < \xi_3 < \xi_5 < \xi_7 < \xi_9$) and $\xi_2, \xi_4, \xi_6, \xi_8$, and ξ_{10} are greater than unity ($\xi_2 < \xi_4 < \xi_6 < \xi_8 < \xi_{10}$).

5.1.4. Termination Criteria for Inverse Code

To determine the most efficient stopping criteria, several rules were compared with each other. Pre-analysis of equation [4.12] suggests that a stopping rule based on the changes in the parameter values at each iteration (Eq. [4.27]) is not a good termination rule since, in some cases, parameters don't change significantly during several iterations then they change suddenly and produce significant reduction in the magnitude of the objective function.

The other termination criterion that was tested was the absolute and relative changes in the magnitude of the objective function in each iteration (Eq. [4.28]).

However, this is a case dependent rule. For small values of δ_1 and δ_2, the algorithm runs repeatedly without significant changes in the magnitude of the function value. For large δ_1 and δ_2 the solution may not be satisfactory. Therefore, the judicious choice of δ_1 and δ_2 is operational and case dependent.

In the optimization problems analyzed in this study, $\left\| \nabla \phi(\beta) \right\|_{\beta = \hat{\beta}}$ seldom converged to zero yet the solution was quite satisfactory. Large numbers of algorithm runs were required to obtain small changes in $\left\| \nabla \phi(\beta) \right\|_{\beta = \hat{\beta}}$ without significant changes in the values of model parameters being optimized. Carrera and Neuman (1986a, 1986b, 1986c) reported similar difficulties.

Finally, critically evaluating these rules, a combined termination criterion was selected to stop the iteration process in the inverse code:

$$if \ (\nabla \phi(\beta)_{\beta = \hat{\beta}} \leq \zeta \ \& \ \frac{\Delta \phi(\beta)}{\phi(\beta)} \leq \eta \ \& \ \phi(\beta) \leq \delta)$$
$$Stop$$
$$else$$
$$Continue \ Optimization \ Loop$$
$$end$$

where ζ, η, and δ are user defined small values.

5.2. Parameter Optimization in Biomolecule Transport in Living Cells

The developed inverse modeling strategy was used to simulate mobility of the GFP-tagged glucocorticoid receptor (GFP-GR) in the nucleus of mouse adenocarcinoma cell

line 3617 and to estimate the optimized values of the molecular diffusion coefficient and binding rate parameters. Before using the numerical model for parameter optimization purposes, it was validated by analytical solution (Oreskes *et al.,* 1994).

5.2.1. Formulation of the Forward Problem

Equation [4.30] was selected as the forward problem to simulate protein transport in the nucleus of mouse adenocarcinoma cell line 3617. The matrix equation [4.32] was used to solve the *forward problem*. An adaptive time step was used to solve the matrix equation. To validate the numerical model with the semi-analytical solution of Sprague *et al.,* (2004), the values of $D_c = 0$, $D_s = 0$ were used, which delete the second partial differential equation from equation [4.30] and collapses it to the mobile-immobile equation . The numerical solution of the forward problem, i.e. equation [4.32], was then compared with the analytical solution and the result depicted in Figures 5.5 and 5.6. As these Figures show there is excellent agreement between the analytical and numerical solutions. Figure 5.5 presents the average fluorescent intensity in the bleach spot, obtained by Eq. [4.33], while Figure 5.6 shows the spatial distribution of the free, $F(r, D_f, K_a^*, K_d, t)$,bound complex ,$C(r, D_f, K_a^*, K_d, t)$, and $F + C(r, D_f, K_a^*, K_d, t)$ GFP-GR inside and outside of bleach spot after photobleaching at times of 0, 0.01, 0.02, 0.05, 0.1, 0.2, 0.5, 1, and 2 seconds for case 13 in Table 5.3.

5.2.2. Formulation of the Inverse Problem: Optimization Scenarios

The following scenarios were considered in the optimization procedure:
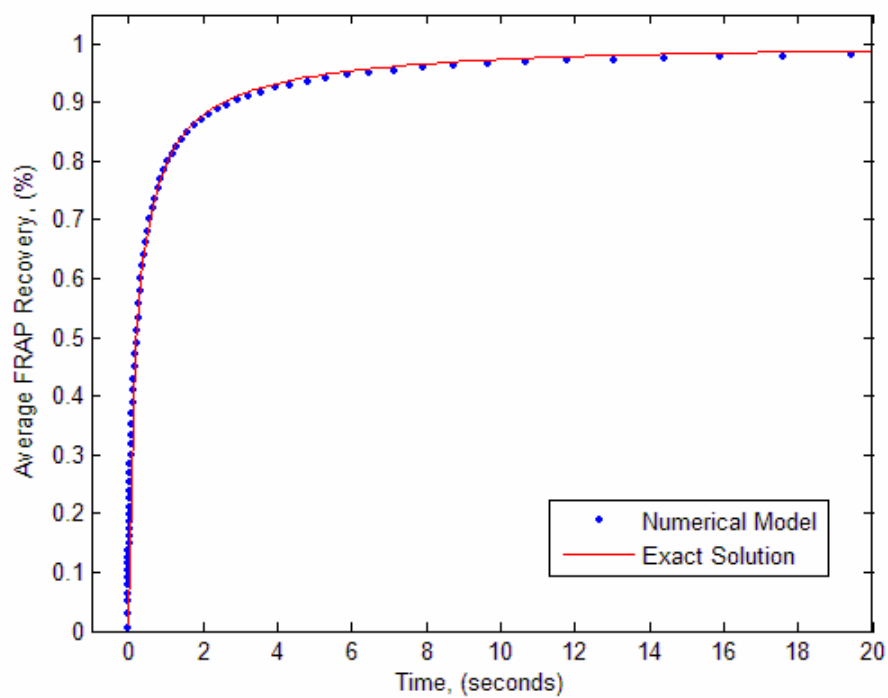
Figure 5.5. Validation of the numerical model with analytical solution.
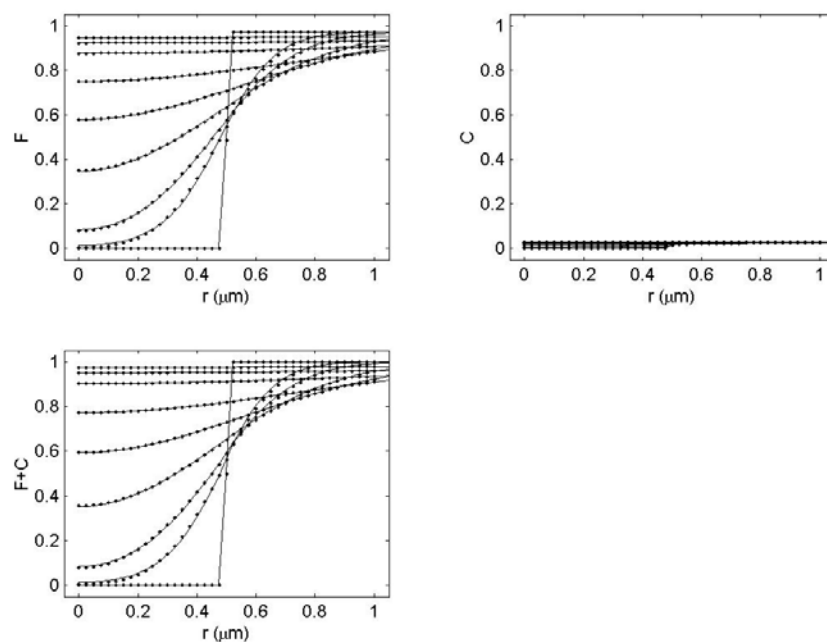
Figure 5.6. Spatial and temporal distribution of fluorescent inside bleach spot after photo bleaching (comparison of analytical (lines) and numerical (dots) solutions).

5.2.2.1. Scenario A: Estimation of Five Parameters for Full Reaction-Diffusion Model

In this case, five model parameters $[D_f, K_a, K_d, D_s, D_c]$ in equation [4.30] were estimated using the developed inverse modeling strategy and the experimental data in Table 4.1. The results are given in Table 5.2 and Figure 5.7, 5.8, and 5.9. The model shows excellent agreement with the experimental data.

Analysis of Table 5.2 reveals that the uncertainties in the estimates of D_f, K_a, and K_d are smaller than those of the diffusion coefficients of the binding sites and bound complex. The later show higher variances and wider confidence intervals. The Root Mean Squared Error (RMSE) and the coefficient of determination are 0.0233 and 0.9914, respectively. Equation [4.30] can describe more than 99 per cent of the temporal and spatial distributions of the fluorescence molecules inside bleached area of the mouse adenocarcinoma cell line 3617 during the course of the FRAP experiment.

If Eigenvalues of the Hessian matrix are positive definite and the gradient of the objective function at the solution is zero, then the solution is a strong local minimum. Table 5.2 shows that the first criterion holds in full but the second one holds only approximately. While the D_f, K_a, and K_d components of the gradient vector at solution are almost zero, the D_s and D_c components are not but the solution is quite satisfactory ($R^2 = 0.9914$ and $RMSE = 0.0233$). In all of the optimization problems studied in this research the gradient vector approached zero but didn't quite reach this limit value, yet the solutions were quite satisfactory with very high coefficient of determinations and very low RMSE.

Figures 5.8a and 5.8b show the temporal and spatial distributions of free GFP-GR

113
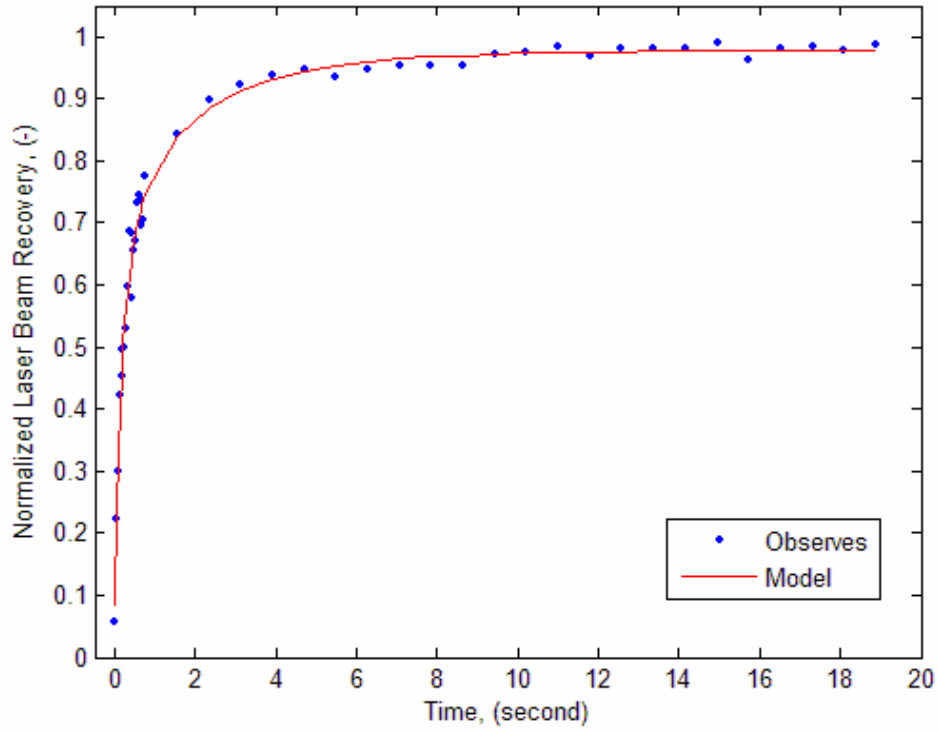
Figure 5.7. Predicted and experimental FRAP recovery for GFP-GR using equation [4.30].

Table 5.2. The results of parameter optimization for scenario A.

Parameter	Opt. Value	LL*	UL*	∇OF	$eigs(H)$	σ_p^2
$D_f(\mu m^2 s^{-1})$	2.1787	1.7332	2.6241	0.0002	0.001	0.0487
$K_a(s^{-1})$	7.2915	5.8936	8.6893	0.0000	0.0049	0.4798
$K_d(s^{-1})$	11.4267	10.7358	12.1175	0.0000	0.0090	0.1172
$D_s(\mu m^2 s^{-1})$	0.0169	-0.2249	0.2588	0.0221	0.4989	0.0143
$D_C(\mu m^2 s^{-1})$	0.0078	-0.0989	0.1146	0.0097	28.5584	0.0028

* 95% confidence interval on the optimized parameters.

114
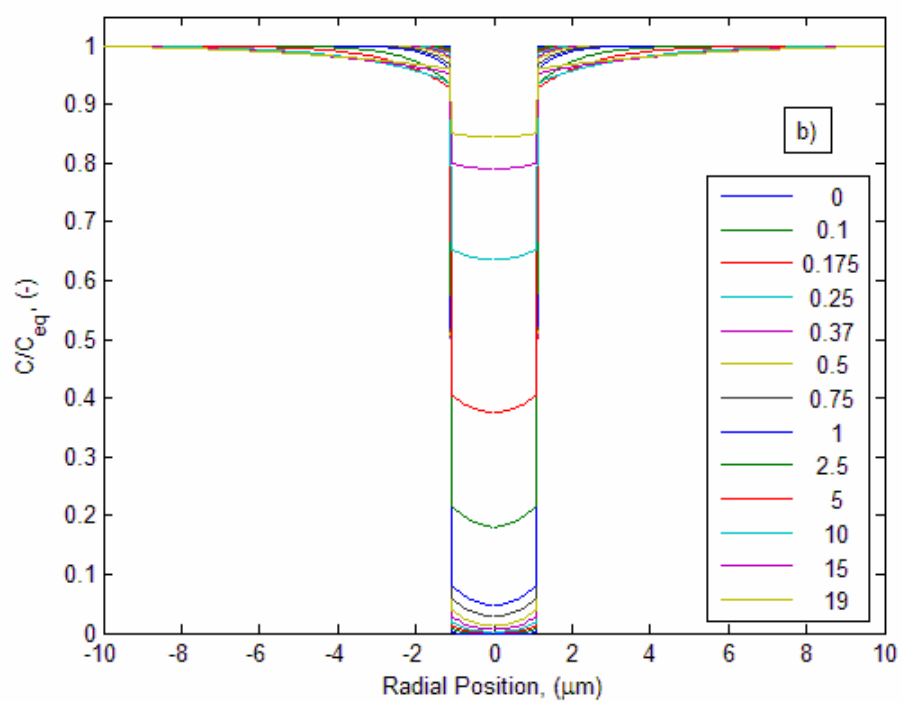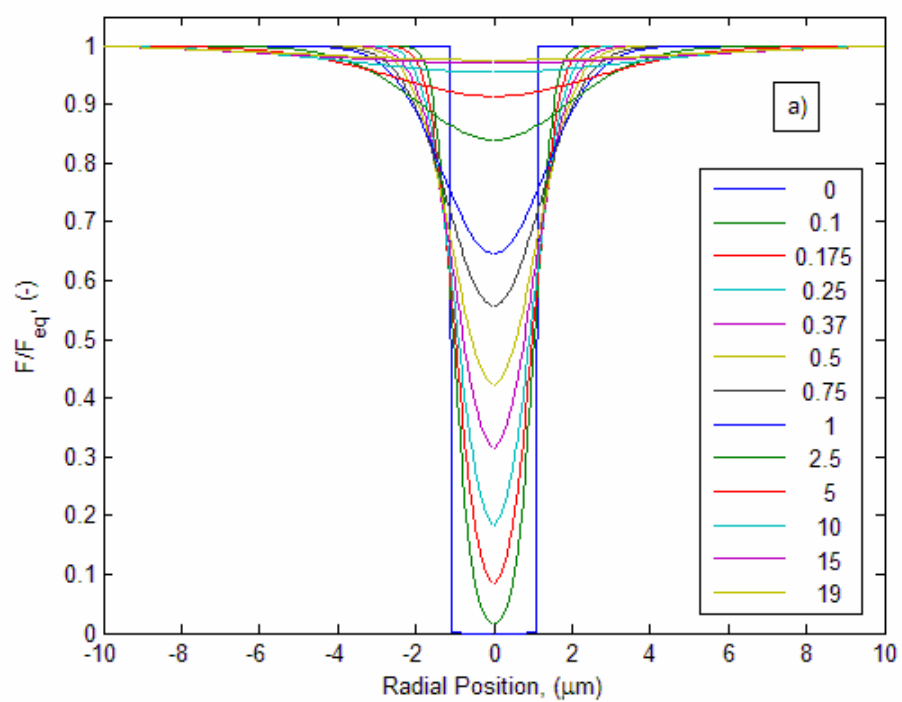
Figure 5.8. Temporal and spatial distribution of free GFP-GR (a) and bound complex (b) inside cell after photochemical bleaching.
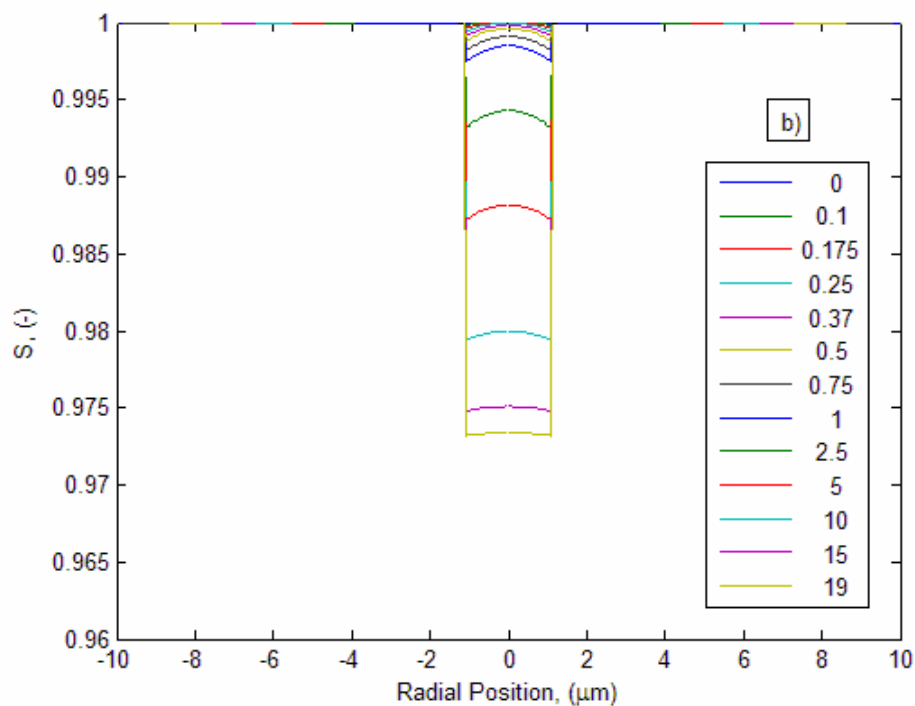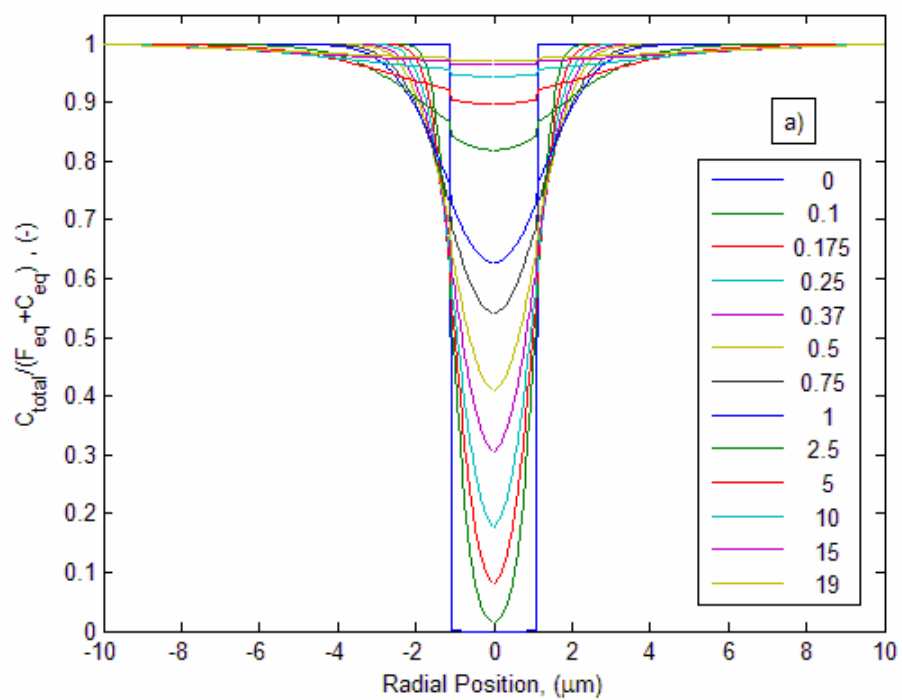
Figure 5.9. Temporal and spatial distribution of total fluorophores (a) and vacant binding sites (b) inside cell after photochemical bleaching.

and bound complex inside the cell after photochemical bleaching. The GFP-tagged free protein and bound complex move toward bleached area from the unbleached region. At the early stages of the experiment, the recovery is very fast but as time goes on the recovery becomes slow and finally reaches the state of equilibrium (in terms of fluorescent distribution inside cell) that the system had before photobleaching (at the end of the experiment the concentration of free protein and bound complex approach F_{eq} and C_{eq}). Note that the fluorophores are not completely recovered due to the loss of *light emission capability* in some of the fluorescence molecules.

Figure 5.9a presents distribution of total fluorescence molecules (free protein and bound complex) inside the nucleus as a function of radial direction over the time course of the FRAP experiment. The confocal microscope detects the fluorescent emission from both of these transport entities and cannot distinguish them. This is one of the shortcomings of the protocol since incorporating the free biomolecule information and the bound complex data in the framework of the multi-objective optimization may produce unique values for the model parameters (as will be discussed 5.3.2.1.2). Again the recovery is very quick at the early stages of the protocol and becomes slow as the experiment proceeds.

Figure 5.9b indicates temporal and spatial distributions of the vacant binding sites inside bleached region during the time course of the FRAP experiment (these four graphs are normalized). The Figure shows that during the experiment, the binding sites decrease slowly. At the beginning of the protocol ($t = 0$) all of the binding sites are vacant but as the experiment proceeds, the free protein from the unbleached zone move toward the bleached area and occupy the vacant binding sites. Therefore, it decreases gradually and

117

finally reaches ninety four per cent of the original concentration at the end of the experiment.

According to Figures 5.7, 5.8, and 5.9 and Table 4.2, the developed numerical model (Eq. [4.32]) and the inverse modeling strategy were successfully applied to simulate and predict the concentration of free biomolecule, bound complex, and vacant binding sites where both of adsorbent and adsorbate are moving transport entities. However, the optimized parameter values may be one of the possible solutions due the ill-posedness of the inverse problem which will be thoroughly discussed in the following sections.

5.2.2.2. Scenario B: Simultaneous Estimation of Mass Transport and Binding Rate Parameters for One-Site-Mobile-Immobile Model

In this scenario, the attempt was to simultaneously estimate the transport and binding parameters of GFP-GR by coupling the experimental data from Table 4.1, the developed optimization algorithm, and the numerical solution of equation [4.30] with $D_c = 0$, $D_s = 0$ (which reduces it to the one-site-mobile-immobile model) through the inverse modeling approach. Tables 5.3 and 5.4 lists the initial guesses and the optimized values for molecular diffusion coefficient (D_f), the pseudo- association rate coefficient (K_a^*), and the free protein-vacant binding site(s) dissociation rate coefficient (K_d). For each run, total concentration of free protein (F_{eq}), total concentration of bound complex (C_{eq}), the Root Mean Squared Error (RMSE), and the coefficient of determination are given as well. The simulated FRAP recovery is compared with the experimental one in Figure 5.10.

Analysis of Tables 5.3 and 5.4 reveals several points regarding the mobility and

Table 5.3. The results of parameter optimization for scenario B.

| run | Initial guesses | | | Optimized values | | | RMSE | R^2 |
	D_f $(\mu m^2 s^{-1})$	K_a^* (s^{-1})	K_d (s^{-1})	D_f $(\mu m^2 s^{-1})$	K_a^* (s^{-1})	K_d (s^{-1})		
1	1.3970	0.0106	0.2439	1.3454	0.0081	0.2490	0.0241	0.9904
2	15.0000	500	86.4000	13.5563	806	83	0.0233	0.9912
3	10.0000	20	50	1.2689	22.8800	538	0.0245	0.9903
4	1.2600	3000	5	79.7179	$1.06*10^4$	168	0.0236	0.9910
5	12.0000	30	490	1.8558	256	489	0.0244	0.9904
6	1.2000	200	49	7.4289	200	42.50000	0.0235	0.9911
7	7.0000	2	470	1.2248	4.7000	540.7200	0.0245	0.993
8	0.7000	202	0.0470	6.6616	56.3620	38.2500	0.0235	0.9910
9	1.5000	0.0010	85	1.2127	$7*10^{-5}$	91.2100	0.0246	0.9902
10	1.5000	0.1000	$1*10^{-5}$	1.2127	0.1874	$1*10^{-5}$	0.0245	0.9903
11	1.5000	$1*10^{-5}$	1	1.4652	0.1974	2.1902	0.0251	0.9900
12	9.2000	500	86.4000	8.3315	468.5600	83.3800	0.0234	0.9911
13	25.0000	0.0010	100	1.2534	1.3557	44.9400	0.0245	0.9903
14	0.2500	0.0010	100	1.2236	0.4235	119.7100	0.0245	0.9903
15	5.0000	400	0.4000	10.1911	396.8000	56.7000	0.0233	0.9911
16	15.0000	4	1400	1.2205	3.8100	1389	0.0245	0.9903
17	4.50000	150	385	4.3970	986	380	0.0242	0.9905
18	10.0000	150	385	8.8610	2458	396	0.0242	0.9905
19	0.4000	0.5000	0.0030	1.6371	0.5211	3.2000	0.0254	0.9901
20[#]	-	-	-	9.2000	500	86.4000	0.0255	0.9886

These values were obtained by Sprague *et al.* (2004).

Table 5.4. Concentration of free GFP-GR and bound complex and average diffusion and binding time for GFP-GR in scenario B.

run	F_{eq}	C_{eq}	$t_b(ms)$	$t_d(ms)$
1	0.9685	0.0315	4016	$1.2345*10^5$
2	0.0934	0.9066	12.0000	1.2407
3	0.9592	0.0408	1.9000	44.0000
4	0.0156	0.9844	6.0000	9.0000
5	0.6564	0.3436	2.0000	3.9100
6	0.1753	0.8247	23.5000	5.0000
7	0.9914	0.0086	1.8000	213.0000
8	0.4043	0.5957	26.1000	18.0000
9	1.000	0.0000	11.0000	15.0000
10	0.0001	0.9999	200	5336
11	0.9173	0.0827	456.6000	5066
12	0.1511	0.8489	12.0000	2.0000
13	0.9707	0.0293	22.3000	738
14	0.9965	0.0035	8.4000	2361
15	0.1250	0.8750	17.6000	2.5200
16	0.9973	0.0027	7.0000	262
17	0.2782	0.7218	2.6000	1.0000
18	0.1388	0.8612	2.50000	0.4000
19	0.8600	0.1400	312.5000	1919
20[*]	0.1474	0.8526	11.6000	2.0000

*These values were obtained by Sprague *et al.* (2004)

120
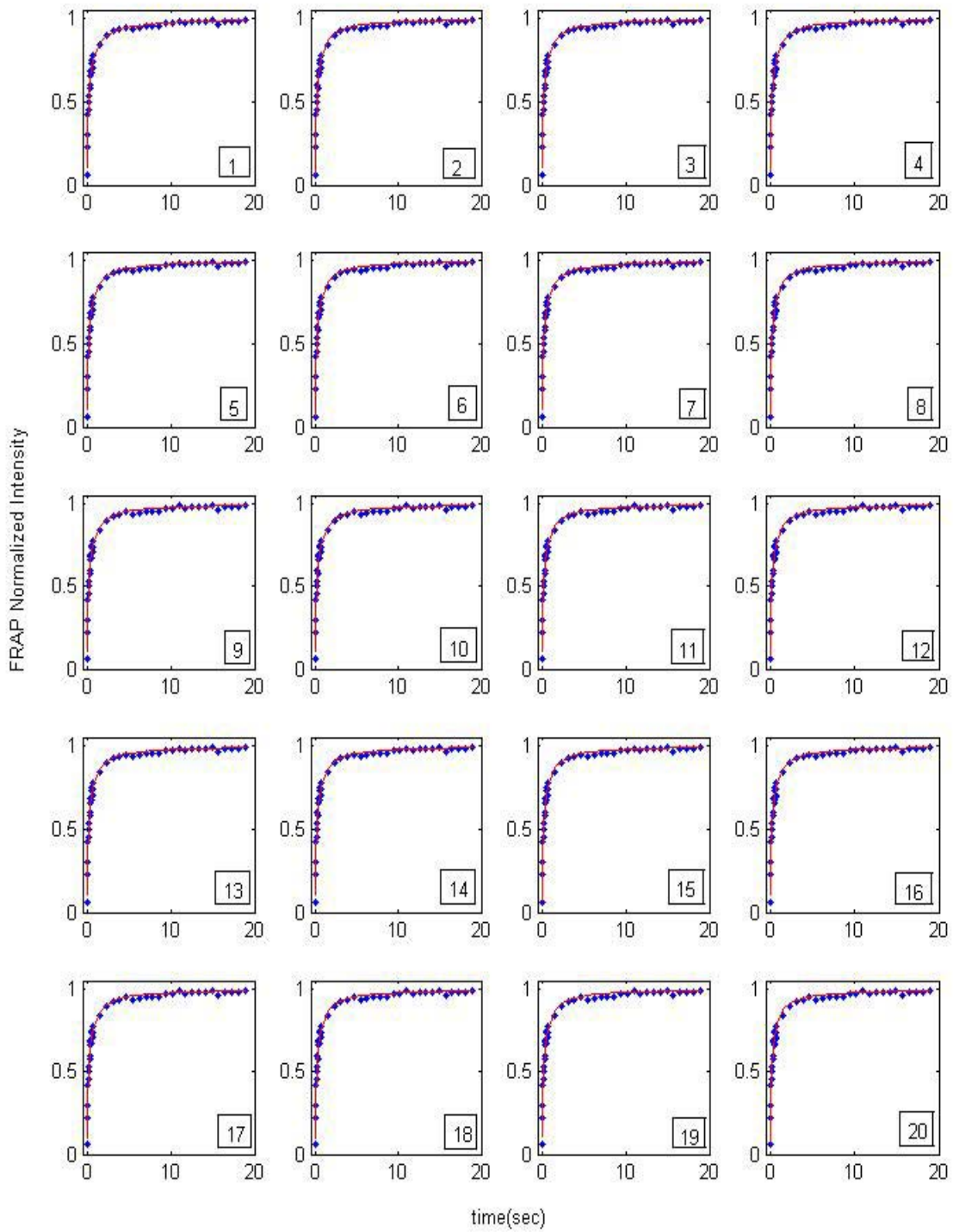
Figure 5.10. Predicted and experimental FRAP recovery curves for GFP-GR using one-site mobile-immobile model.

121

binding of GFP-GR inside the cell nucleus:

First, the primary rate kinetics or single-binding site model, Eq. [2.13], can satisfactorily describe the binding process of the GFP-GR inside nucleus. Therefore, the two-site-mobile-immobile model wasn't developed to simulate the mobility and binding reaction of GFP-GR inside nucleus.

Second, the estimated values for transport and binding parameters by Sprague e*t al.* (2004) are given as run 20 in Tables 5.3 and 5.4 and Figure 5.10 for comparison purpose. As these Tables and Figure 5.10 indicate there is a large number of combinations of three parameters that give essentially the same error level or objective function magnitude and produce excellent fits (only 20 runs were reported). In other words, the inverse problem is not well-posed and doesn't have a unique solution. This explains the conflicting and different parameters values reported in the literature for protein mass transport and binding rate parameters (Berg, 1986; Sprague e*t al.,* 2004, among many others). One of the reasons for the ill-posedness of the inverse problem is that the Fluorescence Recovery after Photobleaching protocol, though useful in studying the dynamics of cells, doesn't provide enough information to uniquely estimate the transport and binding parameters of biomolecules in living cells, simultaneously.

Third, the optimized values of the free molecular diffusion coefficient for GFP-GR range from 1.2 to 80 $\mu m^2 s^{-1}$ where 55 percent of the estimates are less than 2 $\mu m^2 s^{-1}$. These values are far smaller than those reported by previous investigators (Sprague *et al.,* 2004). Since we didn't take into account the effect of convective flux of biomolecules toward bleached area, the optimized values of molecular diffusion coefficient maybe somewhat overestimated in comparison to the "true" value.

Fourth, using equations [2.18] and [2.19] Sprague *et al.* (2004) concluded that 86 per cent of the GFP-GR is bound and only 14 per cent is free. This study suggests that using the FRAP experiment, one cannot identify how much of the biomolecule is free and how much is bound. As Table 5.4 shows the total concentration of free GFP-GR can range from zero to 100 percent. The same is true for concentration of the bound complex.

Fifth, the average binding time per vacant site, calculated by $t_b = 1/K_d$ (Sprague *et al.*, 2004), varies between 0.72 ms to 4.016 s. Again this is in contrast with the findings of Sprague *et al.*, (2004) that the average binding time per vacant site for GFP-GR is 12.7 mili-second.

Sixth, the average time for diffusion of GFP-GR from one site to the next, obtained by $t_d = 1/K_a^*$ (Berg, 1986), ranges between 0.4 ms to 34.3 hours ($1.2345 \times 10^5 s$) while Sprague *et al.*, (2004) reported that it is 2.5 ms and therefore GFP-GR samples the binding sites very quickly.

Finally, using experimental data from the FRAP protocol and by curve fitting, one cannot make conclusions regarding slow or rapid mobility of biomolecules as well as the rates of binding reaction.

These findings are in sharp contrast with the those by Kaufmann and Jain (1990) which claimed that using FRAP, one can simultaneously determine the biomolecule mass transport and binding parameters in vivo. The results of this study also do not confirm the results of Sprague *et al.*, (2004).

To further investigate the reason(s) for the ill-posedness of the inverse problem in FRAP experiment, a data set was generated by solving Eq. [4.32] for a hypothetical cell with prescribed initial and boundary conditions and parameter values: $D_f = 30 \mu m^2 s^{-1}$,

$D_S = 0 \mu m^2 s^{-1}$, $D_C = 0 \mu m^2 s^{-1}$, $K_a^* = 30 s^{-1}$, $K_d = 0.1108 s^{-1}$, and $w = 0.5 \mu m$. The procedure for data generation and perturbation was described in 4.2.2. The resulting signal and noise are depicted in Figure 5.11. The reason for selecting these parameter values for data generation and parameter optimization is that they represent a situation in which the Damkohler number is almost unity and neither of the diffusion and reaction regimes is dominant. Both of these processes are present in the experimental procedure. The parameter values also imply that the free GFP-GR molecules are mobile and the bound complex and the vacant binding sites are relatively immobile. The data were then used for parameter identification in cases C, D, and E below and posedness analysis in section 5.4.
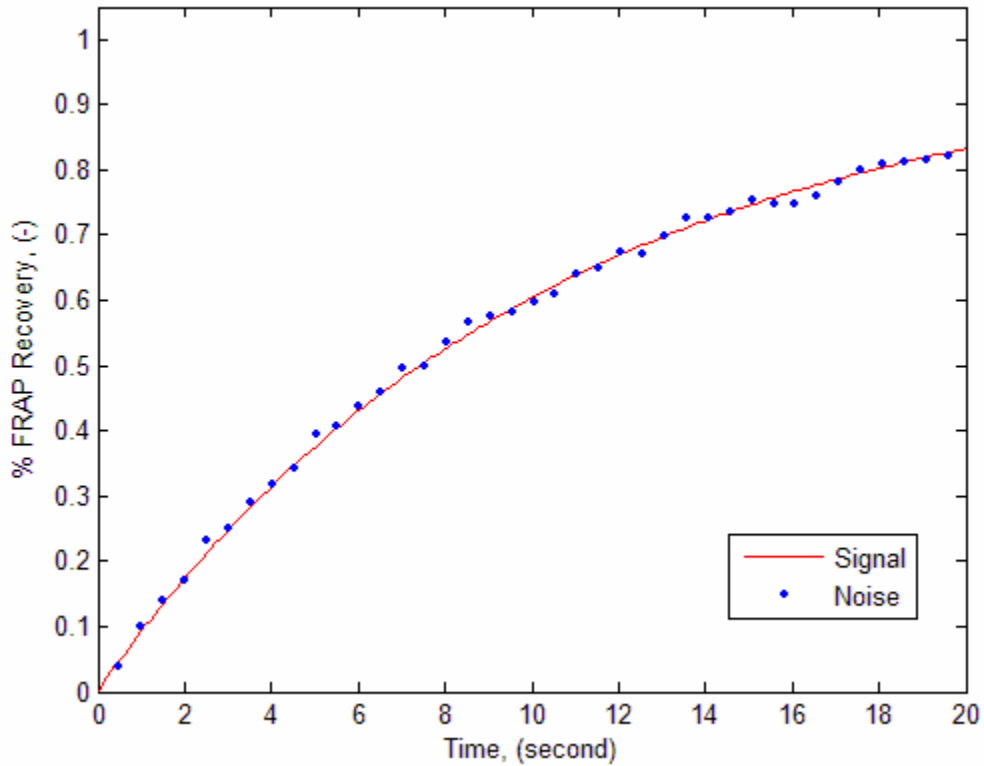
Figure 5.11. The generated noise free and noisy signal for FRAP protocol.

5.2.2.3. Scenario C: Estimation of Single Parameter for Mobile-Immobile Model

The results for this case are presented in Tables 5.5 to 5.7. As these Tables show, the FRAP protocol provides enough information to uniquely estimate one parameter provided that the true values of the other two parameters are known. This is true for both noise free and noisy data. The other important finding is the robustness and efficiency of the developed algorithm which converged to the "true" values of the parameters regardless of the initial guess. The initial guesses for the optimization procedure span twelve orders of magnitudes, but the developed inverse modeling strategy always converged to the "true" parameter values. The values in parentheses are those obtained using corrupted data and matched those obtained with noise free data.

5.2.2.4. Scenario D: Estimation of Two Parameters for Mobile-Immobile Model

In this case pairs of model parameters, under the assumption that the value of the third parameter was known, were estimated. In the first attempt, the optimized values of the binding rate coefficients were determined given a known value of the molecular diffusion coefficient of the GFP-GR. Again the optimization algorithm was used for both noise free and noisy data and the results are given in Table 5.8. As Table 5.8 indicates using the FRAP experiment coupled with the inverse modeling strategy and numerical model, one can uniquely estimate the individual values of the binding rate coefficients given the value of the molecular diffusion coefficient, for both noise free and noisy data, over a wide range of initial guesses.

The results for estimation of the free molecular diffusion coefficient and the dissociation rate parameter, for both noise free and noisy data, are presented in Table 5.9. Analysis of Table 5.9 indicate the FRAP protocol provides enough information to

Table 5.5. The results of optimization for scenario C (estimation of molecular diffusion coefficient in FRAP experiment).

Estimate D_f							
Initial guesses			Optimized values				
D_f $(\mu m^2 s^{-1})$	K_a^* (s^{-1})	K_d (s^{-1})	D_f $(\mu m^2 s^{-1})$	K_a^* (s^{-1})	K_d (s^{-1})	RMSE	R^2
3	30	0.1108	29.9975 (29.8032)	30	0.1108	0.00 (0.01)	1.0000 (0.9984)
5	30	0.1108	29.9968 (29.7362)	30	0.1108	0.00 (0.01)	1.0000 (0.9984)
10	30	0.1108	29.9968 (29.7978)	30	0.1108	0.00 (0.01)	1.0000 (0.9984)
15	30	0.1108	29.9959 (29.7483)	30	0.1108	0.00 (0.01)	1.0000 (0.9984)
20	30	0.1108	29.9972 (29.7490)	30	0.1108	0.00 (0.01)	1.0000 (0.9984)
45	30	0.1108	29.9974 (29.7376)	30	0.1108	0.00 (0.01)	1.0000 (0.9984)
1000	30	0.1108	29.9973 (29.7507)	30	0.1108	0.00 (0.01)	1.0000 (0.9984)
500	30	0.1108	29.9969 (29.7910)	30	0.1108	0.00 (0.01)	1.0000 (0.9984)

Table 5.6. The results of optimization for scenario C (estimation of pseudo-association rate constant in FRAP experiment).

Estimate K_a^*							
Initial guesses			Optimized values				
D_f $(\mu m^2 s^{-1})$	K_a^* (s^{-1})	K_d (s^{-1})	D_f $(\mu m^2 s^{-1})$	K_a^* (s^{-1})	K_d (s^{-1})	RMSE	R^2
30	3.00	0.1108	30	30.0032 (30.3523)	0.1108	0.00 (0.01)	1.000 (0.998)
30	1×10^{-3}	0.1108	30	29.9982 (30.2455)	0.1108	0.00 (0.01)	1.000 (0.998)
30	1×10^{-6}	0.1108	30	30.0031 (30.2468)	0.1108	0.00 (0.01)	1.000 (0.998)
30	1×10^{6}	0.1108	30	30.0030 (30.2478)	0.1108	0.00 (0.01)	1.000 (0.998)
30	1×10^{3}	0.1108	30	30.0031 (30.2507)	0.1108	0.00 (0.01)	1.000 (0.998)
30	300.00	0.1108	30	30.0030 (30.3188)	0.1108	0.00 (0.01)	1.000 (0.998)
30	10.00	0.1108	30	30.0030 (30.2115)	0.1108	0.00 (0.01)	1.000 (0.998)
30	0.050	0.1108	30	30.0030 (30.1655)	0.1108	0.00 (0.01)	1.000 (0.998)

Table 5.7. The results of optimization for scenario C (estimation of dissociation rate coefficient in FRAP experiment).

Estimate K_d							
Initial guesses			Optimized values				
D_f $(\mu m^2 s^{-1})$	K_a^* (s^{-1})	K_d (s^{-1})	D_f $(\mu m^2 s^{-1})$	K_a^* (s^{-1})	K_d (s^{-1})	$RMSE$	R^2
30	30	0.0008	30	30	0.1108 (0.1107)	0.0000 (0.0102)	1.000 (0.998)
30	300	0.8000	30	30	0.1108 (0.1107)	0.0000 (0.0102)	1.000 (0.998)
30	30	0.0001	30	30	0.1108 (0.1107)	0.0000 (0.0102)	1.000 (0.998)
30	30	1.0000	30	30	0.1108 (0.1107)	0.0000 (0.0102)	1.000 (0.998)
30	30	0.0500	30	30	0.1108 (0.1107)	0.0000 (0.0102)	1.000 (0.998)
30	30	0.0010	30	30	0.1108 (0.1107)	0.0000 (0.0102)	1.000 (0.998)
30	30	1×10^{-5}	30	30	0.1108 (0.1108)	0.0000 (0.0102)	1.000 (0.998)
30	30	1×10^{-6}	30	30	0.1108 (0.1107)	0.0000 (0.0102)	1.000 (0.998)

Table 5.8. The results of optimization for scenario D (estimation of two parameters in FRAP experiment: K_a^*-K_d).

Estimate K_a and K_d							
Initial guesses			Optimized values				
D_f $(\mu m^2 s^{-1})$	K_a^* (s^{-1})	K_d (s^{-1})	D_f $(\mu m^2 s^{-1})$	K_a^* (s^{-1})	K_d (s^{-1})	$RMSE$	R^2
30	90	0.005	30	30.0246 (32.7366)	0.1108 (0.1122)	0.00 (0.01)	1.000 (0.99)
30	20	0.01	30	29.9762 (28.8955)	0.1108 (0.1101)	0.00 (0.01)	1.000 (0.99)
30	250	0.01	30	30.0729 (33.7009)	0.1108 (0.1128)	0.00 (0.01)	1.000 (0.99)
30	435	0.0005	30	30.1108 (34.2443)	0.1108 (0.1131)	0.00 (0.01)	1.000 (0.99)
30	10	0.01	30	29.9576 (31.8386)	0.1108 (0.1118)	0.00 (0.01)	1.000 (0.99)
30	100	1	30	30.0027 (36.0428)	0.1108 (0.1141)	0.00 (0.01)	1.000 (0.99)
30	100	$2*10^6$	30	30.0209 (33.8034)	0.1108 (0.1129)	0.00 (0.01)	1.000 (0.99)
30	1000	0.5	30	30.0082 (32.7609)	0.1108 (0.1122)	0.00 (0.01)	1.000 (0.99)

Table 5.9. The results of optimization for scenario D (estimation of two parameters in FRAP experiment: D_f-K_d).

Estimate D_f and K_d							
Initial guesses			Optimized values				
D_f $(\mu m^2 s^{-1})$	K_a^* (s^{-1})	K_d (s^{-1})	D_f $(\mu m^2 s^{-1})$	K_a^* (s^{-1})	K_d (s^{-1})	$RMSE$	R^2
8	30	0.008	30.0111 (27.528)	30	0.1108 (0.1122)	0.000 (0.0101)	1.000 (0.998)
48	30	0.08	29.9972 (29.935)	30	0.1108 (0.1108)	0.000 (0.0101)	1.000 (0.998)
8	30	1	29.9989 (28.204)	30	0.1108 (0.1118)	0.000 (0.0101)	1.000 (0.998)
80	30	1	30.0100 (28.294)	30	0.1108 (0.1117)	0.000 (0.0101)	1.000 (0.998)
150	30	0.01	30.0156 (36.477)	30	0.1108 (0.1077)	0.000 (0.0104)	1.000 (0.998)
0.150	30	0.1	30.0005 (27.822)	30	0.1108 (0.1120)	0.000 (0.0101)	1.000 (0.998)
15	30	0.001	30.0090 (24.555)	30	0.1108 (0.1143)	0.000 (0.0102)	1.000 (0.998)
150	30	0.001	30.0142 (188.225)	30	0.1108 (0.0946)	0.000 (0.0133)	1.000 (0.998)

Table 5.10. The results of optimization for scenario D (estimation of two parameters in FRAP experiment: D_f-K_a^*)

Estimate D_f and K_a^*							
Initial guesses			Optimized values				
D_f $(\mu m^2 s^{-1})$	K_a^* (s^{-1})	K_d (s^{-1})	D_f $(\mu m^2 s^{-1})$	K_a^* (s^{-1})	K_d (s^{-1})	$RMSE$	R^2
50	3	0.1108	3.8162 (6.9081)	4.1352 (7.2953)	0.1108	0.0042 (0.0104)	0.9997 (0.9983)
3	50	0.1108	47.7952 (35.6424)	47.5709 (35.8541)	0.1108	0.0003 (0.0102)	1.0000 (0.9984)
20	25	0.1108	25.2109 (25.2109)	25.2769 (25.2769)	0.1108	0.0001 (0.0001)	1.0000 (1.0000)
25	20	0.1108	24.5737 (24.5737)	24.6488 (24.6488)	0.1108	0.0002 (0.0002)	1.0000 (1.0000)
28	35	0.1108	34.8874 (34.8874)	34.8255 (34.8255)	0.1108	0.0001 (0.0001)	1.0000 (1.0000)
0.1	100	0.1108	89.9205 (89.9205)	89.1097 (89.1097)	0.1108	0.0005 (0.0005)	1.0000 (1.0000)
100	0.1	0.1108	8.5511 (8.5511)	8.8336 (8.8336)	0.1108	0.0017 (0.0017)	1.0000 (1.0000)
28	28	0.1108	28.2015 (28.2015)	28.2282 (28.2282)	0.1108	0.0001 (0.0001)	1.0000 (1.0000)

uniquely estimate the molecular diffusion coefficient and dissociation rate coefficient.

Finally, fixing K_d on the known value, the optimized values of the free molecular diffusion coefficient and pseudo-association rate constant were estimated for both noise free and noisy data. The results are shown in Table 5.10 which indicates that the FRAP experiment doesn't provide enough information for unique simultaneous estimation of the molecular diffusion coefficient and pseudo-association rate constant even for noise free data. One needs to have one of them and try to estimate the other one from the FRAP data using inverse modeling strategy.

It can be argued that the reason for the ill-posedness of the inverse problem lies in the relationship between the free molecular diffusion coefficient and the pseudo-association rate constant. To further investigate the possibility of high inter-correlation between these two parameters, the parameter correlation matrix was calculated using equation [4.71]:

$$COR(P) = \begin{bmatrix} 1.0000 & 0.9890 & -0.2487 \\ 0.9890 & 1.0000 & -0.1196 \\ -0.2487 & -0.1196 & 1.0000 \end{bmatrix}$$

Where the diagonal elements of the matrix are correlation of each parameter with itself which is unity. Correlation between the molecular diffusion coefficient and the free protein-vacant binding site(s) pseudo-association rate constant is very high ($r_{D_f - K_a^*} = 0.989$), while those of $r_{D_f - K_d}$ and $r_{K_a^* - K_d}$ are -0.2487 and -0.1196, respectively.

The signs of the elements of the correlation matrix are physically reasonable because based on the primary rate kinetics, Eq. [2.13], one expects a negative correlation between D_f and K_d as well as between K_a and K_d. We also expect positive correlation

between K_a and D_f.

Based on these results, it's clear that the high inter-correlation between the molecular diffusion coefficient and the pseudo-association rate constant makes it impossible to obtain a unique solution for the inverse problem using the experimental data from the FRAP protocol. The common practice in these situations is to fix one of the parameter and estimate the other one by parameter optimization algorithms.

The biological process behind this phenomenon is of particular interest and requires more investigations. Referring to equation [2.13] one may propose a possible explanation for this high inter-correlation. As the molecular diffusion coefficient increases it promotes the biochemical reaction [2.13] towards right and increases the possibility of interaction between free GFP-GR and the vacant binding site(s), and hence indirectly increases the free protein–to-vacant binding site(s) association rate. The movement of the free GFP-GR toward vacant binding site(s) is a necessary but not sufficient condition for interaction. There may be other reasons for this phenomenon which needs to be investigated.

5.2.2.5. Scenario E: Estimation of Three Parameters for Noise Free FRAP Data

In this scenario, the attempt was to estimate the optimized values of the mass transport and binding rate parameters for noise free data. The results presented in Table 5.12. As the Table indicates, it is impossible to obtain unique simultaneous estimation for mass transport and binding rate parameters even for noise free data. The reason, as pointed out, is the high inter-correlation between the free molecular diffusion coefficient and the pseudo-association rate coefficient.

The proposed approach to uniquely estimate the mass transport and binding rate

130

parameters from the FRAP protocol would be conducting two FRAP experiments on the same class of biomolecule and the same cell in two different regimes. One experiment may be used to measure the molecular diffusion coefficient of the biomolecule independent of binding under diffusion dominant regime. One way to perform this, is using a biomolecule of the same molecular weight and class (but with different surface properties) as the biomolecule under study, but one which doesn't have reaction with the vacant binding site(s). Having determined the diffusion coefficient in diffusion dominant regime, one can determine the individual values of the reaction rate coefficients under either reaction dominant regime or diffusion-reaction regime. Experimentally, this approach is a viable procedure for drugs, antigens, and proteins. This procedure coupled with the parameter optimization algorithms yields the most clinically relevant parameter values to improve the delivery of agents to their targets in cells and tissues.

Table 5.11. The results of optimization for case E (estimation of three parameters for noise free FRAP data).

Estimate D_f, K_d, and K_a^*							
Initial guesses			Optimized values				
D_f $(\mu m^2 s^{-1})$	K_a^* (s^{-1})	K_d (s^{-1})	D_f $(\mu m^2 s^{-1})$	K_a^* (s^{-1})	K_d (s^{-1})	$RMSE$	R^2
20	43	0.01	41.8564	42.7664	0.1112	0.0002	1.0000
200	43	0.01	170.9403	166.9715	0.1106	0.0006	1.0000
27	28	0.01	27.7434	27.6444	0.1107	0.0001	1.0000
29	29	0.01	29.0008	29.0018	0.1108	0.0000	1.0000
29	29	0.001	21.8680	21.5410	0.1104	0.0002	1.0000
29	290	0.0001	276.5849	287.3558	0.1117	0.0005	1.0000
15	500	0.0001	462.2080	491.3985	0.1121	0.0005	1.0000
15	0.5	0.8	3.65890	3.6106	0.1087	0.0043	0.9997

5.3. Parameter Optimization in Water Flow through Partially Saturated Porous Media

The second mass transport problem to be optimized was chosen to be fluid flow in partially saturated porous media. Fluid flow has crucial role in the delivery of drugs and nutrients to cells, tissues, and organs as well as the transport of industrial, agricultural, bacterial, and viral pollutants to surface and groundwater resources, and hence causing carcinogenic and water borne diseases. Therefore, accurate prediction of fluid flow parameters is important in model prediction of fluid flow and species transport in porous materials. As an example of the fluid flow through porous media, the water flow in variably saturated soil was investigated. Both homogeneous and heterogeneous soils were considered.

5.3.1. Formulation of the Forward Problem

Equations [2.21] and [2.23] were selected as *forward problem*. In the following sections, the numerical simulators of these equations were compared with the "exact solution" and with each other in terms of accuracy, mass conservation, possible convergence problem, and oscillatory behavior. The most efficient, mass-conservative, and accurate simulator was selected to be implemented in the framework of the inverse code. The adaptive time step procedure, validation of the numerical simulators of different forms of Richards' equation using both the finite element and finite difference approximations, and mass conservation properties of the simulators were discussed and analyzed in the following sections.

5.3.1.1 Adaptive Time Step

To develop an efficient adaptive time step strategy the values of dt_{max} and dt_{min} were determined by trial and error. To determine dt_{max} in the adaptive time step approach, the simulation started with initial time increment of $\Delta t = 0.1$ day. As Figure 5.12 indicates the finite element simulators (both distributed and lumped stiffness mass matrix) of the h-form and mixed form Richards' equations show appreciable discrepancy with the "exact solution" except for the early stages of the simulation. The result for the finite difference simulation presented in Figure 5.13. Similar to the finite element solution of the Richards' equation, both schemes of the finite difference approximation (fully implicit
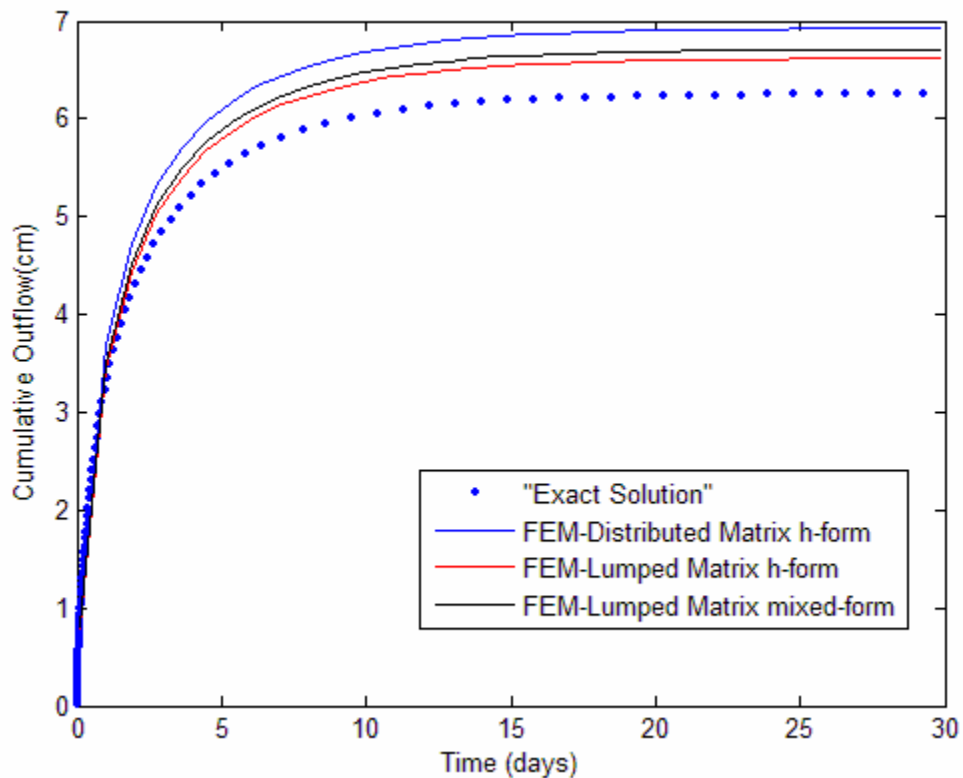
Figure 5.12. Comparison of the linear finite element solution of the h-based form and mixed form Richards' equation with the "exact solution" for initial time increment of $\Delta t = 0.1$ day.
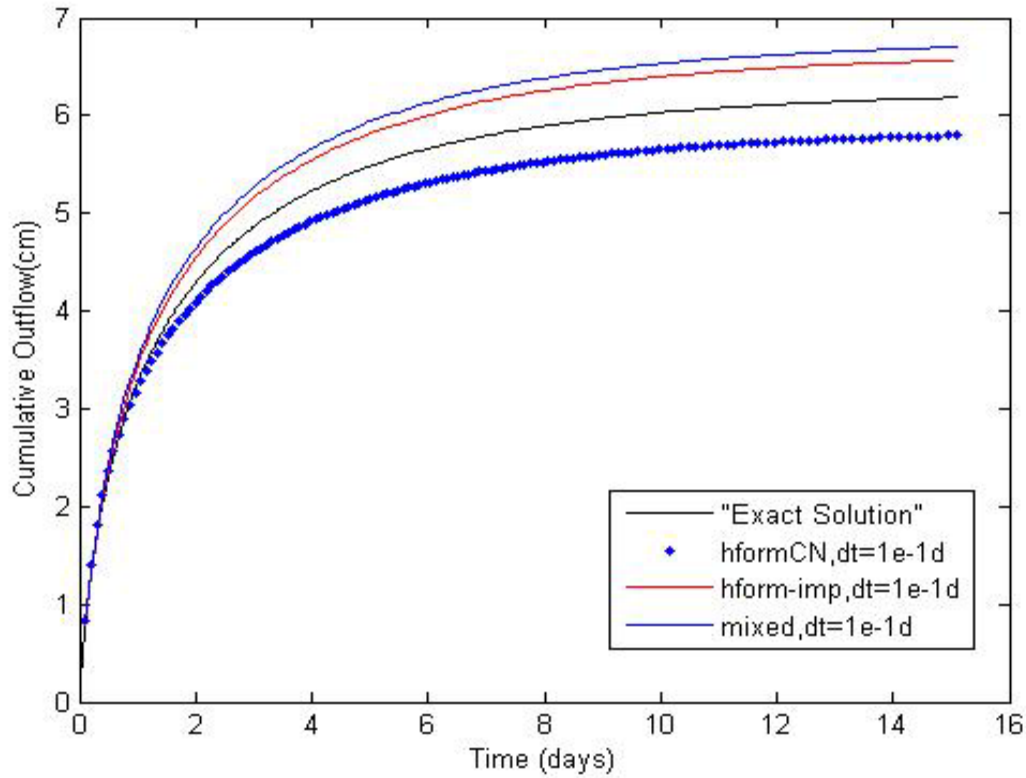
Figure 5.13. Comparison of the finite difference solution of the h-based and mixed forms of the Richards' equation with exact solution for initial time increment of $\Delta t = 0.1$ day.

and Crank-Nicolson) produced poor results for initial time increment of $\Delta t = 0.1$ day. This was more pronounced for the distributed mass matrix formulation in the finite element method and the mixed and fully implicit finite difference schemes. Excellent results were obtained with $\Delta t = 1 \times 10^{-2} day$ which will be discussed in the next section on the validation of the numerical simulators. Therefore, for the drainage experiment considered in this study, the maximum and minimum time increments in the adaptive time step loop were set to $dt_{max} \leq 0.085 day$ and $dt_{min} \geq 1 \times 10^{-4} day$, respectively.

5.3.1.2. Validation of the Numerical Simulators

5.3.1.2.1. h-form Richards' Equation

The numerical solution of the forward model was validated by an "exact solution" (Oreskes *et al.,* 1994). Since it was very difficult or actually impossible to obtain analytical solution for nonlinear Richards' equation without imposing simplifying assumptions about the soil water characteristic relationship, the "exact solution" was obtained by numerical solution of the forward model for dense grid with very fine time step ($\Delta z = 0.1 cm$ and $\Delta t = 1 \times 10^{-9} day$) using prescribed initial and boundary conditions. The soil water hydraulic parameters were as follow: $K_s = 12.50 cmd^{-1}$, $\alpha = 0.014 cm^{-1}$, $n = 1.5$, $\theta_s = 0.33$, $\theta_r = 0.05$, and $\iota = 0.5$. The numerical solutions of the different forms of the one-dimensional Richards' equation obtained on coarse grid ($\Delta z = 2.5 cm$ and $\Delta t = 1 \times 10^{-2} day$) were then compared with the "exact solution". The numerical simulators were compared with the exact solution in terms of the cumulative outflow, calculated by Eq. [4.65], as a function of time.

Figure 5.14 presents the comparison of the linear finite element solution of the h-based form Richards' equation with the "exact solution". Both the distributed and mass lumped schemes show excellent agreement with the exact solution for initial time increment of $\Delta t = 0.01 day$. The result is rather surprising for the distributed mass matrix because, as discussed in chapter two, there are numerous reports about the convergence problem and oscillatory behavior of this scheme. However, as Figure 5.12 indicated earlier, this scheme does have the lowest accuracy when the time increment is large.

The finite difference solution of the h-based form Richards' equation is presented in Figures 5.15a and 5.15b. Both the fully implicit and Crank-Nicolson approximations

135
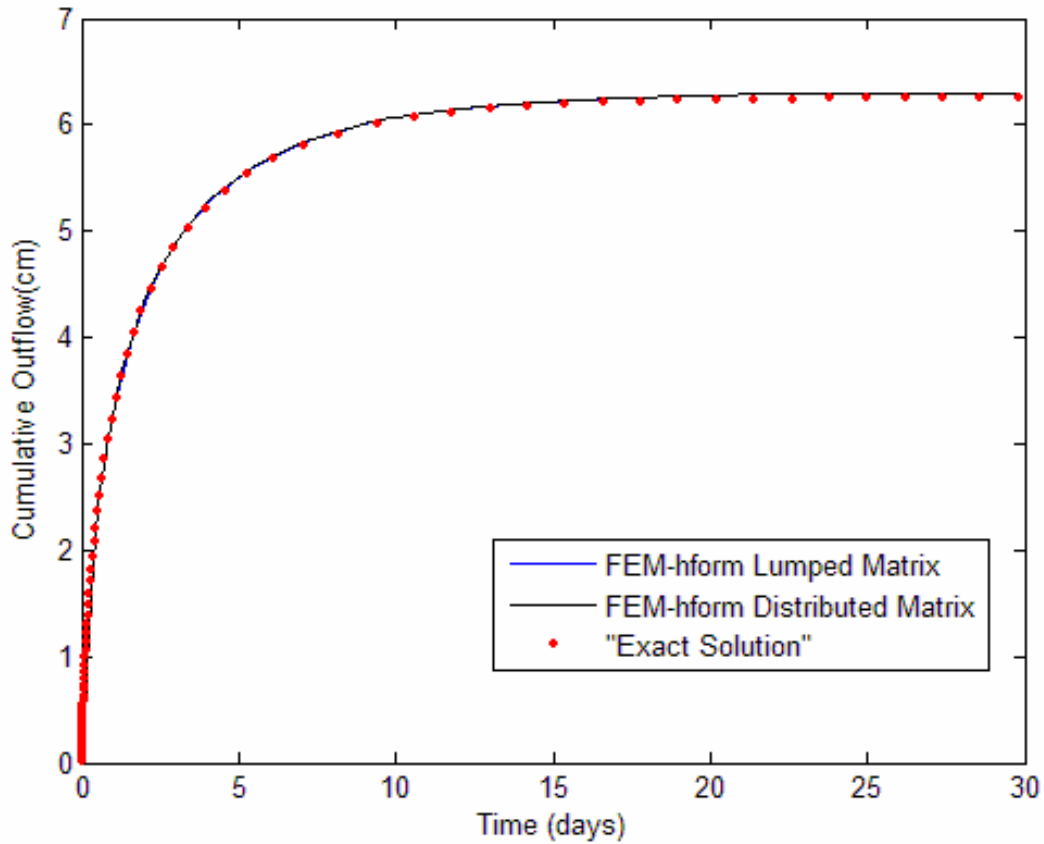
Figure 5.14. Comparison of the linear finite element solution of the h-based form
Richards' equation with the "exact solution" for initial time increment of
$\Delta t = 0.01$ day.

show excellent agreement with the "exact solution" for initial time increment of

$\Delta t = 0.01$ day, though the Crank-Nicolson approach required more Picard iterations to

converge due to the contribution of the explicit scheme in the formulation and produced

poor mass balance for larger time increment which will be discussed in 5.3.1.3. The finite

difference numerical simulators were also used to produce temporal and spatial

distributions of soil moisture content and soil water pressure head profiles during

drainage of a fully saturated soil and infiltration into a homogeneous and very dry soil

which will be compared with those of "exact solution" in Figures 5.17, 5.18, and 5.19.
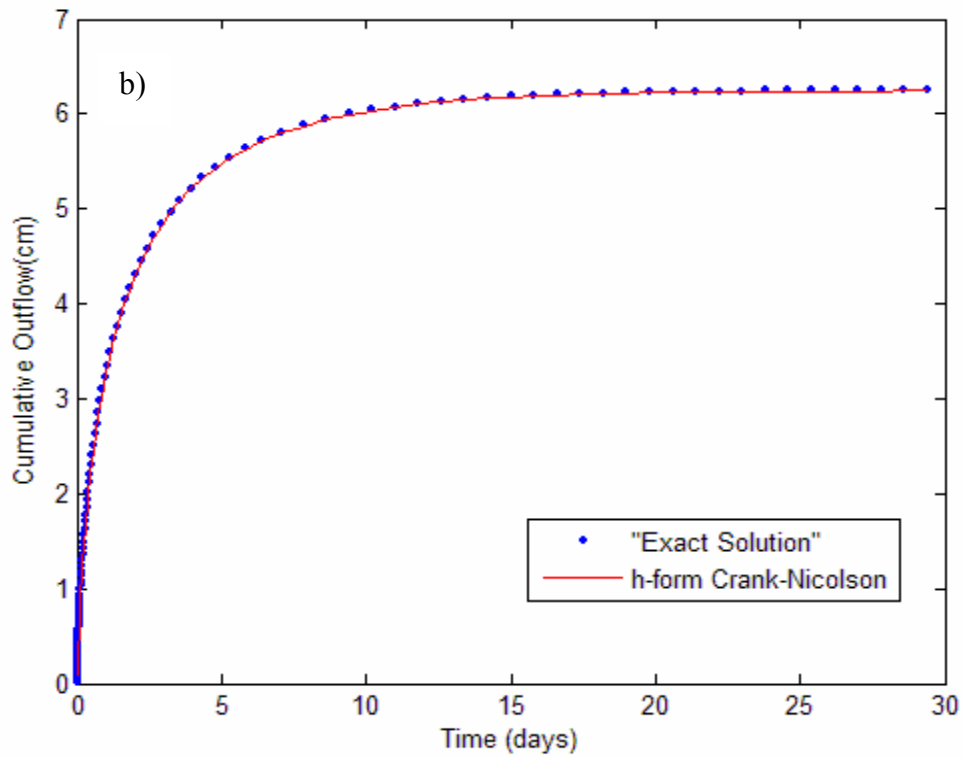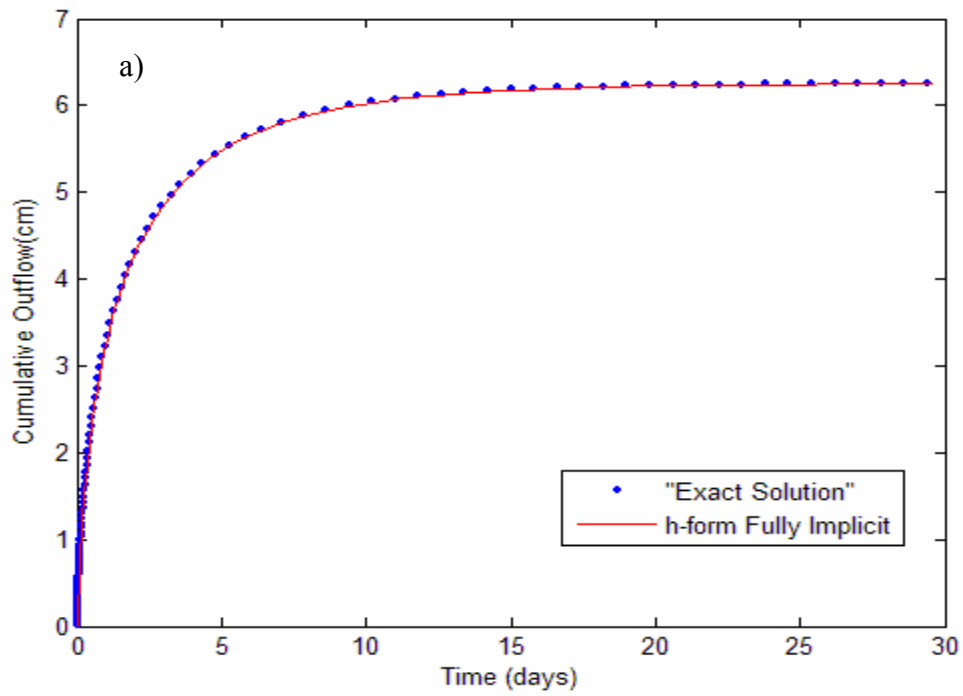
Figure 5.15. Comparison of the finite difference solution of the h-based Richards'
equation with the "exact solution": Fully Implicit scheme (a) and Crank-
Nicolson method (b).

5.3.1.2.2. Mixed-form Richards' Equation

Figure 5.16 presents the comparison of the fully implicit finite difference and the mass lumped linear finite element solutions of the mixed form Richards' equation with the "exact solution". The mass lumped linear finite element solution shows excellent agreement with the "exact solution". However, the finite difference simulator shows some discrepancies as drainage proceeds. It slightly overestimates the outflow from the soil. The temporal and spatial distributions of the soil water pressure head and soil moisture content produced by the linear finite element solution of the mixed form Richards' equation were compared with those of the "exact solution" in Figures 5.17, 5.18, and 5.19.
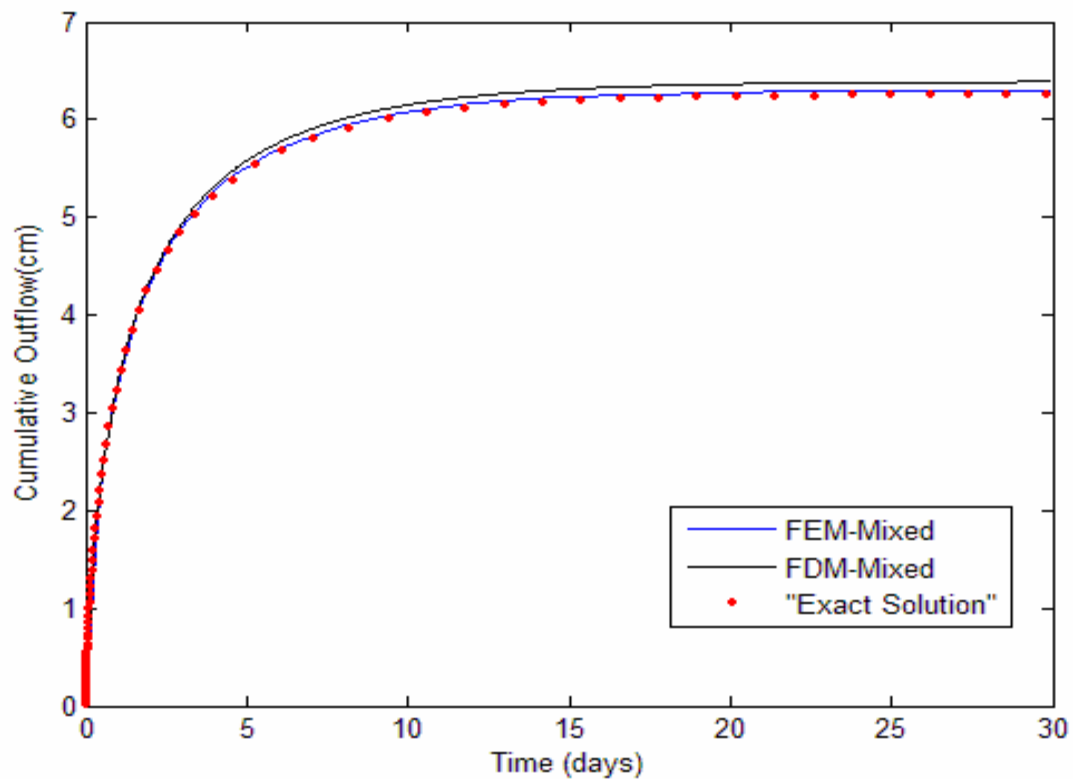
Figure 5.16. Comparison of the linear finite element and finite difference solutions of the mixed form Richards' equation with "exact solution".

5.3.1.2.3. Switching Algorithm

Some investigators reported that the mixed form Richards' equation has shown problems in modeling saturated flow (Gui *et al.*, 2002; Hao *et al.*, 2005). Although the mixed form was successful in modeling water flow in the optimization problems considered in this study, for troublesome situations a mass-conservative switching algorithm was proposed and evaluated with the numerical test problems in the present study. The proposed switching algorithm uses the mixed form of the Richards' equation in the unsaturated zone and switches to the h-based form at and near the saturated zone. A threshold value for soil water pressure head was chosen and incorporated in the code. For soil water pressure heads less than the threshold value, the mixed form of the Richards' equation was used. The algorithm switches to the h-based form for soil water pressure heads equal or greater than the threshold value. To determine the threshold value, different soil water pressure heads were tried and the corresponding mass balance errors were compared with each other. The pressure head value of -2.5 cm ($h_0 = -2.5cm$) produced the lowest error. Similar idea was also reported by others during the preparation of this manuscript (Hao *et al.*, 2005).

The proposed algorithm was tested against two numerical test problems. The first problem was drainage of a fully saturated soil with zero flux boundary condition at the top of the domain and free drainage ($q = K$) boundary condition at the bottom (both boundary conditions are Neumann type). The soil hydraulic parameters that were used to test the switching algorithm are $\alpha = 0.014 cm^{-1}$, $n = 1.5$, $K_s = 12.50 cmd^{-1}$, $\theta_s = 0.33$, $\theta_r = 0.05$, and $\iota = 0.5$.

Figure 5.17 presents the spatial and temporal distributions of the soil water

pressure head during the course of a drainage experiment reproduced by the proposed switching algorithm for times 0.0, 0.02, 0.1, 0.2, 0.5, 1, 2, 5, 10, and 20 days after the initiation of drainage. The solid line shows the reference solution which was obtained by solving the h-form of the Richards' equation using very dense mesh and small time steps as outlined before. The points indicate the switching algorithm solved using a coarse mesh and larger time steps ($\Delta z = 2.5cm$ and $\Delta t = 1\times10^{-2} day$). As the Figure indicates there are excellent agreements between the two solutions.

The second problem is infiltration into a very dry, homogeneous, and semi-infinite soil with uniform initial soil water pressure head ($h_i = -1\times10^4 cm$). The same
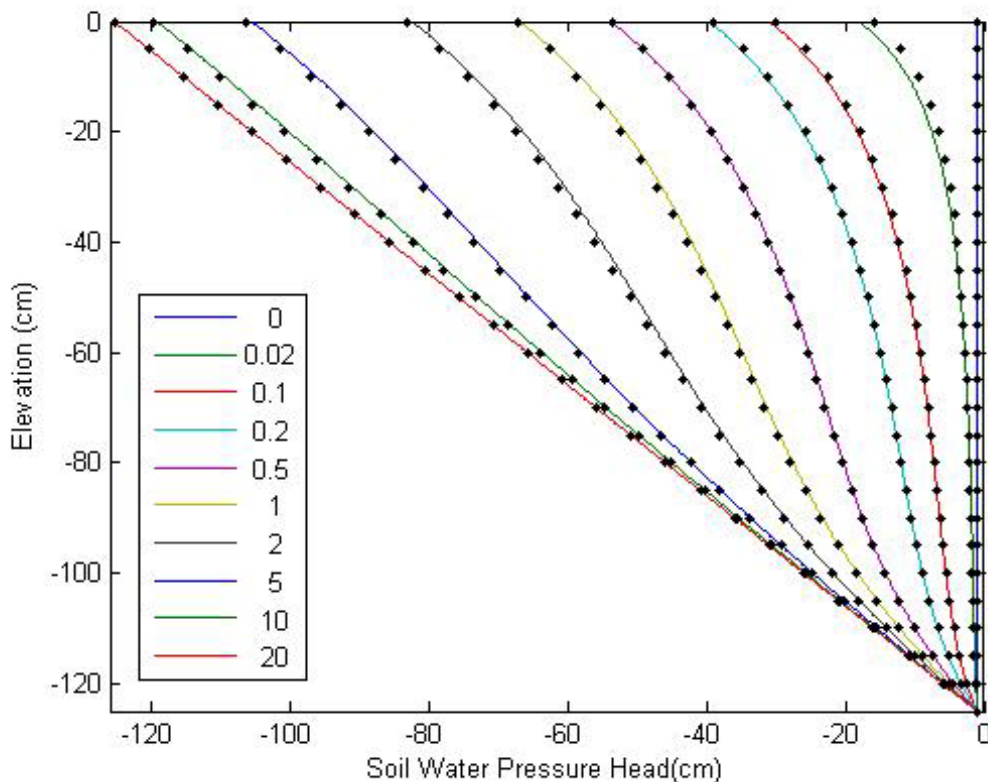
Figure 5.17. Spatial and temporal distributions of soil water pressure head during the course of the drainage experiment generated by the proposed switching algorithm (dots) and the "reference solution"(solid lines). The legend indicates the times after initiation of drainage in days.

140

hydraulic parameters were used to simulate the infiltration experiment. A positive pressure head of 2 cm was used on the soil surface. Infiltration tests were asymptotically carried out by assuming that the experimental conditions were very close to the one-dimensional downward flow with Dirichlet boundary condition on the soil surface and Neumann boundary condition at the lower end of the domain. Figures 5.18 and 5.19 indicate the results of the infiltration experiment generated by the "reference solution", the mixed form of the Richards' equation, and the switching algorithm for infiltration times of 0.0, 0.005, 0.02, 0.05, 0.1, 0.2, 0.35, and 0.5 days. The solid lines show the "reference solution" while the crosses and points represent the mixed form and the proposed switching algorithm, respectively, which were obtained using coarse mesh and larger time steps ($\Delta z = 2.5cm$ and $\Delta t = 1 \times 10^{-5} day$). Figure 5.18 presents the spatial and temporal distribution of the soil water pressure head during infiltration into very dry soils while Figure 5.19 indicates the soil water content distributions. As the Figures show the proposed switching algorithm has excellent agreement with the "exact solution".

5.3.1.3. Mass Conservation Property of the Numerical Simulators

The global mass balance error of the "exact solution" is presented in Figure 5.20. The graph shows perfect global mass balance over the entire domain and at times. This is not the case for the numerical simulators at large time steps. As Figures 5.21 shows both the fully implicit and Crank-Nicolson schemes of the h-based form of the Richards' equation suffer from poor mass balance for $\Delta t = 0.1 day$ and $\Delta z = 2.5cm$. The mass balance error is more pronounced for the Crank-Nicolson method while for the fully implicit method it starts with 10 percent at the beginning of the simulation and approaches 6 percent as the
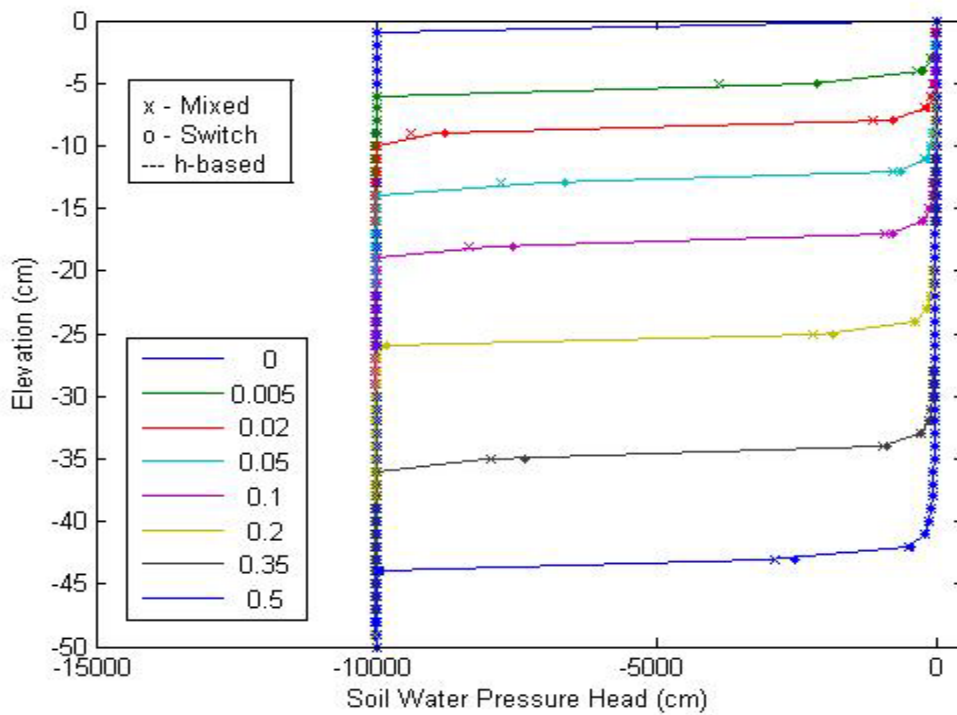
Figure 5.18. Spatial and temporal distributions of the soil water pressure head during the course of an infiltration experiment.
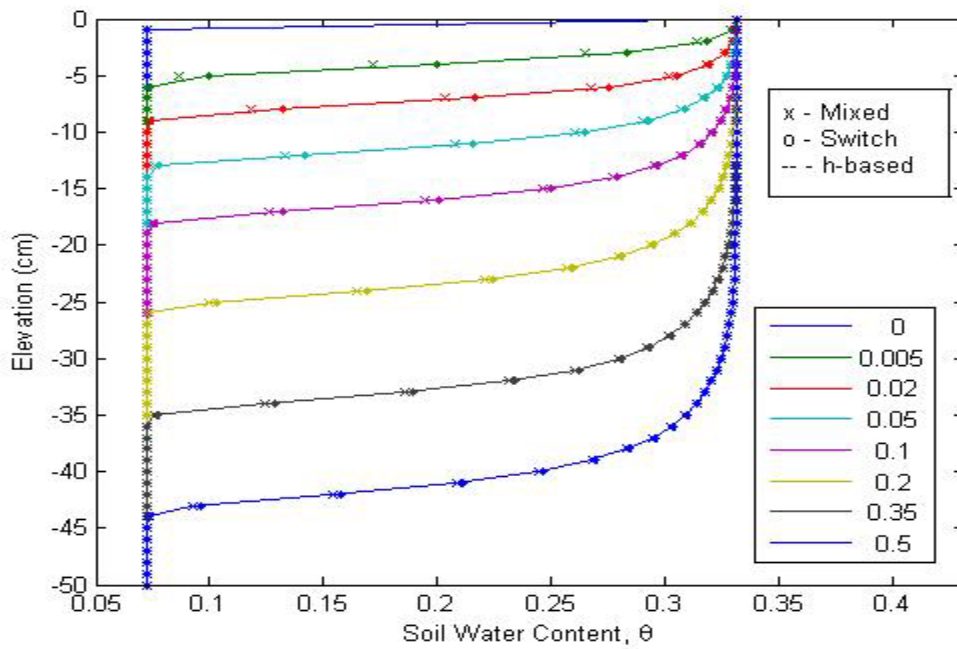
Figure 5.19. Spatial and temporal distributions of the soil water content during the course of an infiltration experiment.
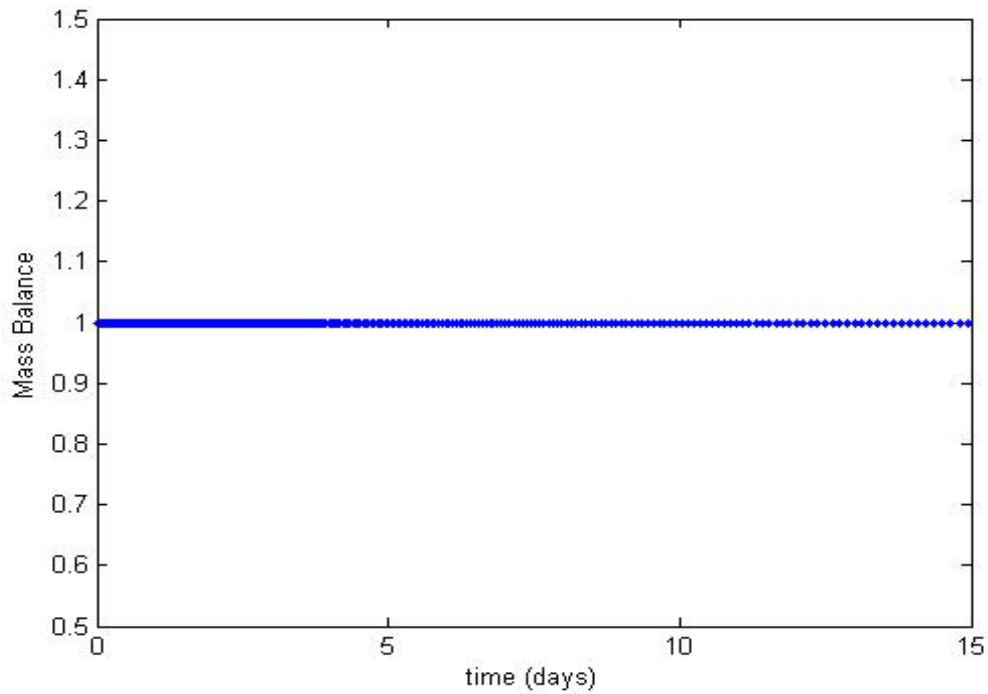
Figure 5.20. Global mass balance error of the "exact solution" simulating drainage
experiment.

simulation proceeds. Similar results obtained for the finite element solution of the h-based form of the Richards' equation. Figure 5.22 presents the global mass balance error of the finite element solution of the h-based Richards' equation using distributed (Figure 5.22a) and lumped (Figure 5.22b) stiffness mass matrices. The error is more pronounced for the distributed mass matrix finite element approximation which starts with 40 percent error at the beginning of the simulation and approaches 10 percent at the end of the solution (for $\Delta t = 0.1\,\text{day}$). The lumped stiffness matrix, as expected, shows better results, in terms of conservation of mass, in comparison with the distributed mass matrix.

Finally, the mass balance property of the mixed form Richards' equation is presented in Figure 5.23. Since the mass-lumped Galerkin based linear finite element solution of the mixed form equation produced similar results, it was not included in the

143
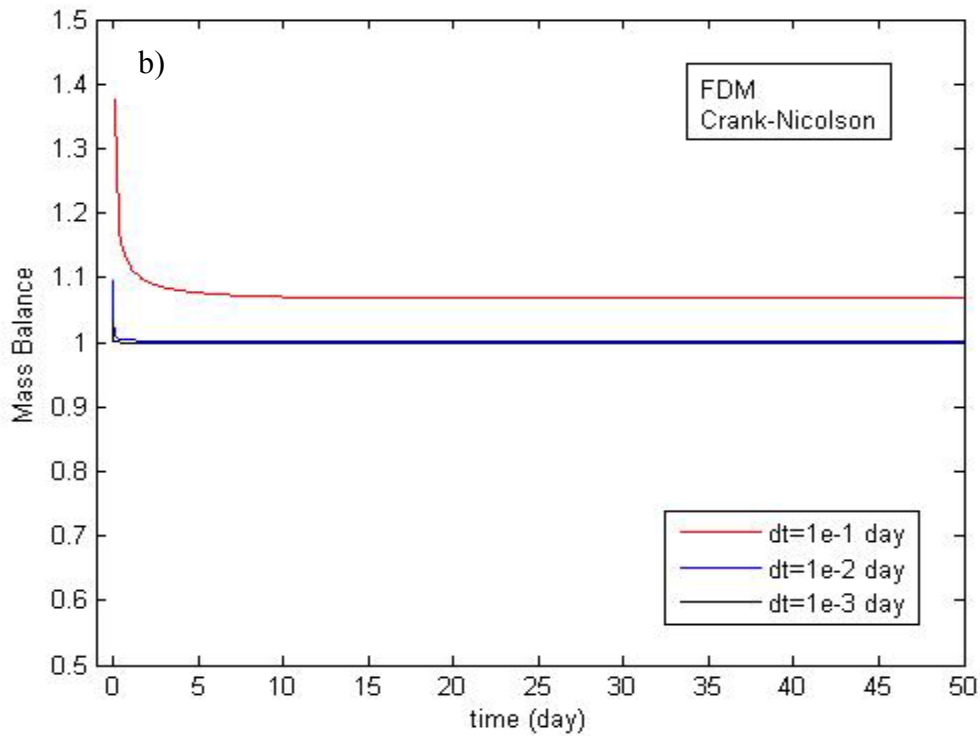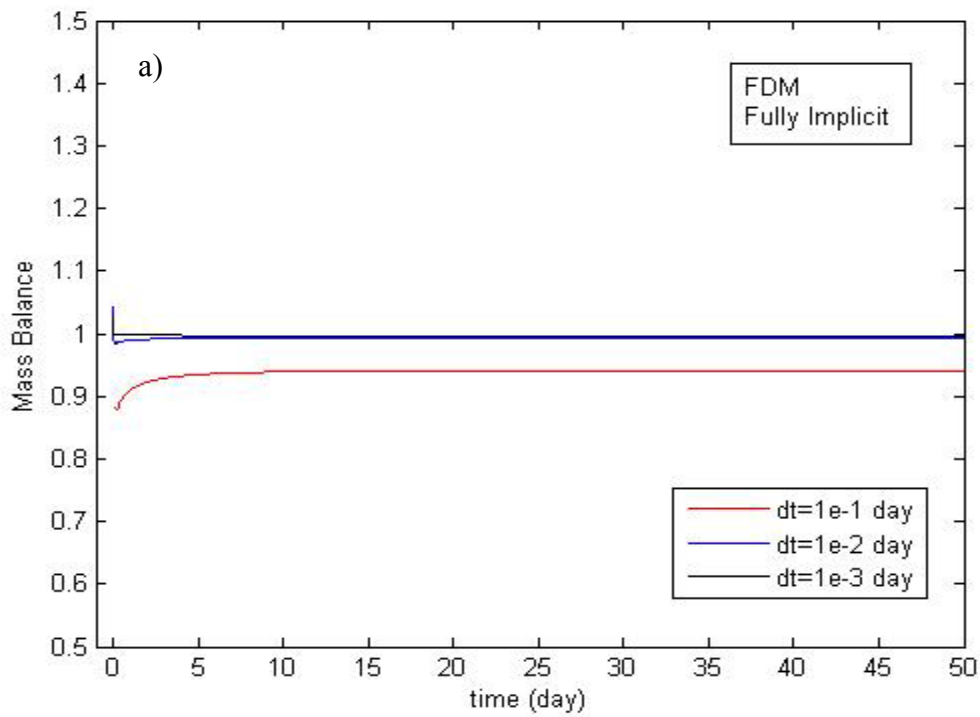
Figure 5.21. Global mass balance error of the finite difference solution of the h-based
Richards' equation (a: fully implicit scheme, b: Crank-Nicolson
formulation) simulating drainage experiment.

144
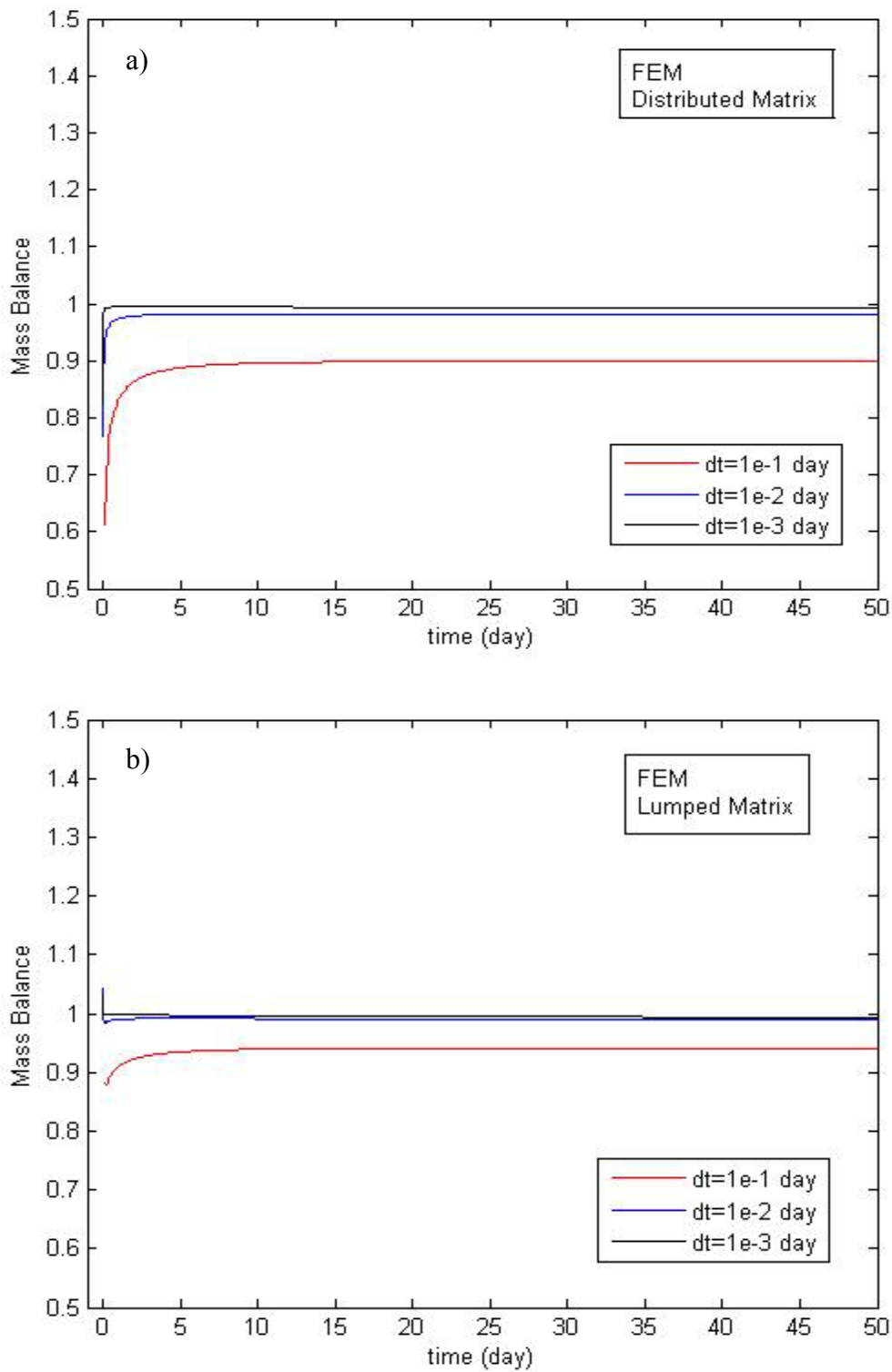
Figure 5.22. Global mass balance error of the finite element solution of the h-based Richards' equation (a: distributed mass matrix, b: lumped mass matrix) simulating drainage experiment.

145
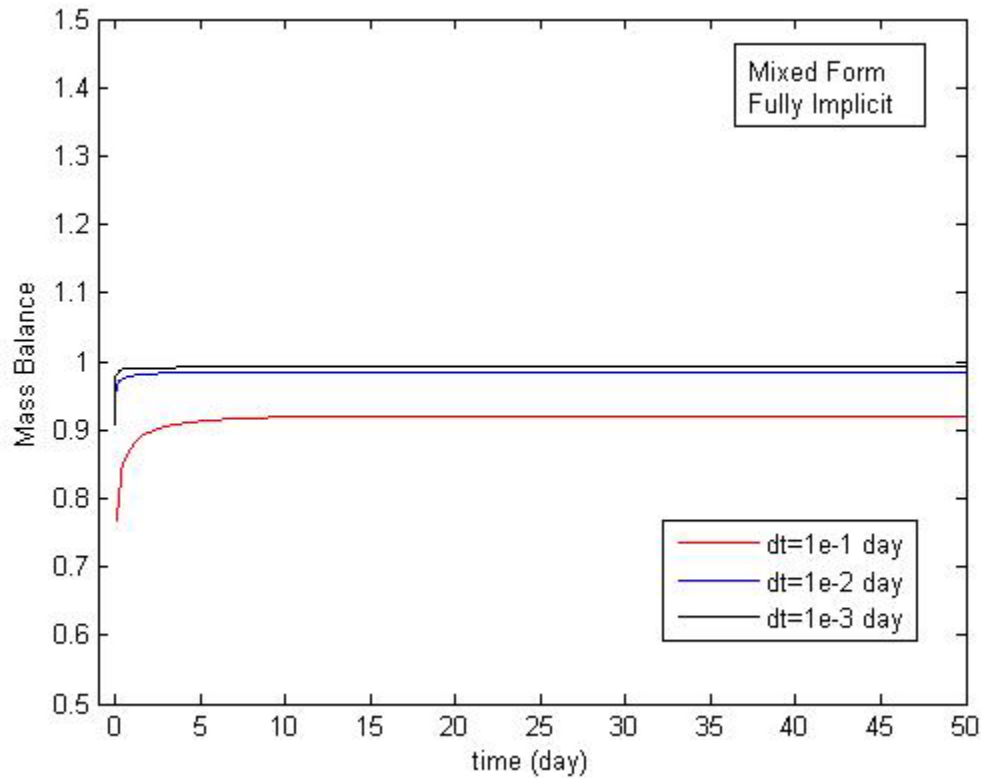
.
Figure 5.23. Global mass balance error for the finite difference simulator (fully implicit
scheme) of the mixed form Richards' equation simulating drainage
experiment.

analysis of the mass balance property and only the results of the finite difference solution
are reported here. For $\Delta t = 0.1\,$day and $\Delta z = 2.5\,cm$ the formulation shows poor mass
balance. The mass balance error at the beginning of the simulation is about 23 percent.
As the simulation proceeds the error becomes smaller but it doesn't vanish. This is in
contrast with the findings of Celia *et al.,* (1990) who claimed that the mixed form of the
Richards' equation is mass conservative for any time steps and any boundary conditions.
The formulation, however, does produce good mass balance results for $\Delta t = 0.01\,$day.

These results were for drainage experiment which is numerically straightforward.
Numerical simulation of infiltration into very dry soils, however, have been challenging

146

in porous media community (van Genuchten, 1982; Milly, 1985; Celia *et al.*, 1990; Kirkland and Hills, 1992; Pan and Wierenga, 1995; Forsyth *et al.*, 1995; Pan e*t al.,* 1996; Diersch and Perrochet, 1999, among many others). As Figure 5.24 shows numerical solution of the h-based form of the Richards' equation ($\Delta t = 1 \times 10^{-5} day$ and $\Delta z = 2.5cm$) shows severe mass balance error while, as Figures 5.25 and 5.26 indicate, the mixed form and the proposed switching algorithm maintain excellent mass balance property for similar mesh .

In conclusion, the distributed mass matrix linear finite element method and the Crank-Nicolson scheme of the finite difference approximation produced poor mass balance and therefore were not selected as the numerical simulator of the forward problem, to simulate water flow in variably saturated porous media, in the framework of the inverse problem. Among the remaining formulations, namely, the mass-lumped linear Galerkin based finite element approximation, the fully implicit finite difference solution of the h-based form and mixed form Richards' equation and the switching algorithm, the optimization uses the mass-lumped Galerkin based linear finite element solution of the mixed form Richards' equation.

The inverse modeling strategy was then applied to simulate partially saturated flow in homogeneous and heterogeneous soils.
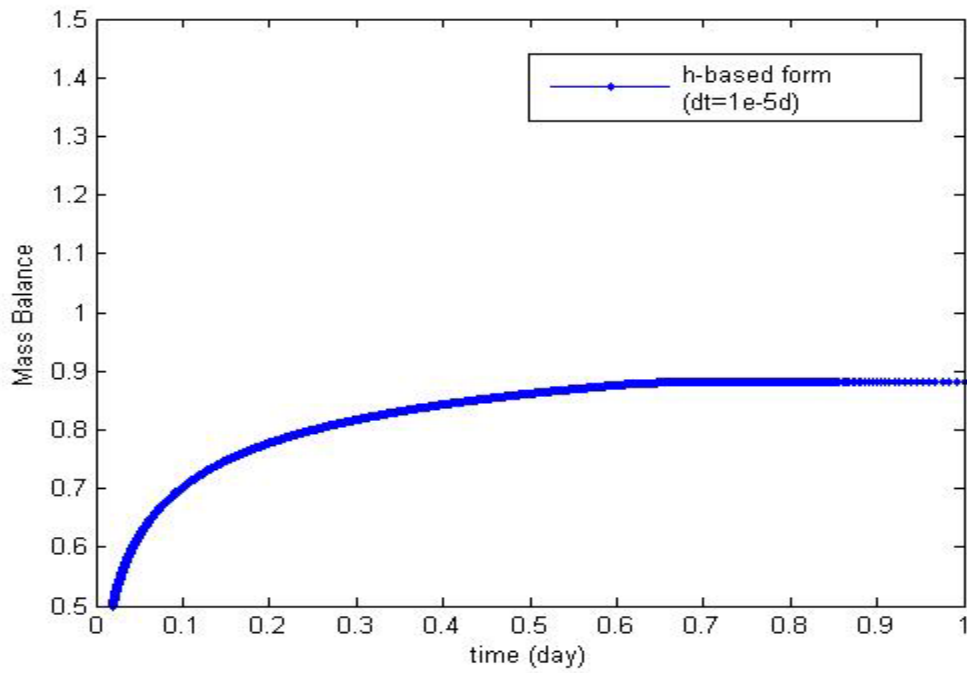
Figure 5.24. Mass conservation property of the h-based form of the Richards' equation for infiltration into very dry soil.
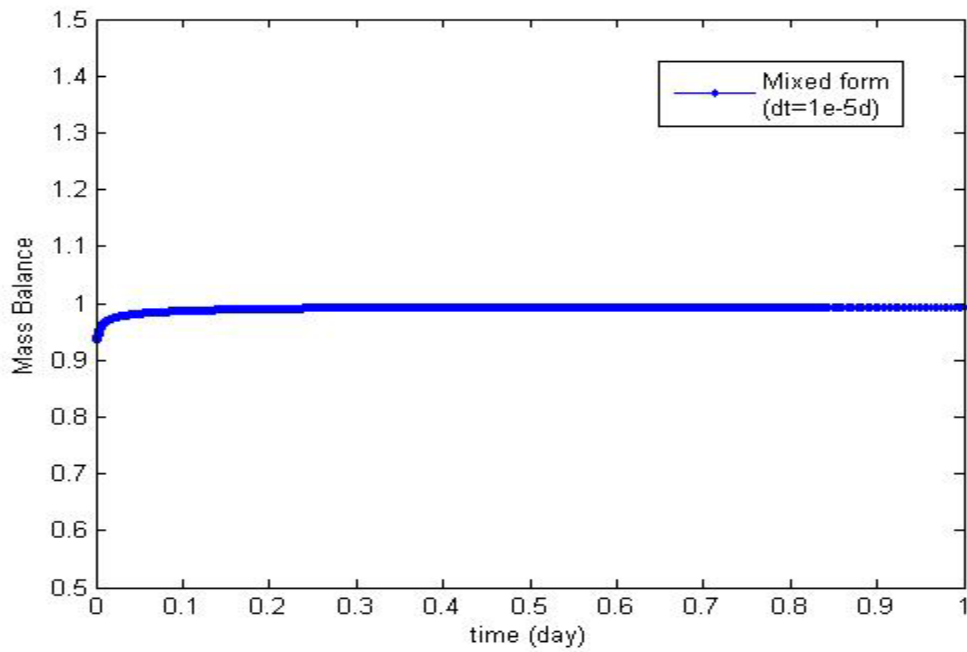
Figure 5.25. Mass conservation property of the mixed form of the Richards' equation for infiltration into very dry soil.

148
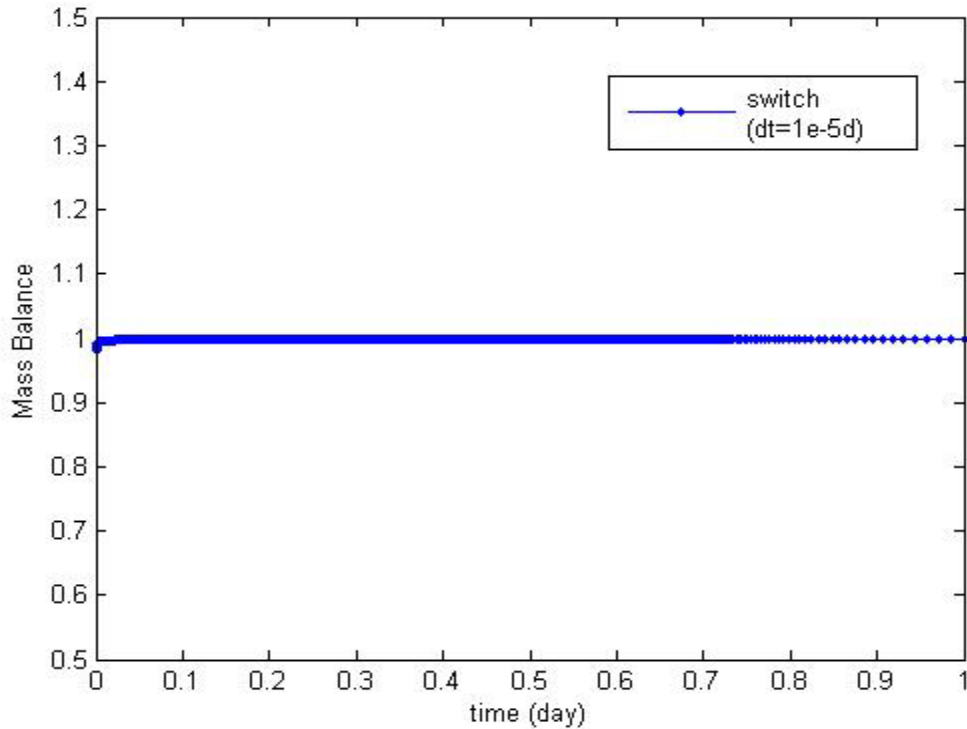
Figure 5.26. Mass conservation property of the proposed switching algorithm for
         infiltration into very dry soil.

5.3.2. Formulation of the Inverse Problem: Optimization Scenarios

The optimization scenarios considered in this section were identification of hydraulic

parameters in water flow through homogeneous and heterogeneous porous media. Both

single-objective and multi-objective optimizations were considered. In flow through

homogeneous soil, both experimental soil water content and soil water pressure head time

and space series were available which made it possible to perform single and multi-

objective optimizations. The data for water flow through heterogeneous variably

saturated soil contained only information on the soil water content time and space series

and therefore a single-objective function was used. Three scenarios were considered and

analyzed; i) single-objective optimization using the soil water content data, ii) single-objective optimization using the soil water pressure head data, and iii) multi-objective optimization using the soil water content and the soil water pressure head data.

To start the optimization, the initial guesses for the parameters were taken from Carsel and Parish (1988) and the parameters were updated iteratively until the stopping criteria were met. The following constraints were imposed on the parameters:

$$K_s \geq 0.01 cmd^{-1} \,, \quad n > 1 \,, \quad \alpha > 0 cm^{-1} \,, \quad \theta_r > 0 \,, \quad -50 \leq \iota \leq 50$$

These constraints were imposed to reduce potential singularity problems in the forward model as all numerical simulators can suffer from singularity when model parameters take unrealistic values (for example large saturated hydraulic conductivity and large values of the residual soil water content simultaneously), though these cases are rare for the soil moisture based Richards' equation (results were not shown).

5.3.2.1. Homogeneous Porous Media

In this scenario, the task was to estimate the optimized values of the hydraulic parameters K_s, α, n, θ_r, and ι, analyze the inverse problem, and compare them with the results of Kool *et al.,* (1987). The data for this case were taken from the drainage experiment on the Bandelier Tuff (described in 4.3.2). To solve the forward problem zero flux boundary condition at the top and free drainage boundary condition at the bottom of the soil profile were applied. The initial soil water content was measured by Abeele (1984) and the corresponding uniform initial condition was applied to solve the *direct problem*. Both *"single objective optimization"* and *"multi-objective optimization"* were considered. In single-objective optimization the information about either the soil water content or soil water pressure head was only incorporated in the optimization. In *multi-objective*

optimization both kind of information (the soil water content data and the soil water pressure head information) were used in the optimization algorithm.

5.3.2.1.1. Single-Objective Optimization

To estimate the optimized values of the parameters $[K_s, \alpha, n, \theta_r, \iota]$, only the soil moisture data were inserted in the objective function (Equation [4.66]). Then the strategy was used to identify the hydraulic parameters. Some of the optimized parameter values are given in Table 5.12. The RMSE for all cases is the same. The gradient of the objective function at the solution, given next to the parameter values in Table 5.12, is close to zero implying that all of these solutions are strong local minima. The positive definiteness of the Hessian (not shown in Table 5.12) confirms this assertion. Table 5.12 shows that the optimized values of K_s, θ_r, and ι are almost stable with values of $6.2 cmd^{-1}, 0.13$, and 2.00, respectively. However, the optimized values of α changes from 0.0015 to 0.0047 and n varies from 9.70 to 42.23. Comparison of rows three and four in Table 5.12 indicates a hyperbolic relationship between these two parameters. As α increases n decreases. This is consistent with the results of parameter response surfaces analysis in the $\alpha - n$ plane.

One may conclude that coupling optimization algorithms with the numerical solution of Richards' equation, and only soil moisture experimental data may not produce unique and stable parameter values for α and n in Mualem-van Genuchten soil water characteristic formula. One possible approach to overcome the non-uniqueness problem regarding α and n is to estimate α separately from the hanging column (Haines apparatus) experiment. It should also be noted that except for very coarse texture soils, the air entry value or the inflection point (α) is not a well-defined point. Therefore, the

Table 5.12. The results of parameter optimization for single objective optimization (soil moisture data only).

Parameter	p	∇OF^{1}	p	∇OF^{2}	p	∇OF^{3}	p	∇OF^{4}	p	∇OF^{5}
$K_s(cmd^{-1})$	6.312	0.0000	6.2550	0.0000	6.2458	0.0001	6.2173	0.0000	6.2176	0.0001
$\alpha(cm^{-1})$	0.0047	-0.0081	0.0037	-0.0020	0.0039	0.0197	0.0027	-0.0042	0.0029	0.0252
n	9.7061	-0.0000	13.6754	0.0000	14.5095	0.0000	19.570	-0.0000	20.6107	0.0000
θ_r	0.1334	0.0000	0.1320	0.0000	0.1321	-0.0001	0.1309	-0.0000	0.1307	-0.0001
ι	1.8492	0.0001	2.0304	0.0000	2.0153	-0.0003	2.1638	-0.0000	2.1567	-0.0003
Parameter	p	∇OF^{6}	p	∇OF^{7}	p	∇OF^{8}	p	∇OF^{9}	$p^{\#}$	$\nabla OF^{\#}$
$K_s(cmd^{-1})$	6.1920	0.0000	6.2024	0.0002	6.1752	0.0000	6.1965	0.0001	25.000	0.0001
$\alpha(cm^{-1})$	0.0019	-0.0095	0.0022	0.0392	0.0013	-0.0227	0.0015	0.0423	0.01433	0.0230
n	28.4561	-0.0000	29.4979	0.0000	41.8688	-0.0000	42.2334	0.0000	1.5060	0.0127
θ_r	0.1300	-0.0000	0.1296	-0.0001	0.1294	-0.0000	0.1287	-0.0001	0.0000	-
ι	2.2593	-0.0000	2.2608	-0.0003	2.3257	-0.0000	2.3380	-0.0002	0.5000	-0.0004

1. $[\, RMSE(\theta) = 0.0091 \quad RMSE(h) = 1.0950m \,]$ 2. $[\, RMSE(\theta) = 0.0091 \quad RMSE(h) = 1.1655m \,]$
3. $[\, RMSE(\theta) = 0.0091 \quad RMSE(h) = 1.1989m \,]$ 4. $[\, RMSE(\theta) = 0.0091 \quad RMSE(h) = 1.1605m \,]$
5. $[\, RMSE(\theta) = 0.0091 \quad RMSE(h) = 1.1941m \,]$ 6. $[\, RMSE(\theta) = 0.0091 \quad RMSE(h) = 1.1808m \,]$
7. $[\, RMSE(\theta) = 0.0091 \quad RMSE(h) = 1.2274m \,]$ 8. $[\, RMSE(\theta) = 0.0091 \quad RMSE(h) = 1.1915m \,]$
9. $[\, RMSE(\theta) = 0.0091 \quad RMSE(h) = 1.2305m \,]$

\# These values were obtained by Kool et al., (1987): $[\, RMSE(\theta) = 0.013 \quad RMSE(h) = 0.3063m \,]$

value obtained by desorption experiment would be a rough estimate. Another possibility is incorporating other kind of experimental data in the objective function and performing *multi-objective optimization* which was considered in this study and will be discussed later in this chapter.

These findings are in contrast with those of Kool *et al.,* (1987) which claimed that "the parameter estimation problem for the two parameters α and n can be solved uniquely using only information on water content profiles during drainage". They also claimed that coupling soil moisture data with soil water pressure head data for one depth (six additional data points) they could uniquely identify the four unknown parameters (the pore connectivity index was assumed to be $\iota = 0.5$). The last two columns of Table 5.12 present their results. The calculated RMSE for this set of parameters is 0.0131 which is 35 percent more than the RMSE (0.0091) of the solutions obtained in this study.

In comparison with the measured value of $K_s = 12.44 cmday^{-1}$, their estimated value for K_s (25 cm/day) is too high especially ponded infiltration gives over-estimated value for saturated hydraulic conductivity (because of the bypass flow). Furthermore, as Figure 5.27 shows this set of parameters produce acceptable fit for water content profile but poor fit for the soil water pressure head data. The same is true for the parameters obtained in this study using only the soil water content information in the optimization procedure. As Figure 5.28 shows the optimized set of parameters produce excellent fit for the soil water content profile and poor fit for the soil water pressure head data.

To further investigate the efficiency of *single-objective optimization* to identify the hydraulic parameters of the variably saturated flow, only soil water pressure head data were used in the objective function. In other words, only the second term in equation
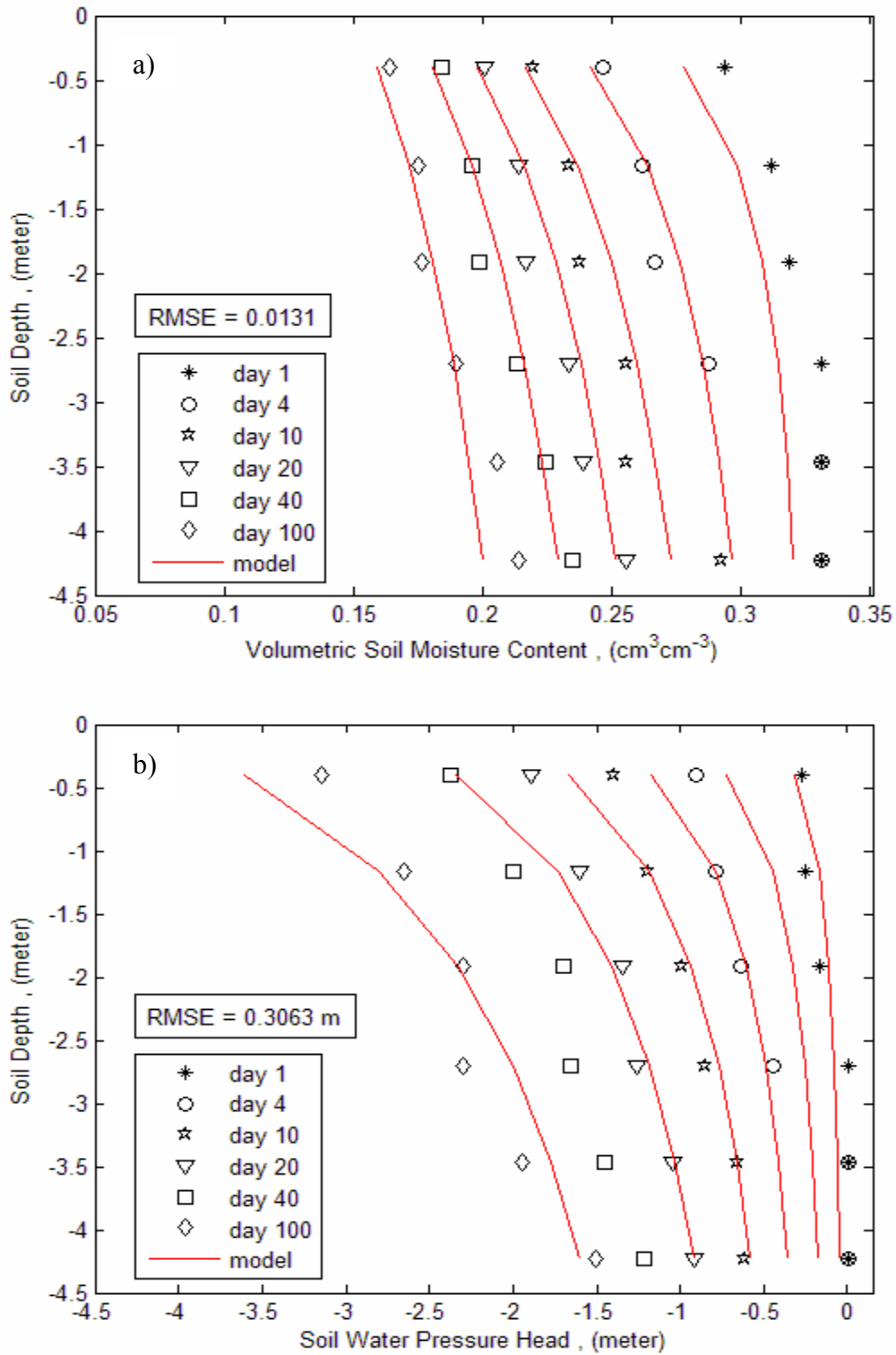
Figure 5.27. Observed and simulated soil water content (a) and pressure head (b) profiles during drainage of Bandelier Tuff using the parameters of Kool *et al.* (1987). The experimental data are from Abeele (1984).
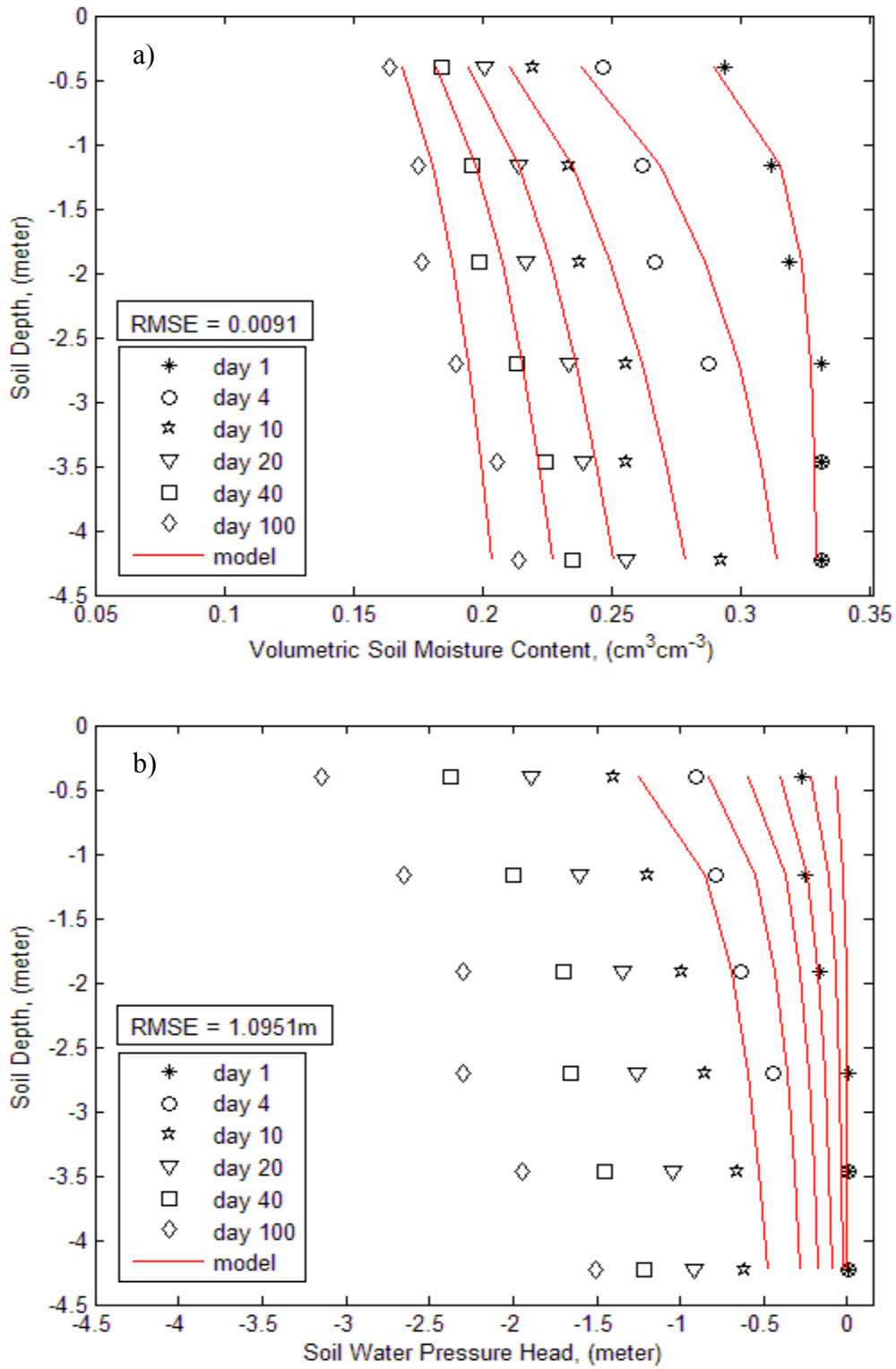
Figure 5.28. Observed and simulated soil water content (a) and pressure head (b) profiles during drainage of Bandelier Tuff. Only the soil water content data were used in the optimization (data from Abeele (1984)).

[4.66] was considered in the objective function. The results of the optimization are depicted in Figure 5.29 in which the optimized values of the parameters produce reasonable fit for the soil water pressure head data but very poor results for the soil water content profile. The results reaffirm that the *single-objective optimization* procedure is not a reliable method to identify the hydraulic parameters of the Mualem-van Genuchten soil water retention relationship and the unsaturated hydraulic conductivity, diffusivity, and soil water capacity functions.

5.3.2.1.2. Multi-Objective Optimization

To identify the hydraulic parameters of the homogeneous soil, the information of the soil water content and soil water pressure head were used together in a *multi-objective optimization* framework, embedded in the proposed inverse modeling strategy. For this purpose, equation [4.67] was used as a weighted complex objective function. The goal was to minimize the objective function so that the optimized hydraulic parameters to be unique and stable and produce the best fits for both soil water content and pressure head profiles. The results are depicted in Figure 5.30 and show reasonable agreements with the soil water content and soil water pressure head profiles. The detailed results of the multi-objective optimization are presented in Table 5.13. The values inside parentheses in the first row are the Mixed Root Mean Squared Error (*RMSE*) which was calculated using equation [4.67]. The only difference with the *single objective optimization* is the residual vector which was defined as follow for multi-objective optimization:

$$r = \frac{(\theta - \hat{\theta})}{\bar{\theta}} + \frac{(h - \hat{h})}{\bar{h}}$$

where θ and $\hat{\theta}$ are the measured and predicted soil water content and h and $\hat{h}$ are the

156
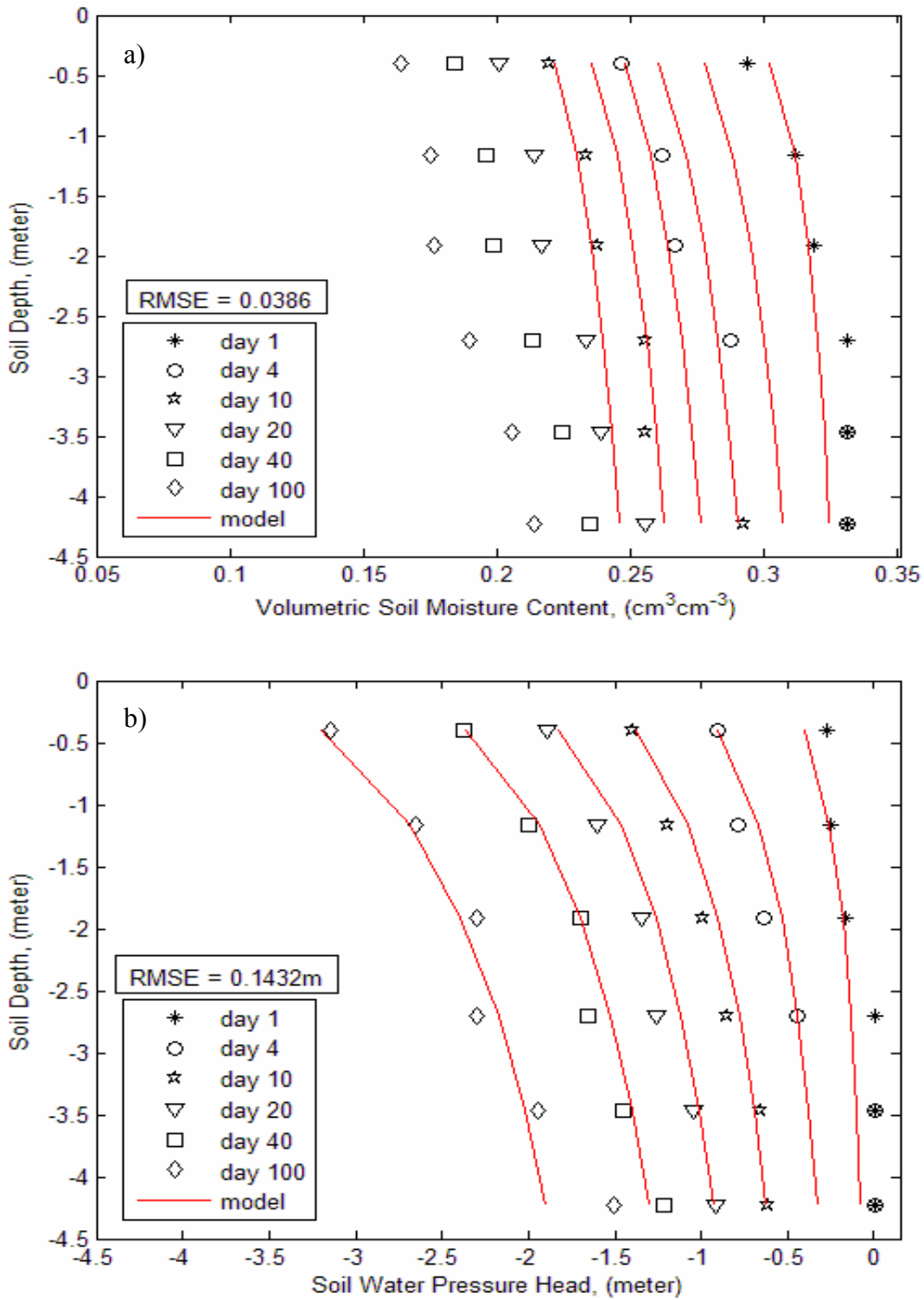
Figure 5.29. Observed and simulated soil water content (a) and pressure head (b) profiles during drainage of Bandelier Tuff. Only the soil water pressure head data were used in the optimization (data from Abeele (1984)).
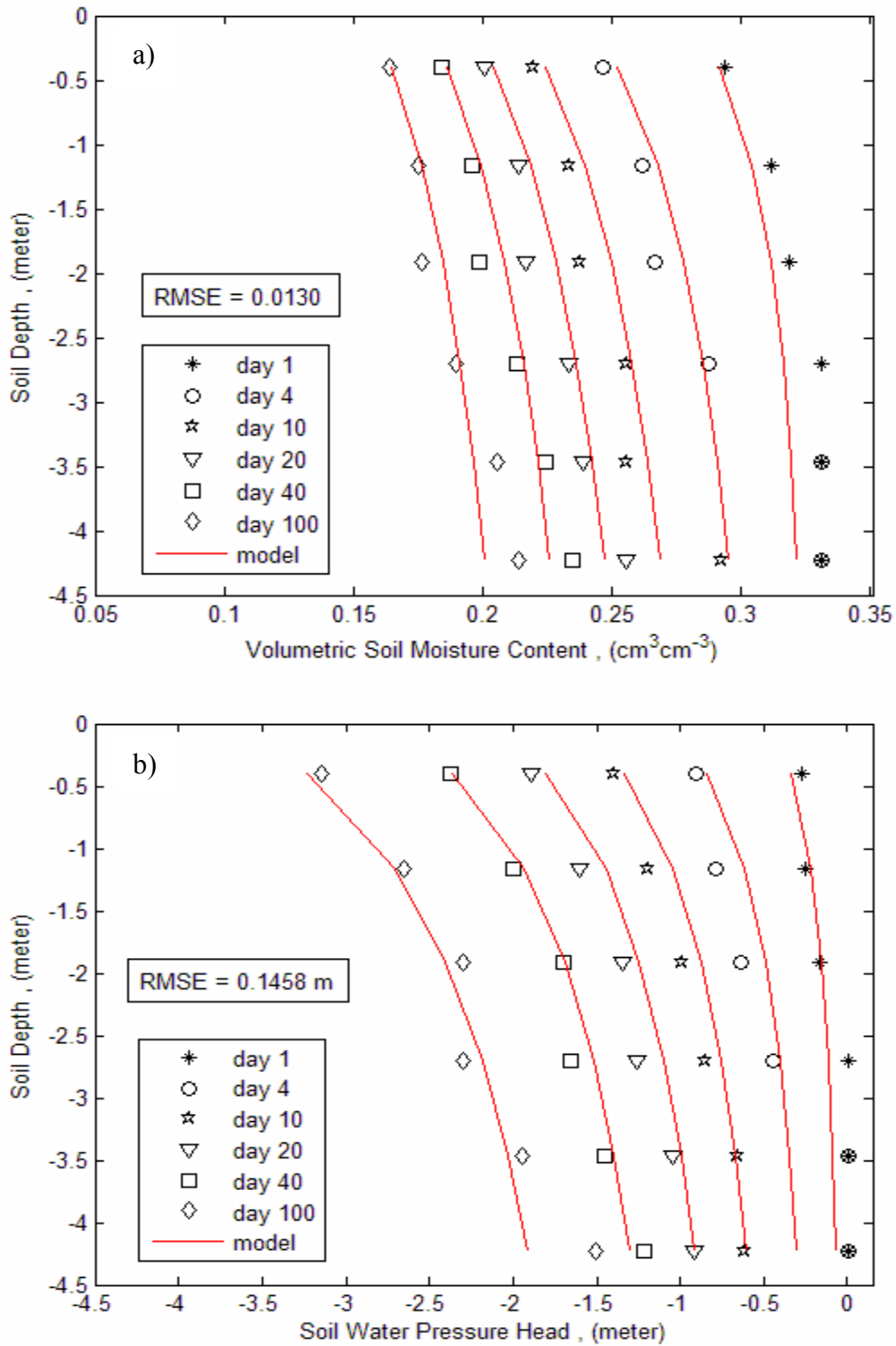
Figure 5.30. Observed and simulated soil water content (a) and pressure head (b) profiles during drainage of Bandelier Tuff using multi-objective optimization (data from Abeele, 1984).

Table 5.13. The results of parameter optimization for multi-objective optimization.

Parameter	p	∇OF^1	p	∇OF^2	p	∇OF^3	p	∇OF^4	p	∇OF^5
$K_s(cmd^{-1})$	12.15	0.0002	13.56	0.0004	14.56	0.0004	12.2500	0.0003	13.0000	0.0004
$\alpha(cm^{-1})$	0.00186	-0.3420	0.00194	-0.0204	0.0021	0.4599	0.00186	-0.1621	0.00192	0.4348
n	3.3850	-0.0001	3.4913	0.0010	3.4913	0.0010	3.4000	0.0002	3.4913	0.0009
θ_r	0.0250	0.0000	0.0314	-0.0003	0.0414	-0.0003	0.0250	0.0001	0.0307	-0.0002
ι	4. 5800	0.0000	4.4056	-0.0009	4.4056	-0.0008	4. 5400	-0.0002	4.4056	-0.0007

Parameter	p	∇OF^6	p	∇OF^7	p	∇OF^8	p	∇OF^9	$p^{\#}$	$\nabla OF^{\#}$
$K_s(cmd^{-1})$	14.56	0.0001	12.30	0.0003	13.5600	0.0004	12.2500	0.0002	25.000	0.0001
$\alpha(cm^{-1})$	0.0021	-0.1504	0.00187	-0.1805	0.00203	0.0316	0.00186	-0.3987	0.01433	0.0230
n	3.4913	-0.0006	3.4913	0.0003	3.4913	0.0009	3.4700	-0.0001	1.5060	0.0127
θ_r	0.0614	0.0003	0.0305	-0.0001	0.0314	-0.0004	0.0300	0.0000	0.0000	-
ι	4.4056	0.0005	4.3900	-0.0004	4.4056	-0.0011	4. 5200	-0.0001	0.5000	-0.0004

1. [$RMSE(\theta) = 0.0130$ $RMSE(h) = 0.1458m$]   2. [$RMSE(\theta) = 0.0140$ $RMSE(h) = 0.1440m$]

3. [$RMSE(\theta) = 0.0145$ $RMSE(h) = 0.1418m$]   4. [$RMSE(\theta) = 0.0130$ $RMSE(h) = 0.1460m$]

5. [$RMSE(\theta) = 0.0135$ $RMSE(h) = 0.1446m$]   6. [$RMSE(\theta) = 0.0147$ $RMSE(h) = 0.1418m$]

7. [$RMSE(\theta) = 0.0130$ $RMSE(h) = 0.1470m$]   8. [$RMSE(\theta) = 0.0140$ $RMSE(h) = 0.1500m$]

9. [$RMSE(\theta) = 0.0131$ $RMSE(h) = 0.1461m$]

These values were obtained by Kool et al., (1987): [$RMSE(\theta) = 0.0130$ $RMSE(h) = 0.3063m$]

measured and predicted soil water pressure head, respectively.

As Table 5.13 shows the optimized values of the parameters are stable, physically reasonable, and the predicted saturated hydraulic conductivity agrees with the measured one. The estimated value for the residual soil water content is also physically realistic. The pore connectivity index (ι) is found to be far greater than the value of 0.5 which has been extensively used in unsaturated flow modeling. The optimized value for $\alpha(cm^{-1})$ is rather small in comparison to common values for Silt and Silty Sand soils (Carsel and Parrish, 1988). The estimated value for n is reasonable which means that the pore size density function is narrow.

Except for the α–related element of the gradient vector, the other elements are close to zero. The calculated Eigenvalues of the Hessian are:

$$eigs(H) = [0.0001 \quad 0.0004 \quad 0.0020 \quad 0.0046 \quad 908.8736]$$

which confirms that the Hessian is positive definite and the solution is at least a strong local minimum because the necessary and sufficient criteria were met. The mixed root mean squared error (0.089) is almost one-third of the RMSE obtained using the parameters of Kool $et\ al.,$ (1987) and Forsyth $et\ al.,$ (1995). Parameter correlation matrix indicates that there are high inter-correlation between $\alpha - n$, $\alpha - \iota$, and $\theta_r - \iota$:

$$
\begin{array}{ccccc}
\underline{K_s} & \underline{\alpha} & \underline{n} & \underline{\theta_r} & \underline{\iota}
\end{array}
$$

$$
COR(P) = \begin{bmatrix}
1.0000 & 0.2857 & -0.6018 & -0.4056 & 0.0451 \\
0.2857 & 1.0000 & -0.8922 & 0.4397 & -0.7805 \\
-0.6018 & -0.8922 & 1.0000 & -0.1709 & 0.6345 \\
-0.4056 & 0.4397 & -0.1709 & 1.0000 & -0.8649 \\
0.0451 & -0.7805 & 0.6345 & -0.8649 & 1.0000
\end{bmatrix}
$$

5.3.2.2. Heterogeneous Porous Media

The developed inverse modeling strategy was also used to estimate the hydraulic parameters of a heterogeneous soil. The experimental data and the physical properties of the soil are presented in Tables 4.2 and 4.3. The upper and lower boundary conditions are the same as for the homogeneous soil but the initial condition is different. The initial water content varies as a function of depth as shown in Figure 5.31 and is formulated as:

$$\theta(z,0) = f(z)$$

A quadratic function was fitted to the water content values in the second column of Table 4.2:

$$\theta(z,0) = -2.9133 \times 10^{6} z^{2} + 5.9528 \times 10^{4} z + 0.4069$$

Similar to the homogeneous soil, the forward problem was solved using the mass-conservative mixed form algorithm. The equation [4.66] was used as the objective function in the optimization procedure. The results of the parameter optimization are presented in Table 5.14 and Figure 5.32. Table 5.14 includes the measured and predicted soil moisture content for each depth over the course of the experiment and the residual vector (the difference between simulated and measured soil moisture contents).

As Figure 5.32 shows the developed inverse modeling algorithm can be successfully used to identify the hydraulic parameters of the partially saturated heterogeneous soils. The coefficients of determinations for depths of 10 cm, 30 cm, 50 cm, 70 cm, and 90 cm are 0.9918, 0.9919, 0.9905, 0.9868, and 0.9750, respectively. The overall coefficient of determination is 0.9908 which implies that the forward model can explain 99 percent of the temporal and spatial soil water content distribution during the course of drainage experiment. The Root Mean Square Error was found to be 0.0045
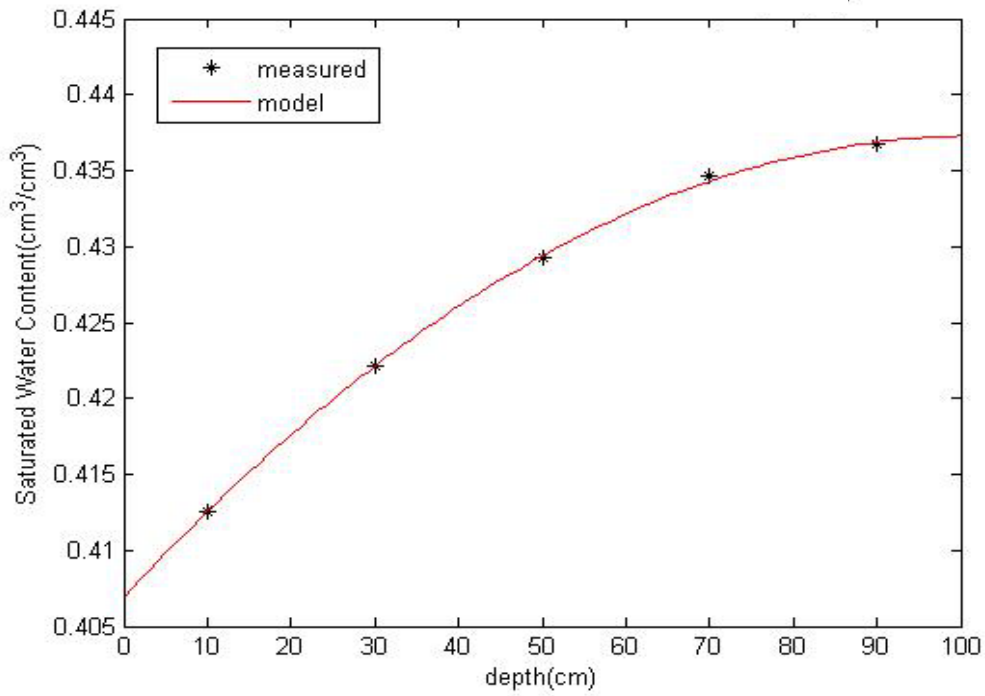
Figure 5.31. Measured and predicted initial water contents as a function of soil depth.
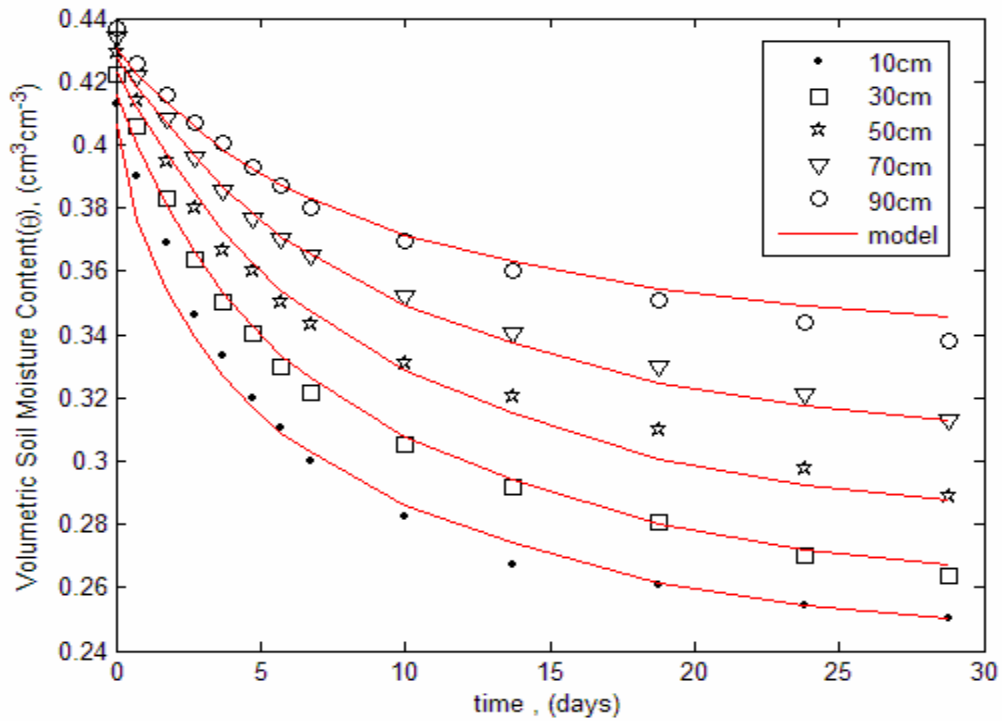
Figure 5.32. Observed and predicted soil water contents during drainage experiment.

Table 5.14. Simulated and observed soil moisture contents for heterogeneous soil.

Depth (cm)	10 cm			30 cm			50 cm			70 cm			90 cm		
Time (day) ↓	model	Exp.	Dev.	model	Exp.	Dev.	model	Exp.	Dev.	model	Exp.	Dev.	model	Exp.	Dev.
0.0000	0.4104	0.4126	0.0022	0.4199	0.4221	0.0022	0.4271	0.4293	0.0022	0.432	0.4336	0.0016	0.4346	0.4368	0.0022
0.7292	0.3786	0.3902	0.0116	0.4031	0.4056	0.0025	0.4144	0.4142	-0.0002	0.4205	0.4216	0.0011	0.4243	0.4257	0.0014
1.7292	0.3553	0.3687	0.0134	0.3828	0.3831	0.0003	0.3988	0.3947	-0.0041	0.4084	0.4081	-0.0003	0.415	0.4158	0.0008
2.7292	0.3402	0.3461	0.0059	0.3679	0.3634	-0.0045	0.3861	0.3801	-0.006	0.3981	0.3957	-0.0024	0.4073	0.4071	-0.0002
3.7292	0.3282	0.3334	0.0052	0.3555	0.3503	-0.0052	0.375	0.3669	-0.0081	0.3888	0.3851	-0.0037	0.4004	0.4004	0
4.7292	0.3189	0.32	0.0011	0.3455	0.34	-0.0055	0.3656	0.36	-0.0056	0.3809	0.3765	-0.0044	0.3946	0.3931	-0.0015
5.7292	0.3109	0.3102	-0.0007	0.3367	0.33	-0.0067	0.3573	0.3501	-0.0072	0.3739	0.37	-0.0039	0.3895	0.3872	-0.0023
6.7292	0.3041	0.3001	-0.004	0.3291	0.3215	-0.0076	0.3499	0.3431	-0.0068	0.3675	0.3648	-0.0027	0.385	0.3801	-0.0049
10.0000	0.2871	0.2824	-0.0047	0.31	0.3052	-0.0048	0.3311	0.3312	0.0001	0.3514	0.3517	0.0003	0.3736	0.3698	-0.0038
13.7500	0.2735	0.267	-0.0065	0.2946	0.2917	-0.0029	0.3158	0.3203	0.0045	0.3381	0.34	0.0019	0.3644	0.3601	-0.0043
18.7500	0.2615	0.2606	-0.0009	0.281	0.2805	-0.0005	0.3022	0.3096	0.0074	0.3263	0.33	0.0037	0.3562	0.3509	-0.0053
23.7917	0.2535	0.2543	0.0008	0.2721	0.27	-0.0021	0.2932	0.2975	0.0043	0.3185	0.3211	0.0026	0.3509	0.3437	-0.0072
28.8125	0.2483	0.2504	0.0021	0.2663	0.2638	-0.0025	0.2874	0.2891	0.0017	0.3134	0.3127	-0.0007	0.3474	0.3378	-0.0096

which is very low.

Since $r^T r / \|J^T J\| = 1.73 \times 10^{-5}$ is less than 1×10^{-3}, this inverse problem can be categorized as the "small residual problem". In such problems, the Levenberg- Marquardt algorithm converges to the solution and its performance is better than quasi- Newton and hybrid algorithms (Gill and Murray, 1978; Nazareth, 1980; Dennis and More, 1977; Denis *et al.,* 1981a; Seber and Wild, 2004).

Table 5.15 presents the optimized values of the hydraulic parameters, 95 percent confidence intervals on the parameters, the variances of the parameter estimates, the gradient of the objective function at the solution, and the Eigenvalues of the Hessian. Except for the pore connectivity index, the 95% confidence intervals are very narrow for the optimized parameters. The variances, and the confidence regions of the optimized parameters indicate that the hydraulic parameters can be identified with more accuracy and small residual errors. Since the estimated value of the residual water content is zero the statistical measures were not reported for this parameter in Table 5.15. The optimized value for the residual soil water content, however, is quite small relative to the expected values.

Again the gradient of the objective function at the solution doesn't reach zero but the results are quite satisfactory. Since the Hessian is positive definite the solution is a strong local minimum.

Table 5.15. The results of parameter optimization for heterogeneous soil.

Parameter	Opt. Value	LL*	UL*	∇OF	$eigs(H)$	σ_p^2
$K_s(cmd^{-1})$	5.9388	5.0009	6.8767	-0.0000	85.5013	0.2204
$\alpha(cm^{-1})$	0.0308	0.0257	0.0359	-0.0002	0.5400	0.00001
n	1.4429	1.3661	1.5197	-0.0000	0.0332	0.0015
θ_r	0.0000	-	-	0.0001	0.0001	0.0018
ι	-4.6735	-6.7135	-2.6335	0.0000	0.0000	1.0428

*95% confidence interval on the optimized parameters.

5.4. Analysis of the Inverse Modeling Strategy

Different techniques were used to analyze the results of the parameter optimization via inverse modeling strategy. First posedness of the inverse problem, in terms of stability and uniqueness, was studied for two mass transport problems. Then the sensitivity of the state variables with respect to model parameter was analyzed followed by the statistical and residual analysis.

5.4.1. Posedness Analysis

To investigate possible ill-posedness of the inverse problem three elements of the posedness, namely existence, stability, and uniqueness of the solution should be analyzed. Existence is not usually a major problem in inverse modeling since there is always a or a set of solutions for inverse problem. Therefore, the uniqueness and stability of the solution were analyzed.

5.4.1.1. Stability Analysis

To perform the stability analysis in inverse problem of GFP-GR (FRAP) a generated data set obtained by solving equation [4.32] for a hypothetical cell with prescribed initial and boundary conditions and parameter values: $D_f = 30 \mu m^2 s^{-1}$, $K_a = 30 s^{-1}$, $K_d = 0.1108 s^{-1}$, $D_c = 0$, $r = 0.5 \mu m$, and $D_s = 0$. Simulated FRAP recovery values were sampled at discrete times for the bleach spot. The data set was then corrupted by adding $N(0, 0.02)$ error term to each "measurement". These noisy "measurements" were then used as input for parameter optimization algorithm and well-posedness analysis of the inverse problem. The results are given in Tables 5.5 to 5.10 in parentheses. As these Tables show small changes in the input data don't generate significant changes in the optimized values of the parameters. Therefore, the cause of the ill-posedness of the inverse problem in case of GFP-GR is not instability.

The same procedure was followed for water flow in variably saturated soils. Both single-objective and multi-objective optimizations were considered. Five percent error with normal probability distribution function, $N(0, 0.05)$, was added to the soil moisture and soil water pressure head data. Table 5.16 presents the results of stability analysis for water flow in heterogeneous soil in which the single-objective optimization was used (only soil moisture information was incorporated in the objective function). Perturbation of the input data didn't change the optimized values of the saturated hydraulic conductivity (K_s), n, and the residual moisture content (θ_r), but it widened the 95 percent confidence intervals on the parameters and increased the variances of estimation from 0.2204, 0.0015, and 0.0018 to 31.4259, 1.0144, and 0.1960, respectively. The changes were pronounced for ι, and α where they changed from -4.6735 and 0.0308 to -

1.6115 and 0.0199, respectively. The estimation uncertainties increased drastically as the scattering increased in the input data.

Similar results were obtained for stability analysis of homogeneous soil (Table 5.17). In this case multi-objective optimization (soil moisture content data and soil water pressure head information incorporated in the objective function) was used. Small changes in input data cause drastic variations in the optimized values of air entry value (α), residual moisture content (θ_r), and pore connectivity index (ι). Other model parameters didn't change significantly (Table 5.17). The RMSE for corrupted data ($RMSE = 0.1511$) is almost two times more than the original data ($RMSE = 0.089$; See Table 5.13). Adding noise to the data increases the variances of parameter estimation which are given in last column of Table 5.17.

The instability analysis clearly demonstrates the importance of the quality of the input data for successful parameter optimization in mass transport problems. Nevertheless, being stable doesn't automatically guarantee that the inverse problem is well-posed. Stability is a necessary but not sufficient criterion for well-posedness of the inverse problem. In addition to being stable, the inverse solution must also be unique in order to be considered well-posed.

Table 5.16. The results of stability analysis of the inverse problem for heterogeneous soil.

Parameter	Opt. Value	LL*	UL*	∇OF	σ_p^2
$K_s\,(cmd^{-1})$	5.6403 (5.9388)	-5.2602	17.1378	0.0000	31.4259
$\alpha(cm^{-1})$	0.0199 (0.0308)	-0.0031	0.0429	0.0025	0.00004
n	1.6365 (1.4429)	-0.5692	3.4550	-0.0003	1.0144
θ_r	0.0000 (0.0000)	-	-	0.0010	0.1906
ι	-1.6115 (-4.6735)	-17.9792	8.6322	-0.0000	44.3610

*95% confidence interval on the optimized parameters.

Table 5.17. The results of stability analysis of the inverse problem for homogeneous soil[#].

Parameter	Opt. Value	LL*	UL*	∇OF	σ_p^2
$K_s\,(cmd^{-1})$	14.6861	10.9745	22.3228	0.0229	7.8939
$\alpha(cm^{-1})$	0.0051	0.0036	0.0077	2604	0.00000
n	2.9500	2.9917	3.0074	6838	0.0000
θ_r	0.0137	-0.3005	0.3653	0.8727	0.0271
ι	5.1901	-5.98886	17.9421	0.0254	35.1032

Data from Abeele (1984)
* 95% confidence interval on the optimized parameters.

5.4.1.2. Uniqueness Analysis

The uniqueness of the inverse problem was first evaluated by construction and analysis of two-dimensional parameter response surfaces of the objective function as a function of pairs of parameters being optimized. Then the three-dimensional parameter hyper-spaces were constructed and analyzed in 5.4.1.2.2.

5.4.1.2.1. Parameter Response Surface

Figures 5.33 and 5.34 represent the response surfaces of the objective function for corrupted synthetic data. The $D_f - K_a^*$ (Figure 5.33) plane indicates a well-defined valley which starts at low values of both parameters and extends linearly to the entire parameter domain. The Figure clearly shows a linear relationship between the molecular diffusion coefficient and the pseudo-association rate constant, thus confirming the high inter-correlation between them and indicates the difficulty of finding unique values for them. Indeed, an infinite number of combinations of the parameters D_f and K_a^* (inside the valley) can give the same objective function value and produce excellent fit. This can be confirmed by a three-dimensional cross section of the D_f-K_a^*-K_d hyper space in Figure 5.34 (shown as $D_f - K_{on} - K_{off}$). In this Figure the value of the dissociation rate coefficient is fixed at the known value ($K_d = 0.1108 s^{-1}$) for the synthetic data (the plot is in logarithmic scale). Any combinations of D_f and K_a^* in the dark blue area produces the same magnitude for the objective function which makes it impossible to obtain a unique solution for the inverse problem. Both Figures show a strong linear positive correlation between D_f and K_a^* confirming the result of the parameter variance-covariance matrix.
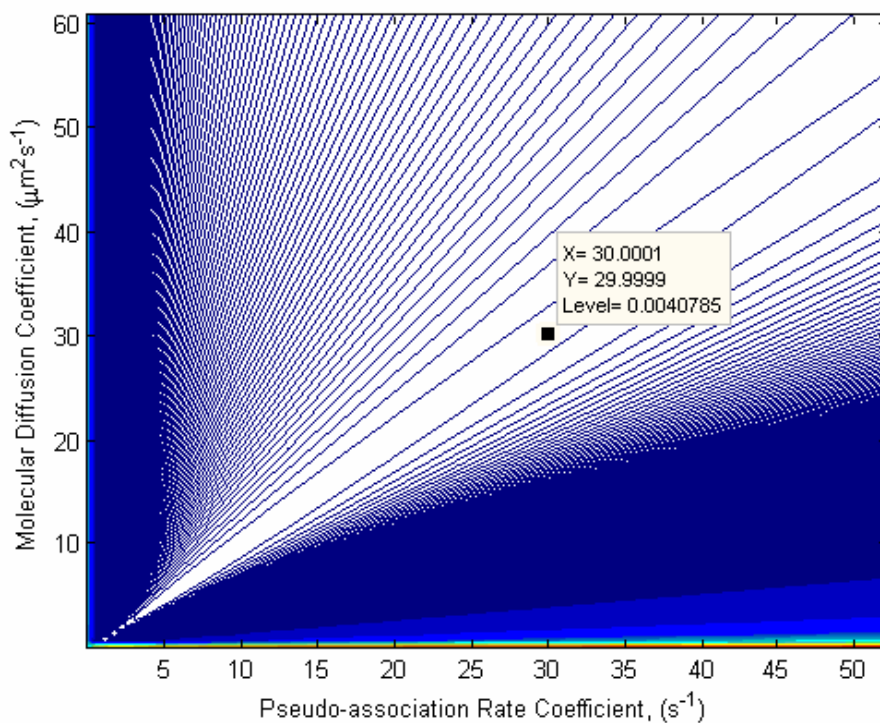
Figure 5.33. Contours of the objective function, $\Phi(\overline{frap})$, in $D_f - K_a^*$ plane (generated data).
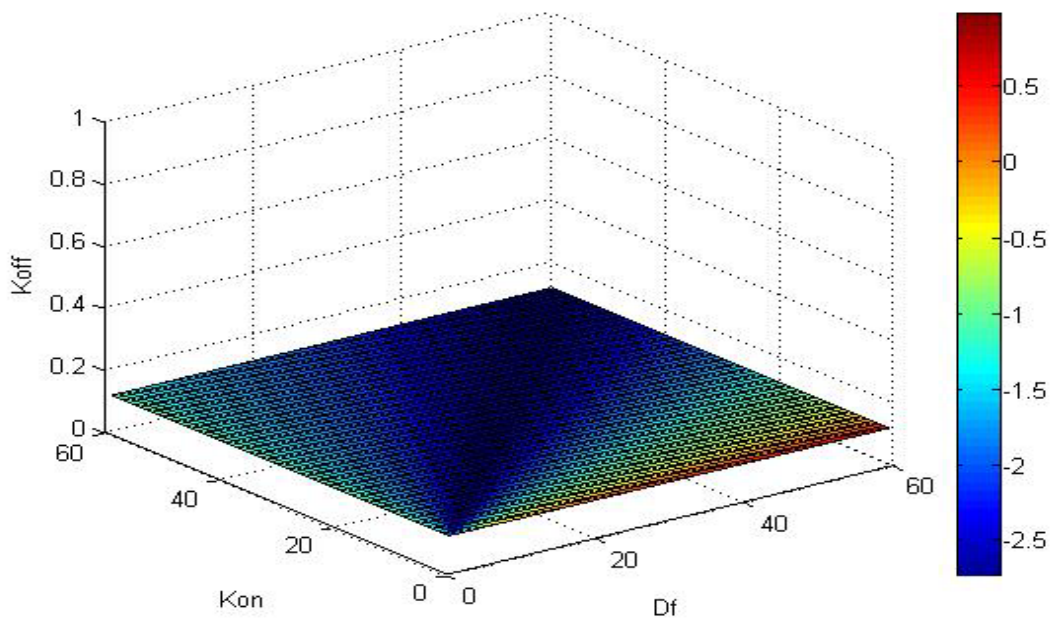
Figure 5.34. A cross section of three-dimensional parameter hyper space (generated data).
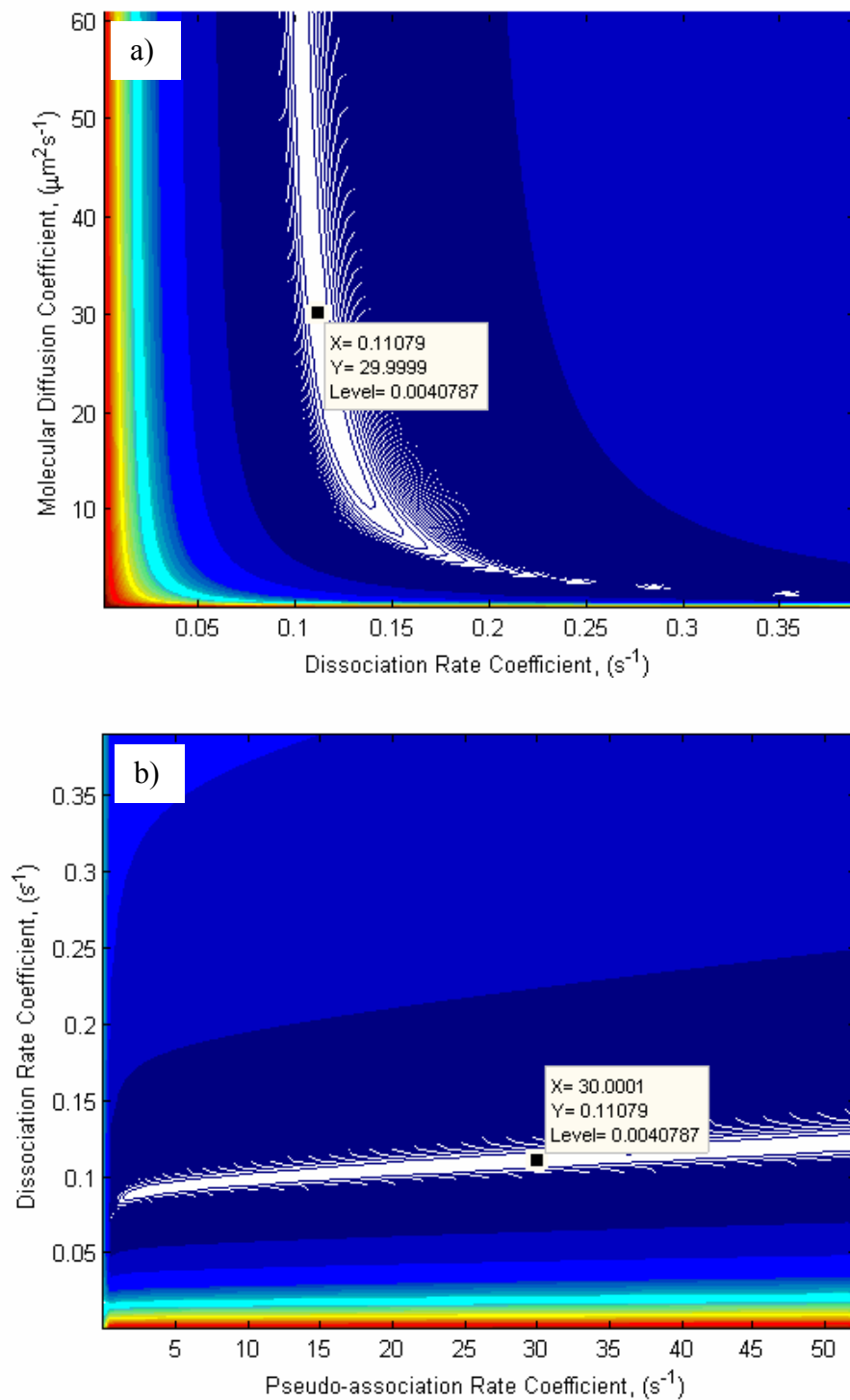
Figure 5.35. Contours of the objective function, $\Phi(\overline{frap})$, in $D_f - K_d$ (a) and $K_a^* - K_d$ (b) planes (generated data).

The contours of the objective function for FRAP in $D_f - K_d$ and $K_a^* - K_d$ planes are presented in Figure 5.35a and 5.35b. Figures indicate that for small values of the biomolecule-free binding site(s) dissociation rate, the objective function is not sensitive to the molecular diffusion coefficient which yields an elongated valley, though closed, in the D_f direction. As K_d increases the objective function becomes sensitive to the changes in the free molecular diffusion coefficient which makes it possible to identify this mass transport parameter. For large values of K_d, the objective function becomes insensitive to the dissociation coefficient which produces an elongated valley in the K_d direction. In a small region where the objective function is sensitive to both parameters, it is possible to identify both parameters easily. Parameter optimization in this zone will produce small estimation variance and narrow confidence intervals.

The contours of the objective function for FRAP in $K_a^* - K_d$ plane shows that the objective function is not sensitive to the pseudo-association rate coefficient when K_a^* increases but it becomes more sensitive when K_a^* decreases. When both parameters are small, there are good chances to identify them with less uncertainty. This is in contrast with the findings of Sprague *et al.* (2004) which reported very high values for these parameters (run 20 in Table 5.1).

A rather surprising feature of the plot in Figure 5.35b is the weak positive linear relationship between K_a^* and K_d which is in contrast with the results of the parameter correlation matrix which gives negative correlation between the two parameters ($r_{K_a^* - K_d} = -0.1196$). The negative correlation between K_a^* and K_d is physically sound

because according to equation [2.13] when K_a^* increases it promotes the reaction towards right, but when K_d increases the biochemical reaction proceeds in the reverse direction.

A possible explanation could be instantaneous binding between GFP-GR and the vacant binding site(s) where adsorption and desorption processes take place dynamically. In other words, the binding process during the experimental course of the FRAP protocol (which take several seconds to several minutes) has a dynamic nature.

Figure 5.33 shows several apparent local minima when both the free molecular diffusion coefficient and the pseudo-association rate constant are small. To further investigate the possibility of obtaining local minimum for inverse problem when the model parameters are small, one of the possible solutions ($D_f = 3\mu m^2 s^{-1}, K_a^* = 0.03 s^{-1}$, and $K_d = 0.1824 s^{-1}$) was used to construct response surfaces. The results are depicted in Figures 5.36 and 5.37. The important implication of these Figures is that the bound response surface doesn't automatically guarantee a unique solution for inverse problem. In other parts of the parameter domain, another set or sets of parameters may produce a local minima or even global minimum. The second finding is that the behavior of the objective function varies in different sub-spaces of the parameter domain.

These findings were also confirmed by analysis of the two-dimensional response surfaces for water flow in homogeneous and heterogeneous soils. Uniqueness analysis of the inverse problem in case of water flow in heterogeneous soil was accomplished by constructing ten pairs of response surfaces for the parameter vector $[K_s, \alpha, n, \theta_r, \iota]$ as discussed in 4.4.2.2.1. The results are presented in Figures 5.38 to 5.42. The only available data for this case was the soil water content information which was used as
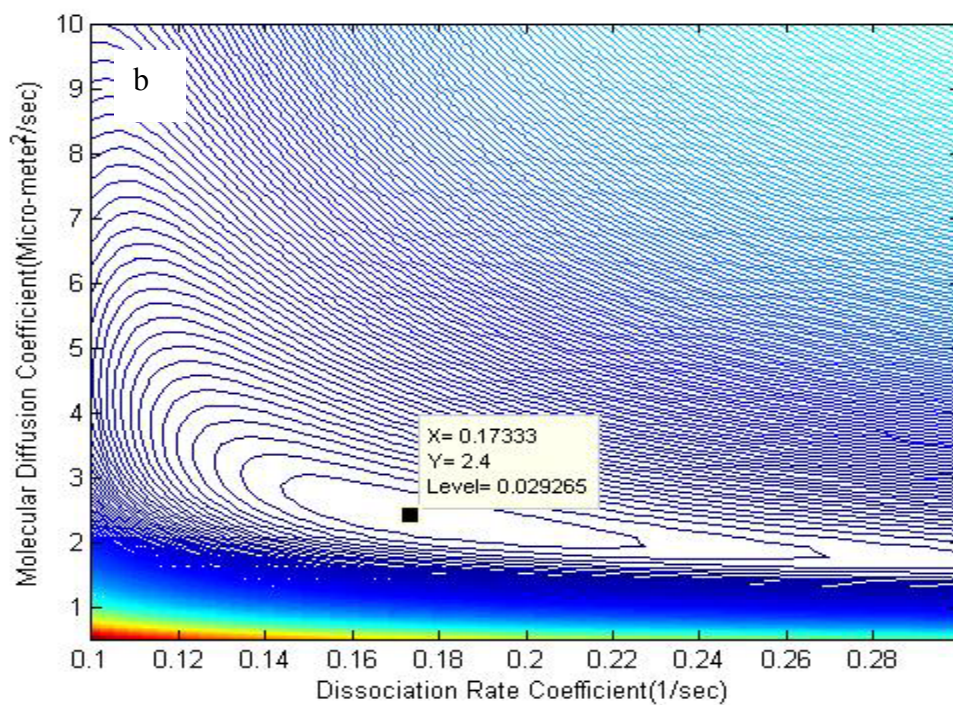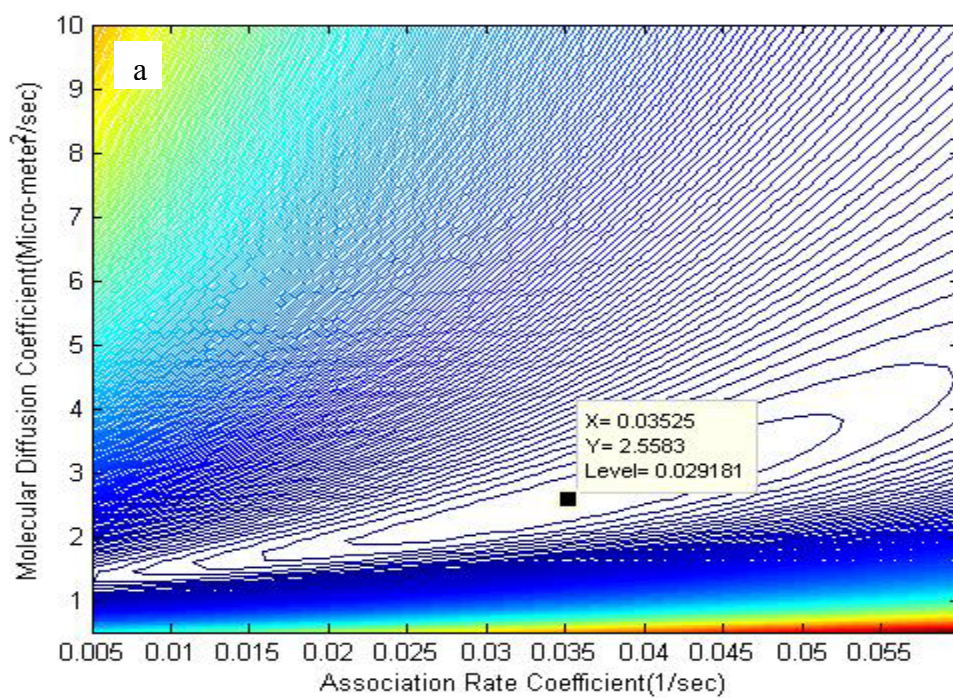
Figure 5.36. Contours of the objective function, $\Phi(\overline{frap})$, in $D_f - K_a^*$ (a) and $D_f - K_d$ (b) planes (experimental data).
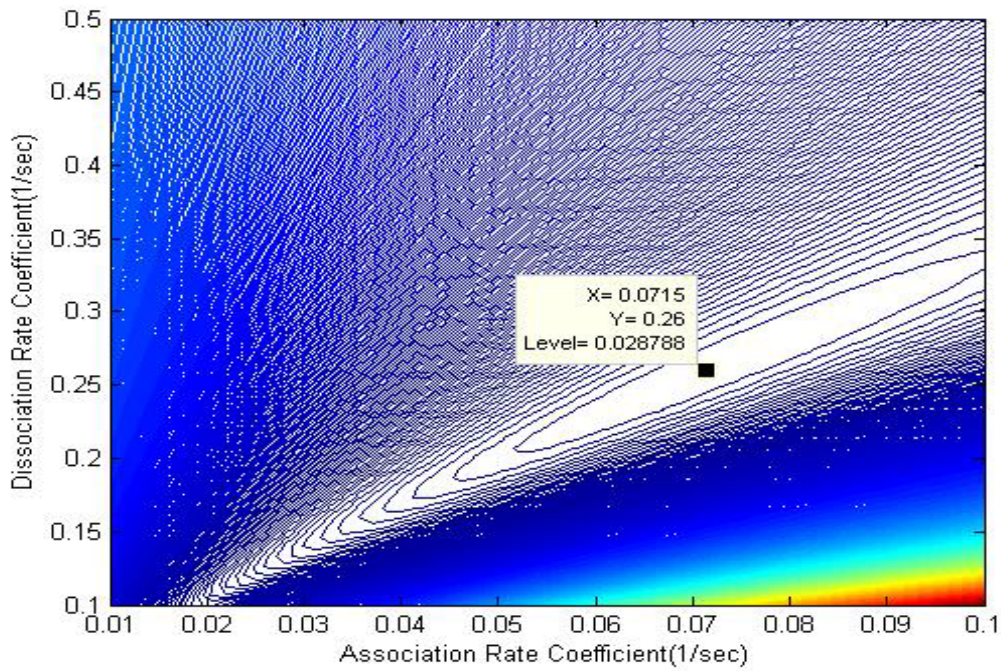
Figure 5.37. Contours of the objective function, $\Phi(\overline{frap})$, in $K_a^* - K_d$ plane (experimental data).

objective function. The magnitude of the objective function (denoted as Level) along with the minimum values of the parameters (denoted as X and Y) are given in the plots.

The $K_s - \alpha$ and $K_s - n$ planes in Figures 5.38a and 5.38b show well defined valleys which start at small value of K_s and large values of α and n and extend in parabolic shape in K_s direction. The response surfaces show an inverse relationship between K_s and α as well as K_s and n in terms of their effects on the objective function $\Phi(\theta)$. An increase in K_s in higher subspace of the parameter space and corresponding decrease in α and n in lower subspace will produce the same behavior in the objective function, $\Phi(\theta)$.

Figure 5.38. Contours of the objective function, $\Phi(\theta)$, for heterogeneous soil in $K_s - \alpha$ (a) and $K_s - n$ (b) planes.

Analysis of the hyperbolic shape of $\Phi(\theta)$ in Figure 5.38a suggests that for higher values of α (lower values of K_s), the objective function becomes insensitive to α but in lower subspace of α (higher values of K_s) it becomes insensitive to K_s. In middle part of the parameter space both parameters are more identifiable ($0.025 < \alpha < 0.036, cm^{-1}$ and $5 < K_s < 7, cmday^{-1}$).

The hyperbolic behavior of the objective, $\Phi(\theta)$, in Figure 5.38b indicates that K_s is more identifiable in the middle part of the domain of n ($1.385 < n < 1.45$). It also suggests that n is more identifiable in the relatively small subspace of K_s ($4 < K_s < 7, cmday^{-1}$). The objective function becomes insensitive to K_s in lower values of n (higher values of K_s) and actually extends parallel to K_s direction. On the other hand, $\Phi(\theta)$ becomes insensitive to n in lower values of K_s and higher values of n ($K_s < 2cmday^{-1}$). The plot in this region is almost parallel to n.

Figure 5.39a presents the response surface plot of the objective function $\Phi(\theta)$ in $\alpha - n$ direction. Again, the response surfaces show an inverse relationship between α and n in terms of their effects on the objective function. An increase in α in higher subspace of the parameter domain and corresponding decrease in n in lower subspace cause the same response in the objective function, $\Phi(\theta)$. The hyperbolic shape of $\Phi(\theta)$ suggests that for higher values of α (lower values of n), the objective function becomes insensitive to α but in lower subspace of α (higher values of n) it becomes insensitive to n. In middle part of the plot, both parameters are more identifiable but there are an infinite combinations of parameters α and n around the error level $\Phi(\theta) = 0.0099$
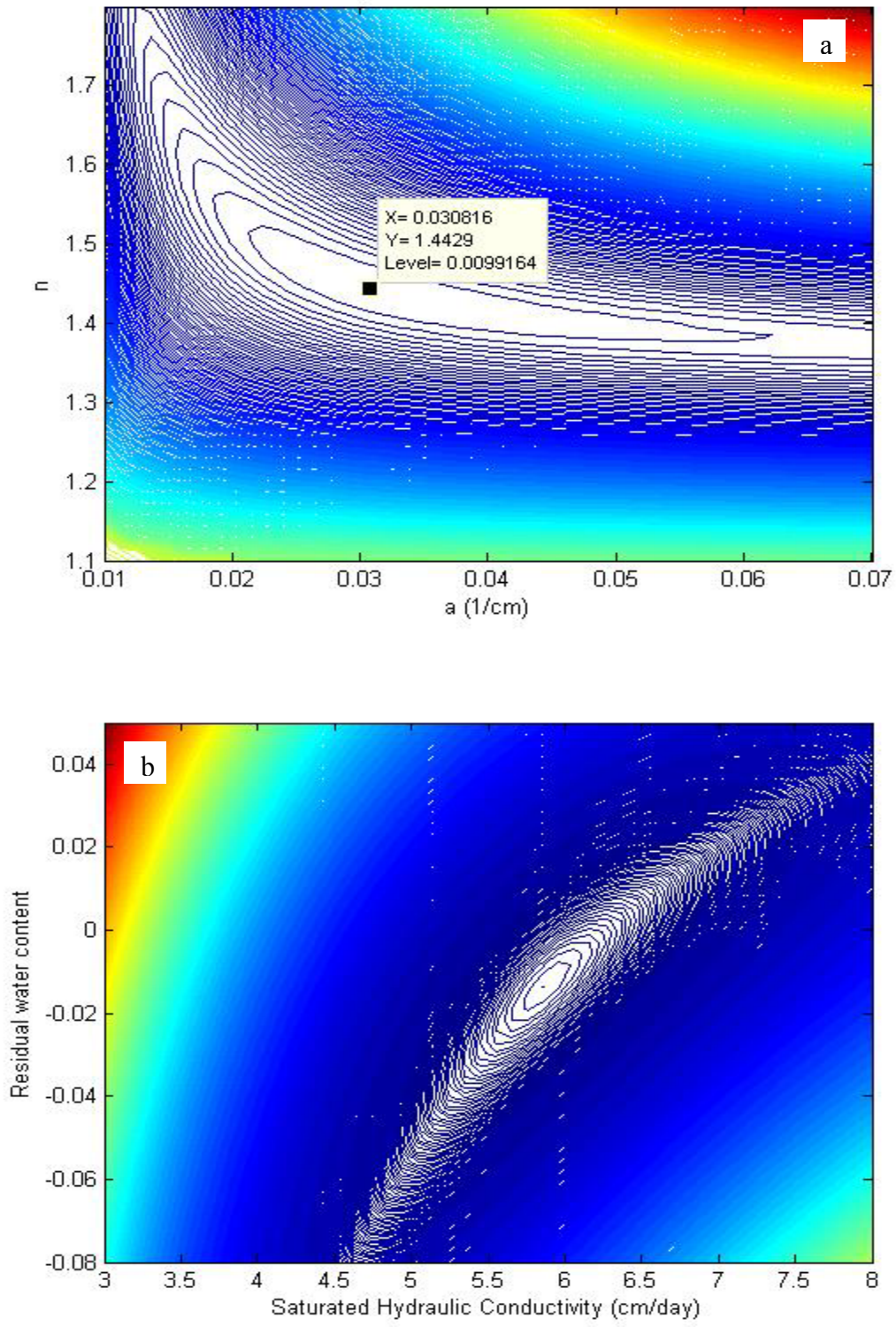
Figure 5.39. Contours of the objective function, $\Phi(\theta)$, for heterogeneous soil in $\alpha - n$ (a) and $K_s - \theta_r$ (b) planes.

(denoted as $Level = 0.0099164$ in the plot) that can produce almost $\Phi(\theta) = 0.0099$. This indicates that the bottom of the objective function at the vicinity of the solution is very flat and it is very difficult or essentially impossible to obtain unique values for α and n. Note that values of n between almost $1.41 < n < 1.45$ and values of α between almost $0.025 < \alpha < 0.04 cm^{-1}$ produce the function value (error level) of $\Phi(\theta) = 0.0099$ which confirms that the bottom of the penalty function is flat near to the solution (any points inside the internal ellipsoid in Figure 5.39a produce $\Phi(\theta) = 0.0099$ with minor differences in the sixth or seventh digit). This conclusion is consistent with the result of Table 5.12, which itself is a result of single-objective parameter optimization in which just the soil moisture content data were used in the formulation of the objective function. Table 5.12 showed that using only the soil moisture data in the parameter optimization procedure, produce stable values for K_s, ι, and θ_r while different initial guesses for the parameters produced different optimized values for α and n.

Figure 5.39b shows the response surface plot of the objective function $\Phi(\theta)$ in the $K_s - \theta_r$ plane. The plot shows well defined minimum. K_s and θ_r in all of the response surfaces converged to $5.9 cmday^{-1}$ and zero which are their optimized values obtained through inverse modeling (see Table 5.15). In other words, the inverse modeling and the response surfaces produced the same values for the saturated hydraulic conductivity and residual water content. In some of the response surfaces the optimized value of θ_r was negative, which is physically unrealistic. The reason for these minor differences is that the constrained optimization was used to identify the hydraulic parameters. In the inverse code lower and upper constraints were imposed on the

parameters being optimized. In case of the residual water content, if it becomes less than 0.001, the algorithm replaces it with zero and continues to run. Without these limitations, the algorithm may find negative value for θ_r.

This is again consistent with the result of Table 5.12 in which stable optimized values were obtained for K_s and θ_r using the developed inverse modeling strategy regardless of the initial guesses for the parameters.

Figures 5.40a, 5.40b, and 5.41a show the response surface plots of the objective function $\Phi(\theta)$ in the $\theta_r - n$, $\theta_r - \alpha$, and $\iota - \theta_r$ planes. The objective function have very well defined minimum in all of the three plots. In other words, the soil water content data produces useful information to identify θ_r with. This is somewhat expected since the residual water content, by definition, is the water content at $1500 kPa$ soil water matric potential head. Therefore, it should be better estimated by the soil moisture data. This is consistent with the results of hydraulic parameter optimization (see Table 5.15) and also with the results of parameter sensitivity analysis which will be discussed later in 5.4.2.2.

Contours of the objective function, $\Phi(\theta)$, in $\iota - n$, $\iota - K_s$, and $\iota - \alpha$ planes are presented in Figures 5.41b, 5.42a, and 5.42b. The $\iota - n$ plane in Figure 5.41b shows a well defined valley which starts at low ι and middle n and extends in logarithmic shape through almost the entire parameter space. The response surfaces show a direct relationship between ι and n in terms of their effects on the objective function. An increase in n and higher value of ι generates the same response in the objective function, $\Phi(\theta)$ which makes it very difficult to obtain a unique solution for ι and n. Again, this is somewhat expected since both of these parameters are exponents in the Mualem-van Genuchten models (ι is exponent in the Mualem's equation (2.25) and n in
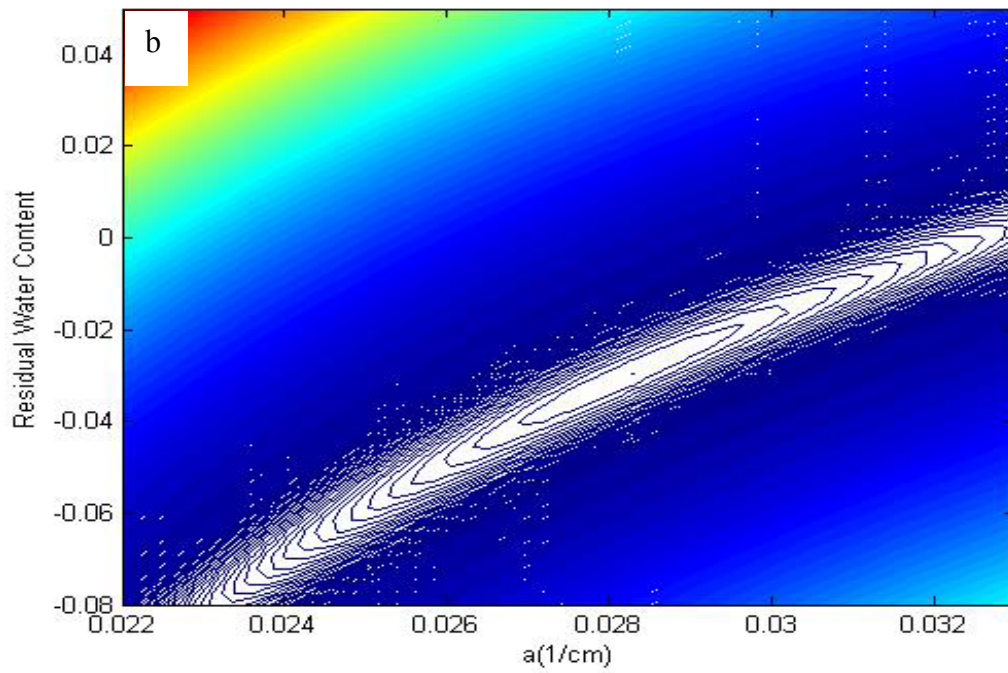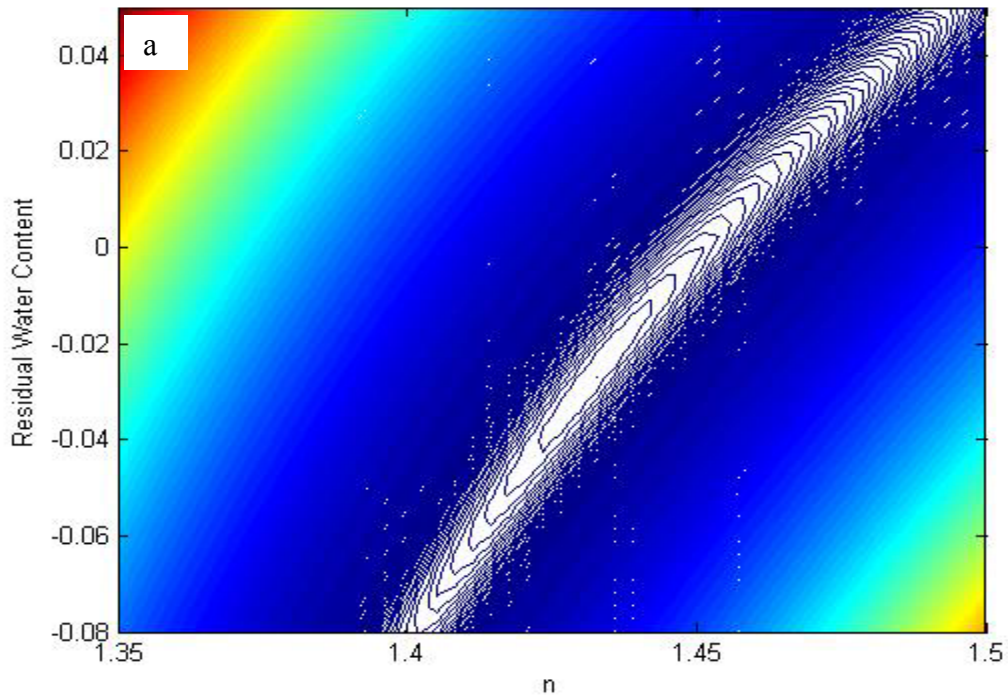
Figure 5.40. Contours of the objective function, $\Phi(\theta)$, for heterogeneous soil in $\theta_r - n$ (a) and $\theta_r - \alpha$ (b) planes.
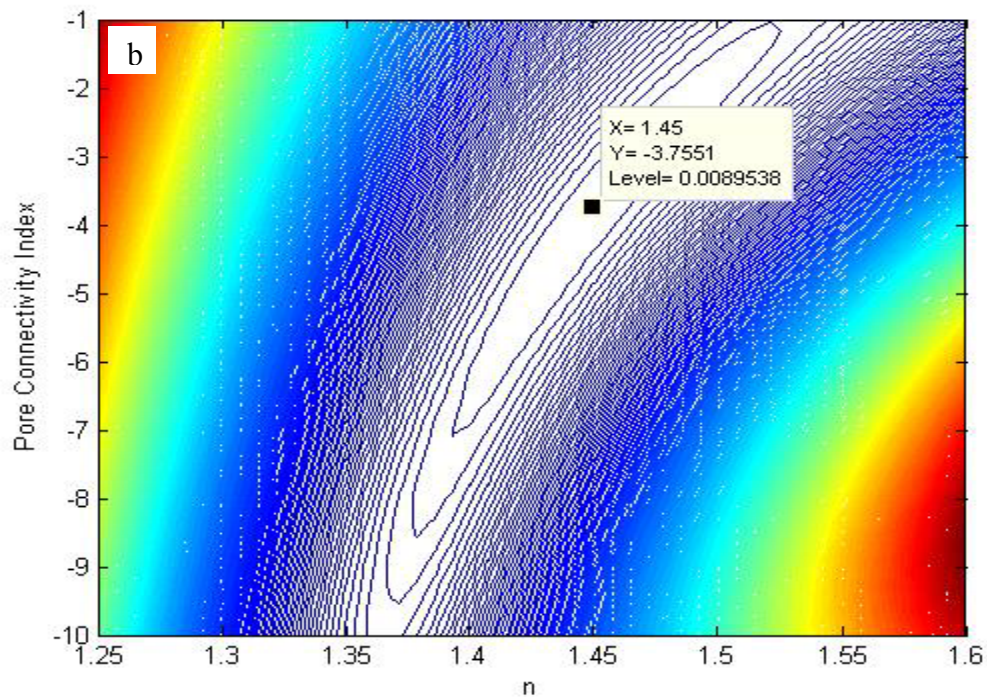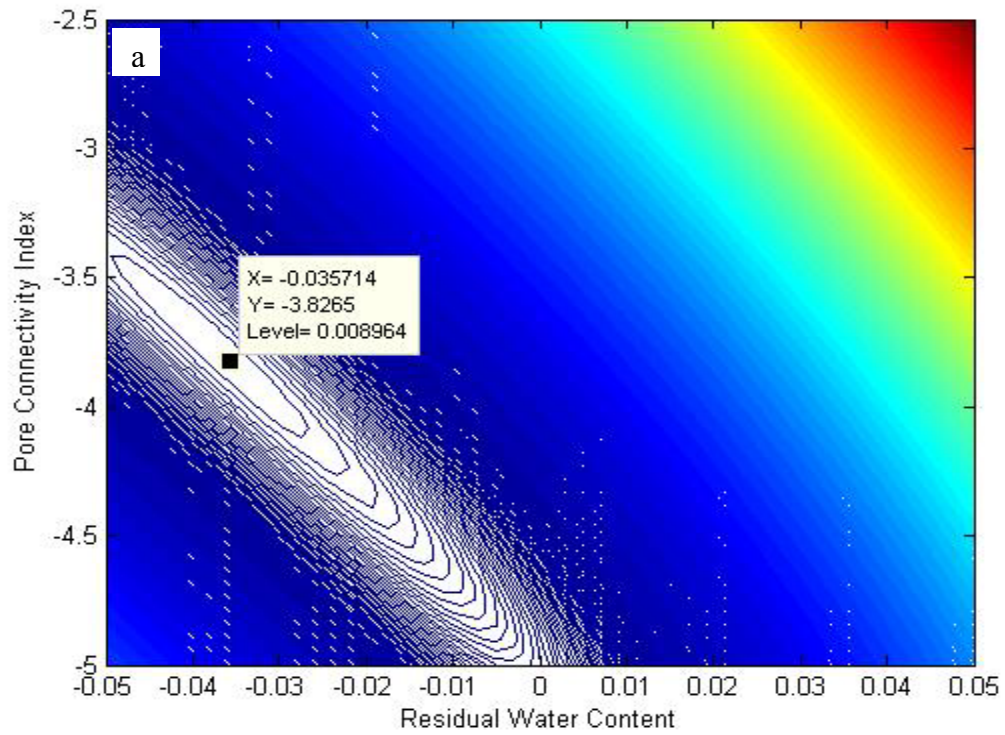
Figure 5.41. Contours of the objective function, $\Phi(\theta)$, for heterogeneous soil in $\iota - \theta_r$ (a) and $\iota - n$ (b) planes.
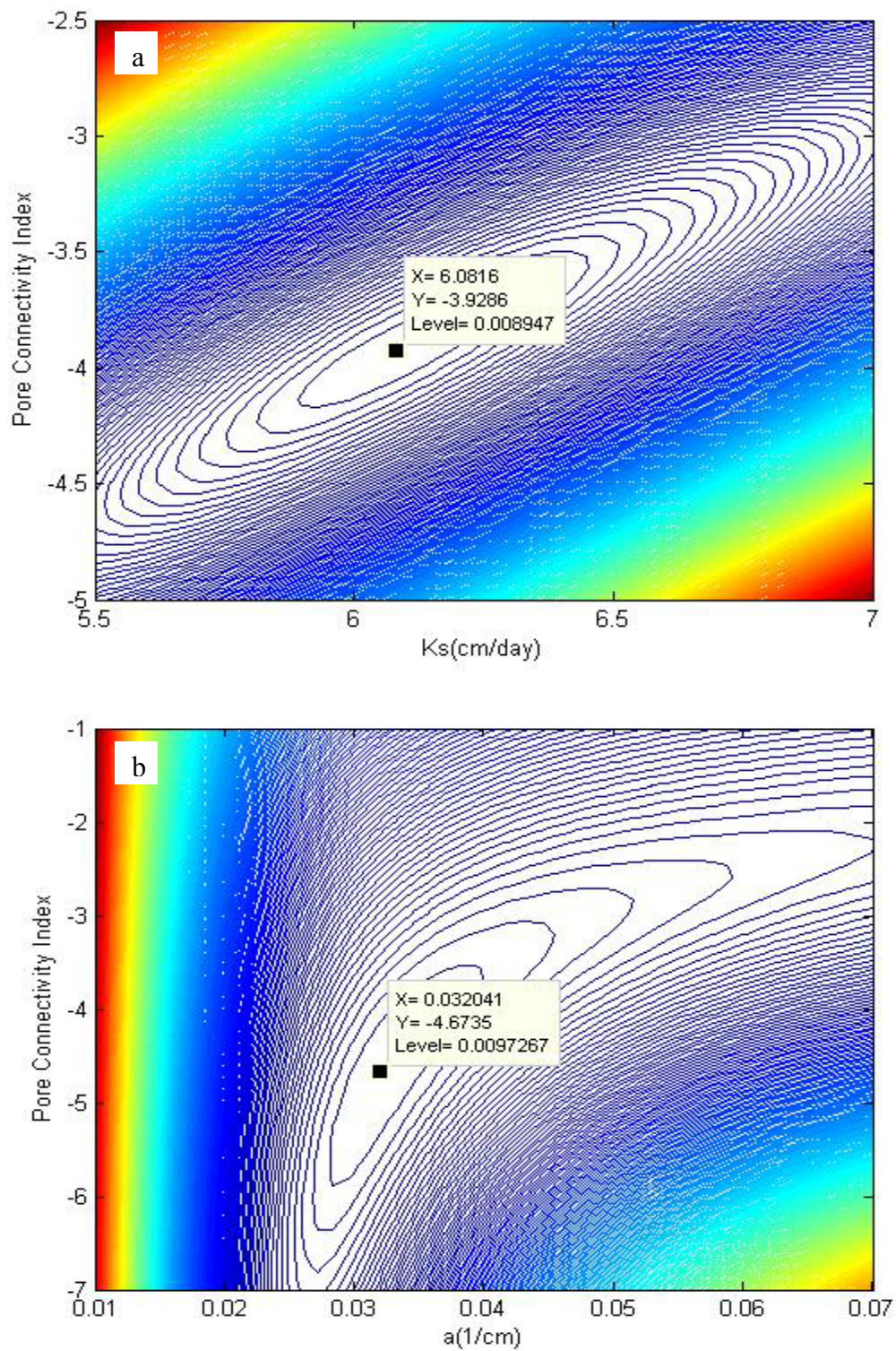
Figure 5.42. Contours of the objective function, $\Phi(\theta)$, for heterogeneous soil in $\iota - K_s$ (a) and $\iota - \alpha$ (b) planes.

the van Genuchten'n empirical formula (2.24)). Furthermore, there is high inter-correlation between these two parameters thus making them less identifiable. Any values inside the internal ellipsoid produce an objective function value of $\Phi(\theta) = 0.00895$. Indeed, there are infinite combinations of parameters ι and n inside the ellipsoid that can produce the same error level. This indicates that the objective function is insensitive to ι since for parameter values of n between 1.4 and 1.5 ($1.4 < n < 1.5$), the pore connectivity index (ι) varies form -7 to -1 ($-7 < \iota < -1$). These inferences are consistent with the results of Table 5.15 in which the parameter confidence interval for ι is wider than other parameters ($-6.7135 < \iota = -4.6735 < -2.6335$) and the estimation variance for this parameter ($\sigma_\iota^2 = 1.0428$) is the highest among the optimized values of the hydraulic parameters. The finding is also consistent with the results of parameter sensitivity analysis, will be discussed in 5.4.2.2, which showed that $\Phi(\theta)$ is almost insensitive to the pore connectivity index (ι) in the Mualem's model.

Other explanation for the wide valley in Figure 5.41b, which produces very small function value, is that the bottom of the objective function at the vicinity of the solution is very flat and it is very difficult to find unique values for the pore connectivity index (ι).

Figure 5.42a shows the response surface plot of the objective function $\Phi(\theta)$ in the $\iota - K_s$ plane. The response surfaces indicate a logarithmic relationship between ι and K_s in terms of their effects on the objective function. A higher value of ι and an increase in K_s yields the same response in the objective function, $\Phi(\theta)$, which makes it very difficult to obtain a unique set for ι and K_s. Again, any combinations of ι and K_s inside the well-defined internal ellipsoid will produce an objective function value (error level)

of $\Phi(\theta) = 0.008947$ which is very small. This is another indication that the objective function is very flat in the $\iota - K_s$ direction.

Figure 5.42b shows contours of the objective function $\Phi(\theta)$ in the $\iota - \alpha$ plane. Analysis of the logarithmic shape of $\Phi(\theta)$ in Figure 5.42b suggests that for higher values of α and ι, the objective function becomes insensitive to α but in lower values of α and ι, it becomes insensitive to ι. Indeed, in higher values of α it becomes parallel to α and in lower values of this parameter it becomes parallel to ι. In middle part of the parameter domain, both parameters are more identifiable ($(0.027 < \alpha < 0.037)$ and $-5.5 < \iota < -3.5$)) and the objective function produces a well-defined minimum.

Another ten pairs of response surfaces were constructed for the homogeneous soil using the soil water content and the pressure head information in a multi-objective function ($\Phi(\theta+h)$) framework. The data for developing these response surfaces were taken from Abeele (1984). These planes are depicted in Figures 5.43 through 5.47. While the combined objective function is not sensitive to θ_r, it produces well-defined minimum for $K_s - n$, $K_s - \iota$, $K_s - \theta_r$, $\iota - n$, $\iota - \alpha$, and other planes. Using more information clearly increases the identifiability of the model parameters. Except for the $K_s - \theta_r$ plane, which generates a well-defined minimum, the contours of the objective function $\Phi(\theta+h)$, in $\alpha - \theta_r$, $n - \theta_r$, and $\iota - \theta_r$ planes are almost parallel with the θ_r direction thus implying that this parameter is very difficult to identify from the available soil moisture content and pressure head information through parameter optimization approach. The best way to identify this parameter is to measure it in pressure plate apparatus at $1500 kP$ pneumatic pressure.
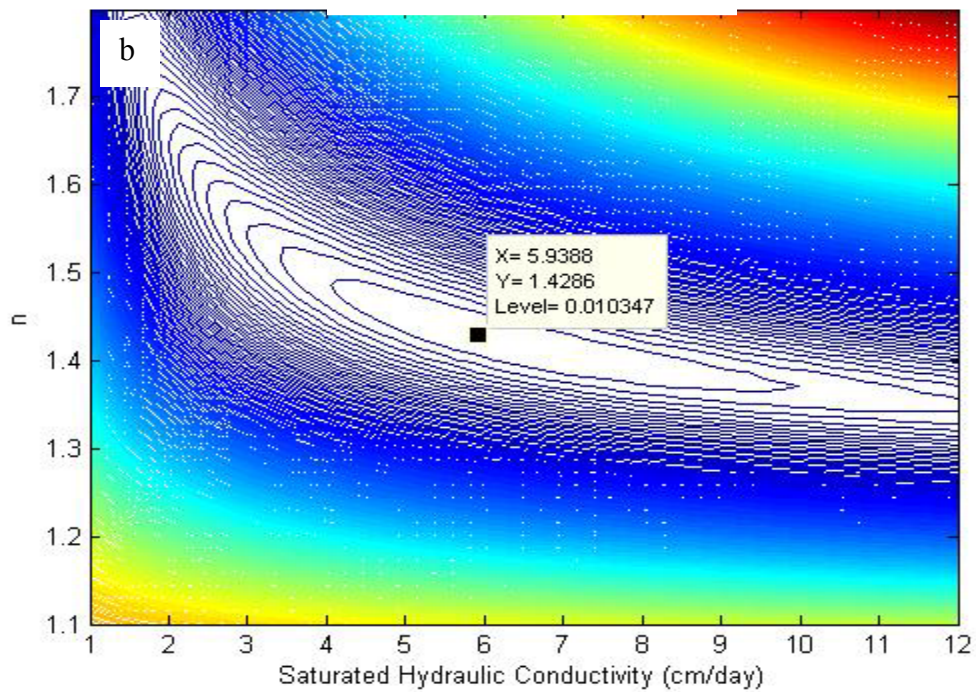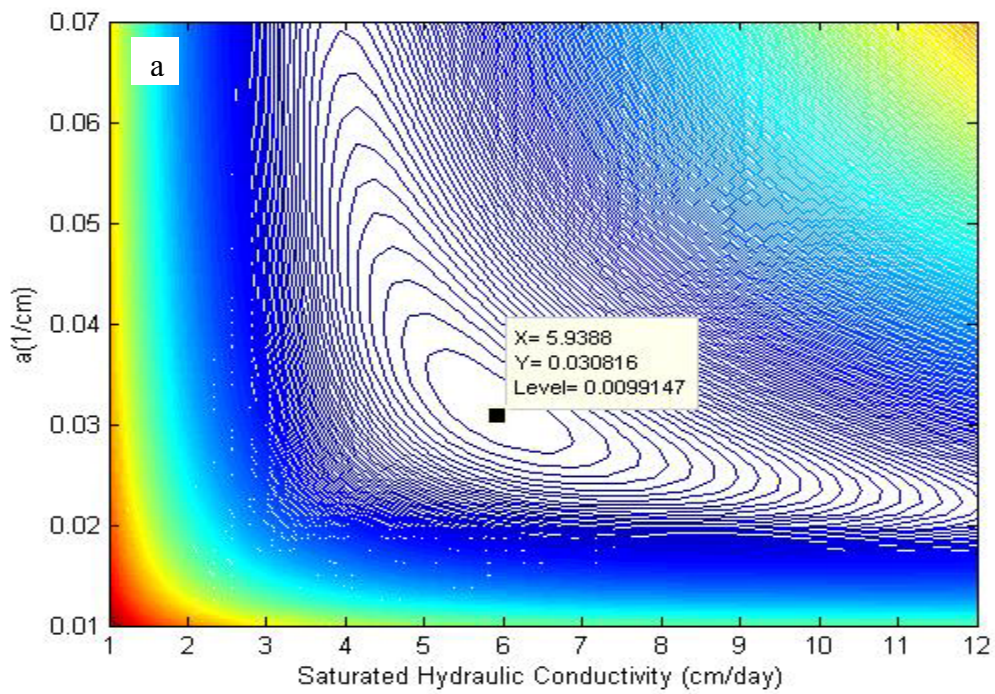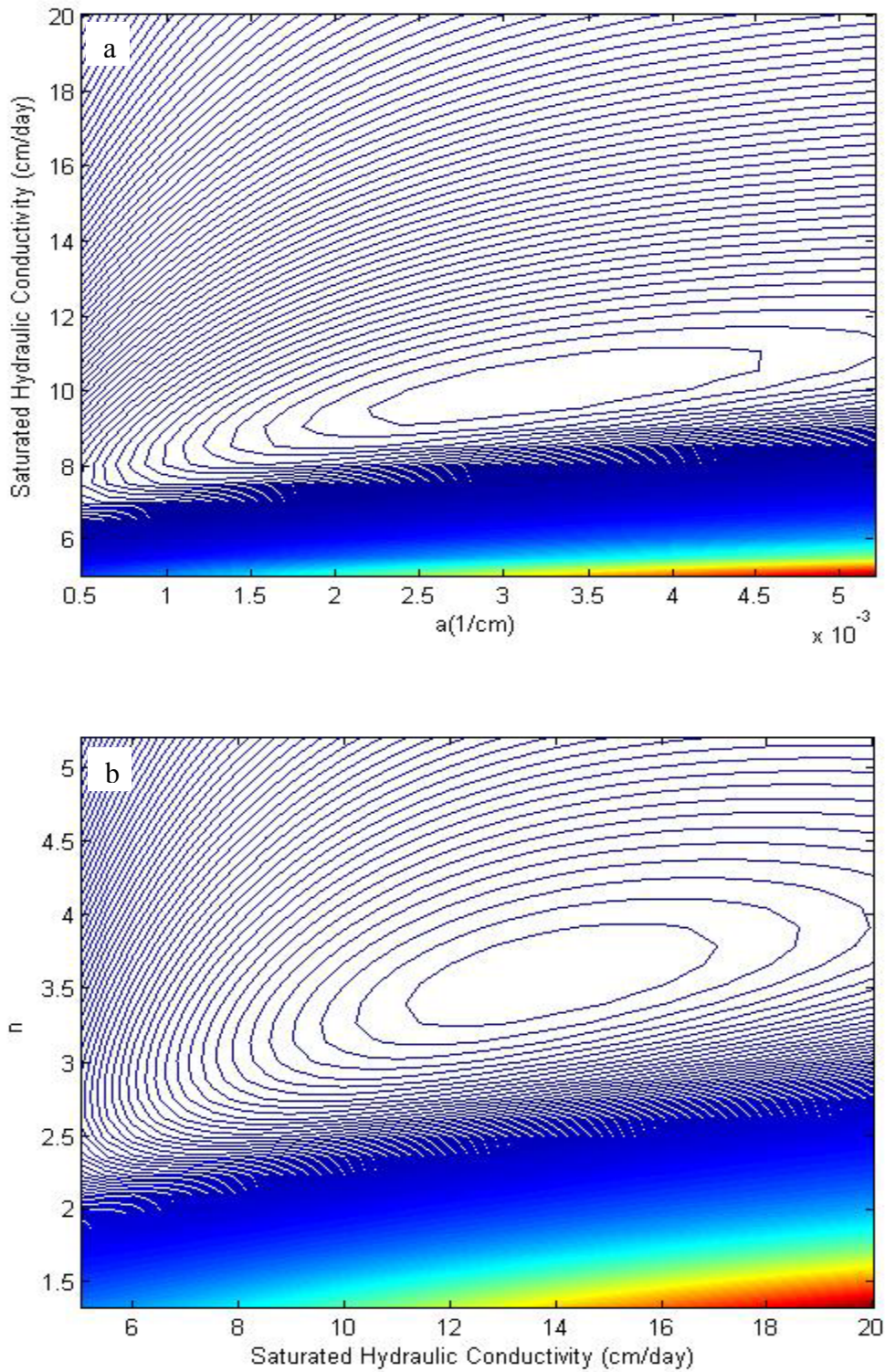
Figure 5.43. Contours of the objective function, $\Phi(\theta + h)$, for homogeneous soil in $K_s - \alpha$ (a) and $K_s - n$ (b) planes.
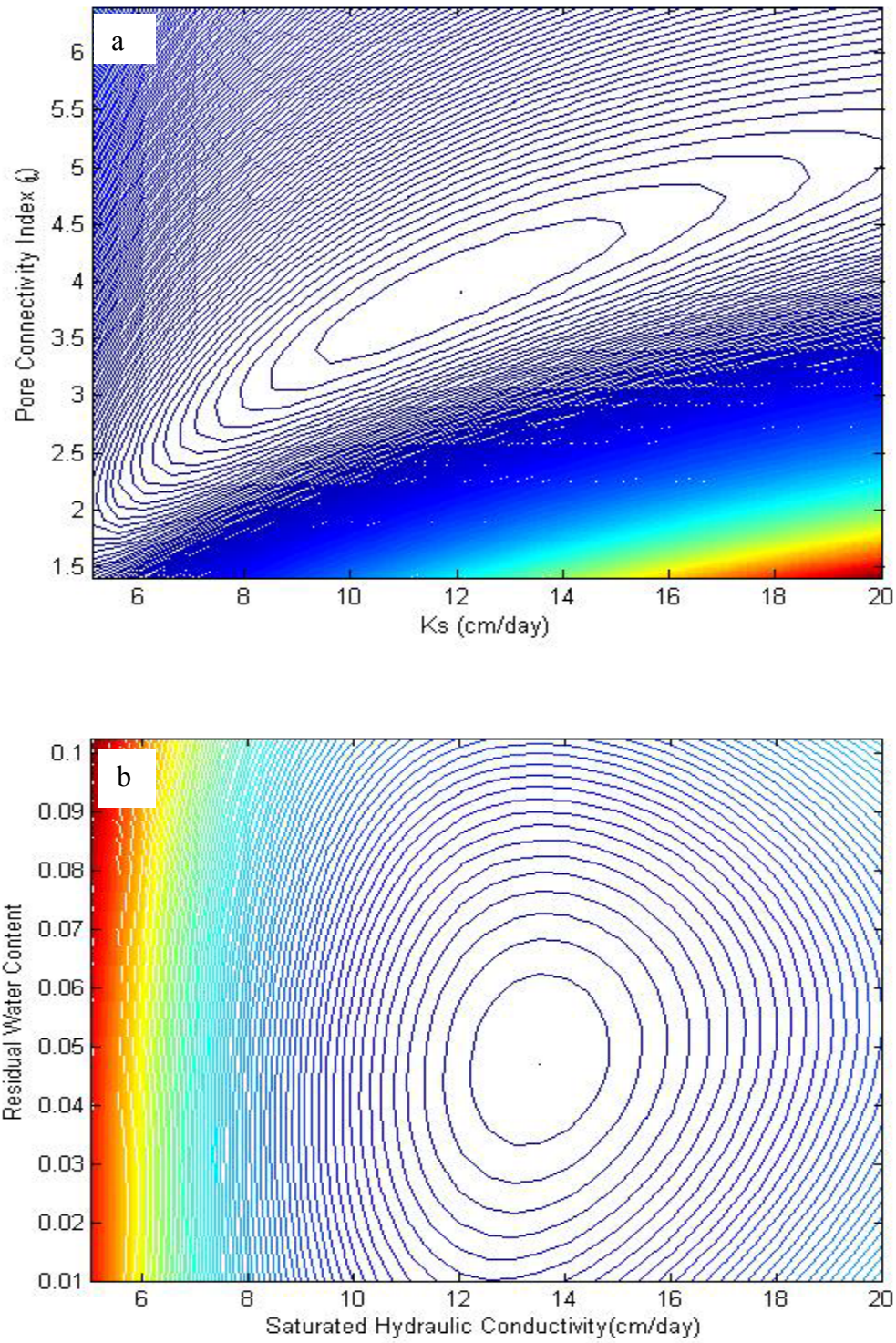
Figure 5.44. Contours of the objective function, $\Phi(\theta + h)$, for homogeneous soil in $K_s - \iota$ (a) and $K_s - \theta_r$ (b) planes.
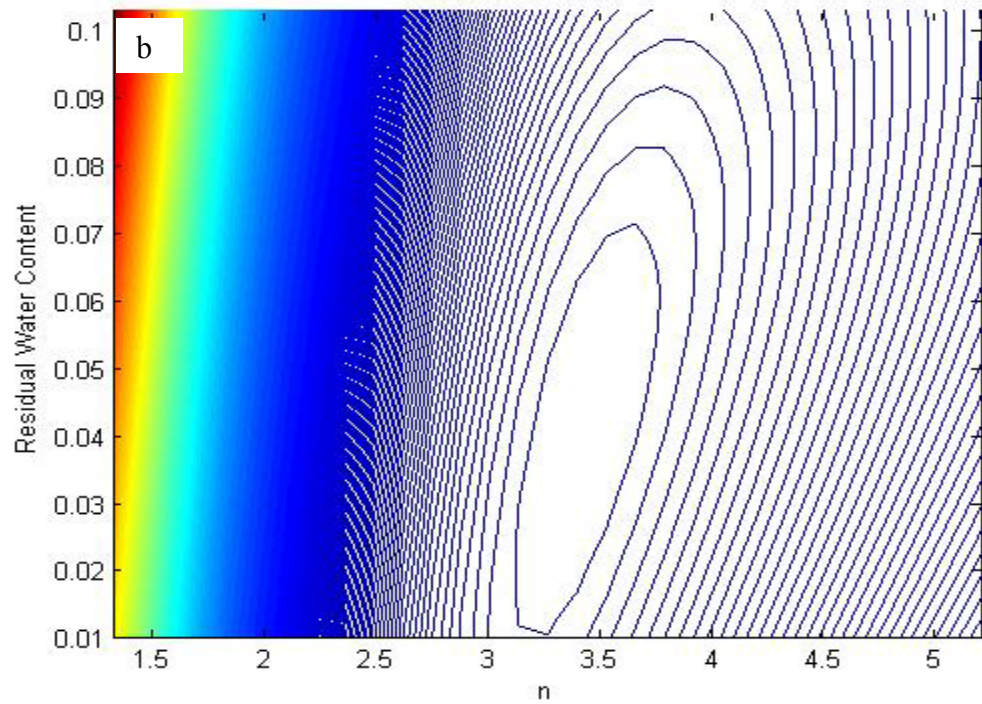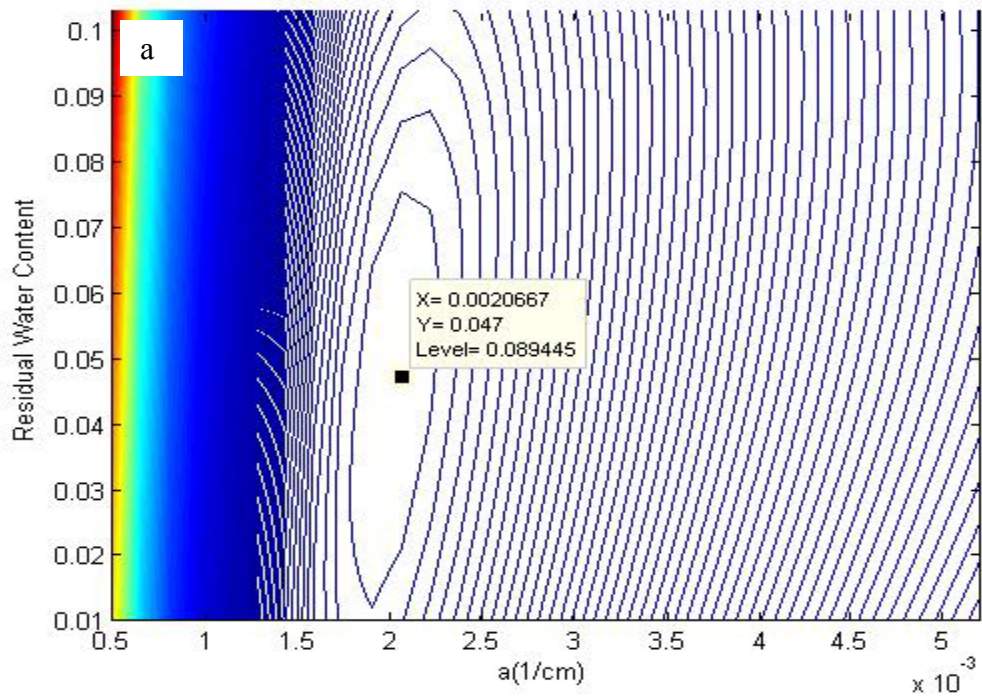
Figure 5.45. Contours of the objective function, $\Phi(\theta + h)$, for homogeneous soil in $\alpha - \theta_r$ (a) and $n - \theta_r$ (b) planes.
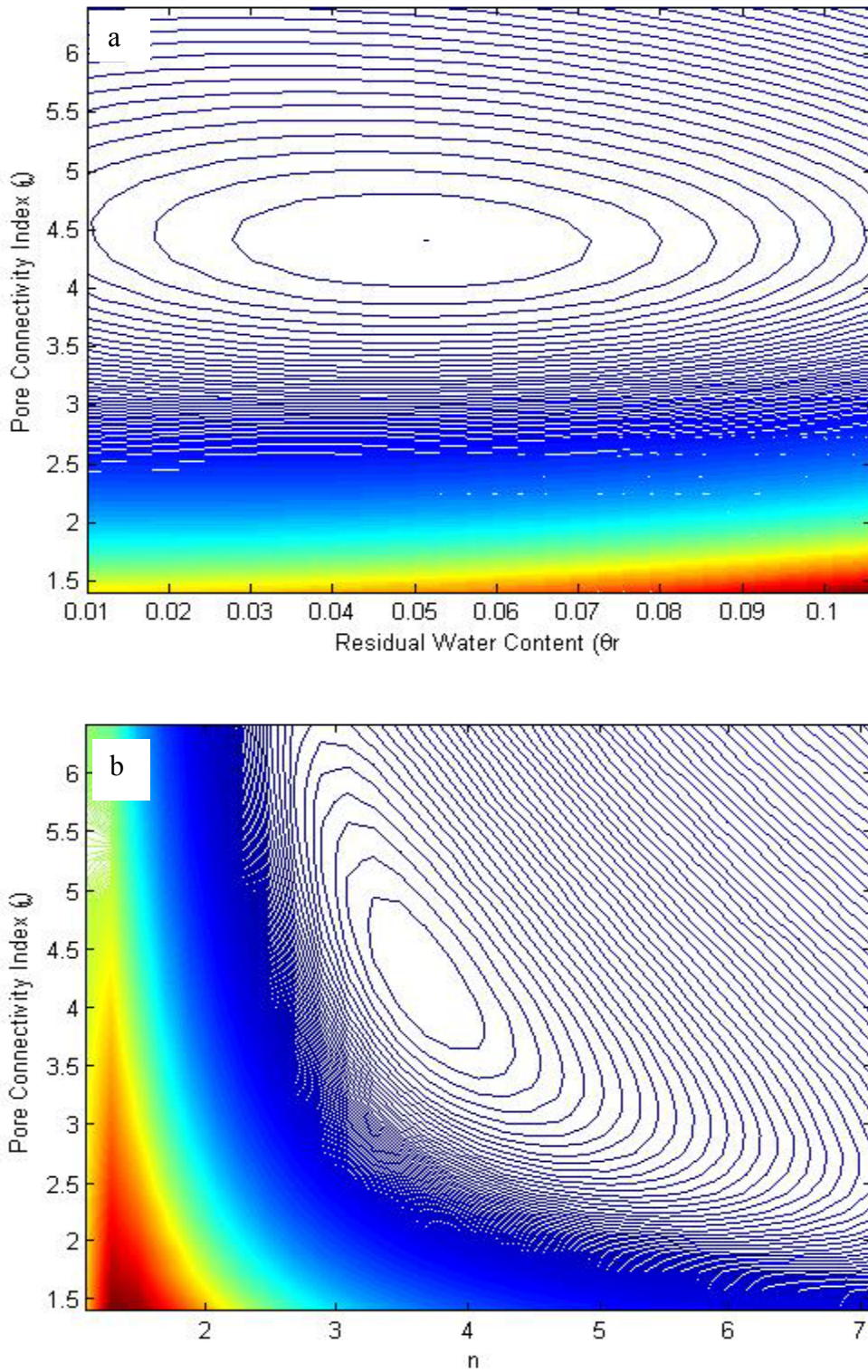
Figure 5.46. Contours of the objective function, $\Phi(\theta + h)$, for homogeneous soil in $\iota - \theta_r$ (a) and $\iota - n$ (b) planes.
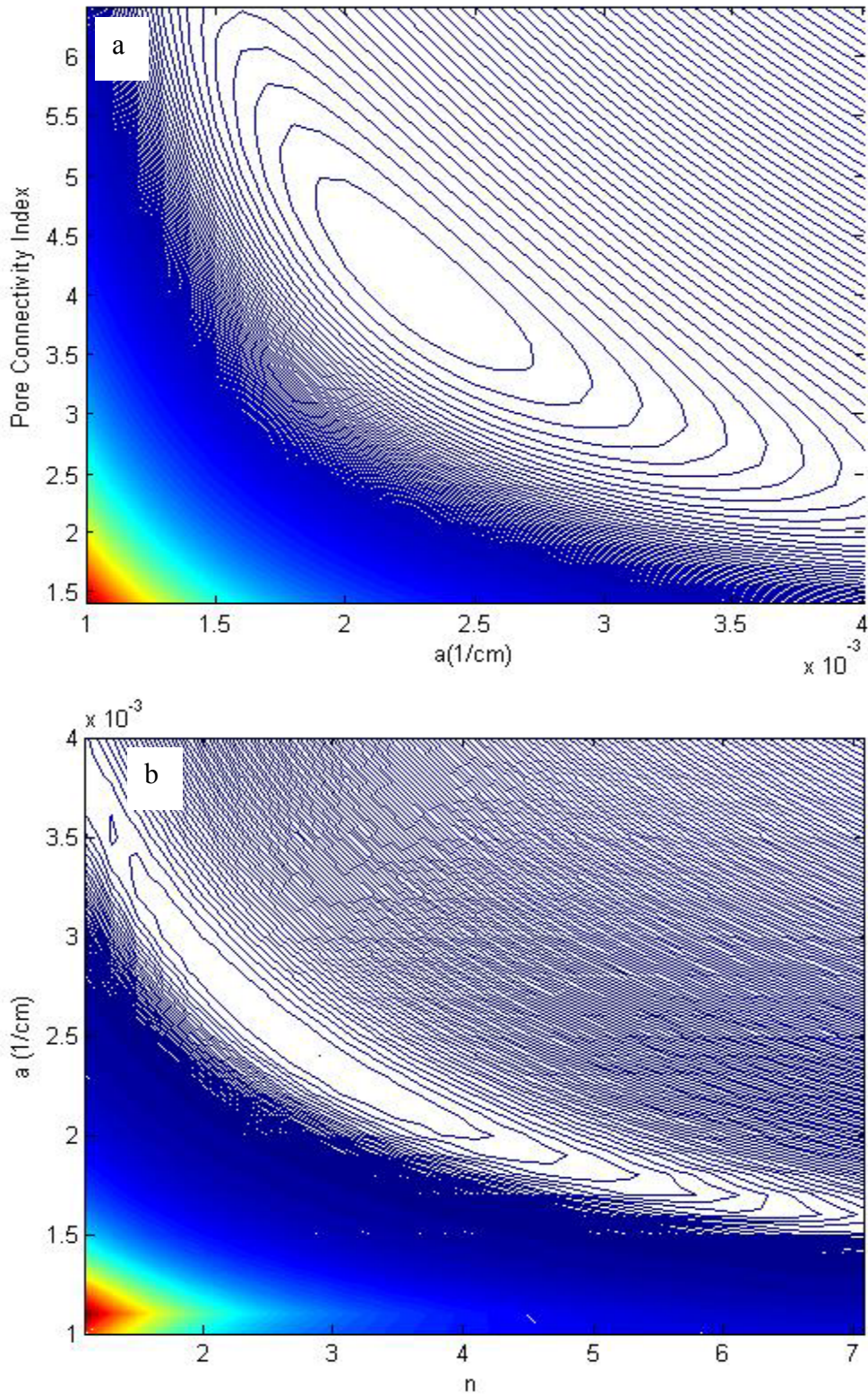
Figure 5.47. Contours of the objective function, $\Phi(\theta + h)$, for homogeneous soil in $\iota - \alpha$ (a) and $\alpha - n$ (b) planes.

The $\alpha - n$ plane in Figure 5.47 shows a small local minimum next to the main well defined ellipsoid. This and other small local minima may be caused by minor oscillations of the numerical solution of the partial differential equations governing mass transport processes in porous media.

The important findings from the analysis of the two-dimensional parameter response surfaces can be summarized as:

First, the objective function $\Phi(\overline{frap})$ is not sensitive enough to the fluorescent recovery data to easily and reliably identify the mass transport coefficients through inverse modeling approach. In response surfaces this lack of sensitivity is characterized by elongated valley parallel to the direction of the diffusion coefficient.

Second, the soil moisture content information and combination of the soil water pressure head and the soil water content provide enough information to identify the saturated hydraulic conductivity of partially saturated soil.

Third, response surfaces, though very useful in analyzing the identifiability of the parameters being optimized, are only two-dimensional cross sections of a full $p - dimensional$ parameter hyper-space. Other local minima may exist in different regions of the parameter space which don't show up in the response surfaces. A well-defined minimum in two-dimensional planes doesn't automatically guarantee that no other minima exist and that the inverse problem is unique.

Fourth, several small local minima in the two-dimensional plane may be produced by minor oscillation of the numerical simulator. Care should be exercised in interpreting these minima.

Fifth, the response surfaces should be constructed and studied in conjunction with the parameter sensitivity analysis, residual analysis, and goodness of fit measures. Otherwise it may lead to misleading results regarding the uniqueness of the inverse problem.

5.4.1.2.2. Parameter Hyper-Space

Since response surfaces are only two-dimensional cross sections of a whole $p-dimensional$ parameter domain, analysis of the behavior of the objective function in full hyper-space will reveal how the function might behave in the whole space. To gain a broader perspective about the identifiability of the model parameters through inverse modeling, a three-dimensional parameter hyper-space was constructed for the FRAP experimental data (Table 4.1) and depicted in Figure 5.48 (note that the image is in logarithmic scale). The graph shows the behavior of the objective function in whole parameter space and presents envelops on which the magnitude of the objective function is the same. The 3-D image shows that the minimum is a plane or envelop (not a distinctive point). The dark blue area shows parameter values which produce the lowest function value. In very small values of D_f the objective function extends almost linearly throughout K_d direction implying that $\Phi(\overline{frap})$ is insensitive to K_d (this confirms the results obtained by two-dimensional response surfaces in Figure 5.36b). In very large values of D_f (and very small values of K_d) the objective function extends parallel to D_f axis and becomes insensitive to this parameter (any values of D_f in the light blue area produces the same error value). This is consistent with the results of Figure 5.35a. The

192
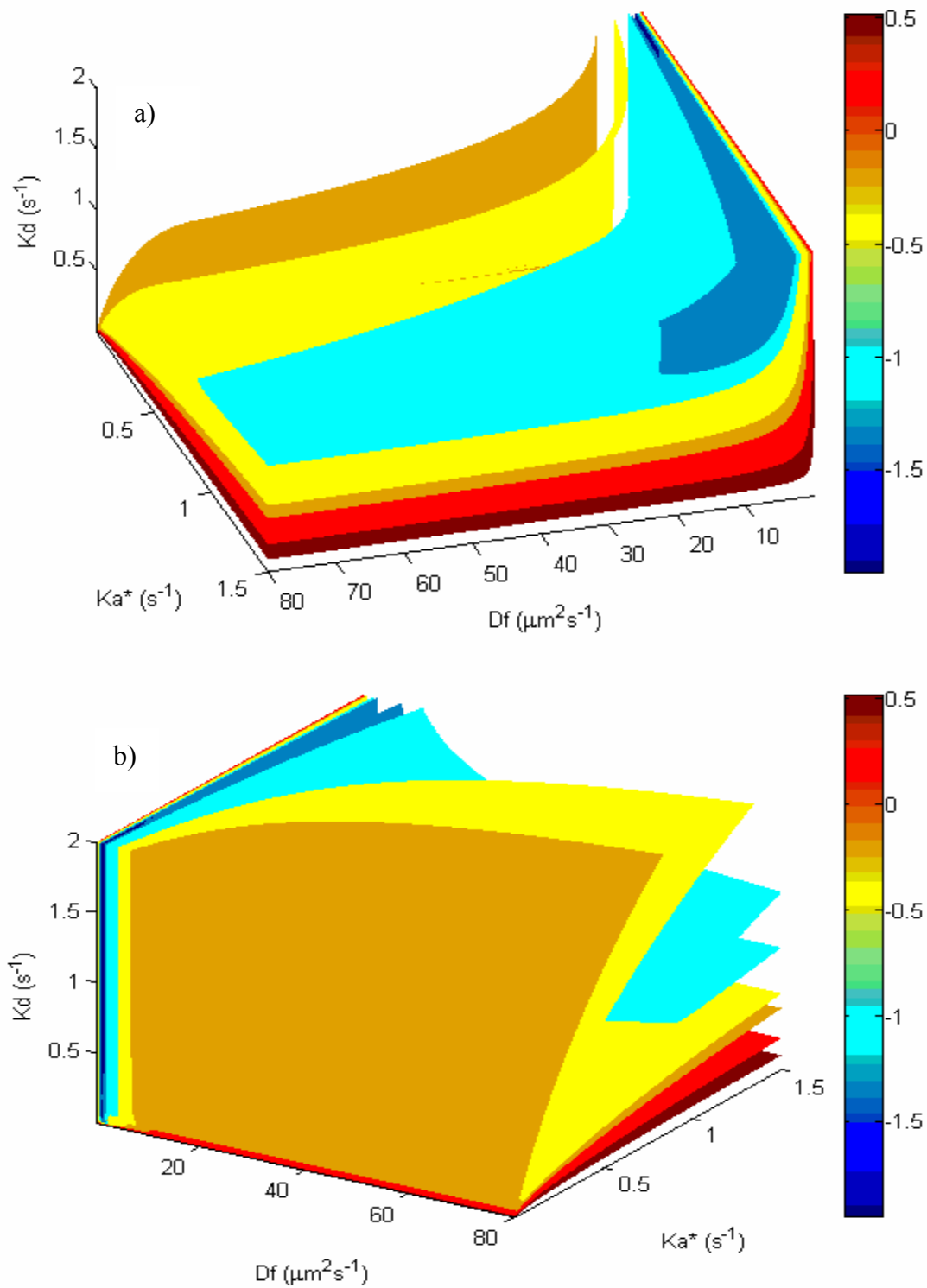
Figure 5.48. Three-dimensional parameter hyper-space of the objective function $\Phi(\overline{frap})$ in $D_f - K_a^* - K_d$ direction.

hyper-space also shows that the minimum is in lower subspace of K_a^* and D_f. Note that the blue area, which has the lowest error value, coincides with $K_a^* < 1s^{-1}$ and $D_f < 10\mu m^2 s^{-1}$.

The graph clearly shows that it is impossible to obtain a unique solution for model parameters in one-site mobile-immobile model. The result obtained by parameter hyper-space is consistent with the results of two-dimensional parameter response surface plot.

To fully understand the behavior of the objective functions $\Phi(\theta + h)$, $\Phi(\theta)$, and $\Phi(h)$ in whole parameter space a 5-dimensional hyper-space should be constructed and demonstrated which is not technically plausible in foreseeable future. However, the behavior of the objective function $\Phi(\theta + h)$ in $K_s - \alpha - n$ direction was constructed and presented in Figure 5.49 in two different perspectives.

The three-dimensional parameter hyper-space in $K_s - \alpha - n$ indicates that even using multi-objective optimization does not result in unique solution for inverse problem in case of water flow through homogeneous soil but the range of optimized values for model parameters are smaller than the single-objective optimization which is consistent with the parameter optimization (compare Tables 5.12 and 5.13). The optimum value of the saturated hydraulic conductivity is between $10 \le K_s \le 15 (cmd^{-1})$, that of α is between $1 \times 10^{-3} \le \alpha \le 2 \times 10^{-3}$ (cm^{-1}), and that of n is between $3 \le n \le 8$. Note that the residual soil moisture content (θ_r) and pore connectivity index (ι) were kept at the optimized values.

Two-dimensional slices of the objective function $\Phi(\theta + h)$ in $\alpha - n$, $K_s - n$, and $K_s - \alpha$ directions are given in Figure 5.50. There are well defined minimum planes in
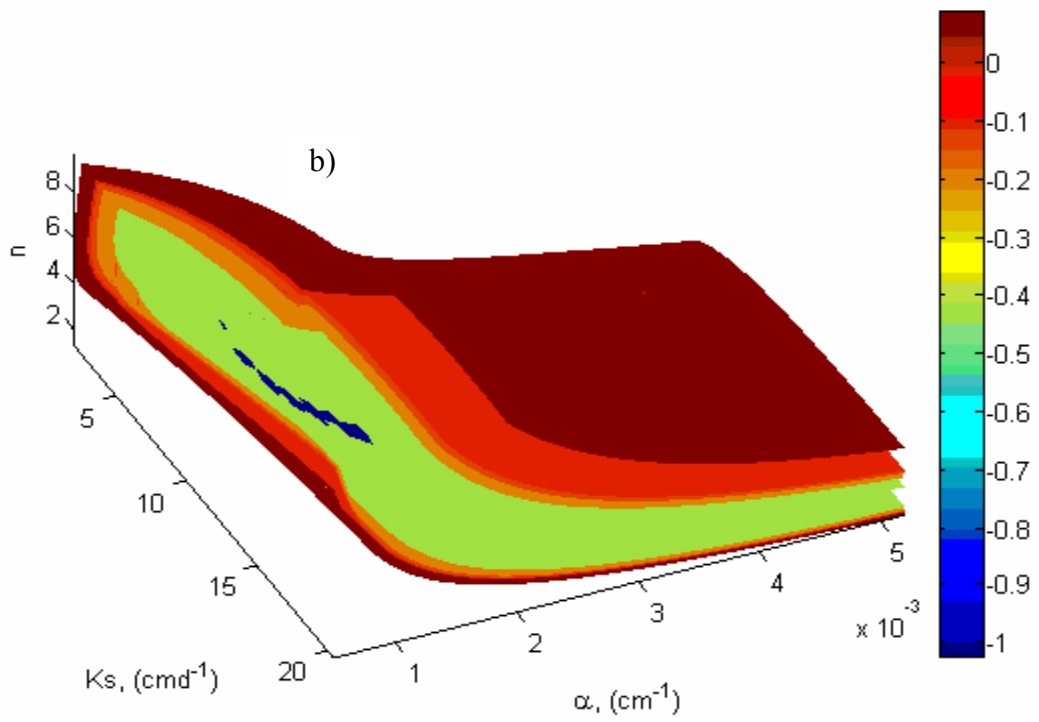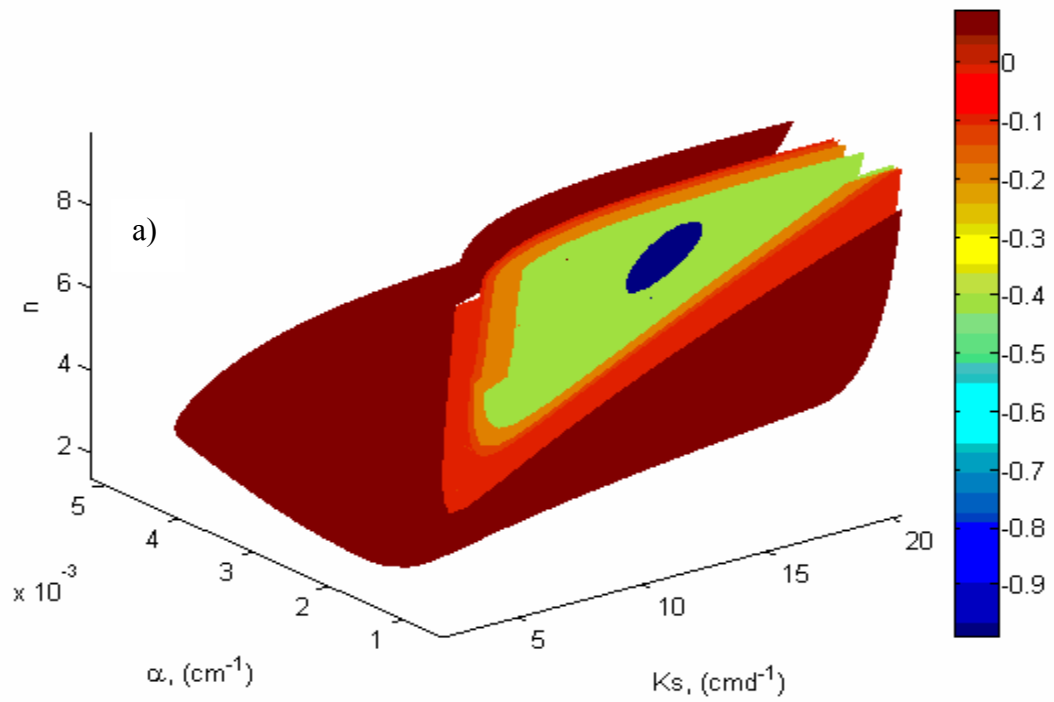
Figure 5.49. Three-dimensional parameter hyper-space of the objective function $\Phi(\theta + h)$ in $K_s - \alpha - n$ direction.
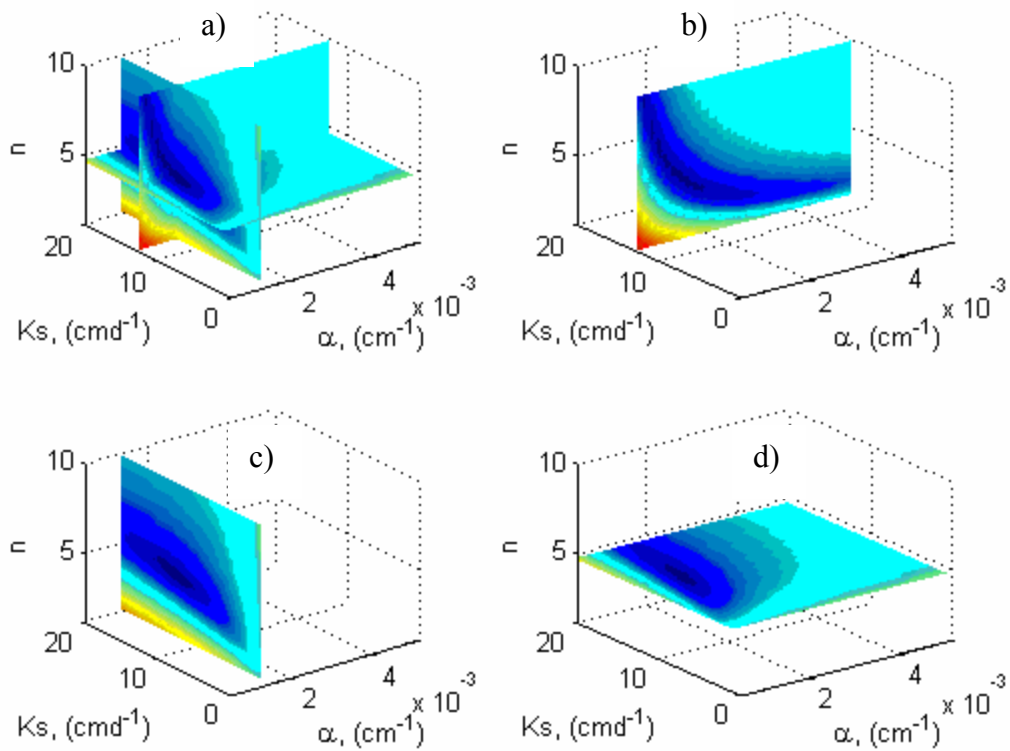
Figure 5.50. Two-dimensional slices of the objective function $\Phi(\theta + h)$ in (a): $K_s - \alpha - n$ direction, b): $\alpha - n$ direction (K_s is constant), c): $K_s - n$ direction (α is constant), and $K_s - \alpha$ direction (n is constant).

$K_s - n$ and $K_s - \alpha$ directions but in $\alpha - n$ direction there is a well defined hyperbola similar to the response surface plot in Figure 5.47b. The result of parameter slices is consistent with the parameter response surface plots and parameter hyper-space. All of them show that the optimized values of the saturated hydraulic conductivity in conjunction with the air entry value (α) and n can be well estimated using soil moisture content and soil water pressure head information in the context of the inverse modeling strategy. However, simultaneous unique estimation of α and n is difficult.

5.4.2. Sensitivity Analysis

5.4.2.1. Biomolecule Transport in Living Cells

The relative sensitivity of the *laser beam recovery*, $\overline{frap}$, with respect to changes in free molecular diffusion coefficient (D_f) of GFP-GR, the pseudo-association rate constant (K_a^*), and the dissociation rate constant (K_d) is presented in Figures 5.51, 5.52, and 5.53. The graphs were generated for several possible solutions in Table 5.3 and the result will only be presented for one solution of the parameter space. The absolute sensitivity of $\overline{frap}$ with respect to model parameters is presented in Appendix B.

Figure 5.51 indicates that the relative sensitivity of the $\overline{frap}$ with respect to changes in D_f increases from the beginning of the FRAP experiment and reaches its peak in less than one second after the initiation of experiment. Then, it rapidly decreases as the experiment proceeds. Indeed after one second it becomes insensitive to the molecular diffusion coefficient (D_f) of GFP-GR and it will be very difficult or essentially impossible to identify D_f from the FRAP protocol.

Figure 5.52 presents the distribution of the sensitivity of $\overline{frap}$ with respect to changes in K_a^* over time course of the FRAP experiment. The sensitivity rapidly increases at the beginning of the experiment and during a time span less than two seconds it reaches its peak. As time of experiment increases $\overline{frap}$ becomes insensitive to the changes in pseudo-association rate constant. Again, $\overline{frap}$ becomes insensitive to the experimental data in the middle and late stages of the FRAP procedure so that it is very difficult to quantify the pseudo-association rate constant from the protocol by inverse
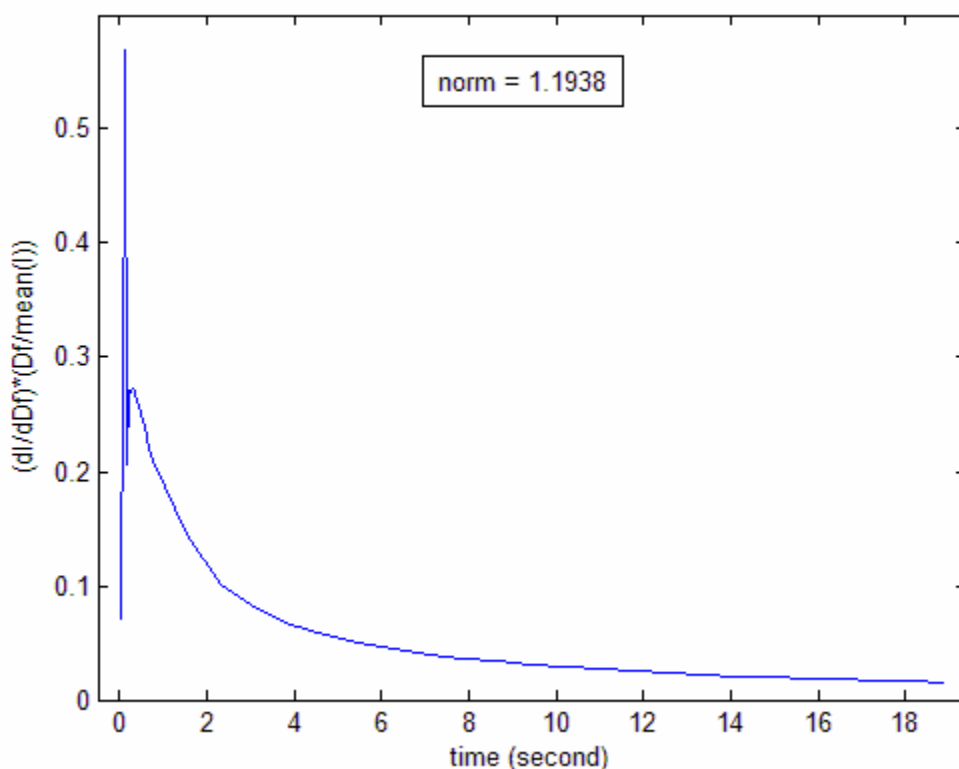
Figure 5.51. Distribution of the relative sensitivity of $\overline{frap}$ with respect to changes in D_f over time course of the FRAP experiment.

modeling.

Finally, Figures 5.53 shows the time distribution of the relative sensitivity of $\overline{frap}$ with respect to changes in K_d. Again, the sensitivity quickly increases at the initial periods of the FRAP experiment and reaches its peak in less than two seconds. Then it sharply decreases and eventually becomes insensitive to the dissociation rate constant. Except for the early stages of the experiment, the protocol doesn't provide useful information to estimate the dissociation rate by nonlinear parameter optimization algorithms.

Parameter sensitivity analysis of the FRAP protocol indicates that:
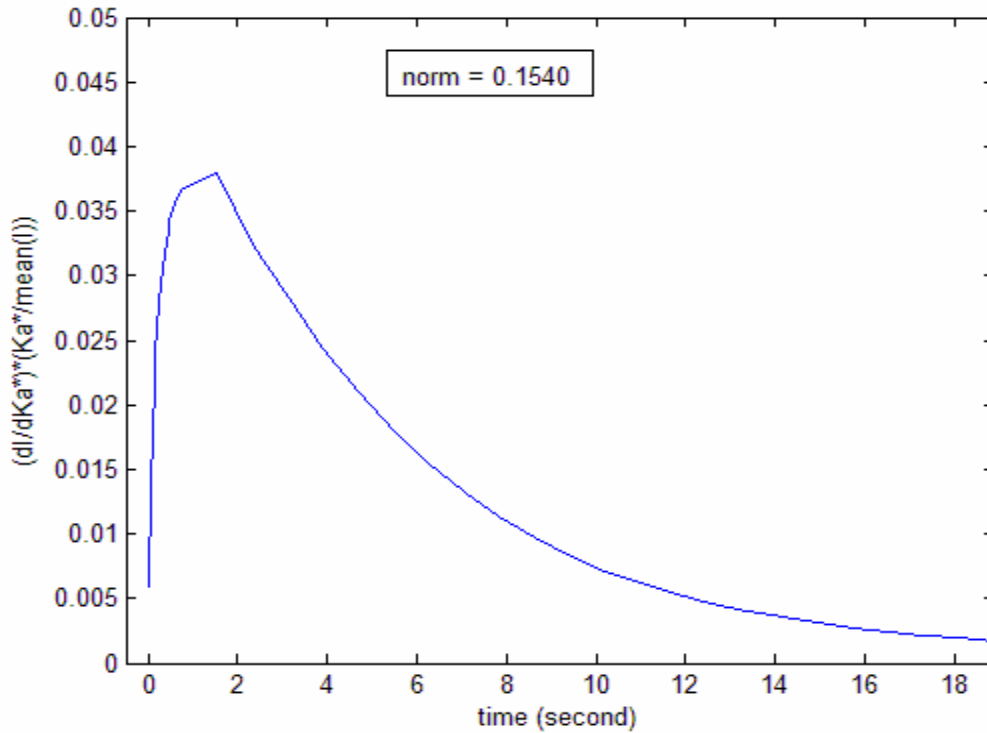
Figure 5.52. Distribution of the relative sensitivity of $\overline{frap}$ with respect to changes in K_a^* over time course of the FRAP experiment.

First, the protocol provides the most useful and sensitive information at the early stages of the experiment. For reliable and accurate parameter estimation, more data should be collected at the early stages of the experiment. For GFP-GR the effective time to perform FRAP experiment is less than five seconds. After that it regains the state of equilibrium which it had before the photochemical bleaching and becomes insensitive to model parameters. This poses enormous challenges in developing innovative techniques to improving the quality of the protocol and to gathering sufficient data points at the beginning of the experiment. One of the shortcomings of the protocol, at the present time, is that the procedure cannot collect enough data points at the early stages of the
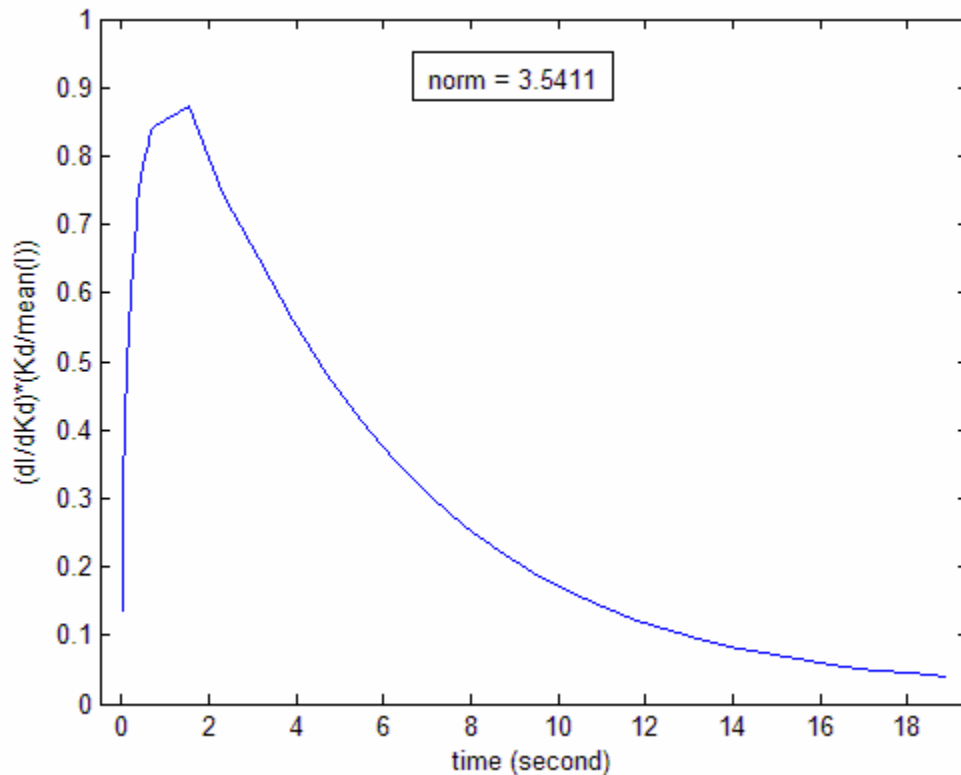
Figure 5.53. Distribution of the relative sensitivity of $\overline{frap}$ with respect to changes in K_d over time course of the FRAP experiment.

experiment.

Second, in parameter optimization by inverse modeling more weight should be given to the data in the early stages of the experiment.

Third, sensitivity of $\overline{frap}$ with respect to different parameters varies by several orders of magnitude. Comparing the norm of the sensitivity and the shape of the graphs in Figures 5.51, 5.52, and 5.53 indicate that K_d is the most sensitive and the most identifiable parameter followed by D_f and K_a^*. This is consistent with the results of

Tables 5.5 to 5.10 where in all of the optimization scenarios, the optimized value of the dissociation rate coefficient approached the "true" value.

5.4.2.2. Water Flow through Partially Saturated Porous Media

Parameter sensitivity analysis was performed for both single objective and multi-objective optimization. In single objective optimization, the sensitivities of the soil water content to changes in model parameters K_s, α, n, θ_r, and ι were calculated and are depicted in Figures 5.54b, 5.55b, 5.56b, 5.57b, and 5.58b. The norm of the columns of the last normalized Jacobian matrix in the optimization procedure was used as a measure to compare the sensitivity of the soil water content with respect to changes in different hydraulic parameters. The soil depths in which measurements were made, are given in the legend.

The same procedure was followed for multi-objective optimization in which the objective function is the weighted soil water content and weighted soil water pressure head ($\Phi(\theta + h)$). The sensitivity of $\Phi(\theta + h)$ with respect to changes in the hydraulic parameters is depicted in Figures 5.54a, 5.55a, 5.56a, 5.57a, and 5.58a. The results are first given for the Los Alamos National Lab data (Abeele, 1984) in which all of the soil characteristics (soil texture, measurements, initial and boundary conditions, etc) are similar except for the objective functions. Since the relative sensitivity is dimensionless, one can compare the sensitivity of the state variables with respect to different parameters and sensitivity of different parameters with each other.

Comparing Figures 54a and 54b, the following remarks can be made about the sensitivity of the objective functions with respect to parameters:
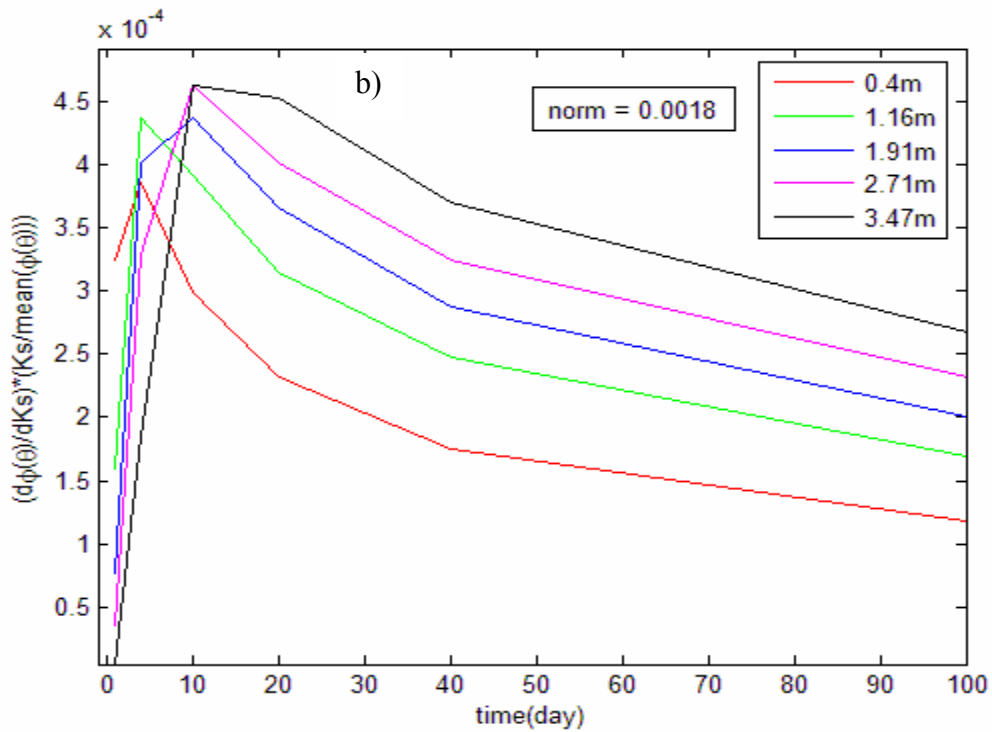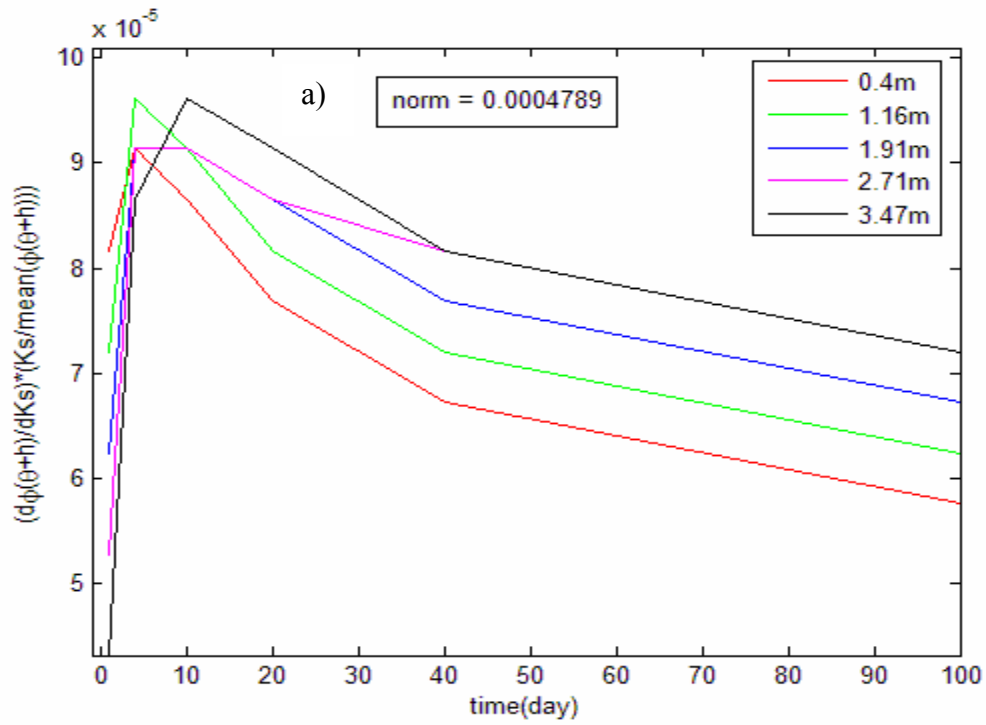
Figure 5.54. Time-depth distribution of the relative sensitivity of $\Phi(\theta+h)$ and $\Phi(\theta)$ with respect to changes in K_s for multi-objective (a) and single-objective optimization (b).

Sensitivity of $\Phi(\theta)$ and $\Phi(\theta+h)$ with respect to changes in K_s is highest at the early stages of the drainage experiment. As drainage proceeds the sensitivity of $\Phi(\theta)$ and $\Phi(\theta+h)$ with respect to changes in K_s decreases. The rate of decrease for the surface layer ($z = 40$cm) is faster than for the subsurface layers. Therefore, to obtain reliable estimate for K_s more data points should be collected at the beginning of the experiment or more weight should be given to the early data points in the parameter optimization algorithm. Comparing Figures 5.54a and 5.54b and the norms of the sensitivities in the single objective and multi-objective optimizations indicate that adding additional information (soil water matric potential head data) to the soil water content data doesn't increase the identifiability of K_s which is surprising. This suggests that saturated hydraulic conductivity should be better identified using the soil moisture content data (with more data at the early stages of drainage) rather than both soil moisture and soil water pressure head data to $\Phi(\theta)$.

Comparing Figures 5.55a and 5.55b and the norms of the relative sensitivities indicate that additional information increases the identifiability of α by four order of magnitude. α is the most sensitive and identifiable parameter for both single and multi-objective optimization. This is consistent with the narrow 95 percent confidence interval on the parameter in Tables 5.14 and 5.15. As drainage proceeds the sensitivity of the objective function with respect to α decreases in the upper layers of coarse texture soil but it stays constant for lower layers of sand. Again the sensitivity analysis indicates that the information gathered at the surface layers and at the early stages of drainage experiment increases the identifiability of the parameter.
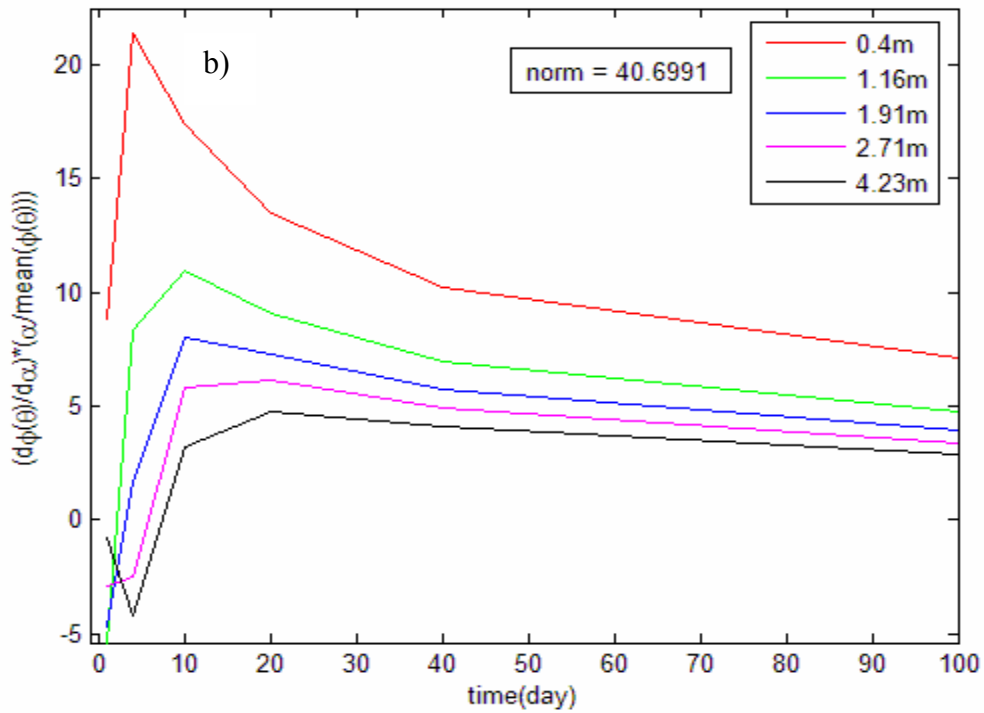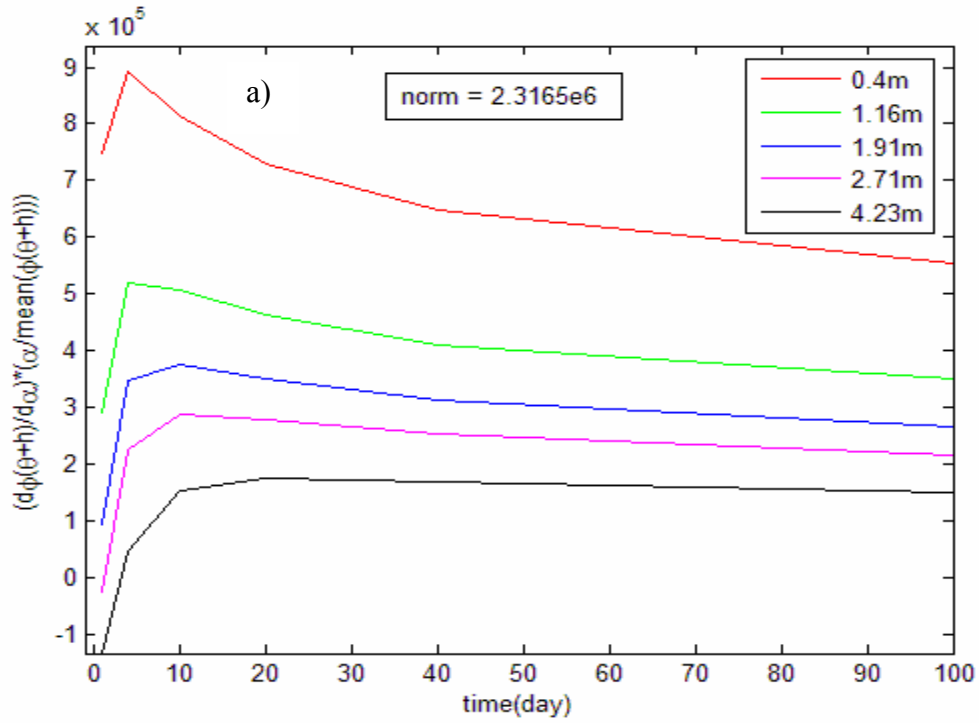
Figure 5.55. Time-depth distribution of the relative sensitivity of $\Phi(\theta + h)$ and $\Phi(\theta)$ with respect to changes in α for multi-objective (a) and single-objective optimization (b).

Since n is exponent in the van Genuchten soil water retention model (Eq. [2.24]), one expects the highest sensitivity for this parameter, but according to Figure 5.56 the relative sensitivity of $\Phi(\theta + h)$ with respect to n is less than α. As soil becomes drier the sensitivity increases but the rate of increase is not high in comparison with α, and stays constant over the time course of the drainage experiment for multi-objective optimization. For single-objective optimization, after a drastic increase in the sensitivity, it decreases as drainage proceeds. The sensitivity curves for n do not have a well-defined peak in multi-objective optimization but they do in single-objective optimization. Another surprising result is that additional information does not increase the identifiability of n as much as α. However, comparison of the norms of the sensitivities for the two cases, in Figure 5.56, reaffirms that adding soil water pressure head data to soil moisture content data increases the identifiability of the parameter two-folds.

Comparing norms the sensitivities in Figure 5.57 indicates that additional information actually decreases the identifiability of θ_r. This is somewhat expected because θ_r is the residual soil water content and it should be well identified by the soil moisture data in very dry zone of the soil water characteristic curve rather than with the soil water pressure head data. As drainage proceeds the sensitivities of $\Phi(\theta)$ and $\Phi(\theta + h)$ with respect to θ_r increase. The rate of increase for $\Phi(\theta)$ in the surface layer ($z = 40$cm) is greater than $\Phi(\theta + h)$ in subsurface layers. It doesn't have a well-defined peak in both multi-objective and single-objective optimizations. Figure 5.57 clearly shows that the identifiability of θ_r is high in the drier part of the soil water characteristic curve.
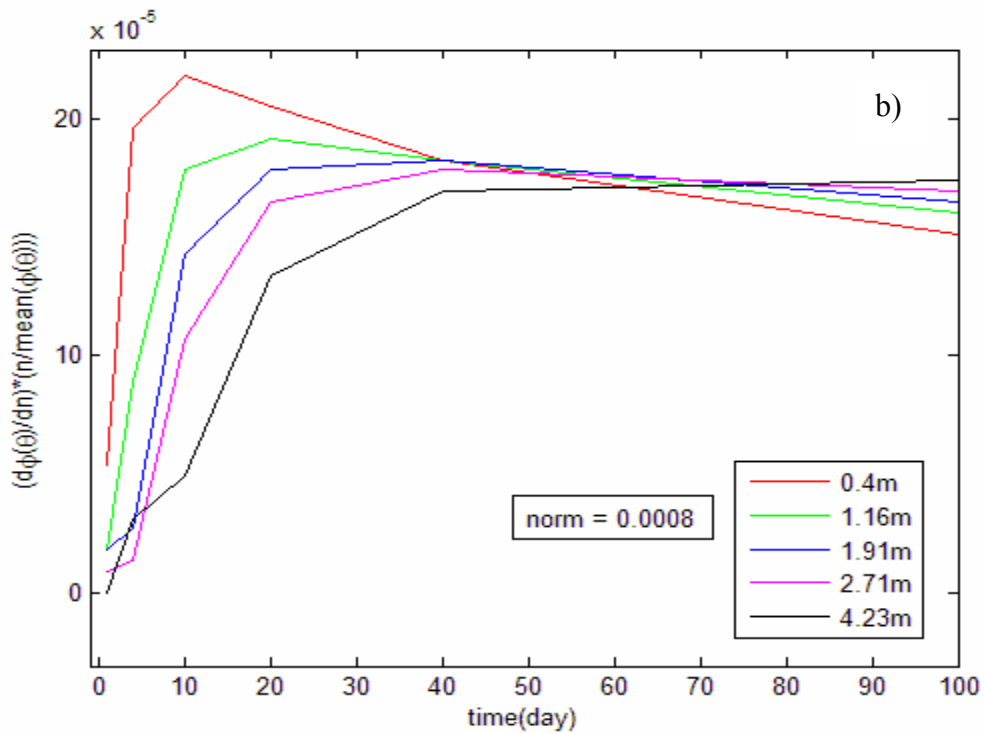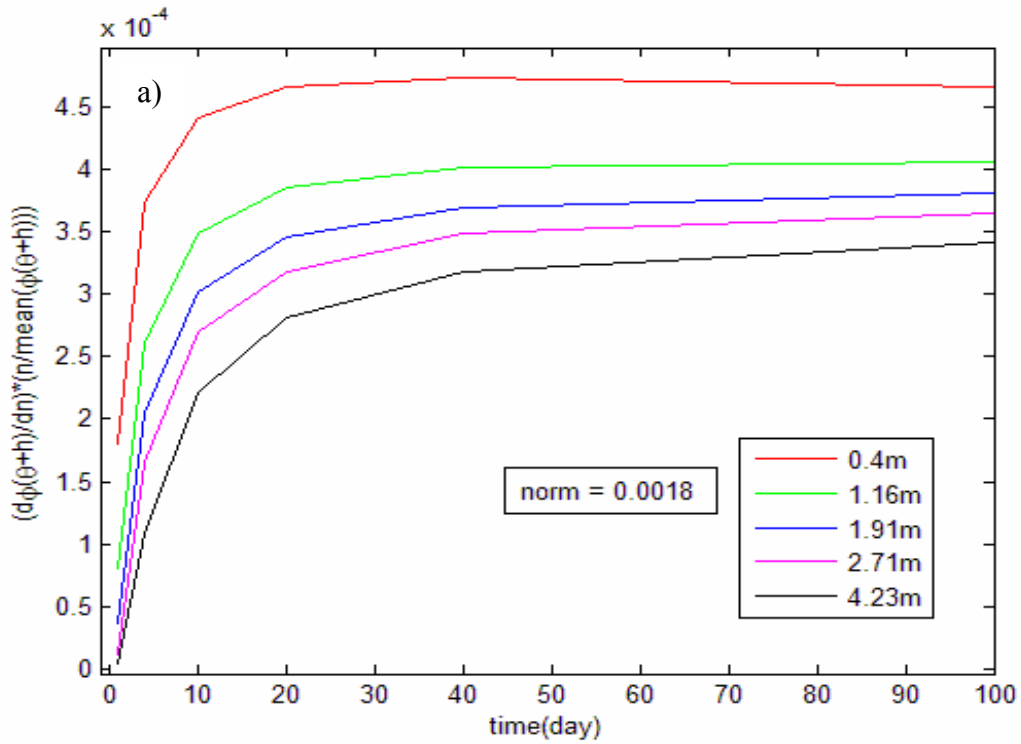
Figure 5.56. Time-depth distribution of the relative sensitivity of $\Phi(\theta+h)$ and $\Phi(\theta)$ with respect to changes in n for multi-objective (a) and single-objective optimization (b).
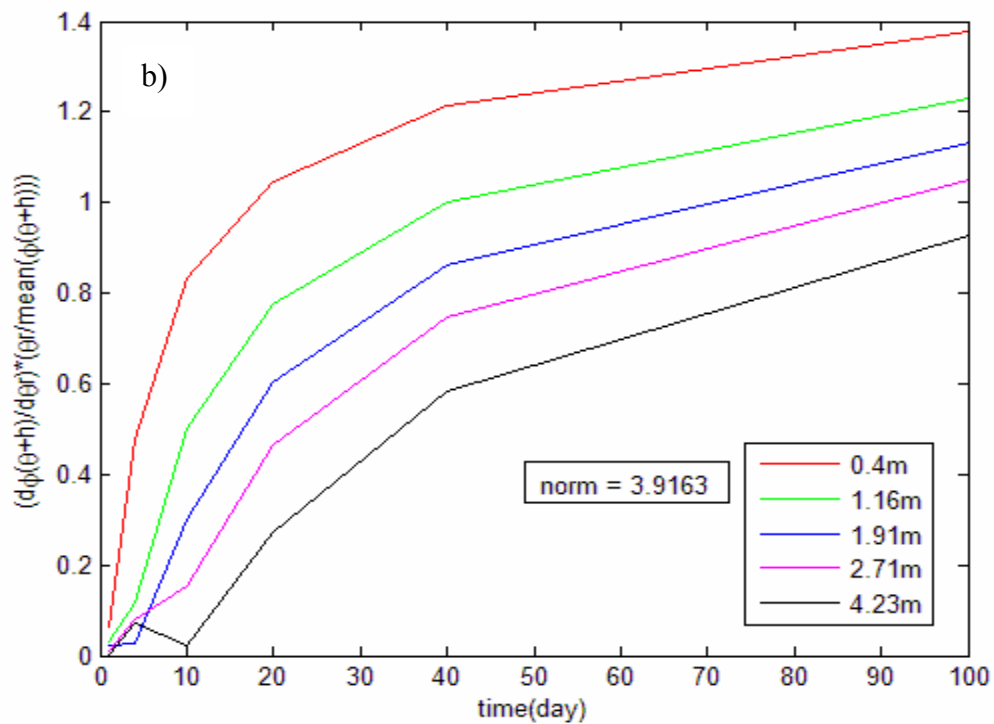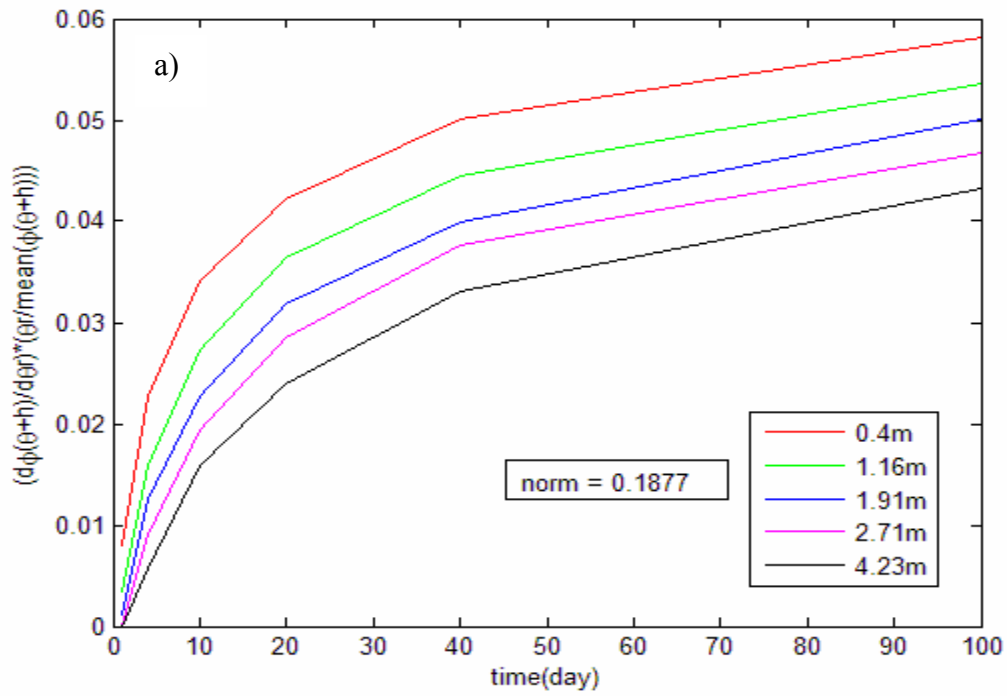
Figure 5.57. Time-depth distribution of the relative sensitivity of $\Phi(\theta+h)$ and $\Phi(\theta)$ with respect to changes in θ_r for multi-objective (a) and single-objective optimization (b).
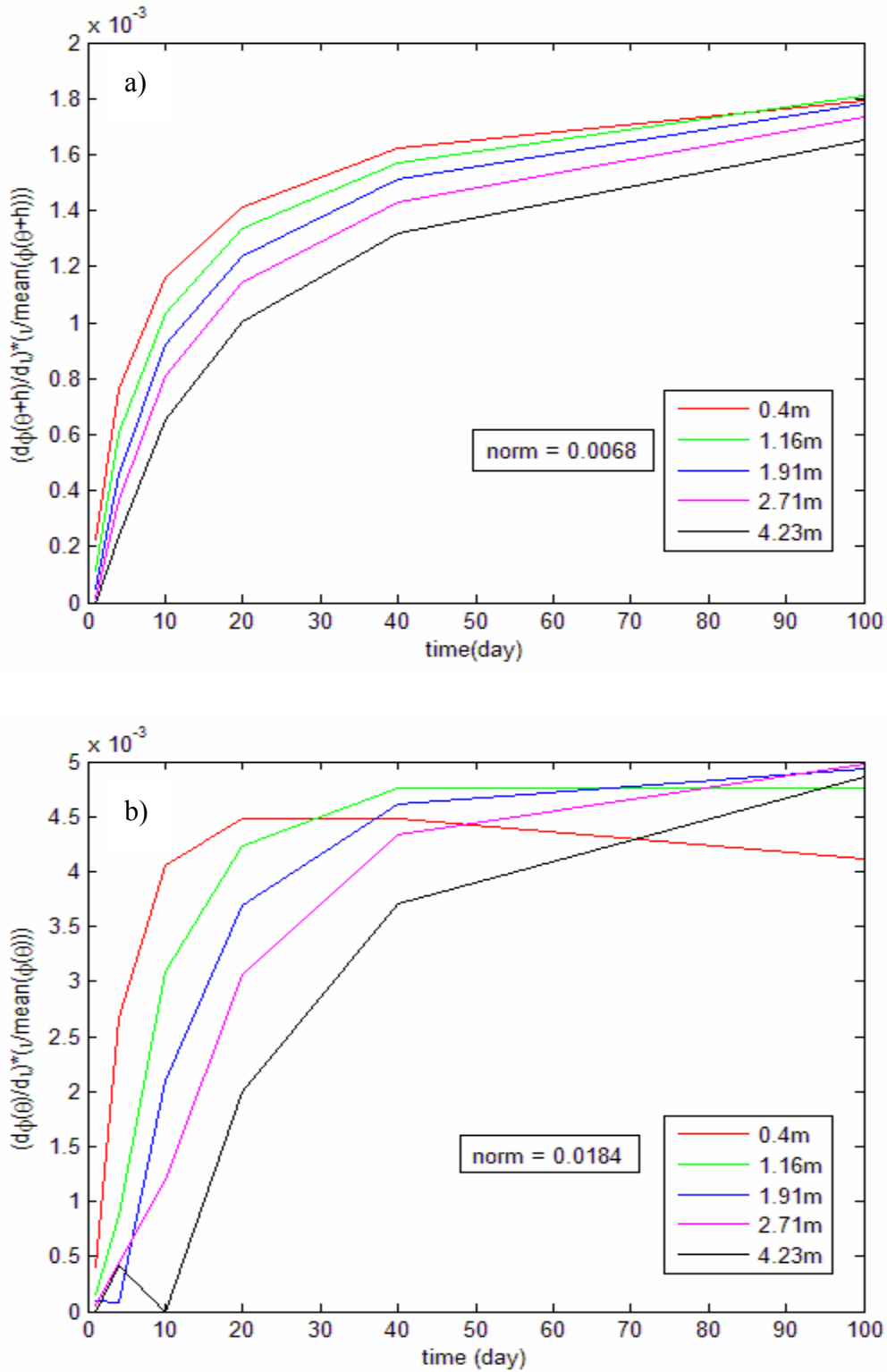
Figure 5.58. Time-depth distribution of the sensitivity of $\Phi(\theta+h)$ and $\Phi(\theta)$ with respect to changes in ι for multi-objective (a) and single-objective optimization (b).

Sensitivity of $\Phi(\theta)$ and $\Phi(\theta+h)$ with respect to changes in pore connectivity index (ι) increases during the course of the drainage experiment. The increase is more pronounced for surface layer indicating that for successful estimation of ι more data should be collected at the surface layer and in dry parts of the soil. Additional information to the objective function slightly decreases the identifiability of ι. This can be shown by comparing Figures 5.58a and 5.58b and comparing the norm of the sensitivities.

The relative sensitivity of soil moisture content with respect to changes in model parameters K_s, α, n, θ_r, and ι, for heterogeneous soil, is presented in Figures 5.59, 5.60, 5.61, 5.62, and 5.63. Comparing the norms of the sensitivities, the same inferences can be made. Again α is the most sensitive model parameter followed by the residual soil moisture content. The remaining parameters have almost the same identifiability.

Overall, the saturated hydraulic conductivity is more identifiable using soil moisture content data in the wetter range of the soil water characteristic curve (early times in the drainage experiment) while the identifiability of other parameters increases as soil becomes drier. It implies that more data points should be collected at the beginning of the drainage experiment to reliably identify K_s and at the same time more data sets should be used from the upper layer of soil during time course of the drainage experiment. To make soil more drier one option is to use a bare soil surface. This will however add the evaporation flux as another unknown that must be identified through the inverse modeling strategy. This is not recommended. Instead collecting more data points in layers close to soil surface and giving them more weight may increase the identifiability of the hydraulic parameters.
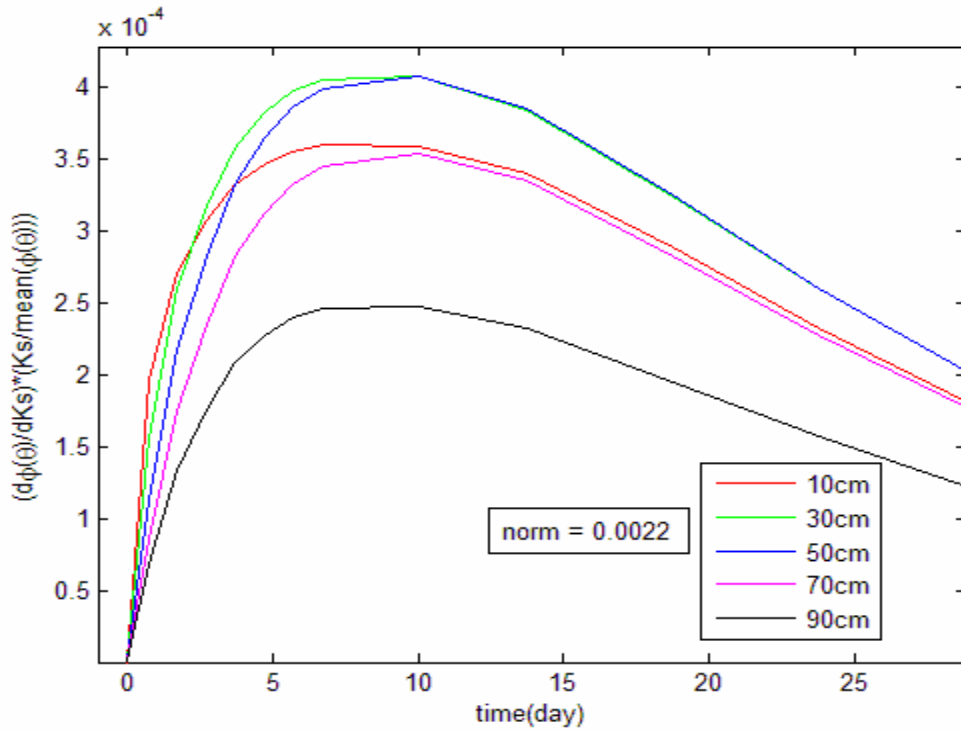
Figure 5.59. Time-depth distribution of the relative sensitivity of $\Phi(\theta)$ with respect to changes in K_s for single-objective optimization for heterogeneous soil.
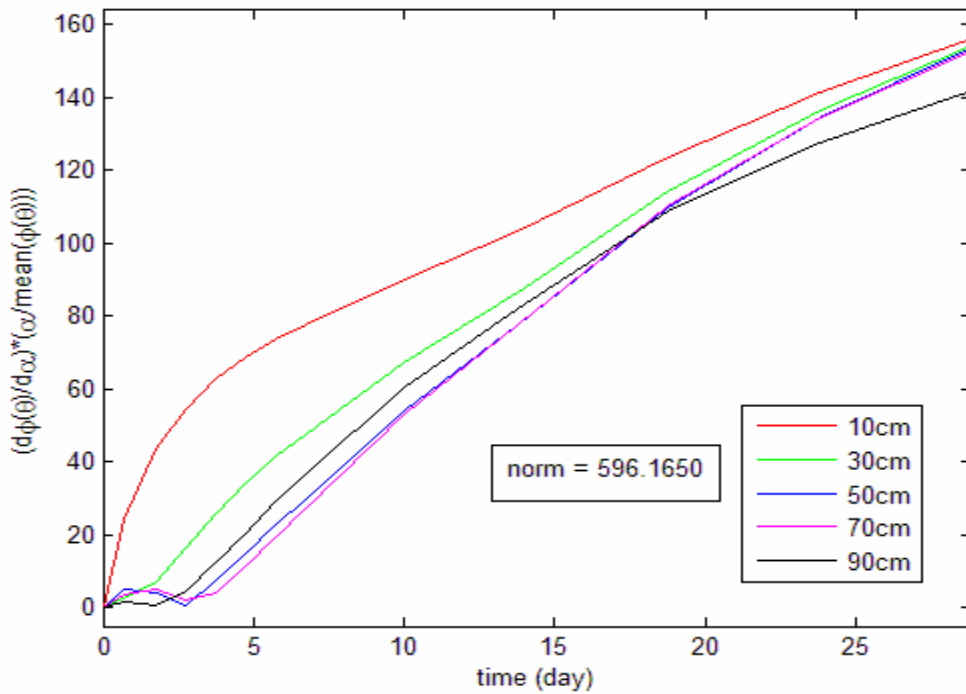
Figure 5.60. Time-depth distribution of the relative sensitivity of $\Phi(\theta)$ with respect to changes in α for single-objective optimization for heterogeneous soil.
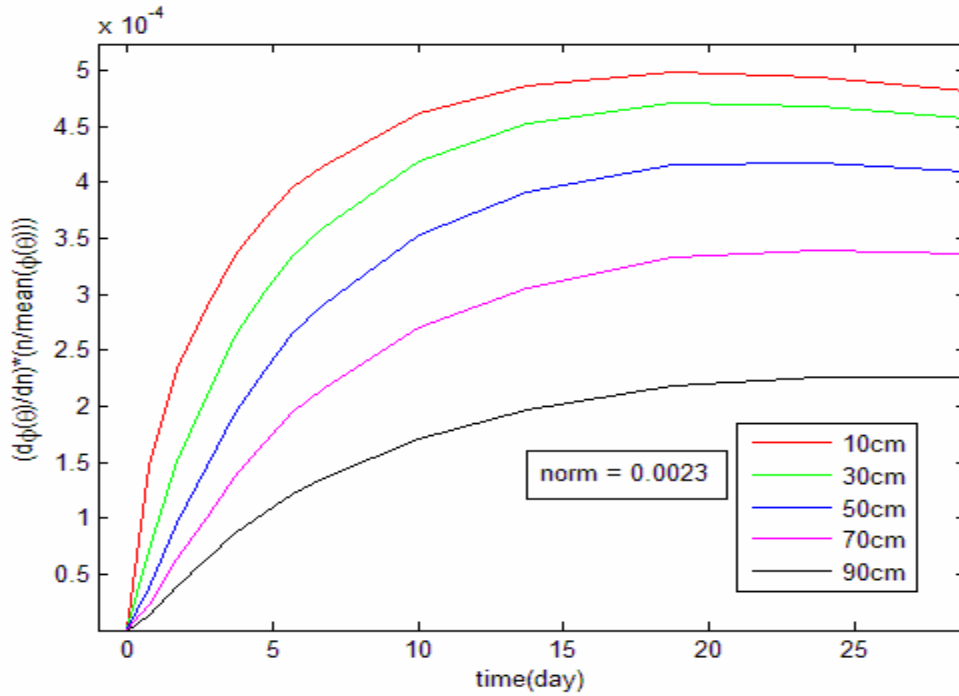
Figure 5.61. Time-depth distribution of the relative sensitivity of $\Phi(\theta)$ with respect to changes in n for single-objective optimization for heterogeneous soil.
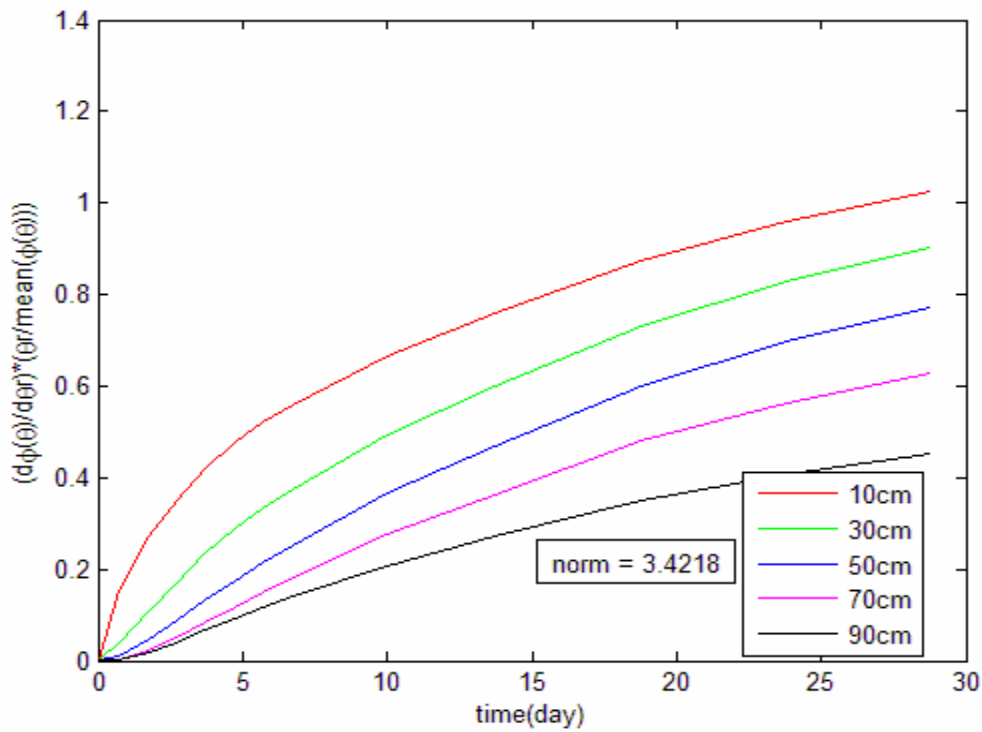
Figure 5.62. Time-depth distribution of the relative sensitivity of $\Phi(\theta)$ with respect to changes in θ_r for single-objective optimization for heterogeneous soil.
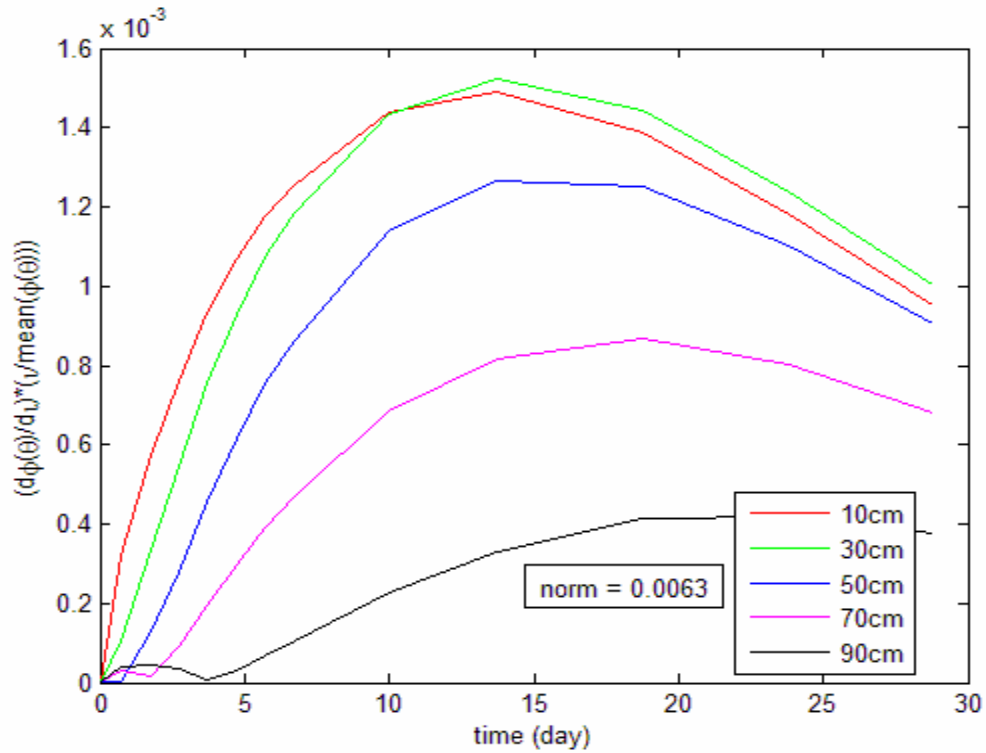
Figure 5.63. Time-depth distribution of the relative sensitivity of $\Phi(\theta)$ with respect to changes in ι for single-objective optimization for heterogeneous soil.

In conclusion, sensitivity analysis of the state variable(s) with respect to model parameters should be used as a prerequisite and starting point for the design of experiment, data collection, and sampling plan. It also should be done before the consideration of inverse modeling for a case study since it reveals what can and what cannot be identified by optimization.

5.4.3. Residual Analysis

Different means were used to analyze the residuals of the state variables. The errors were plotted against the state variables to visually examine possible trends, oscillations, correlations, equality of variances, and to determine whether the mean of the residuals is

zero and if they are normally distributed. These qualitative methods were coupled with the quantitative hypotheses tests which are discussed below.

5.4.3.1. Hypothesis Test on the Residuals' Mean

The *t-statistic* was used to verify if the mean of the residuals is zero. The residuals are given in appendix C. For FRAP experiment the following *null and alternative hypotheses* were stated:

$$H_0 : \mu = 0$$
$$H_A : \mu \neq 0$$

The mean and standard deviation of the residuals in case of FRAP experiment with five unknown parameters (full reaction-diffusion model) were 0.0012 and 0.0224 with sample size $n = 43$. The *t-statistic* was calculated as:

$$t = \frac{0.0012 - 0}{0.0224 / \sqrt{43}} = 0.3478$$

In case of FRAP experiment with three unknown parameters (one-site-mobile-immobile model), the mean and standard deviation of residuals were -0.0029 and 0.0234 with sample size $n = 43$. The *t-statistic* was calculated as:

$$t = \frac{-0.0029 - 0}{0.0234 / \sqrt{43}} = -0.8127$$

For 42 degrees of freedom, the *tabled t-values* for different levels of significance are given in Table 5.18. The calculated *t-statistic* was then compared with the *tabled t-values* at different levels of significance and the results summarized in Table 5.18. As the Table indicates the *null hypothesis* (mean of the residuals is zero) can not be rejected even at 20 per cent level of significance. The possibility of committing *error type one* is extremely slim.

Table 5.18. The results of hypothesis test on the residuals' mean in FRAP model.

α	0.01	0.05	0.1	0.2
t-value	2.8120	2.0175	1.6820	1.3020
Decision	*Accept H_0*	*Accept H_0*	*Accept H_0*	*Accept H_0*

In case of water flow through homogeneous soil (data from Abeele, 1984), the mean and standard deviation of the residuals for soil moisture content data were -0.0023 and 0.0120. The mean and standard deviation of the residuals for soil water pressure head data were $-0.0025m$ and $0.0188m$. The sample size for both cases was 36. The *t-statistic* was calculated as:

For soil moisture content data:

$$t = \frac{-0.0023 - 0}{0.0120/\sqrt{36}} = -1.1467$$

For soil water pressure head data:

$$t = \frac{-0.0025 - 0}{0.01371/\sqrt{36}} = -0.1094$$

For different levels of significance and degree of freedom $v = n - 1 = 35$ the tabled t-values are given in Table 5.19.

As the Table indicates the *null hypothesis* (mean of the residuals is zero) can not be rejected even at 20 per cent level of significance for both data sets. Again, the possibility of committing *error type one* is unlikely.

Table 5.19. The results of hypothesis test on the residuals' mean in case of water flow through homogeneous soil.

α	0.01	0.05	0.1	0.2
t-value	2.7240	2.03	1.69	1.306
Decision on θ	*Accept H_0*	*Accept H_0*	*Accept H_0*	*Accept H_0*
Decision on h	*Accept H_0*	*Accept H_0*	*Accept H_0*	*Accept H_0*

In case of water flow through heterogeneous soil, the mean, standard deviation, and the sample size were 7.6615×10^{-4}, 0.0046, and 65, respectively. The *t-statistic* was calculated as:

$$t = \frac{7.6615 \times 10^{-4} - 0}{0.0046 / \sqrt{65}} = 1.3428$$

For degree of freedom 64, the *tabled t-values* for different levels of significances are given in Table 5.20. The null hypothesis cannot be rejected even at 10 per cent level of significance.

In conclusion, hypothesis tests on the mean of the residuals show that the errors have zero mean and therefore, the first criterion for development and use of the nonlinear optimization, through least square method, was met.

Table 5.20. The results of hypothesis test on the residuals' mean in case of water flow through heterogeneous soil.

α	0.01	0.05	0.1	0.2
t-value	2.6540	1.9970	1.6690	1.295
Decision	*Accept H_0*	*Accept H_0*	*Accept H_0*	*Reject H_0*

5.4.3.2. Hypothesis Test on the Equality of the Residuals' Variance

To verify if residuals have constant variance they were divided into different sections. In FRAP experiment, one of the possible residuals (from Appendix C) was chosen and the residual plot versus laser beam recovery was divided into three regions. The variance in each region was calculated and compared with each other using the Bartlett test. The residuals were divided into three groups as:

$$S_1^2 = S^2(residuals(1:5)) = 9.2651 \times 10^{-4}$$
$$S_2^2 = S^2(residuals(6:24)) = 9.3655 \times 10^{-4}$$
$$S_3^2 = S^2(residuals(25:33)) = 9.3126 \times 10^{-5}$$

The pooled weighted variance was found to be (using Eq. [4.79]) $S_p^2 = 7.1030 \times 10^{-4}$. The *Bartlett's statistic* was calculated as $T = 9.5454$ which is less than the *upper critical value* of the χ^2 for two degrees of freedom ($k = 3$) at one per cent level of significance ($\chi^2_{(0.01,2)} = 10.60$). It is, however, more than the tabled value for five per cent level of significance. At one percent level of significance the *null hypothesis* (the residuals have constant variance) cannot be rejected. Based on this test and analysis of residual plot versus laser beam recovery, it is concluded that the residuals, in case of GFP-GR transport in living cells, have equal variance.

In case of soil moisture data in water flow through homogeneous soil (drainage of Bandelier tuff, data from Abeele, 1984) the residuals were divided into three subsections:

$$S_1^2 = S^2(residuals(1:8)) = 2 \times 10^{-5}$$
$$S_2^2 = S^2(residuals(9:14)) = 3.6323 \times 10^{-5}$$
$$S_3^2 = S^2(residuals(14:24)) = 6.28 \times 10^{-5}$$

The pooled weighted variance was found to be $S_p^2 = 4.22 \times 10^{-5}$. The *Bartlett statistic* was calculated by Eq. [4.78] and was found to be 2.3348. For degree of freedom 2, the upper critical values of the chi-square distribution are given in Table 5.21 for different levels of significance. As the Table indicates the null hypothesis (residuals have constant variance) cannot be rejected even at twenty per cent level of significance. Therefore, the residuals of soil moisture profiles in case of water flow through homogeneous soil have constant variance.

Table 5.21. The results of hypothesis test on the equality of the residuals' variance in case of water flow through homogeneous soil (soil moisture content data).

α	0.01	0.05	0.1	0.2
critical	10.60	7.380	5.99	4.61
Decision	*Accept H_0*	*Accept H_0*	*Accept H_0*	*Accept H_0*

The same procedure was followed for residuals of soil water pressure head. The residuals were divided into three subsections and the corresponding variances were calculated:

$$S_1^2 = S^2(residuals(1:8)) = 0.0057m$$
$$S_2^2 = S^2(residuals(9:14)) = 0.0078m$$
$$S_3^2 = S^2(residuals(14:24)) = 0.0086m$$

The pooled variance was calculated and obtained as $S_p^2 = 0.0175m$. The *Bartlett's statistic* was found to be 5.9186. For three degrees of freedom ($k=3$) the *critical values* of the χ^2 are given in Table 5.22. As the Table shows the null hypothesis

(residuals of soil water pressure head have constant variance) cannot be rejected even at 20 per cent level of significance. Therefore, the errors in soil water pressure head data and soil moisture content profile have constant variance.

In case of soil moisture content data for water flow through heterogeneous soil, the residuals were categorized into five cells with sample size of $N_i = 13$ (initial total sample size was $N = 65$). The *Bartlett's statistic* was found to be $T = 10.4470$ which is less than $\chi^2_{(0.05,4)} = 11.14$ and $\chi^2_{(0.01,4)} = 14.86$. Therefore, the null hypothesis cannot be rejected implying that the residuals of soil moisture content profile have constant variance.

Since the residuals in all three optimization problems considered in this study were normally distributed (will be discussed in 5.4.3.3), the Levene test was not used to verify the equality of variances. In conclusion, the second criterion of the nonlinear optimization, which assumes that the residuals have constant variance, was met.

Table 5.22. The results of hypothesis test on the equality of the residuals' variance in case of water flow through homogeneous soil (soil water pressure head profile).

α	0.01	0.05	0.1	0.2
critical	12.84	9.35	7.81	6.25
Decision	*Accept H_0*	*Accept H_0*	*Accept H_0*	*Accept H_0*

5.4.3.3. Hypothesis Test on the Correlation of the Residuals

To test possible correlation among residuals, the following hypothesis test was stated:

$$H_0 : \rho = 0$$
$$H_A : \rho \neq 0$$

In the case of FRAP experiment with five unknown parameters the residuals were divided into two sub-groups:

$$r_1 = r(1:end-1)$$
$$r_2 = r(2:end)$$

The correlation coefficient ($R = 0.2569$) was then calculated and was used to obtain the *critical t-statistics* (with sample size $n = 42$):

$$t = \frac{0.2569}{\sqrt{\dfrac{1-0.066}{42-2}}} = 1.6812$$

In case of FRAP experiment with three unknown parameters the same procedure was followed and the *critical t-statistics* was calculated as:

$$t = \frac{0.1931}{\sqrt{\dfrac{1-0.0373}{42-2}}} = 1.2447$$

These *critical t-statistics* were then compared with the *tabled t-values* at different levels of significances and the results presented in Table 5.23. As the Table indicates the *null hypothesis* (residuals are uncorrelated) can not be rejected even at the 20 per cent level of significance. The possibility of having *error type one* is almost zero.

In case of water flow through homogeneous soil the same procedure was followed for both residuals of soil moisture content ($R = 0.4117$) and soil water pressure head ($R = 0.4170$) data (with sample size $n = 42$). The *t-statistics* was calculated as:

For soil moisture content data:

$$t = \frac{0.4117}{\sqrt{\dfrac{1-0.1695}{35-2}}} = 2.5952$$

For soil water pressure head data:

$$t = \frac{0.4170}{\sqrt{\dfrac{1-0.1739}{35-2}}} = 2.6357$$

For different levels of significance and degree of freedom $v = n - 2 = 33$, the tabled t-values are presented in Table 5.24.

As the Table indicates the *null hypothesis* (residuals are uncorrelated) can not be rejected at one per cent level of significance for both data sets but at five and more per cent level of significance the alternative hypothesis (residuals are correlated) can be accepted.

Table 5.23. The results of hypothesis test on the correlation of residuals in FRAP model.

α	0.01	0.05	0.1	0.2
t-value	2.7040	2.0210	1.6820	1.3030
Decision	*Accept H_0*	*Accept H_0*	*Accept H_0*	*Accept H_0*

Table 5.24. The results of hypothesis test on correlation of residuals in case of water flow through homogeneous soil.

α	0.01	0.05	0.1	0.2
t-value	2.7350	2.035	1.6936	1.3084
Decision on θ	*Accept H_0*	*Reject H_0*	*Reject H_0*	*Reject H_0*
Decision on h	*Accept H_0*	*Reject H_0*	*Reject H_0*	*Reject H_0*

The same procedure was followed to test possibility of correlation among residuals in case of water flow through heterogeneous soil. The correlation coefficient was calculated ($R = 0.7256$) and inserted in the *critical t-statistics* formula:

$$t = \frac{0.7256}{\sqrt{\dfrac{1-0.5265}{64-2}}} = 8.3029$$

The results are summarized in Table 5.25. Since the *critical t-value* is greater than the *tabled values* in any levels of significance, the null hypothesis is rejected which means that the errors are correlated.

Table 5.25. The results of hypothesis test on correlation of residuals in case of water flow through heterogeneous soil.

α	0.01	0.05	0.1	0.2
t-value	2.6540	1.9970	1.6690	1.295
Decision	*Reject H_0*	*Reject H_0*	*Reject H_0*	*Reject H_0*

To investigate the reasons for correlation among the residuals the errors were plotted against the state variables and presented in Figures 5.64, 5.65, and 5.66. As these Figures show there are no visible trends or oscillations for residuals in case of full reaction-diffusion and one-site-mobile-immobile FRAP models. However, for water flow through homogeneous soil there is a slightly visible trend and in case of water flow through heterogeneous soil the trend is more visible (Figure 5.66). Since the data in theses cases are space and time series, one may expect autocorrelation among state variable(s) and among the corresponding residuals in different time and/or space scales.

To further investigate possibility of significant autocorrelation among the residuals, the serial correlation coefficients were calculated for both time series and space series and the results summarized in Tables 5.26 and 5.27. In time series, for a selected
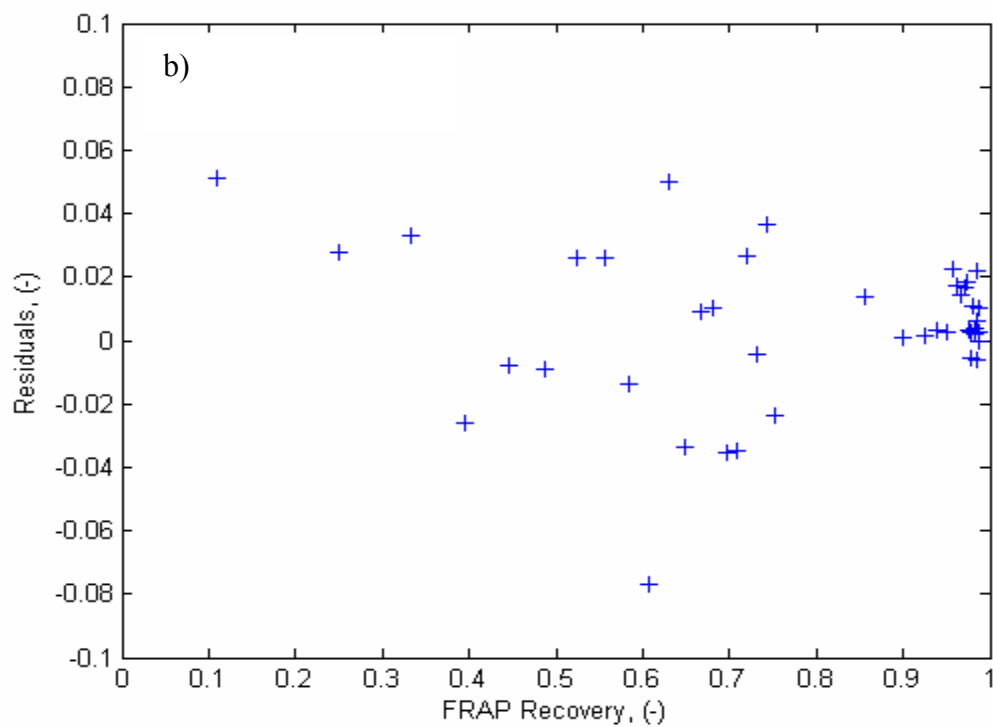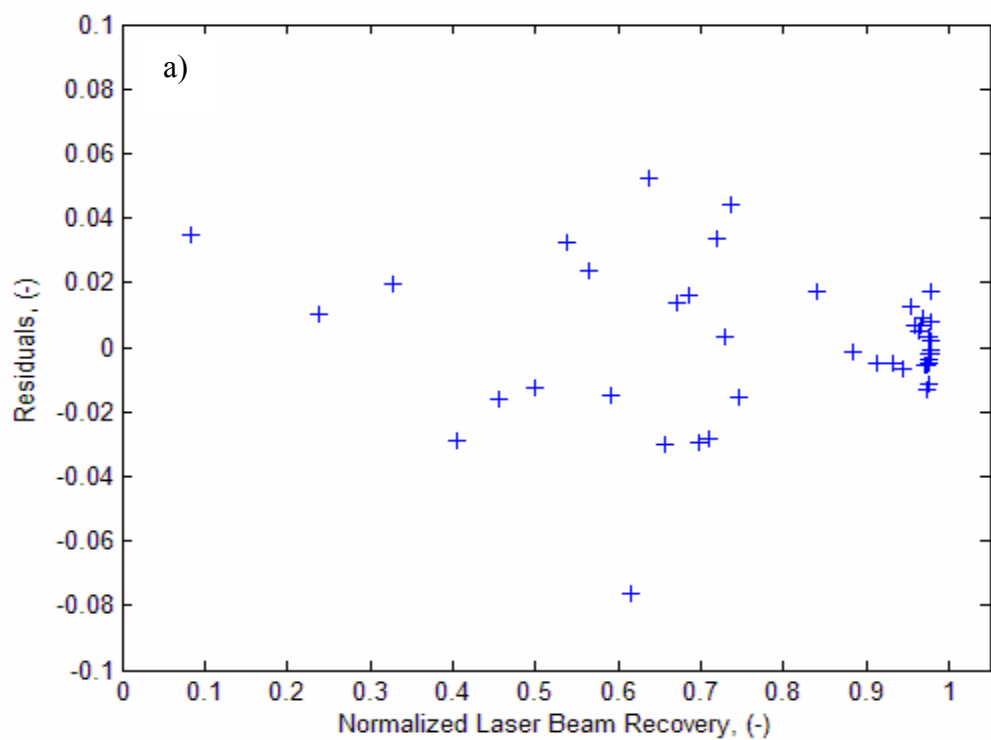
Figure 5. 64. Residuals versus normalized laser beam recovery in FRAP experiment: a) the full reaction-diffusion model b) one-site-mobile-immobile model.
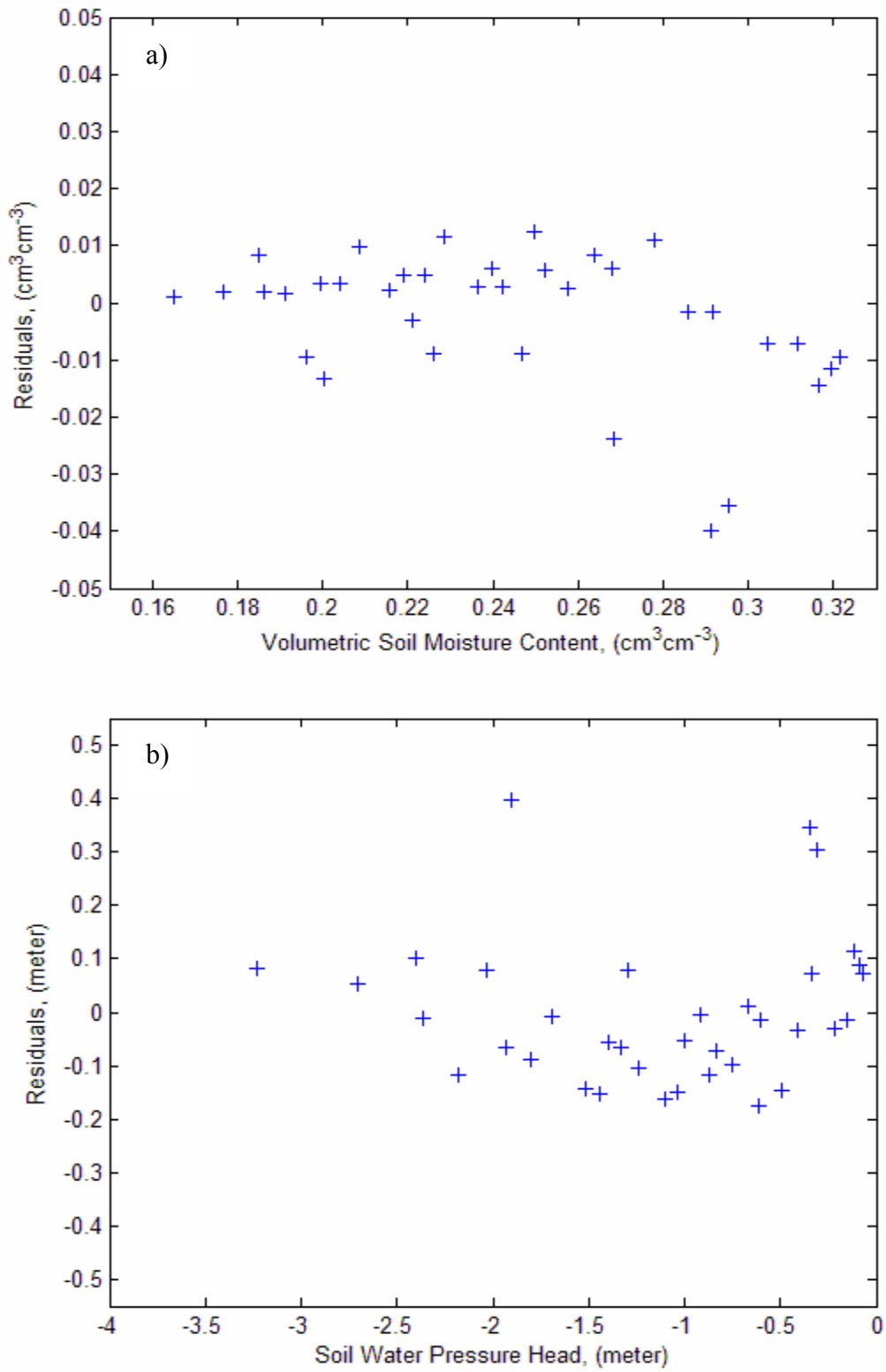
Figure 5.65. Residuals of soil water content (a) and soil water pressure head (b) profiles in drainage of homogeneous soil using multi-objective optimization.
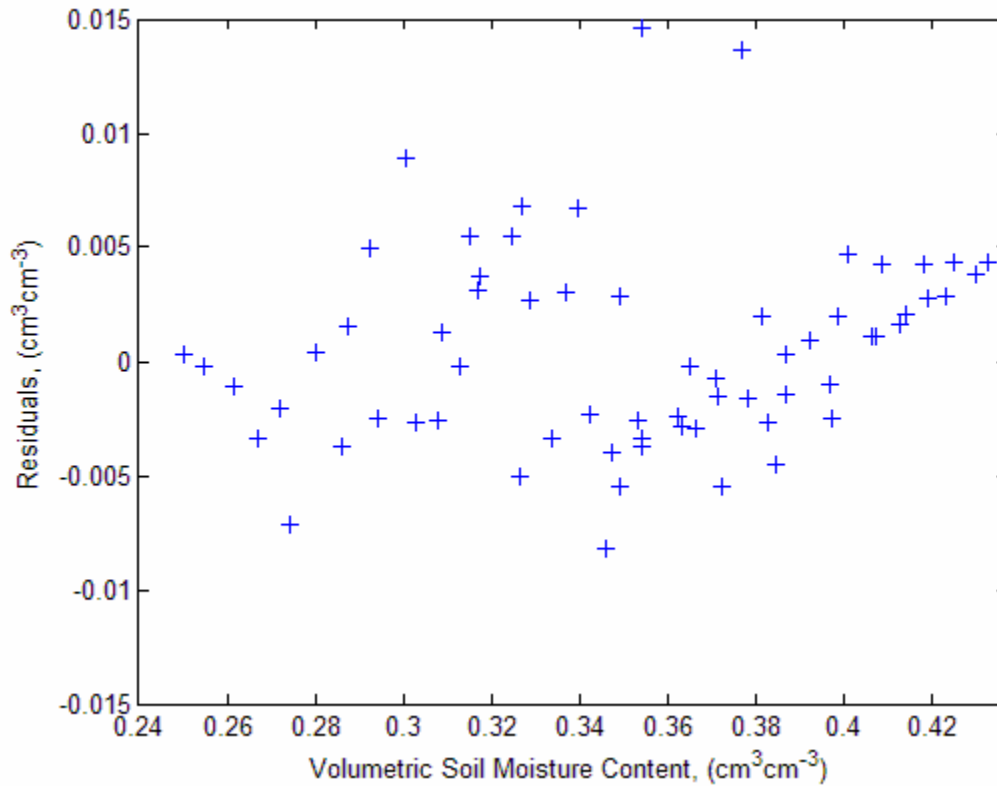
Figure 5.66. Residuals of soil water content profiles in drainage of heterogeneous soil.

depth the serial correlations were calculated for different time steps (i.e. depth one over all times, depth two over all times, and so on). In space series, the serial correlations were calculated for selected time over all depths.

First the serial correlation coefficients for time series of water flow through homogeneous soil are discussed. The means, standard deviations, and serial correlation coefficients are presented in Tables 5.26 and 5.27 for six different depths over all measurement times. The standard deviations for all depths are almost equal except for two depths 391cm and 423cm. For soil moisture content data, the serial correlation coefficients are high and the null hypothesis is rejected (except for depths 391cm and

423cm) at the levels of significance $\alpha = 0.05(t_{5,0.05} = 0.7290)$ and $\alpha = 0.01(t_{5,0.01} = 0.882)$.

This means that there are significant correlations among residuals in different time increments.

As Table 5.27 indicates, for soil water pressure head data the serial correlation coefficient are not significant even at the level of significance $\alpha = 0.01(t_{5,0.01} = 0.882)$ which confirms the residual distribution pattern in Figure 5.65b. The serial correlation coefficient for depth 271cm is exceptionally high which is not acceptable from the statistical point of view (because it is against the trend).

The same procedure was followed to verify if there is significant serial correlation among soil moisture content and soil water pressure head data in space series. The results summarized in Tables 5.28 and 5.29. For soil moisture data (Table 5.28) the serial correlation coefficients are not significant at both levels of significance ($\alpha = 0.05(t_{5,0.05} = 0.7290)$ and $\alpha = 0.01(t_{5,0.01} = 0.882)$). Therefore, the null hypothesis (the residuals are uncorrelated) cannot be rejected in space series.

For soil water pressure head data, the means, standard deviations, and the serial correlation coefficients are given in Table 5.29. The Table shows that there are not significant serial correlations among soil water pressure head data in different depths at a given time. In other words, *the null hypothesis* (the errors are uncorrelated) cannot be rejected at the level of significance $\alpha = 0.05(t_{5,0.05} = 0.7290)$ and $\alpha = 0.01(t_{5,0.01} = 0.882)$.

In case of water flow through heterogeneous soil, the same procedure was applied and the means, standard deviations, and serial correlation coefficients are presented in Table 5.30 for five different depths over all measurement times. For this case, the serial correlation coefficients in time series are significant and *the null hypothesis* (the errors

Table 5.26. The results of serial correlation analysis for time series in case of water flow through homogeneous soil (soil moisture data).

Depth (cm)	$\bar{x}(-)$	s	R	Decision
40	0.0045	0.0058	0.9139	*Reject H_0*
116	0.0037	0.0077	0.9262	*Reject H_0*
191	0.0099	0.0061	0.9811	*Reject H_0*
271	0.0009	0.0092	0.9879	*Reject H_0*
391	0.0088	0.0184	-0.0162	*Accept H_0*
423	0.0169	0.0132	0.2230	*Accept H_0*

Table 5.27. The results of serial correlation analysis for time series in case of water flow through homogeneous soil (soil water pressure head data).

Depth (cm)	$\bar{x}(cm)$	$s(cm)$	R	Decision
40	0.0150	0.0529	0.1978	*Accept H_0*
116	0.0600	0.0695	0.0865	*Accept H_0*
191	0.0248	0.0729	0.3271	*Accept H_0*
271	0.0507	0.1046	0.9529	*Reject H_0*
391	0.0908	0.1542	0.1192	*Accept H_0*
423	0.1603	0.1617	-0.2466	*Accept H_0*

Table 5.28. The results of serial correlation analysis for space series in case of water flow through homogeneous soil (soil moisture data).

Time (day)	$\bar{x}(-)$	s	R	Decision
1	-0.1010	0.0057	-0.2864	*Accept H_0*
4	-0.1274	0.2285	0.6865	*Accept H_0*
10	0.0024	0.1358	-0.1874	*Accept H_0*
20	0.0380	0.0073	0.4180	*Accept H_0*
40	0.0470	0.0073	0.6908	*Accept H_0*
100	0.0561	0.0091	0.7418	*Accept H_0*

Table 5.29. The results of serial correlation analysis for space series in case of water flow through homogeneous soil (soil water pressure head data).

Time (day)	$\bar{x}(cm)$	$s(cm)$	R	Decision
1	0.7324	0.5712	0.0077	*Accept H_0*
4	0.8211	2.2333	0.6509	*Accept H_0*
10	-0.2831	0.6057	0.3107	*Accept H_0*
20	-0.6034	0.6060	0.0695	*Accept H_0*
40	-0.1530	0.7538	-0.2797	*Accept H_0*
100	0.7933	1.7058	0.0483	*Accept H_0*

Table 5.30. The results of serial correlation analysis for time series in case of water flow through heterogeneous soil (soil moisture data).

Depth (cm)	$\bar{x}$	s	R	Decision
10	0.003	0.0066	0.7953	*Reject* H_0
30	0.0009	0.0036	0.7838	*Reject* H_0
50	0.00075	0.0048	0.7174	*Reject* H_0
70	0.0015	0.0027	0.6787	*Reject* H_0
90	0.0005	0.0039	0.9282	*Reject* H_0

are uncorrelated) is rejected at the level of significance $\alpha = 0.05(t_{5,0.05} = 0.4760)$. This mans that there is significant correlations among residuals in different time increments for a given depth.

The result of serial correlation analysis for space series (in case of water flow through heterogeneous soil) are presented in Table 5.31. Since the calculated serial correlation coefficients are less than the tabled one (Pearson test) at the level of significance $\alpha = 0.05(t_{12,0.05} = 0.805)$, the null hypothesis cannot be rejected. This implies that there is no significant correlation among the residuals in space series. The serial correlation coefficient for the second time is abnormally high which is against the observed trend and is not statistically acceptable.

In conclusion, correlation analysis shows that the residuals are uncorrelated in cases of FRAP experiment data, soil water pressure head data (both time series and space

series), and soil moisture content data in space series. However, the soil moisture content data are correlated in time series.

5.4.3.4. Hypothesis Test on the Normality of the Residuals

One of the assumptions of the least squares theory is the normality of the residuals. In other words, it is assumed that the errors are normally distributed. To analyze the normality of the errors two qualitative and two quantitative methods were used: 1) Error frequency analysis and normal probability plots, and 2) Hypothesis tests on the normality of the residuals using the chi-square and Kolmogorov-Smirnov one sample tests.

Error frequency analysis was first performed for the FRAP experiment by constructing residuals histograms. The histograms are presented in Figures 5.67a and 5.67b for the full reaction-diffusion model and one-site-mobile-immobile equation, respectively. The Figures visibly show that the errors are normally distributed. This was confirmed by the analysis of the normal probability plots and the chi-square hypothesis test on the normality of the random variable. The normal probability plots were constructed and depicted in Figures 5.68a (for the full reaction-diffusion model) and 5.68b (for one-site-mobile-immobile model). Again, the normal probability plots suggest that the residuals are normally distributed.

Residual frequency analysis and normal probability plots, though useful in figuring out the underlying probability distribution function, are only qualitative means to study possible normal distribution of random variable. To verify normality of the errors in case of FRAP experiment, the chi-square test was used and the following hypotheses were stated:

Table 5.31. The results of serial correlation analysis for space series in case of water flow through heterogeneous soil (soil moisture data).

Time (day)	$\bar{x}(cm)$	$s(cm)$	R	Decision
0.0000	0.0063	0.00025	-0.6067	*Accept H_0*
0.7292	0.006	0.0048	0.8090	*Reject H_0*
1.7292	0.0038	0.0064	0.2827	*Accept H_0*
2.7292	-0.0004	0.0043	-0.1641	*Accept H_0*
3.7292	-0.0018	0.0046	-0.6951	*Accept H_0*
4.7292	-0.0058	0.0024	-0.2940	*Accept H_0*
5.7292	-0.0014	0.0022	-0.1144	*Accept H_0*
6.7292	-0.003	0.0017	0.0567	*Accept H_0*
10.0000	-0.0052	0.0029	0.2080	*Accept H_0*
13.7500	-0.0008	0.0049	0.1765	*Accept H_0*
18.7500	0.0021	0.0049	-0.7277	*Accept H_0*
23.7917	0.0022	0.0041	-0.2857	*Accept H_0*
28.8125	-0.0020	0.0037	-0.3514	*Accept H_0*
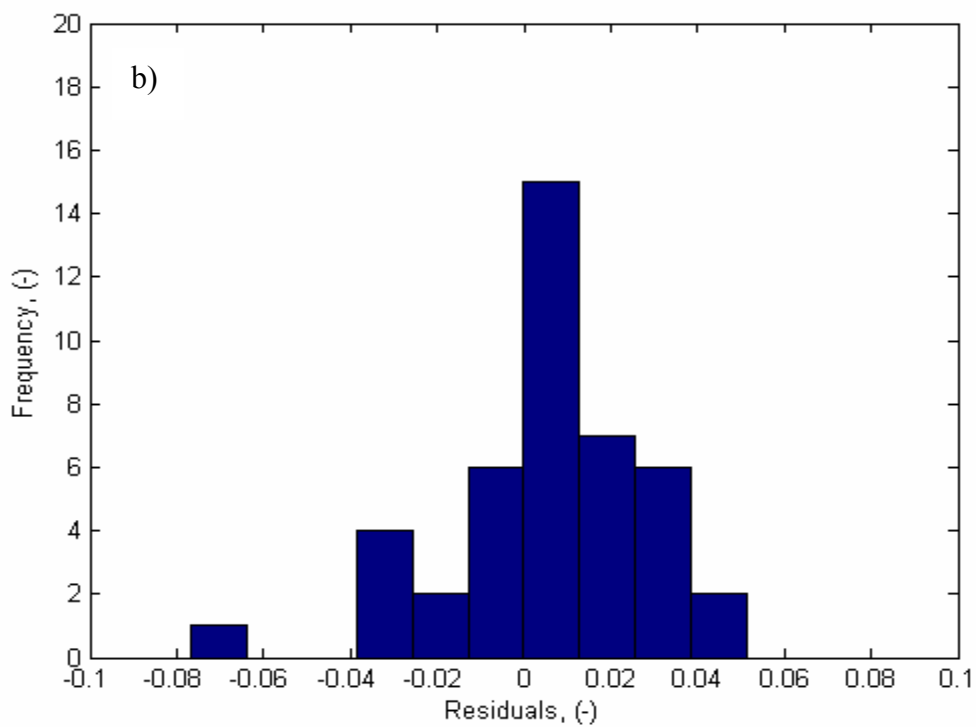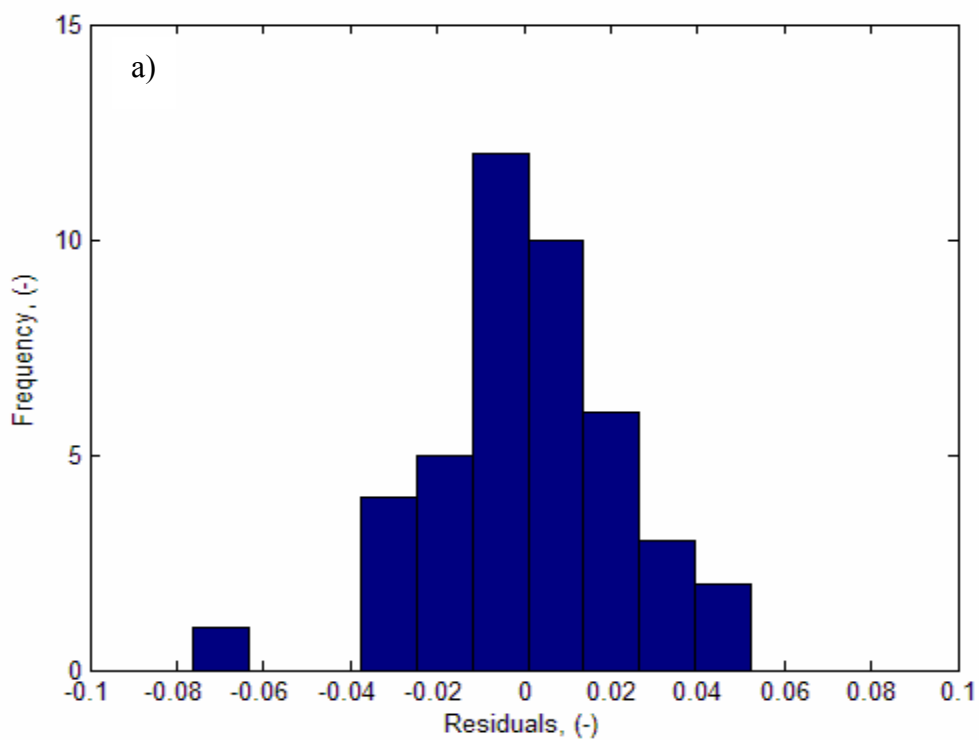
Figure 5.67. Histograms of residuals for FRAP experiment: a) full reaction-diffusion model, and b) one-site-mobile-immobile model.

231
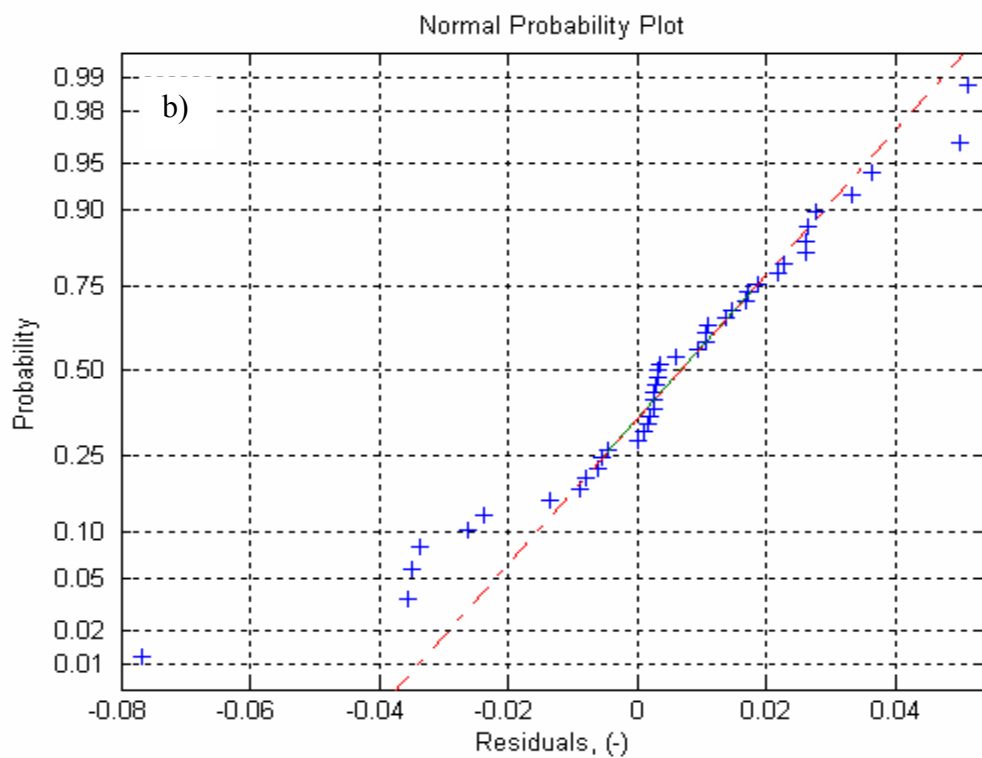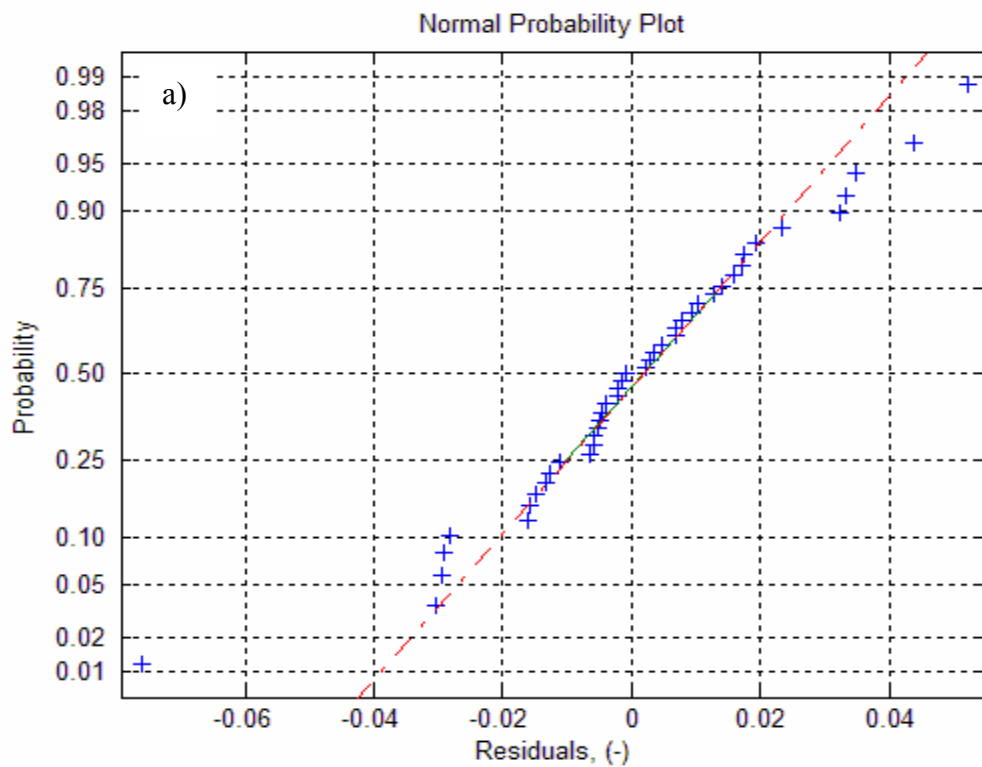
Figure 68. Normal probability plot for FRAP experiment: a) full reaction-diffusion model, and b) one-site-mobile-immobile model.

$$H_0 : r = N(0.0012, 0.0224)$$
$$H_A : r \neq N(0.0012, 0.0224)$$

Since the calculated χ^2 (3.6190) is less than the *tabled value* ($\chi^2_{(0.80,2)}$ = 4.61), the *null hypothesis* (the residuals are normally distributed) cannot be rejected even at 20 per cent level of significance implying that the residual are normally distributed. Similarly, the result of chi-square test for residuals of the one-site-mobile-immobile model showed that errors are *strongly* normally distributed.

In case of water flow through homogeneous soil, the histograms of errors (for multi-objective optimization) are depicted in 5.69a and 5.69b. The corresponding normal probability plots are given in Figures 5.70a and 5.70b. These Figures do not show apparent normal distribution for residuals of soil moisture content and soil water pressure head. To verify the normal distribution of errors in soil moisture content profile, the chi-square test was used and the following null and alternative hypotheses were stated:

Since the calculated χ^2 (3.8795) is less than the tabled value ($\chi^2_{(1-\alpha,v)}$ = 5.9915) *the null hypothesis* (residuals are normally distributed) cannot be rejected at 5 per cent level of significance which means that the residuals in soil water content data (data from Abeele, 1984) are normally distributed.

For soil water pressure head profile in case of multi-objective optimization of water flow through homogeneous soil (drainage of Bandelier tuff), the following hypotheses were tested:

$$H_0 : r = N(-0.0025, 0.0137)$$
$$H_A : r \neq N(-0.0025, 0.0137)$$
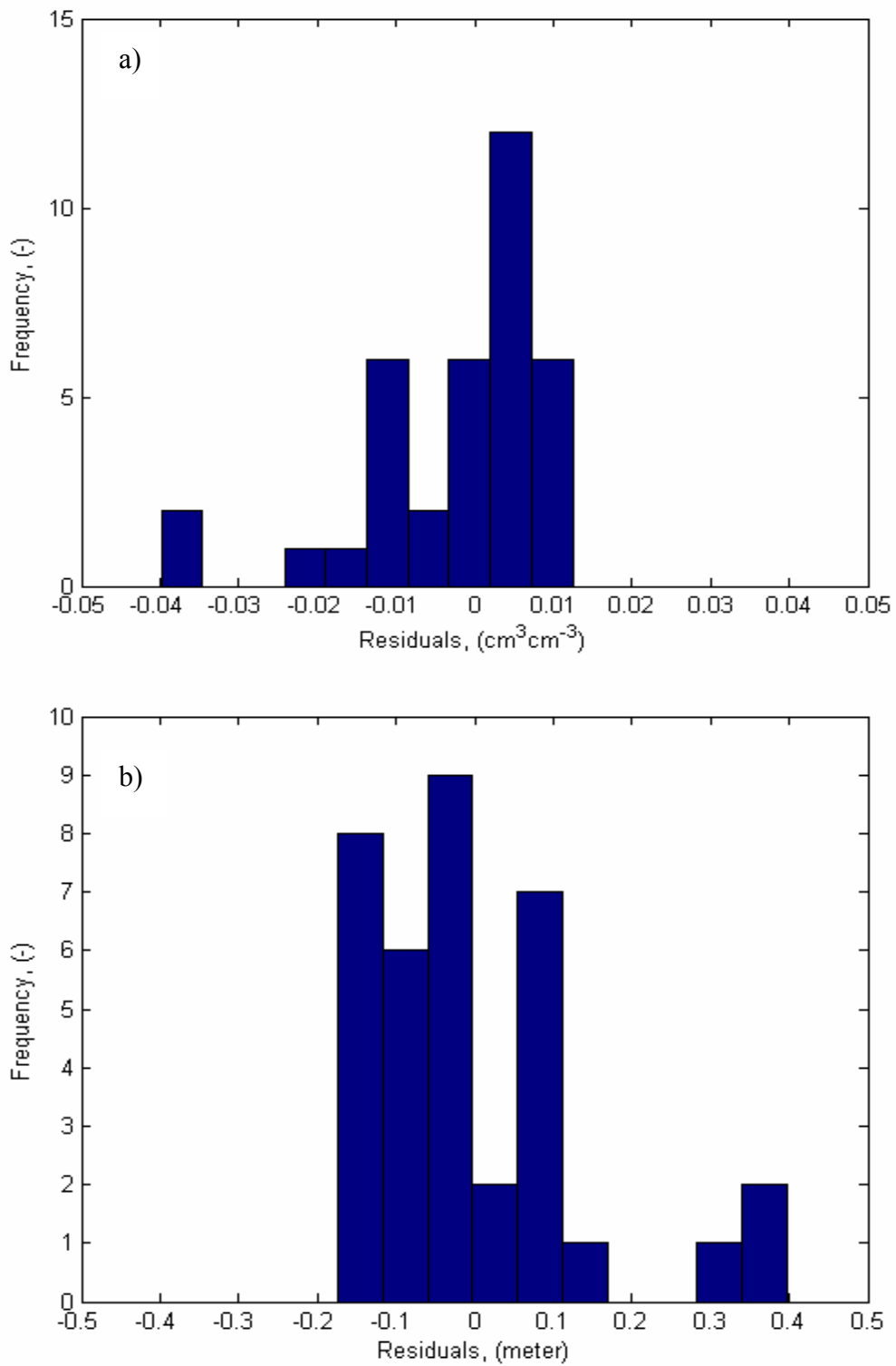
Figure 5.69. Error frequency histograms for: (a) soil water content profile and (b) soil water pressure head profile in drainage of homogeneous soil (multi-objective optimization).
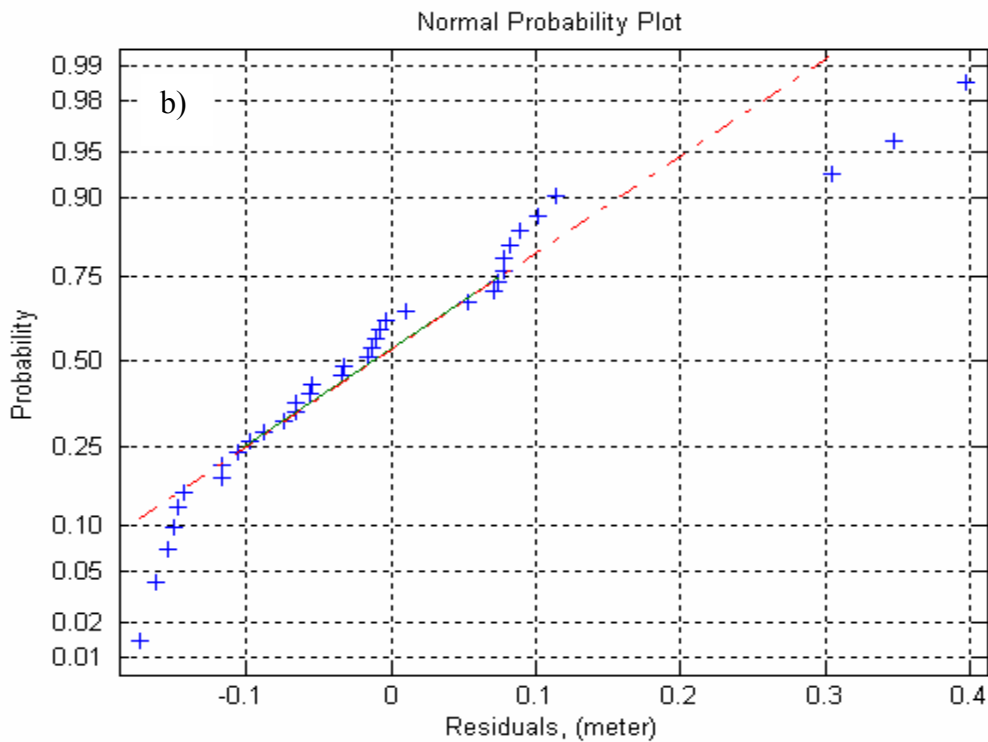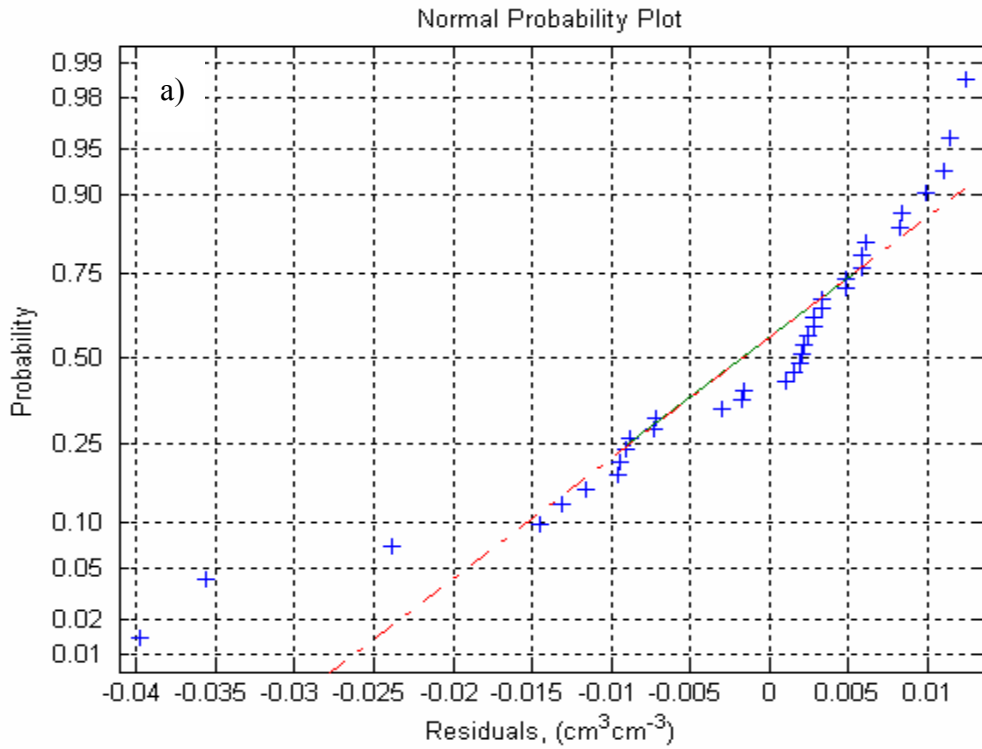
Figure 5.70. Normal probability plot for: (a) soil water content profile and (b) soil water pressure head profile in drainage of homogeneous soil (multi-objective optimization).
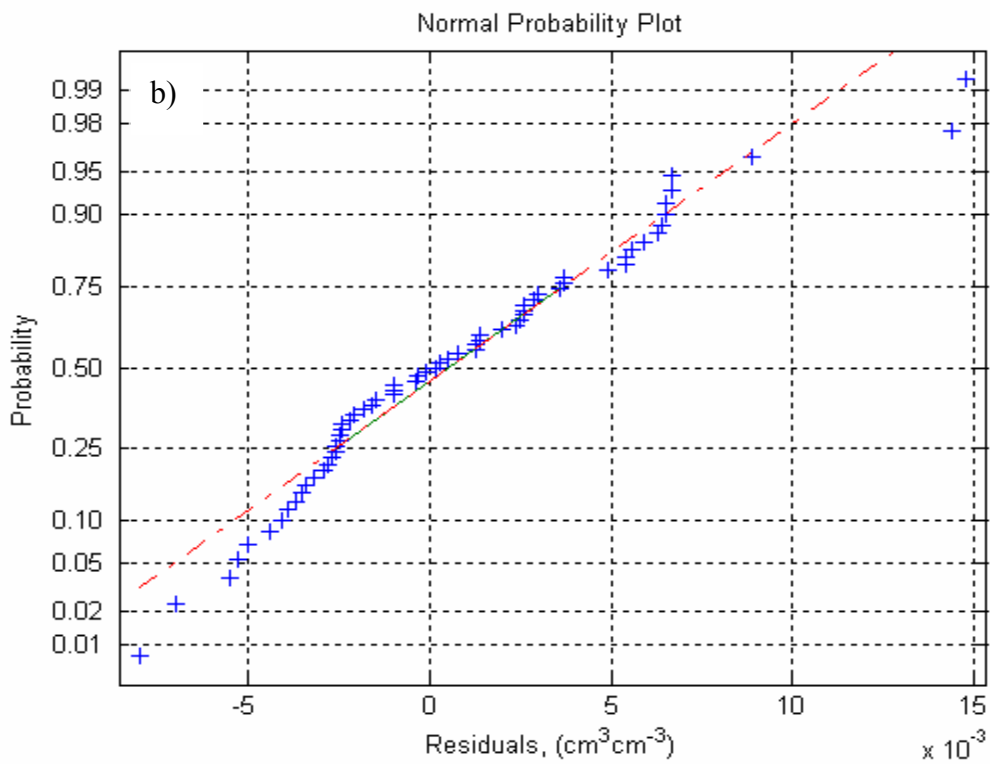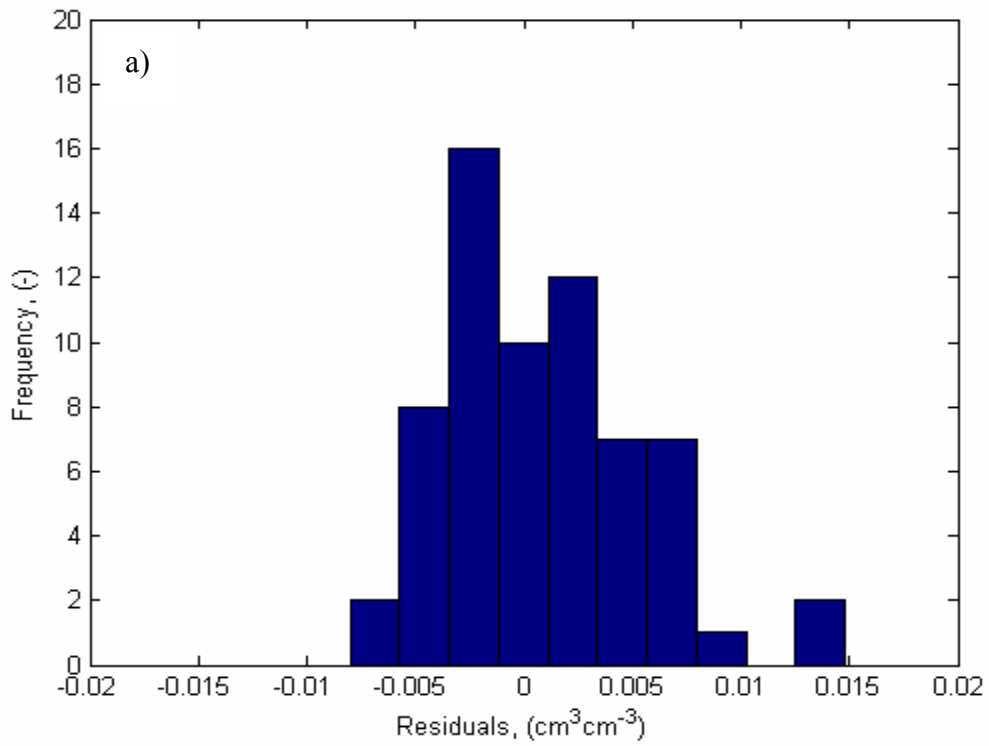
Figure 5.71. a) Histograms of residuals for soil water content profile in drainage of heterogeneous soil, and Normal probability plot.

The same procedure was followed to calculate the observed and expected error frequencies and merge the cells when the observed frequency was less than five. Since the calculated χ^2 (5.5156) is less than the *tabled critical value* at 10 percent level of significance ($\chi^2_{(1-\alpha,v)}$ = 5.9915), *the null hypothesis* (errors are normally distributed) is accepted indicating that the residuals in soil water pressure head data are normally distributed.

The chi-square test is a powerful test when the sample size is large. However, combining cells when the expected error frequencies are less than five looses information and hence decreases the power of the test. Furthermore for very small samples this test is not applicable (McCuen, 2003). To overcome these limitations, the Kolmogorov-Smirnov one sample test is usually used since it treats each observation separately and does not loose information through merging of categories. This test is more powerful than the chi-square test when sample size is not large.

The Kolmogorov-Smirnov one sample test was used to verify if the residuals in soil moisture content and soil water pressure head data (in case of drainage of Bandelier tuff: Data from Abeele, 1984) are normally distributed (in case of FRAP experiment, the Kolmogorov-Smirnov one sample test was not used because the evidence (normal probability plot, error frequency analysis, and chi-square test) strongly indicate that the residuals are normally distributed). The detailed calculation and analysis of the test are given in Appendix C. The results are only highlighted here:

For soil moisture content data

Sample test statistic = 0.140

α	Critical	Decision

0.20	0.178	*Accept H_0*
0.15	0.190	*Accept H_0*
0.10	0.203	*Accept H_0*
0.05	0.227	*Accept H_0*
0.01	0.272	*Accept H_0*

For soil water pressure head data:

Sample test statistic = 0.150

α	Critical	Decision
-------	--------	--------
0.20	0.178	*Accept H_0*
0.15	0.190	*Accept H_0*
0.10	0.203	*Accept H_0*
0.05	0.227	*Accept H_0*
0.01	0.272	*Accept H_0*

These results indicate that *the null hypothesis* (the errors are normally distributed) cannot be rejected even at twenty per cent level of significance. Therefore, the residuals in both cases are concluded to be *strongly* normally distributed.

Finally, for residuals of the drainage experiment in heterogeneous soil the error frequency and normal probability plot were constructed and depicted in Figures 5.71a and 5.71b. Both Figures show visible normal probability distribution function for the residuals. However, to verify that the residuals are normally distributed, in a quantitative way, the following hypotheses were tested:

$$H_0 : r = N(7.6615 \times 10^{-4}, 0.0046)$$
$$H_A : r \neq N(7.6615 \times 10^{-4}, 0.0046)$$

For this case there were seven cells. Since the information regarding the mean and standard deviation were taken from sample (not provided by population), therefore the

degree of freedom is $v = k - 2 - 1 = 4$.

The *calculated chi-square statistic* ($\chi^2 = 11.6606$) for this case is greater than the *critical value* at five per cent level of significance ($\chi^2_{(0.05,4)} = 11.14$). Therefore *the null hypothesis* (errors are normally distributed) cannot be accepted at 5 per cent level of significance and the *alternative hypothesis* (errors are not normally distributed) is accepted which implies that the residual are not normally distributed. However, the calculated χ^2 is less than *the tabled value* at one per cent level of significance ($\chi^2_{(0.01,4)} = 14.86$). This implies that the null hypothesis should be accepted and, therefore, the residuals are normally distributed.

This is a typical situation showing the power of the chi-square test. The sample size is initially large ($n = 65$), but combining the categories with expected probabilities less than five, leads to seven cells ($k = 7$). Furthermore, by reducing two degrees of freedom for mean and standard deviation of the sample, more information is lost.

To overcome the uncertainty, the Kolmogorov-Smirnov one sample test was used to verify that the residuals are normally distributed. The detailed results are given in Appendix C. The highlights of the test can be summarized as:

Sample test statistic = 0.096

α	Critical	Decision
0.20	0.133	*Accept* H_0
0.15	0.141	*Accept* H_0
0.10	0.151	*Accept* H_0
0.05	0.169	*Accept* H_0
0.01	0.202	*Accept* H_0

The Kolmogorov-Smirnov one sample test indicates that *the null hypothesis* (the errors are normally distributed) cannot be rejected even at the 20 per cent level of significance implying that the residuals are strongly normally distributed.

In conclusion, detailed residual analysis indicates that:

1) Residuals have zero mean,

2) Residuals have constant variance,

3) Residuals are normally distributed,

4) Residuals are uncorrelated (except for time series of water flow in homogeneous and heterogeneous soil at 5 or more per cent levels of significance).

Therefore, the necessary and sufficient criteria for least square parameter optimization, which were used in this study, were met except, to some extent, in the heterogeneous soil optimization.

CHAPTER 6: SUMMARY AND CONCLUSION

........Carrying a few books like a beast.
Sa'adi

6.1. Summary

The objectives of this study were to develop, evaluate, apply, and analyze an inverse modeling strategy to identify model parameters in mass transport problems in different biosystems. An important goal of the study was to formulate an inverse modeling methodology which is capable of solving single and multi-objective optimization problems. The strategy treated model parameters identification problem as a nonlinear optimization problem in which the forward model was solved iteratively until satisfactory results were obtained.

The forward problem consisted of one or more nonlinear partial differential equations governing mass transport phenomena in different biological systems. The problem was solved numerically by means of both the Galerkin based linear finite element method and the finite difference approximation. The accuracy and mass conservation properties of the numerical simulators were verified against exact and reference solutions prior to apply as forward model in the inverse problem. An adaptive time stepping approach was used to decrease CPU time, maintain small truncation error, and increase efficiency of the numerical simulators.

In inverse problem, the partial derivatives of the objective function with respect to model parameters were approximated by one-sided and two-sided finite difference approximations. At the beginning of the optimization, the strategy uses the former, which

is computationally cheap but not accurate, and as the solution approaches the minimum it switches to the later which is more accurate but computationally expensive. These derivatives were used to form the Jacobian matrix and to obtain the gradient of the objective function in each iteration. The Osborne-Moré extended version of the Levenberg-Marquardt algorithm was used in the inverse code. Using and critically analyzing different termination criteria to asses the accuracy of the inverse results, a mixed termination criterion was used to stop the algorithm. The developed inverse modeling strategy was then applied to identify model parameters in two different biological mass transport problems.

In the field of molecular biology, the experimental data from Fluorescence Recovery after Photobleaching (FRAP) protocol was coupled with the optimization algorithm and the numerical solution of a system of three coupled nonlinear partial differential equations to identify the optimized values of the mass transport and binding parameters for GFP-tagged glucocorticoid receptor. The following results were obtained:

1. The FRAP protocol provides enough information to uniquely estimate one parameter.

2. Coupling the experimental data obtained by the FRAP protocol with the inverse modeling strategy one can uniquely estimate the individual values of the binding rate coefficients (rather than their ratio) given the value of the molecular diffusion coefficient.

3. The FRAP experiment doesn't provide enough information for unique simultaneous estimation of the molecular diffusion coefficient and the pseudo-association rate constant. One needs to have one of them and to estimate the other

242

one from the FRAP data using the parameter optimization approach via inverse modeling strategy. This issue results from high inter-correlation between molecular diffusion coefficient and the pseudo-association rate parameter. The high intercorrelation makes it impossible to obtain unique solution for inverse problem using the experimental data from FRAP protocol.

4. The cause of the ill-posedness of the inverse problem was non-uniqueness not instability. Small changes in the input data didn't induce significant changes in the optimized values of the model parameters.

5. One possible approach to uniquely estimate the mass transport and binding parameters from the FRAP protocol is conducting two FRAP experiments on the same class of biomolecule and cell in two different regimes. One experiment may be used to measure the molecular diffusion coefficient of the biomolecule independent of binding in diffusion dominant regime. A way to perform this is using a biomolecule of the same molecular weight, class, and surface charge properties as of the biomolecule under study which doesn't have reaction with the vacant binding site(s). Having determined the diffusion coefficient, one can determine the individual values of the reaction rate parameters by conducting other FRAP experiment in reaction dominant or diffusion-reaction dominant regime.

The second mass transport problem investigated was water flow in partially saturated porous media. The developed parameter optimization strategy could successfully be used to identify hydraulic parameters for both single and multi-objective optimization problems in homogeneous and heterogeneous soils. In case of

heterogeneous soil, only soil water content information was available which was used in the framework of the single objective optimization to identify the hydraulic parameters. The results showed excellent agreement with the experimental data. In case of homogeneous soil, using only the soil moisture content data in the objective function produced good fit for soil moisture content profiles but poor results for soil water pressure head profiles. Also, the optimized values of n and $\alpha(cm^{-1})$ (in the van Genuchten model) were not unique. On the other hand, incorporating only soil water pressure head information in the objective function yielded excellent fit for soil water pressure head profiles but poor results for soil water content profile. Incorporating both kind of information in the objective function, in the framework of multi-objective optimization, produced excellent result for both soil water content and pressure head profiles. The optimized parameter values were stable.

Posedness of the inverse problem was investigated using stability and uniqueness analyses. To study the stability of the inverse problem, input data were perturbated. They were then used in the optimization algorithm and the results were compared with the optimized parameters. It was found that instability was not the cause of ill-posedness of the inverse problem in case of protein transport in living cells. The uniqueness of the inverse problem was studied by construction and analysis of parameter response surfaces and parameter hyper spaces. It was found that closed parameter response surfaces don't automatically guarantee a unique solution for the inverse problem. To fully understand the behavior of the objective function in whole parameter space, $p-dimensional$ parameter hyper-spaces should be constructed and analyzed.

A Parameter sensitivity analysis was carried out to determine where and when the

objective function has the highest sensitivity to the collected data and with respect to the changes in the model parameters being estimated. Parameter sensitivity analysis of the FRAP protocol indicated that the procedure provides the most sensitive information at the early stages of the experiment. Therefore, in parameter optimization, more weight should be given to the data in the beginning of the experiment. The dissociation rate coefficient is the most sensitive and hence the most identifiable parameter followed by the pseudo-association rate and free molecular diffusion coefficients. For GFP-GR the effective time to perform FRAP experiment is less than five seconds. After that the system essentially regains the state of equilibrium which it had before the photobleaching.

Sensitivity analysis, in case of water flow through partially saturated porous media, indicated that the sensitivity to the saturated hydraulic conductivity is highest in the wet region of the soil water characteristic curve. To obtain reliable estimate for this parameter, more data points should be collected at the beginning of the experiment or more weight should be given to early data points in the parameter optimization algorithm.

Comparing the norm of the sensitivities in single objective and multi-objective optimization indicated that additional information increases the identifiability of the air entry value (α) drastically. Additional information about the system (soil water pressure head data) remarkably increased the identifiability of α. The air entry value is the most sensitive and the most identifiable parameter for both single and multi-objective optimizations. This is confirmed by narrow confidence interval of the parameter obtained by the optimization.

Additional information slightly increased the identifiability of n and ι but it did not increase the sensitivity of the saturated hydraulic conductivity. It also decreased the

identifiability of the residual soil water content (θ_r). The parameter can be well identified using soil moisture data from dry zone of the soil water characteristic curve.

Residual analysis indicates that the errors are uncorrelated, and have constant variance and almost zero mean. Hypothesis test on the error probability density function shows that the residuals are normally distributed.

6.2. Conclusion

The development of the inverse modeling strategy was successful in incorporating a mass-conservative, efficient, and accurate numerical simulator (to solve the forward problem), an efficient optimization algorithm, a mixed stopping rule, and an efficient strategy to control the direction and size of the search in each iteration. The application of the strategy was successful in modeling protein transport in living cells and identifying model parameters in the Fluorescence Recovery after Photobleaching. The developed inverse modeling strategy was also successfully applied to quantify hydraulic parameters in water flow through homogeneous and heterogeneous partially saturated porous media, with both single-objective and multi-objective optimizations. The optimization algorithm was successfully used to analyze the posedness of the inverse problem in two mass transport optimization problems in different biological systems using parameter three-dimensional hyper-spaces and two-dimensional response surfaces. Parameter sensitivity analysis, residual analysis, and hypotheses tests on the normality of the error probability density function, and error variance indicated that the errors are uncorrelated, normally distributed, and have constant variance. Overall, the objectives of this study, which were "*develop, apply, and analyze an inverse modeling strategy to identify model parameters in mass transport problems in different biological systems*", were met successfully.

CHAPTER 7: RECOMMENDATIONS FOR FUTURE RESEARCH

With them the seed of wisdom did I sow
And with my own hand labour'd it to go
And this was all the Harvest that I reap'd
"I came like water, and like wine I go".
Khayyam

The inverse modeling strategy described in this study was developed, validated, analyzed, and applied in two different biological mass transport problems. The strategy offers the characteristics needed for parameter identification in sophisticated models and systems of partial differential equations governing transport phenomena in porous materials. However, ill-posedness of the inverse problems remains a major challenge. Future research should be aimed at tackling ill-posedness problems and developing innovative techniques to collect experimental data.

Specific recommendations are as follows:

1. Developing state-of-the-art techniques to study in vivo molecular dynamics (e.g. extending non-invasive methods to gather more information from biological systems) and collect more experimental data at the early stages of the FRAP protocol which are not feasible with current state of the techniques.

2. Further investigations are required to explain the high intercorrelation between the molecular diffusion coefficient and the pseudo-association rate coefficient, and to understand the underlying biological process behind this phenomenon.

3. Future research should focus on the comparison of the gradient based inverse modeling strategies with the large scale genetic algorithm and Monte Carlo–

Markov Chain (MCMC) methods in modeling flow and transport processes in biological systems.

4. Regularization and incorporation of a priori information regarding model parameters should be a focus of the future research in modeling biomolecule transport in living cells, tissues, and organs and variably saturated flow and transport through porous media.

5. More attention should be paid to stochastic inverse modeling approaches in modeling transport phenomena in biological systems.

6. Future investigations are required regarding the applications of inverse modeling approaches in multi-phase flow systems.

7. Sophisticated water retention functions such as bimodal and hysteretic models should be incorporated in the framework of the inverse modeling of flow and transport through partially saturated porous media.

8. Information theory, Generalized Likelihood Uncertainty Estimation (GLUE) methodology, and equifinality are suggested to be focal points of future research in modeling complex and highly heterogeneous bioenvironmental systems.

8. Appendices

Appendix A

Matrix Assembly in Finite Element Methods

Referring to Figure 4.2 one can identify the linear basis function in every element. Since the descending slope line passes through the points $(x_1, y_1) = (0,1)$ and $(x_2, y_2) = (\Delta z, 0)$, the linear basis function for this part of the element (i.e., the first node) can be developed as:

$$\phi_i = 1 - \frac{z}{\Delta z}$$

Using the same idea the linear basis function for ascending slope is (note that the ascending slope line passes through points $(x_1, y_1) = (0,0)$ and $(x_2, y_2) = (\Delta z, 1)$:

$$\phi_j = \frac{z}{\Delta z}$$

Using these linear basis functions, one can assemble the stiffness mass and global matrices in the finite element approximation of the Richards' equation. First, the stiffness mass matrix is assembled:

$$C(h)\frac{\partial h}{\partial t} \cong \sum_{i=1}^{2} C_i \phi_i(z)\frac{\partial \hat{h}}{\partial t}$$

Element 1:

$$\int_0^L \{\phi_i(z)[C_1\phi_i(z) + C_2\phi_j(z)] * \frac{\partial}{\partial t}[h_1\phi_i(z) + h_2\phi_j(z)]\}dz +$$

$$\int_0^L \{\phi_j(z)[C_1\phi_i(z) + C_2\phi_j(z)] * \frac{\partial}{\partial t}[h_1\phi_i(z) + h_2\phi_j(z)]\}dz$$

$Node1$:

$$\int_0^L \phi_i(z)[C_1\phi_i(z) + C_2\phi_j(z)][\phi_i(z) + \phi_j(z)]dz$$

$Node2$:

$$\int_0^L \phi_j(z)[C_1\phi_i(z) + C_2\phi_j(z)][\phi_i(z) + \phi_j(z)]dz$$

$$B_{11} = \int_0^L \phi_i(z)C_1\phi_i(z)\phi_i(z)dz + \int_0^L \phi_i(z)C_2\phi_j(z)\phi_i(z)dz$$

$$B_{12} = \int_0^L \phi_i(z)C_1\phi_i(z)\phi_j(z)dz + \int_0^L \phi_i(z)C_2\phi_j(z)\phi_j(z)dz$$

$$B_{21} = \int_0^L \phi_j(z)C_1\phi_i(z)\phi_i(z)dz + \int_0^L \phi_j(z)C_2\phi_j(z)\phi_i(z)dz$$

$$B_{22} = \int_0^L \phi_j(z)C_1\phi_i(z)\phi_j(z)dz + \int_0^L \phi_j(z)C_2\phi_j(z)\phi_j(z)dz$$

$$B_{11} = C_1\int_0^L \phi_i^3(z)dz + C_2\int_0^L \phi_i^2(z)\phi_j(z)dz =$$

$$C_1\int_0^L (1-z/\Delta z)^3 dz + C_2\int_0^L (1-z/\Delta z)^2(z/\Delta z)dz$$

$$B_{12} = C_1\int_0^L \phi_i^2(z)\phi_j(z)dz + C_2\int_0^L \phi_i(z)\phi_j^2(z)dz =$$

$$C_1\int_0^L (1-z/\Delta z)^2(z/\Delta z)dz + C_2\int_0^L (1-z/\Delta z)(z/\Delta z)^2 dz$$

$$B_{21} = C_1\int_0^L \phi_i^2(z)\phi_j(z)dz + C_2\int_0^L \phi_i(z)\phi_j^2(z)dz =$$

$$C_1\int_0^L (1-z/\Delta z)^2(z/\Delta z)dz + C_2\int_0^L (1-z/\Delta z)(z/\Delta z)^2 dz$$

$$B_{22} = C_1\int_0^L \phi_i(z)\phi_j^2(z)dz + C_2\int_0^L \phi_j^3(z)dz =$$

$$C_1\int_0^L (1-z/\Delta z)(z/\Delta z)^2 dz + C_2\int_0^L (z/\Delta z)^3 dz$$

$$B_{11} = \Delta z(\frac{C_1}{4} + \frac{C_2}{12}) = \frac{\Delta z}{12}(3C_1 + C_2)$$

$$B_{12} = \Delta z(\frac{C_1}{12} + \frac{C_2}{12}) = \frac{\Delta z}{12}(C_1 + C_2)$$

$$B_{21} = \Delta z(\frac{C_1}{4} + \frac{C_2}{12}) = \frac{\Delta z}{12}(C_1 + C_2)$$

$$B_{22} = \Delta z(\frac{C_1}{12} + \frac{C_2}{4}) = \frac{\Delta z}{12}(C_1 + 3C_2)$$

Element 2:

*Node*1 :

$$\int_0^L \phi_i(z)[C_2\phi_i(z) + C_3\phi_j(z)][\phi_i(z) + \phi_j(z)]dz$$

*Node*2 :

$$\int_0^L \phi_j(z)[C_2\phi_i(z) + C_3\phi_j(z)][\phi_i(z) + \phi_j(z)]dz$$

or :

$$B_{22} = \int_0^L \phi_i(z)C_2\phi_i(z)\phi_i(z)dz + \int_0^L \phi_i(z)C_3\phi_j(z)\phi_i(z)dz$$

$$B_{23} = \int_0^L \phi_i(z)C_2\phi_i(z)\phi_j(z)dz + \int_0^L \phi_i(z)C_3\phi_j(z)\phi_j(z)dz$$

$$B_{32} = \int_0^L \phi_j(z)C_2\phi_i(z)\phi_i(z)dz + \int_0^L \phi_j(z)C_3\phi_j(z)\phi_i(z)dz$$

$$B_{33} = \int_0^L \phi_j(z)C_2\phi_i(z)\phi_j(z)dz + \int_0^L \phi_j(z)C_3\phi_j(z)\phi_j(z)dz$$

or:

$$B_{22} = C_2\int_0^L \phi_i^3(z)dz + C_3\int_0^L \phi_i^2(z)\phi_j(z)dz =$$

$$C_2\int_0^L (1-z/\Delta z)^3 dz + C_3\int_0^L (1-z/\Delta z)^2(z/\Delta z)dz$$

$$B_{23} = C_2\int_0^L \phi_i^2(z)\phi_j(z)dz + C_3\int_0^L \phi_i(z)\phi_j^2(z)dz =$$

$$C_2\int_0^L (1-z/\Delta z)^2(z/\Delta z)dz + C_3\int_0^L (1-z/\Delta z)(z/\Delta z)^2 dz$$

$$B_{32} = C_2\int_0^L \phi_i^2(z)\phi_j(z)dz + C_3\int_0^L \phi_i(z)\phi_j^2(z)dz =$$

$$C_2\int_0^L (1-z/\Delta z)^2(z/\Delta z)dz + C_3\int_0^L (1-z/\Delta z)(z/\Delta z)^2 dz$$

$$B_{33} = C_2\int_0^L \phi_i(z)\phi_j^2(z)dz + C_3\int_0^L \phi_j^3(z)dz =$$

$$B_{22} = \Delta z(\frac{C_2}{4} + \frac{C_3}{12}) = \frac{\Delta z}{12}(3C_2 + C_3)$$

$$B_{23} = \Delta z(\frac{C_2}{12} + \frac{C_3}{12}) = \frac{\Delta z}{12}(C_2 + C_3)$$

$$B_{32} = \Delta z(\frac{C_2}{4} + \frac{C_3}{12}) = \frac{\Delta z}{12}(C_2 + C_3)$$

$$B_{33} = \Delta z(\frac{C_2}{12} + \frac{C_3}{4}) = \frac{\Delta z}{12}(C_2 + 3C_3)$$

Continuing the same procedure will lead to the formation of the stiffness mass matrix:

$$[B] = \frac{\Delta z}{12}\begin{pmatrix} 3C_1+C_2 & C_1+C_2 & 0 & ... & 0 \\ C_1+C_2 & C_1+6C_2+C_3 & C_2+C_3 & . & . \\ . & . & . & . & . \\ . & . & C_{N-2}+C_{N-1} & C_{N-2}+6C_{N-1}+C_N & C_{N-1}+C_N \\ 0 & 0 & .... & C_{N-1}+C_N & C_{N-1}+3C_N \end{pmatrix}$$

It must be mentioned that in assembling the mass matrix the upper limit of integration of the basis function is Δz, and the following integrals are equivalent:

$$\int_0^L (1-z/\Delta z)(z/\Delta z)^2\, dz = \int_0^L (1-z/\Delta z)^2 (z/\Delta z)\, dz = \frac{L}{12} = \frac{\Delta z}{12}$$

$$\int_0^L (z/\Delta z)^3\, dz = \int_0^L (z/\Delta z)^3\, dz = \frac{L}{4} = \frac{\Delta z}{4}$$

Similarly the matrix $[A]$ is assembled to form:

$$[A] = \frac{1}{2\Delta z}\begin{pmatrix} K_1 + K_2 & -K_1 - K_2 & 0 & \cdots & & 0 \\ -K_1 - K_2 & K_1 + 2K_2 + K_3 & -K_2 - K_3 & & & \cdot \\ \cdot & \cdot & \cdot & \cdot & & \cdot \\ \cdot & \cdot & -K_{N-2} - K_{N-1} & K_{N-2} + 2K_{N-1} + K_N & -K_{N-1} - K_N \\ 0 & 0 & \cdots & K_{N-1} - K_N & K_{N-1} + K_N \end{pmatrix}$$

And finally the driving force vector $\{F\}$ can be written as:

$$\{F\} = \frac{1}{2}\begin{bmatrix} K_1 + K_2 \\ K_3 - K_1 \\ \cdot \\ \cdot \\ K_{i+1} - K_{i-1} \\ \cdot \\ \cdot \\ K_n - K_{n-1} \end{bmatrix} + \begin{bmatrix} q_0(t) \\ 0 \\ 0 \\ \cdot \\ \cdot \\ \cdot \\ 0 \\ 0 \\ -q_L(t) \end{bmatrix}$$

where $q_0(t)$ is the net flux (precipitation + irrigation - evapotranspiration) at the soil surface, and $q_L(t)$ is the imposed drainage flux at the bottom of the soil (van Genuchten, 1978).

Appendix B

Sensitivity Matrices

and

Absolute Sensitivities of the State Variables

The absolute and relative sensitivities of the state variables: laser beam recovery in the Fluorescence Recovery after Photobleaching (FRAP), soil moisture content, soil water pressure head were calculated using the columns of the last Jacobian matrix at the end of the optimization. The Jacobian matrices for three state variables are presented in Tables B1, B2, B3, B4, and B5. The absolute sensitivities of the state variables with respect to changes in model parameters are presented in the following Figures.
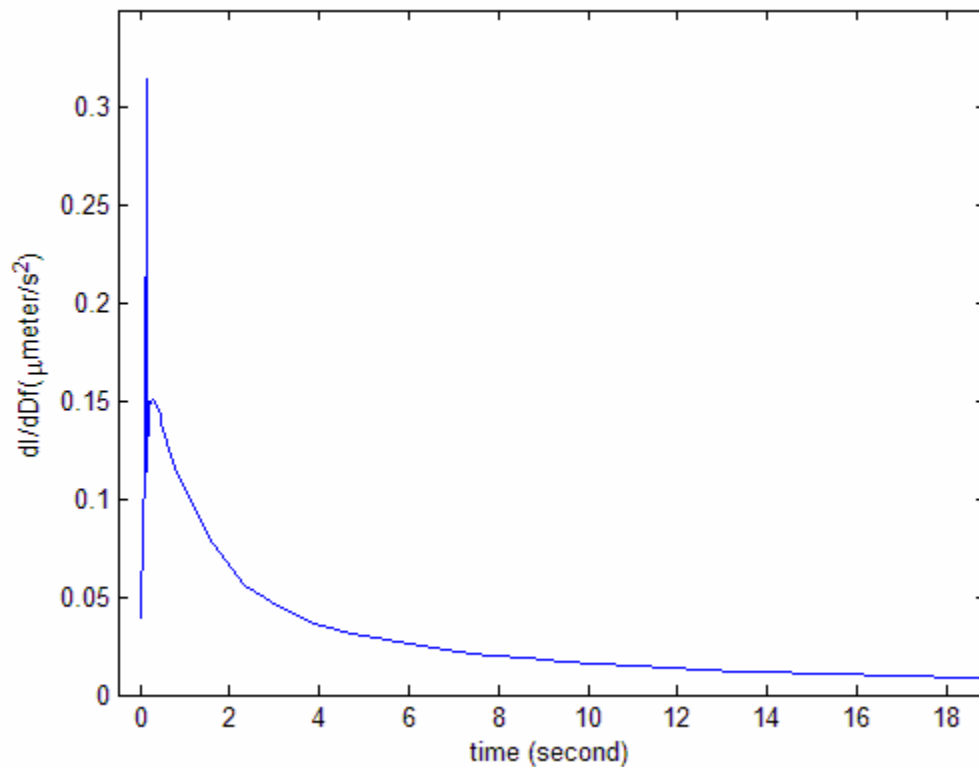
Figure B1. Distribution of the absolute sensitivity of $\overline{frap}$ with respect to changes in D_f over time course of the FRAP experiment.

Table B1. Sensitivity matrix for one-site-mobile-immobile model in FRAP experiment.

$\dfrac{\partial \bar{frap}}{\partial D_f}$	$\dfrac{\partial \bar{frap}}{\partial K_a}$	$\dfrac{\partial \bar{frap}}{\partial K_d}$
0.0391	-0.4315	0.0188
0.0880	-0.9916	0.0433
0.1132	-1.3082	0.0573
0.3150	-1.5621	0.0046
0.1144	-1.7420	0.0764
0.1502	-1.8953	0.0846
0.1493	-2.0290	0.0902
0.1507	-2.1381	0.0956
0.1497	-2.2329	0.1003
0.1479	-2.3115	0.1043
0.1454	-2.3785	0.1078
0.1424	-2.4372	0.1111
0.1392	-2.4860	0.1139
0.1358	-2.5288	0.1164
0.1324	-2.5643	0.1187
0.1291	-2.5945	0.1207
0.1257	-2.6208	0.1226
0.1225	-2.6422	0.1243
0.1193	-2.6605	0.1259
0.1163	-2.6751	0.1273
0.0806	-2.7695	0.1314
0.0557	-2.3575	0.1407
0.0442	-2.0577	0.1369
0.0368	-1.7784	0.1298
0.0316	-1.5286	0.1213
0.0277	-1.3103	0.1122
0.0247	-1.1219	0.1028
0.0222	-0.9602	0.0935
0.0202	-0.8225	0.0846
0.0185	-0.7053	0.0762
0.0171	-0.6058	0.0683
0.0158	-0.5214	0.0610
0.0147	-0.4497	0.0544
0.0138	-0.3890	0.0483
0.0129	-0.3376	0.0429
0.0122	-0.2939	0.0380
0.0115	-0.2569	0.0336
0.0109	-0.2253	0.0298
0.0104	-0.1985	0.0263
0.0099	-0.1757	0.0233
0.0094	-0.1562	0.0206
0.0090	-0.1395	0.0182
0.0086	-0.1252	0.0161

Table B2. Sensitivity matrix for diffusion-reaction model in FRAP experiment.

$\dfrac{\partial \overline{frap}}{\partial D_f}$	$\dfrac{\partial \overline{frap}}{\partial K_a}$	$\dfrac{\partial \overline{frap}}{\partial K_d}$	$\dfrac{\partial \overline{frap}}{\partial D_S}$	$\dfrac{\partial \overline{frap}}{\partial D_C}$
0.0064	-0.0002	0.0008	0.0000	0.0941
0.0165	-0.0013	0.0054	0.0017	0.1852
0.0220	-0.0022	0.0081	0.0049	0.1975
0.0256	-0.0028	0.0097	0.0096	0.2043
0.0273	-0.0031	0.0105	0.0141	0.2080
0.0281	-0.0033	0.0108	0.0193	0.2110
0.0283	-0.0034	0.0109	0.0246	0.2133
0.0280	-0.0035	0.0108	0.0290	0.2148
0.0274	-0.0035	0.0106	0.0344	0.2164
0.0265	-0.0034	0.0103	0.0399	0.2178
0.0256	-0.0034	0.0100	0.0454	0.2190
0.0245	-0.0033	0.0096	0.0511	0.2203
0.0237	-0.0033	0.0094	0.0557	0.2213
0.0226	-0.0032	0.0090	0.0614	0.2226
0.0218	-0.0031	0.0088	0.0662	0.2237
0.0208	-0.0031	0.0084	0.0720	0.2250
0.0200	-0.0030	0.0082	0.0766	0.2261
0.0192	-0.0030	0.0080	0.0813	0.2272
0.0185	-0.0029	0.0078	0.0860	0.2284
0.0177	-0.0028	0.0075	0.0916	0.2298
0.0100	-0.0021	0.0052	0.1609	0.2457
0.0065	-0.0015	0.0038	0.1923	0.2460
0.0040	-0.0009	0.0022	0.2019	0.2368
0.0018	-0.0001	0.0002	0.2008	0.2238
-0.0000	0.0008	-0.0019	0.1948	0.2097
-0.0015	0.0018	-0.0042	0.1870	0.1961
-0.0027	0.0027	-0.0065	0.1788	0.1836
-0.0036	0.0037	-0.0087	0.1706	0.1722
-0.0043	0.0045	-0.0108	0.1630	0.1621
-0.0048	0.0054	-0.0127	0.1559	0.1530
-0.0052	0.0061	-0.0145	0.1495	0.1450
-0.0054	0.0069	-0.0163	0.1434	0.1376
-0.0055	0.0075	-0.0178	0.1380	0.1311
-0.0056	0.0081	-0.0193	0.1330	0.1252
-0.0056	0.0087	-0.0207	0.1284	0.1199
-0.0056	0.0092	-0.0219	0.1243	0.1152
-0.0055	0.0097	-0.0230	0.1204	0.1109
-0.0055	0.0102	-0.0241	0.1168	0.1069
-0.0054	0.0106	-0.0250	0.1135	0.1033
-0.0052	0.0109	-0.0260	0.1104	0.0999
-0.0051	0.0113	-0.0268	0.1076	0.0969
-0.0050	0.0116	-0.0275	0.1049	0.0940

Table B3. Sensitivity matrix for multi-objective optimization (data from Abeele, 1984).

$\dfrac{\partial\theta}{\partial K_s}$	$\dfrac{\partial\theta}{\partial\alpha}$	$\dfrac{\partial\theta}{\partial n}$	$\dfrac{\partial\theta}{\partial\theta_r}$	$\dfrac{\partial\theta}{\partial\iota}$
0.0017	6.7314	0.0045	-0.0007	-0.0014
0.0019	8.0445	0.0093	-0.0020	-0.0048
0.0018	7.3365	0.0110	-0.0030	-0.0073
0.0016	6.5745	0.0116	-0.0037	-0.0089
0.0014	5.8277	0.0118	-0.0044	-0.0102
0.0012	4.9776	0.0116	-0.0051	-0.0113
0.0015	2.6184	0.0020	-0.0003	-0.0007
0.0020	4.6760	0.0065	-0.0014	-0.0038
0.0019	4.5771	0.0087	-0.0024	-0.0065
0.0017	4.1623	0.0096	-0.0032	-0.0084
0.0015	3.6962	0.0100	-0.0039	-0.0099
0.0013	3.1462	0.0101	-0.0047	-0.0114
0.0013	0.8296	0.0009	-0.0001	-0.0003
0.0019	3.1229	0.0051	-0.0011	-0.0029
0.0019	3.3823	0.0075	-0.0020	-0.0058
0.0018	3.1493	0.0086	-0.0028	-0.0078
0.0016	2.8139	0.0092	-0.0035	-0.0095
0.0014	2.3919	0.0095	-0.0044	-0.0112
0.0011	-0.2195	0.0003	0.0000	-0.0001
0.0019	2.0300	0.0041	-0.0008	-0.0023
0.0019	2.5889	0.0067	-0.0017	-0.0051
0.0018	2.5058	0.0079	-0.0025	-0.0072
0.0017	2.2684	0.0087	-0.0033	-0.0090
0.0015	1.9331	0.0091	-0.0041	-0.0109
0.0010	-0.8208	0.0000	0.0000	0.0000
0.0019	1.1881	0.0033	-0.0006	-0.0018
0.0020	1.9889	0.0060	-0.0015	-0.0045
0.0019	2.0423	0.0074	-0.0023	-0.0067
0.0017	1.8911	0.0083	-0.0031	-0.0087
0.0015	1.6255	0.0088	-0.0040	-0.0106
0.0009	-1.2067	-0.0001	0.0000	0.0000
0.0018	0.4050	0.0027	-0.0005	-0.0015
0.0020	1.3894	0.0055	-0.0014	-0.0041
0.0019	1.5820	0.0070	-0.0021	-0.0063
0.0017	1.5255	0.0079	-0.0029	-0.0083
0.0015	1.3363	0.0085	-0.0038	-0.0104

Table B4. Sensitivity matrix for single-objective optimization (soil moisture data, data from Abeele, 1984).

$\dfrac{\partial \theta}{\partial K_s}$	$\dfrac{\partial \theta}{\partial \alpha}$	$\dfrac{\partial \theta}{\partial n}$	$\dfrac{\partial \theta}{\partial \theta_r}$	$\dfrac{\partial \theta}{\partial \iota}$
0.0063	0.3903	0.0012	-0.0358	-0.0016
0.0075	0.9417	0.0044	-0.2746	-0.0107
0.0058	0.7647	0.0049	-0.4796	-0.0163
0.0045	0.5928	0.0046	-0.6021	-0.0180
0.0034	0.4510	0.0041	-0.6976	-0.0180
0.0023	0.3119	0.0034	-0.7922	-0.0165
0.0031	-0.2368	-0.0004	0.0179	0.0006
0.0085	0.3688	0.0020	-0.0674	-0.0035
0.0076	0.4822	0.0040	-0.2881	-0.0124
0.0061	0.3986	0.0043	-0.4465	-0.0170
0.0048	0.3065	0.0041	-0.5759	-0.0191
0.0033	0.2104	0.0036	-0.7072	-0.0191
0.0015	-0.2067	-0.0004	0.0119	0.0004
0.0078	0.0732	0.0006	0.0157	0.0003
0.0085	0.3538	0.0032	-0.1736	-0.0084
0.0071	0.3215	0.0040	-0.3473	-0.0148
0.0056	0.2519	0.0041	-0.4963	-0.0185
0.0039	0.1726	0.0037	-0.6506	-0.0198
0.0007	-0.1277	-0.0002	0.0059	0.0002
0.0064	-0.1097	-0.0003	0.0455	0.0018
0.0090	0.2564	0.0024	-0.0887	-0.0048
0.0078	0.2708	0.0037	-0.2676	-0.0123
0.0063	0.2183	0.0040	-0.4307	-0.0174
0.0045	0.1499	0.0038	-0.6032	-0.0200
0.0003	-0.0708	-0.0001	0.0028	0.0001
0.0049	-0.1874	-0.0006	0.0481	0.0020
0.0091	0.1808	0.0017	-0.0306	-0.0021
0.0084	0.2354	0.0033	-0.2067	-0.0101
0.0068	0.1965	0.0039	-0.3792	-0.0162
0.0049	0.1355	0.0039	-0.5655	-0.0198
0.0001	-0.0334	-0.0000	0.0011	0.0000
0.0036	-0.1848	-0.0007	0.0416	0.0017
0.0090	0.1410	0.0011	0.0124	0.0000
0.0088	0.2097	0.0030	-0.1559	-0.0080
0.0072	0.1805	0.0038	-0.3348	-0.0149
0.0052	0.1253	0.0039	-0.5326	-0.0195

Table B5. Sensitivity matrix for water flow through heterogeneous soil.

$\dfrac{\partial\theta}{\partial K_s}$	$\dfrac{\partial\theta}{\partial\alpha}$	$\dfrac{\partial\theta}{\partial n}$	$\dfrac{\partial\theta}{\partial\theta_r}$	$\dfrac{\partial\theta}{\partial\iota}$
0.0000	-0.0000	0.0000	-0.0000	0.0000
0.0035	0.3461	0.1080	-0.0541	-0.0017
0.0050	0.6374	0.1756	-0.0970	-0.0029
0.0058	0.8057	0.2188	-0.1263	-0.0039
0.0064	0.9381	0.2552	-0.1524	-0.0047
0.0067	1.0340	0.2819	-0.1730	-0.0054
0.0069	1.1141	0.3032	-0.1906	-0.0060
0.0070	1.1783	0.3188	-0.2047	-0.0064
0.0070	1.3856	0.3557	-0.2461	-0.0072
0.0065	1.5986	0.3745	-0.2815	-0.0074
0.0054	1.9225	0.3807	-0.3269	-0.0066
0.0042	2.1858	0.3735	-0.3598	-0.0054
0.0032	2.3933	0.3622	-0.3841	-0.0041
0.0000	-0.0000	0.0000	-0.0000	0.0000
0.0028	-0.0465	0.0516	-0.0121	-0.0006
0.0048	0.0978	0.1122	-0.0378	-0.0017
0.0060	0.2416	0.1576	-0.0603	-0.0028
0.0068	0.3886	0.1989	-0.0833	-0.0039
0.0074	0.5148	0.2308	-0.1030	-0.0048
0.0077	0.6309	0.2569	-0.1209	-0.0055
0.0079	0.7286	0.2762	-0.1357	-0.0060
0.0079	1.0464	0.3231	-0.1814	-0.0072
0.0074	1.3520	0.3482	-0.2217	-0.0076
0.0061	1.7790	0.3593	-0.2734	-0.0069
0.0047	2.1055	0.3538	-0.3106	-0.0057
0.0035	2.3546	0.3428	-0.3381	-0.0044
0.0000	-0.0000	0.0000	-0.0000	0.0000
0.0019	-0.0768	0.0258	-0.0028	-0.0000
0.0040	-0.0718	0.0700	-0.0152	-0.0007
0.0053	-0.0034	0.1077	-0.0292	-0.0014
0.0063	0.1016	0.1450	-0.0455	-0.0023
0.0070	0.2148	0.1754	-0.0610	-0.0031
0.0074	0.3338	0.2013	-0.0760	-0.0039
0.0077	0.4419	0.2211	-0.0890	-0.0044
0.0079	0.8167	0.2714	-0.1317	-0.0058
0.0074	1.1803	0.3008	-0.1710	-0.0064
0.0061	1.6724	0.3180	-0.2226	-0.0061
0.0048	2.0370	0.3165	-0.2600	-0.0052
0.0036	2.3103	0.3081	-0.2878	-0.0041
0.0000	-0.0001	0.0000	0.0000	0.0000
0.0014	-0.0535	0.0147	-0.0008	0.0001
0.0031	-0.0896	0.0449	-0.0070	-0.0001
0.0043	-0.0542	0.0727	-0.0161	-0.0005
0.0053	0.0298	0.1011	-0.0278	-0.0010
0.0059	0.1340	0.1250	-0.0395	-0.0015

0.0064	0.2503	0.1458	-0.0513	-0.0020
0.0066	0.3590	0.1622	-0.0618	-0.0024
0.0069	0.7419	0.2059	-0.0969	-0.0035
0.0065	1.1109	0.2341	-0.1301	-0.0042
0.0054	1.6011	0.2545	-0.1743	-0.0044
0.0043	1.9589	0.2576	-0.2068	-0.0039
0.0032	2.2249	0.2531	-0.2313	-0.0032
0.0000	-0.0002	0.0000	0.0000	0.0000
0.0011	-0.0333	0.0096	-0.0003	0.0002
0.0024	-0.0387	0.0280	-0.0047	0.0002
0.0032	0.0137	0.0456	-0.0117	0.0001
0.0039	0.1109	0.0632	-0.0207	-0.0000
0.0043	0.2197	0.0779	-0.0296	-0.0002
0.0046	0.3334	0.0909	-0.0384	-0.0004
0.0047	0.4349	0.1012	-0.0460	-0.0006
0.0049	0.7720	0.1301	-0.0708	-0.0013
0.0046	1.0803	0.1507	-0.0936	-0.0018
0.0039	1.4781	0.1683	-0.1239	-0.0023
0.0031	1.7645	0.1734	-0.1464	-0.0022
0.0023	1.9761	0.1725	-0.1635	-0.0019
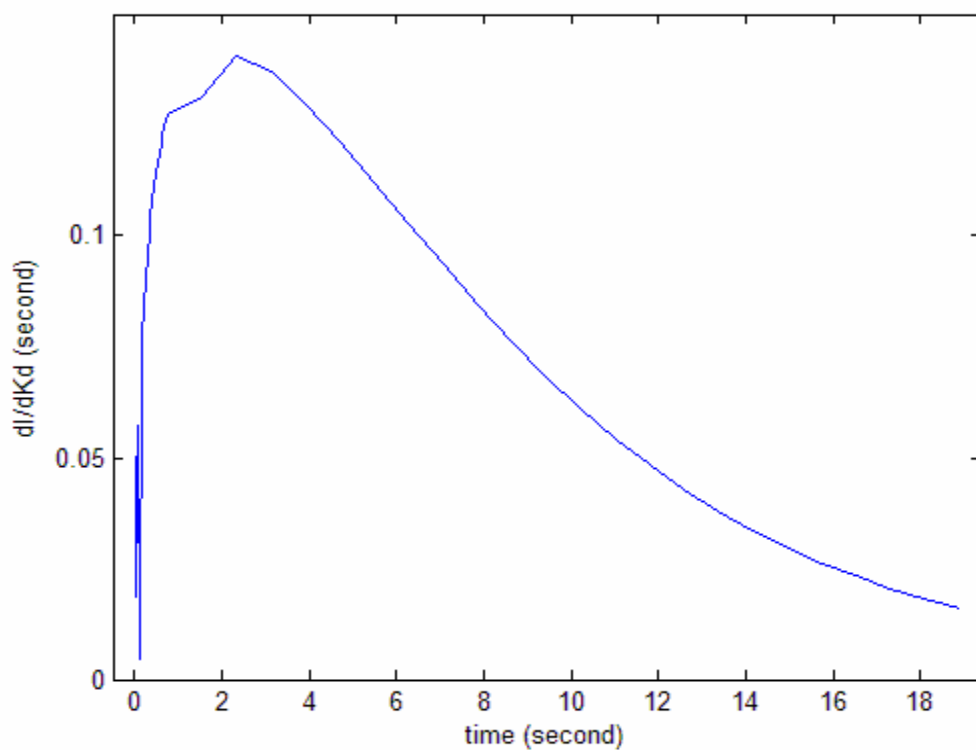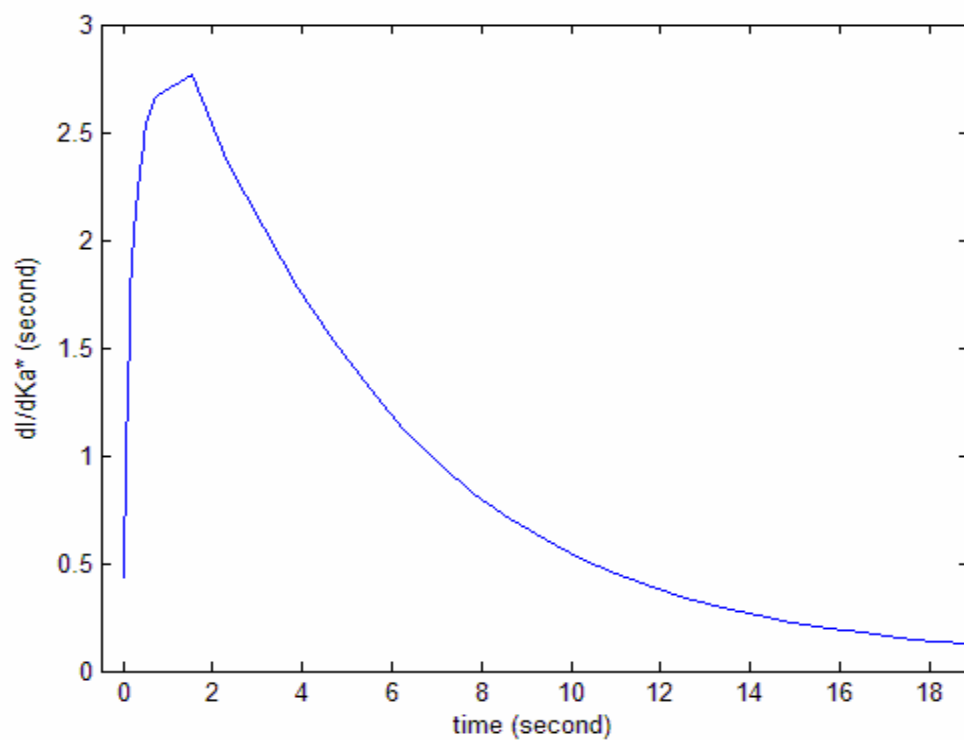
Figure B2. Distribution of the absolute sensitivity of $\overline{frap}$ with respect to changes in K_a^* (a) and K_d (b) over time course of the FRAP experiment.
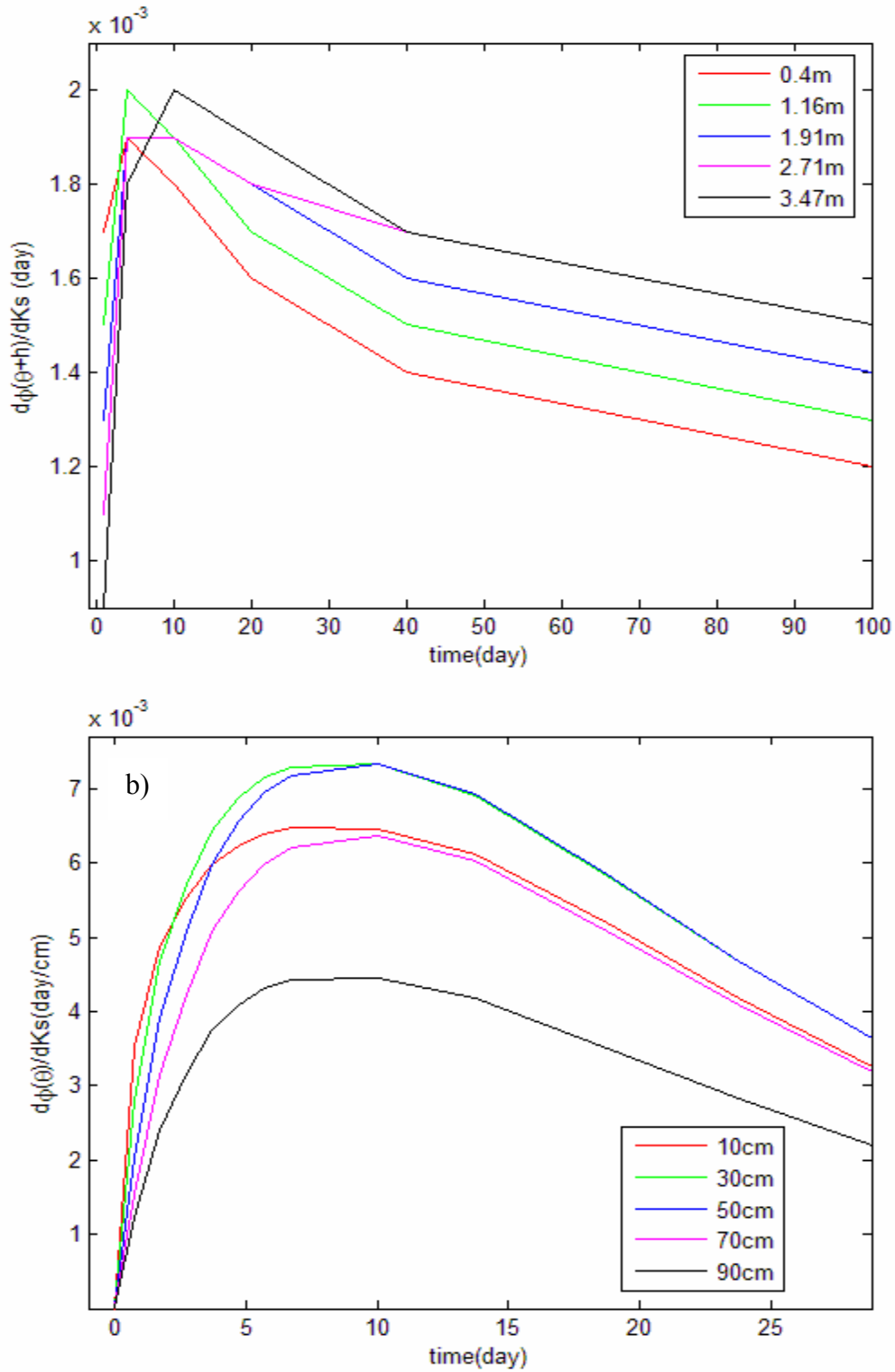
Figure B3. Time-depth distribution of the absolute sensitivity of the objective function with respect to K_s for multi-objective (a) and single-objective optimization (b).
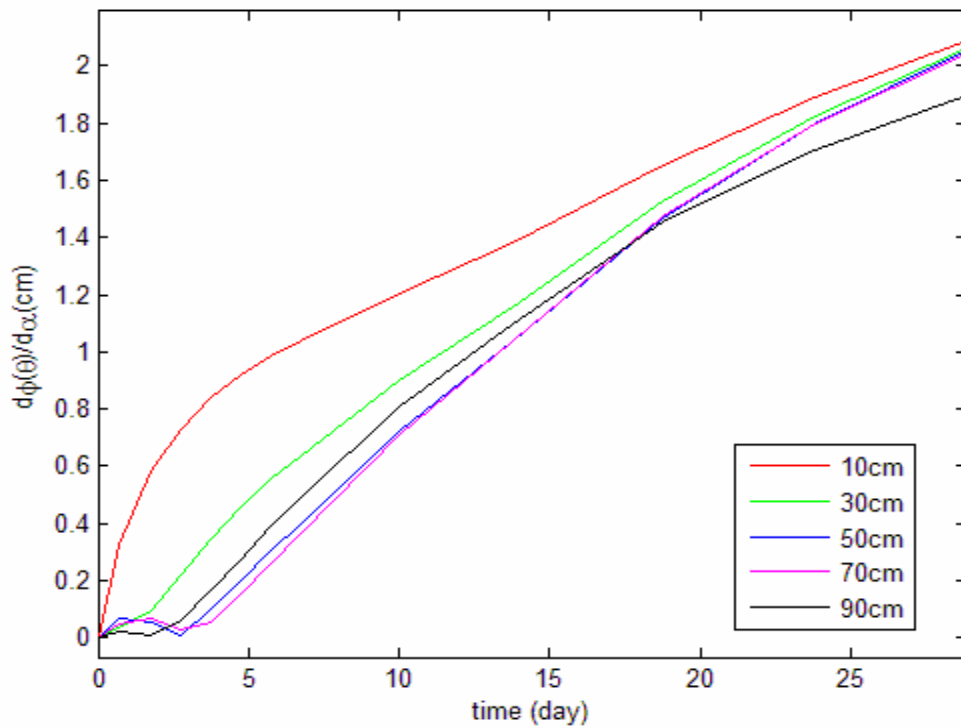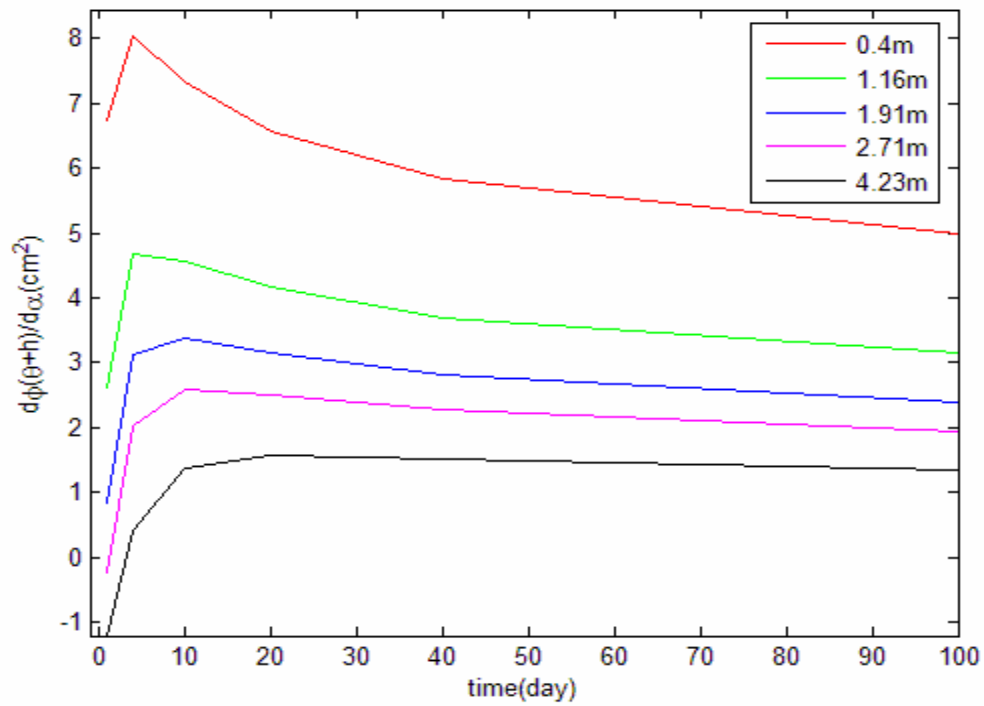
Figure B4. Time-depth distribution of the absolute sensitivity of the objective function with respect to α for multi-objective (a) and single-objective optimization (b).
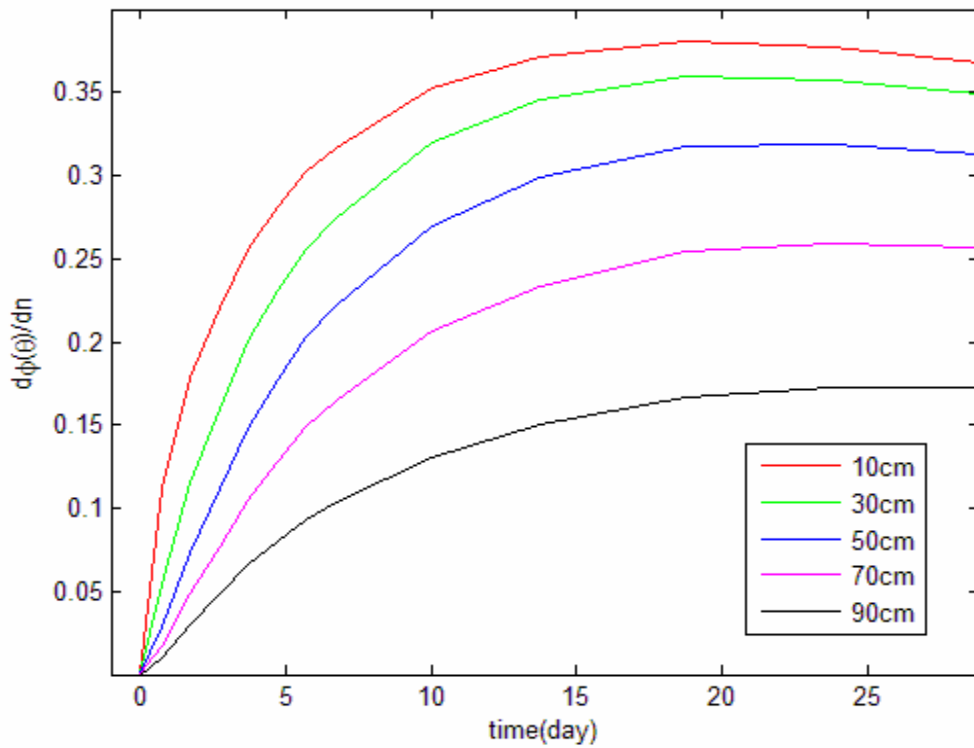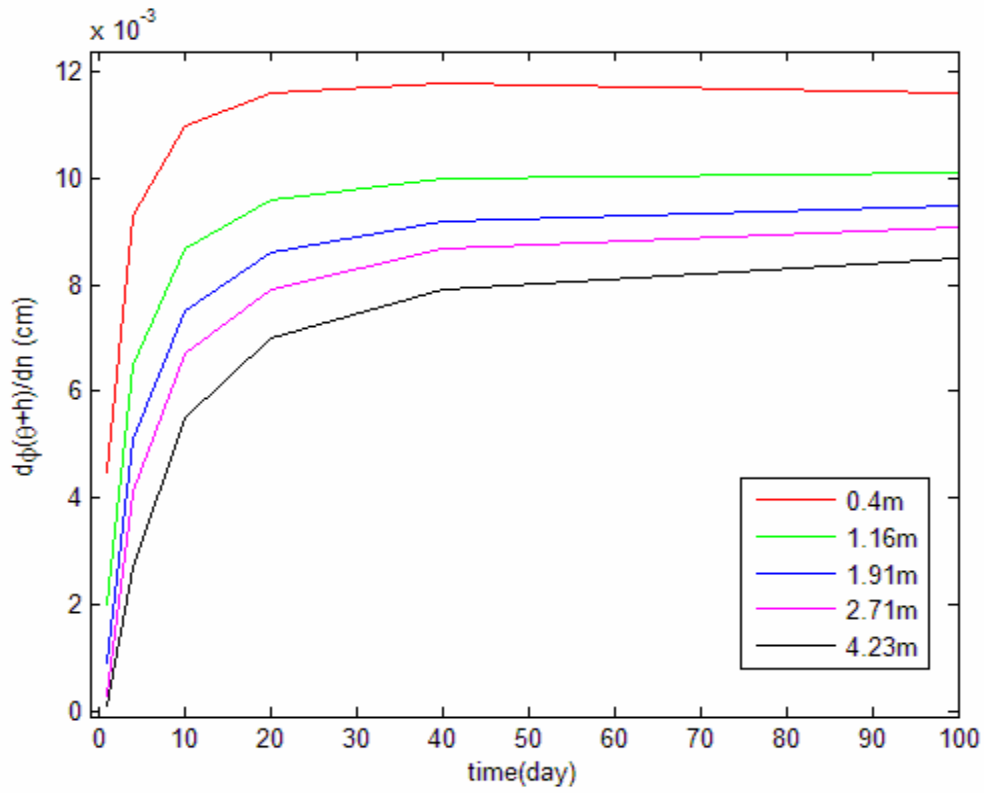
Figure B5. Time-depth distribution of the absolute sensitivity of the objective function with respect to *n* for multi-objective (a) and single-objective optimization
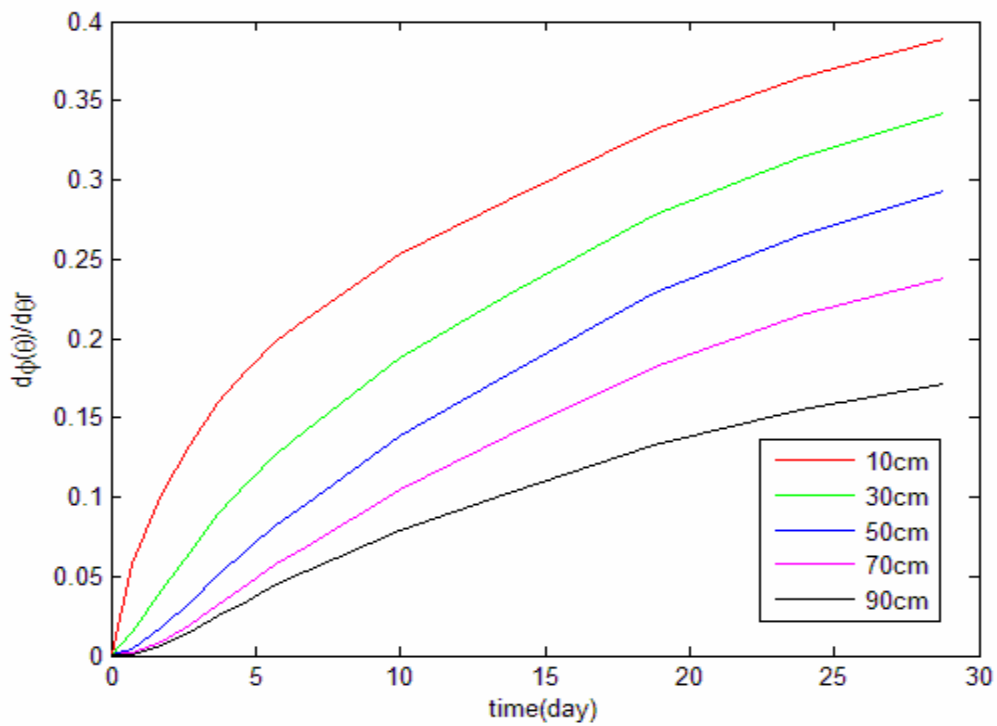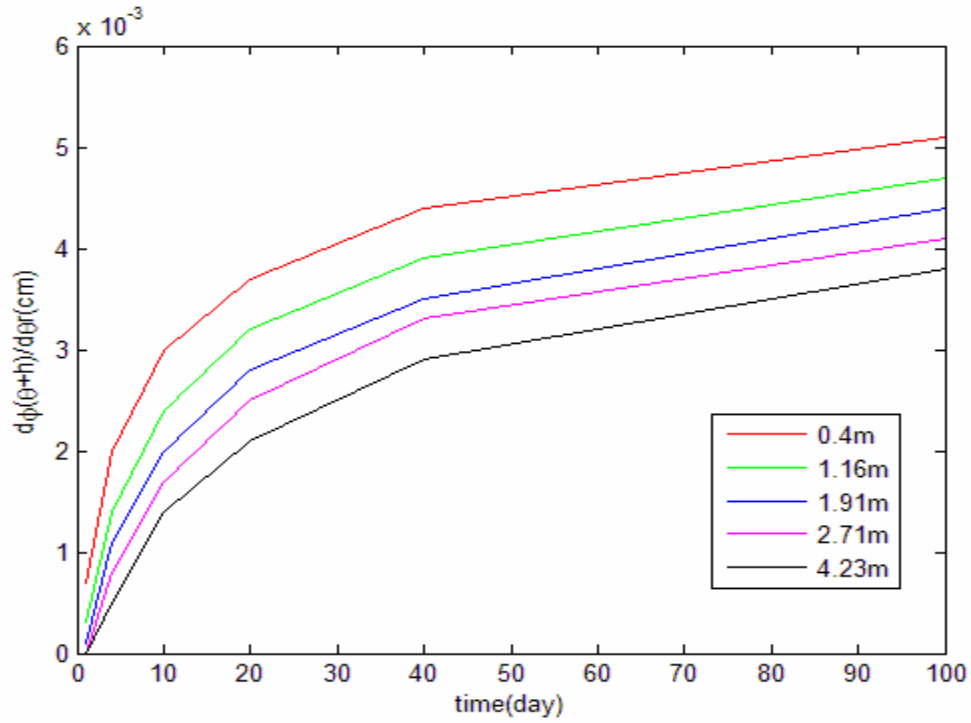
Figure B6. Time-depth distribution of the absolute sensitivity of the objective function with respect to θ_r for multi-objective (a) and single-objective optimization (b).
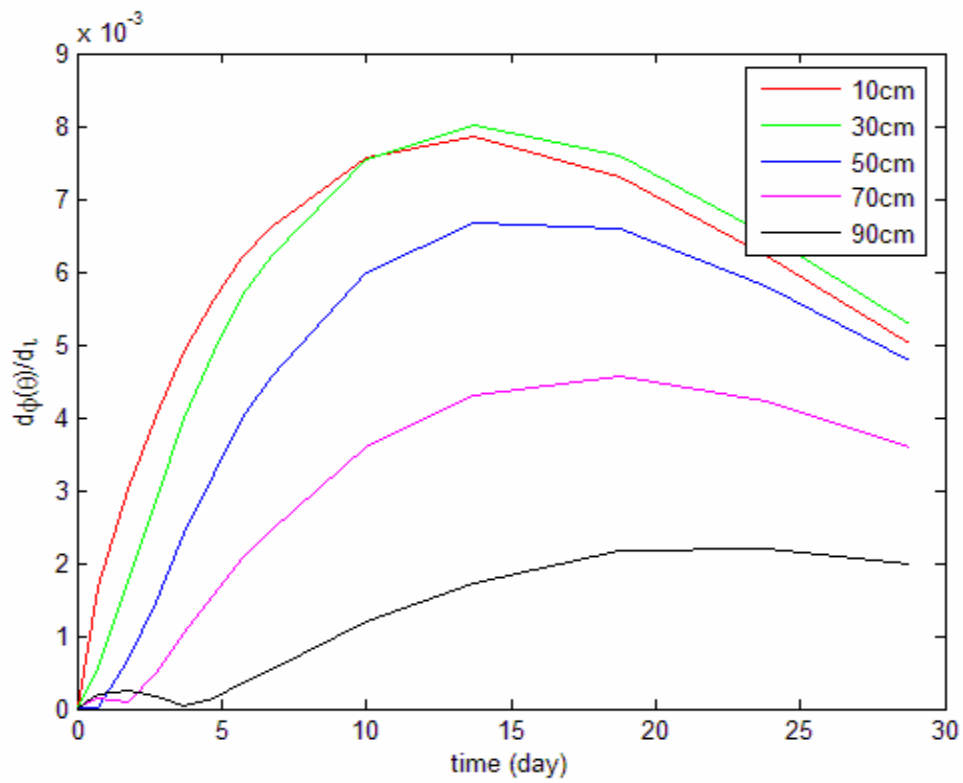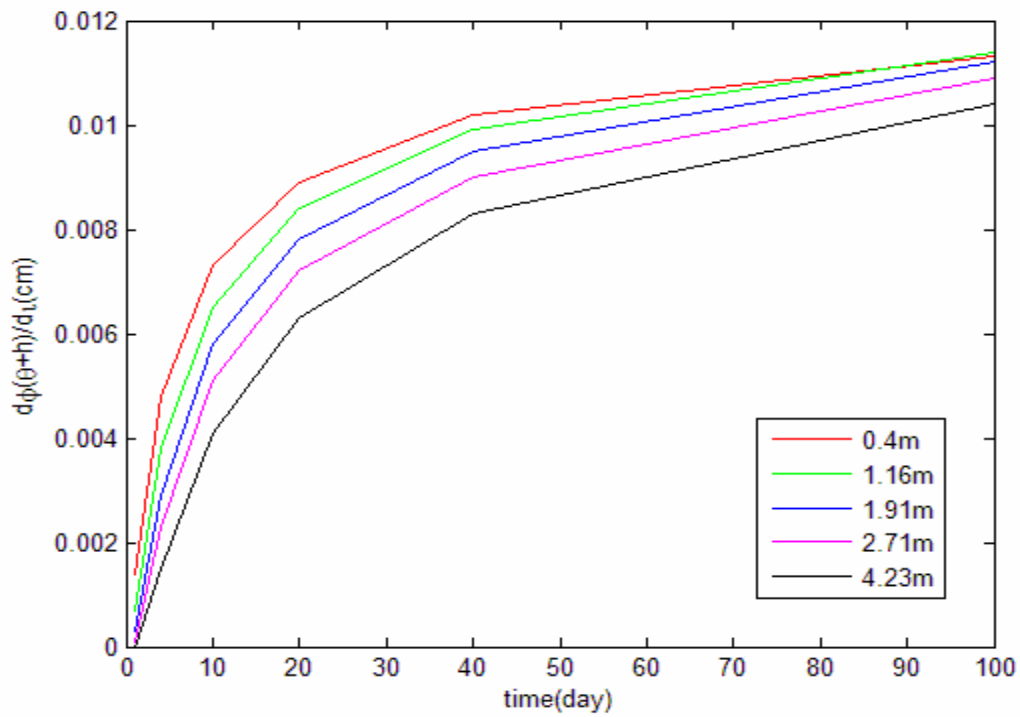
Figure B7. Time-depth distribution of the sensitivity of the objective function with respect to ι for multi-objective (a) and single-objective optimization (b).

Appendix C

Residuals of the State Variables
(Laser beam Recovery, Soil Moisture Content, and Soil water Pressure Head)

Residuals of the FRAP Recovery for Reaction-Diffusion Model

```
0.0347   0.0325   0.0140   0.0440  -0.0066  -0.0057  -0.0021
0.0103   0.0234   0.0158  -0.0157   0.0127  -0.0057  -0.0112
0.0193  -0.0149  -0.0293   0.0173   0.0068  -0.0133   0.0174
-0.0292 -0.0761  -0.0281  -0.0014   0.0047   0.0035   0.0022
-0.0160  0.0523   0.0334  -0.0047   0.0070  -0.0050  -0.0009
-0.0128 -0.0304   0.0030  -0.0052   0.0093  -0.0039   0.0078 -0.0021
```

Residuals of the FRAP Recovery for One-Site-Mobile-Immobile Model

Run 1:

```
-0.0516 -0.0276  -0.0106  -0.0366   0.0053   0.0006  -0.0021
-0.0285 -0.0278  -0.0116   0.0238  -0.0152   0.0005   0.0073
-0.0344  0.0121   0.0345  -0.0093  -0.0102   0.0081  -0.0208
0.0249   0.0753   0.0341   0.0062  -0.0087  -0.0086  -0.0052
0.0065  -0.0513  -0.0270   0.0068  -0.0117   0.0002  -0.0016
0.0076   0.0324   0.0041   0.0055  -0.0143  -0.0007  -0.0098 0.006
```

Run 2:

```
-0.0525 -0.0300  -0.0112  -0.0357   0.0081   0.0015  -0.0019
-0.0304 -0.0299  -0.0119   0.0249  -0.0128   0.0013   0.0074
-0.0368  0.0103   0.0345  -0.0060  -0.0082   0.0087  -0.0208
0.0223   0.0738   0.0344   0.0098  -0.0070  -0.0081  -0.0051
0.0039  -0.0525  -0.0265   0.0102  -0.0103   0.0005  -0.0016
0.0050   0.0315   0.0048   0.0087  -0.0132  -0.0004  -0.0099  0.0005
```

Run 3:

```
-0.0495 -0.0226  -0.0104  -0.0406  -0.0027  -0.0019  -0.0025
-0.0242 -0.0234  -0.0122   0.0192  -0.0220  -0.0015   0.0071
-0.0291  0.0156   0.0331  -0.0197  -0.0159   0.0066  -0.0210
0.0306   0.0780   0.0320  -0.0051  -0.0134  -0.0098  -0.0052
0.0123  -0.0495  -0.0297  -0.0038  -0.0155  -0.0007  -0.0015
0.0131   0.0334   0.0007  -0.0038  -0.0174  -0.0013  -0.0097  0.0008
```

Run 4:

```
-0.0288 -0.0228  -0.0118  -0.0425  -0.0036  -0.0024  -0.0029
-0.0186 -0.0239  -0.0138   0.0173  -0.0228  -0.0019   0.0067
-0.0263  0.0149   0.0315  -0.0215  -0.0166   0.0061  -0.0213
0.0320   0.0771   0.0303  -0.0065  -0.0141  -0.0102  -0.0055
```

```
 0.0130  -0.0506  -0.0315  -0.0050  -0.0161  -0.0011  -0.0018
 0.0132   0.0321  -0.0011  -0.0048  -0.0180  -0.0017  -0.0099   0.0005
```

Run 5:

```
-0.0473  -0.0223  -0.0102  -0.0406  -0.0027  -0.0019  -0.0026
-0.0234  -0.0231  -0.0121   0.0192  -0.0220  -0.0015   0.0070
-0.0286   0.0159   0.0332  -0.0197  -0.0159   0.0066  -0.0210
 0.0310   0.0783   0.0321  -0.0051  -0.0134  -0.0098  -0.0052
 0.0127  -0.0493  -0.0296  -0.0038  -0.0155  -0.0007  -0.0016
 0.0134   0.0336   0.0008  -0.0038  -0.0175  -0.0014  -0.0097   0.0008
```
Run 6:

```
-0.0094  -0.0217  -0.0138  -0.0456  -0.0054  -0.0035  -0.0036
 0.0008  -0.0236  -0.0160   0.0140  -0.0244  -0.0029   0.0060
-0.0158   0.0146   0.0290  -0.0249  -0.0181   0.0052  -0.0219
 0.0381   0.0763   0.0276  -0.0095  -0.0154  -0.0110  -0.0061
 0.0166  -0.0519  -0.0344  -0.0075  -0.0173  -0.0019  -0.0024
 0.0154   0.0305  -0.0041  -0.0070  -0.0191  -0.0025  -0.0105   0.0000
```

Run 7:

```
-0.0495  -0.0221  -0.0099  -0.0402  -0.0026  -0.0019  -0.0025
-0.0240  -0.0229  -0.0118   0.0196  -0.0219  -0.0014   0.0071
-0.0288   0.0161   0.0336  -0.0194  -0.0158   0.0066  -0.0209
 0.0310   0.0785   0.0325  -0.0048  -0.0133  -0.0097  -0.0051
 0.0127  -0.0490  -0.0293  -0.0036  -0.0155  -0.0007  -0.0015
 0.0135   0.0339   0.0011  -0.0037  -0.0174  -0.0013  -0.0096   0.0008
```

Run 8:

```
-0.0573  -0.1759  -0.1471  -0.1552  -0.0294  -0.0158  -0.0119
-0.0985  -0.1761  -0.1450  -0.0921  -0.0451  -0.0143  -0.0018
-0.1423  -0.1350  -0.0958  -0.0888  -0.0363  -0.0054  -0.0294
-0.1042  -0.0697  -0.0932  -0.0547  -0.0317  -0.0209  -0.0132
-0.1338  -0.1938  -0.1512  -0.0424  -0.0320  -0.0112  -0.0092
-0.1384  -0.1071  -0.1173  -0.0354  -0.0325  -0.0112  -0.0170   0.0063
```

Run 9:

```
-0.0136   0.0896   0.1088   0.0700   0.0305   0.0158   0.0095
 0.0386   0.0923   0.1060   0.1281   0.0070   0.0150   0.0185
 0.0498   0.1337   0.1502   0.0577   0.0098   0.0219  -0.0101
 0.1218   0.1974   0.1477   0.0533   0.0097   0.0046   0.0052
 0.1125   0.0704   0.0843   0.0429   0.0054   0.0128   0.0084
 0.1202   0.1532   0.1131   0.0350   0.0017   0.0114  -0.0001   0.0099
```

Run 10:

```
-0.0457  -0.0087   0.0027  -0.0296  -0.0006  -0.0008  -0.0018
-0.0156  -0.0094   0.0005   0.0298  -0.0202  -0.0005   0.0077
-0.0183   0.0297   0.0456  -0.0136  -0.0143   0.0075  -0.0203
 0.0428   0.0919   0.0441  -0.0009  -0.0120  -0.0089  -0.0046
 0.0254  -0.0358  -0.0180  -0.0006  -0.0142   0.0001  -0.0010
 0.0267   0.0469   0.0121  -0.0013  -0.0163  -0.0006  -0.0091   0.0013
```

Run 11:

```
-0.0457  -0.0087   0.0027  -0.0296  -0.0006  -0.0008  -0.0018
-0.0156  -0.0094   0.0005   0.0298  -0.0202  -0.0005   0.0077
-0.0183   0.0297   0.0456  -0.0136  -0.0143   0.0075  -0.0203
 0.0428   0.0919   0.0441  -0.0009  -0.0120  -0.0089  -0.0046
 0.0254  -0.0358  -0.0180  -0.0006  -0.0142   0.0001  -0.0010
 0.0267   0.0469   0.0121  -0.0013  -0.0163  -0.0006  -0.0091   0.0013
```

Run 12:

```
-0.0189  -0.0220  -0.0119  -0.0430  -0.0041  -0.0027  -0.0031
-0.0126  -0.0233  -0.0140   0.0167  -0.0232  -0.0022   0.0065
-0.0231   0.0153   0.0312  -0.0223  -0.0170   0.0059  -0.0214
 0.0342   0.0773   0.0300  -0.0072  -0.0144  -0.0104  -0.0056
 0.0145  -0.0505  -0.0319  -0.0056  -0.0164  -0.0013  -0.0020
 0.0143   0.0321  -0.0016  -0.0054  -0.0183  -0.0019  -0.0101   0.0004
```

Run 13:

```
-0.0485  -0.0221  -0.0100  -0.0404  -0.0027  -0.0019  -0.0025
-0.0231  -0.0229  -0.0119   0.0194  -0.0220  -0.0014   0.0071
-0.0284   0.0161   0.0335  -0.0195  -0.0159   0.0066  -0.0209
 0.0312   0.0785   0.0324  -0.0050  -0.0134  -0.0098  -0.0052
 0.0129  -0.0490  -0.0294  -0.0037  -0.0155  -0.0007  -0.0015
 0.0136   0.0338   0.0010  -0.0037  -0.0174  -0.0013  -0.0096   0.0008
```

Run 14:

```
-0.0485  -0.0221  -0.0100  -0.0404  -0.0027  -0.0019  -0.0025
-0.0231  -0.0229  -0.0119   0.0194  -0.0220  -0.0014   0.0071
-0.0284   0.0161   0.0335  -0.0195  -0.0159   0.0066  -0.0209
 0.0312   0.0785   0.0324  -0.0050  -0.0134  -0.0098  -0.0052
 0.0129  -0.0490  -0.0294  -0.0037  -0.0155  -0.0007  -0.0015
 0.0136   0.0338   0.0010  -0.0037  -0.0174  -0.0013  -0.0096   0.0008
```

Run 15:

```
-0.0106  -0.0205  -0.0116  -0.0433  -0.0045  -0.0030  -0.0033
-0.0044  -0.0221  -0.0138   0.0164  -0.0236  -0.0024   0.0064
-0.0183   0.0163   0.0313  -0.0230  -0.0174   0.0057  -0.0216
 0.0373   0.0782   0.0300  -0.0079  -0.0148  -0.0106  -0.0058
 0.0169  -0.0498  -0.0320  -0.0062  -0.0167  -0.0015  -0.0021
 0.0162   0.0326  -0.0018  -0.0059  -0.0186  -0.0021  -0.0102   0.0002
```


Run 16:

```
-0.0497  -0.0227  -0.0104  -0.0407  -0.0027  -0.0019  -0.0025
-0.0243  -0.0235  -0.0123   0.0191  -0.0220  -0.0015   0.0071
-0.0292   0.0156   0.0331  -0.0197  -0.0159   0.0066  -0.0210
 0.0305   0.0780   0.0320  -0.0051  -0.0134  -0.0098  -0.0052
 0.0122  -0.0495  -0.0298  -0.0038  -0.0155  -0.0007  -0.0015
 0.0130   0.0334   0.0007  -0.0038  -0.0174  -0.0014  -0.0097   0.0008
```


Run 17:

```
-0.0432  -0.0223  -0.0105  -0.0409  -0.0029  -0.0020  -0.0026
-0.0223  -0.0232  -0.0124   0.0189  -0.0222  -0.0016   0.0070
-0.0280   0.0158   0.0330  -0.0200  -0.0161   0.0065  -0.0210
 0.0314   0.0781   0.0319  -0.0054  -0.0136  -0.0099  -0.0052
 0.0128  -0.0494  -0.0299  -0.0040  -0.0157  -0.0008  -0.0016
 0.0135   0.0334   0.0005  -0.0040  -0.0176  -0.0014  -0.0097   0.0007
```


Run 18:

```
-0.0426  -0.0232  -0.0114  -0.0417  -0.0031  -0.0022  -0.0027
-0.0225  -0.0241  -0.0133   0.0181  -0.0224  -0.0017   0.0069
-0.0285   0.0149   0.0321  -0.0206  -0.0163   0.0064  -0.0211
 0.0307   0.0772   0.0310  -0.0058  -0.0137  -0.0100  -0.0053
 0.0121  -0.0504  -0.0308  -0.0044  -0.0158  -0.0009  -0.0017
 0.0126   0.0325  -0.0004  -0.0043  -0.0177  -0.0015  -0.0098   0.0007
```


Run 19:

```
-0.0495  -0.0242  -0.0112  -0.0433  -0.0083  -0.0051  -0.0048
-0.0245  -0.0247  -0.0132   0.0161  -0.0270  -0.0044   0.0050
-0.0302   0.0147   0.0319  -0.0277  -0.0204   0.0038  -0.0230
 0.0290   0.0773   0.0305  -0.0133  -0.0175  -0.0124  -0.0071
 0.0104  -0.0502  -0.0316  -0.0111  -0.0193  -0.0032  -0.0034
 0.0113   0.0327  -0.0015  -0.0102  -0.0209  -0.0037  -0.0114  -0.0009
```

```
-0.0223  -0.0380  -0.0273  -0.0564  -0.0074  -0.0044  -0.0043
-0.0217  -0.0395  -0.0290   0.0037  -0.0261  -0.0038   0.0054
-0.0349  -0.0009   0.0165  -0.0307  -0.0196   0.0044  -0.0225
 0.0206   0.0612   0.0156  -0.0134  -0.0167  -0.0118  -0.0067
-0.0003  -0.0664  -0.0460  -0.0104  -0.0185  -0.0026  -0.0030
-0.0012   0.0165  -0.0153  -0.0093  -0.0202  -0.0032  -0.0110  -0.0005
```

Residuals of the Soil Moisture Content Data in Case of Water Flow Through Homogeneous Soil

```
-0.0016  -0.0073  -0.0072  -0.0145  -0.0116  -0.0096
 0.0058   0.0059   0.0110  -0.0017  -0.0398  -0.0356
 0.0048   0.0061   0.0124   0.0024   0.0084  -0.0239
 0.0034   0.0049   0.0115   0.0028   0.0029  -0.0088
 0.0020   0.0034   0.0099   0.0022  -0.0029  -0.0090
 0.0010   0.0020   0.0083   0.0016  -0.0095  -0.0132
```

Residuals of the Soil Water Pressure Head Data in Case of Water Flow Through Homogeneous Soil

```
 0.0710  -0.0319  -0.0158   0.1136   0.0892   0.0735
-0.0734  -0.1738  -0.1472  -0.0343   0.3473   0.3050
-0.0663  -0.1505  -0.1170  -0.0969   0.0100  -0.0130
-0.0875  -0.1540  -0.1059  -0.1621  -0.0546  -0.0035
-0.0101  -0.0663  -0.0077  -0.1431  -0.0565   0.0776
 0.0827   0.0528   0.1019  -0.1171   0.0783   0.3974
```

Residuals of the Soil Moisture Content Data in Case of Water Flow Through Heterogeneous Soil

```
 0.0063   0.0064    0.0065    0.0059    0.0065
 0.0144   0.0056    0.0026    0.0036    0.0037
 0.0148   0.0024   -0.0022    0.0014    0.0025
 0.0067  -0.0028   -0.0044   -0.0010    0.0013
 0.0067  -0.0026   -0.0055   -0.0015    0.0020
 0.0030  -0.0024   -0.0025   -0.0018    0.0008
 0.0013  -0.0035   -0.0039   -0.0010    0.0002
-0.0026  -0.0050   -0.0041   -0.0004   -0.0027
-0.0037  -0.0025    0.0026    0.0026   -0.0016
-0.0070  -0.0024    0.0054    0.0029   -0.0029
-0.0010   0.0005    0.0089    0.0054   -0.0032
-0.0001  -0.0021    0.0049    0.0037   -0.0053
 0.0003  -0.0034    0.0014   -0.0003   -0.0080
```

Appendix D

*Kolmogorov-Smirnov One Sample Test on the Normality of the
Residuals*

Table D1. *Kolmogorov-Smirnov One Sample Test on the Normality of the Residuals in Case of Water Flow through Homogeneous Soil – Soil Moisture Data (data from Abeele, 1984).*

CELL	X	Sample probability	Expected probability	Absolute difference
1	-43823.00000	0.02778	0.00100	0.02678
2	-39544.00000	0.05556	0.00267	0.05289
3	-26596.00000	0.08333	0.03304	0.05029
4	-17137.00000	0.11111	0.12558	0.01447
5	-13749.00000	0.13889	0.18402	0.04513
6	-11463.00000	0.16667	0.23163	0.06496
7	-10994.00000	0.19444	0.24224	0.04780
8	-9357.00000	0.22222	0.28109	0.05886
9	-7628.00000	0.25000	0.32512	0.07512
10	-6949.00000	0.27778	0.34313	0.06535
11	-6208.00000	0.30556	0.36324	0.05768
12	-5701.00000	0.33333	0.37720	0.04387
13	-3453.00000	0.36111	0.44086	0.07975
14	-1036.00000	0.38889	0.51104	0.12215
15	-422.00000	0.41667	0.52886	0.11219
16	374.00000	0.44444	0.55190	0.10746
17	2478.00000	0.47222	0.61185	**<u>0.13962</u>**
18	2722.00000	0.50000	0.61861	0.11861
19	2915.00000	0.52778	0.62397	0.09619
20	3164.00000	0.55556	0.63087	0.07532
21	5223.00000	0.58333	0.68595	0.10261
22	5318.00000	0.61111	0.68839	0.07728
23	5476.00000	0.63889	0.69251	0.05362
24	5966.00000	0.66667	0.70493	0.03826
25	6676.00000	0.69444	0.72255	0.02811
26	6946.00000	0.72222	0.72916	0.00694
27	7247.00000	0.75000	0.73639	0.01361
28	8138.00000	0.77778	0.75712	0.02065
29	8187.00000	0.80556	0.75823	0.04732
30	8237.00000	0.83333	0.75936	0.07397
31	10317.0000	0.86111	0.80404	0.05707
32	10546.00000	0.88889	0.80862	0.08027
33	11027.00000	0.91667	0.81807	0.09860
34	12634.00000	0.94444	0.84738	0.09707
35	13852.00000	0.97222	0.86739	0.10483
36	15704.00000	1.00000	0.89429	0.10571

Sample test statistic =   0.140

α	Critical	Decision
0.20	0.178	*Accept Ho*
0.15	0.190	*Accept Ho*
0.10	0.203	*Accept Ho*
0.05	0.227	*Accept Ho*
0.01	0.272	*Accept Ho*

Table D2. *Kolmogorov-Smirnov One Sample Test on the Normality of the Residuals in Case of Water Flow through Homogeneous Soil – Soil Water Pressure Head Data (data from Abeele, 1984).*

CELL	X	Sample probability	Expected probability	Absolute difference
1		0.02778	0.12093	0.09316
2		0.05556	0.12664	0.07108
3		0.08333	0.12697	0.04363
4		0.11111	0.13097	0.01986
5		0.13889	0.13781	0.00108
6		0.16667	0.16455	0.00212
7		0.19444	0.16929	0.02515
8	-75266.0000	0.22222	0.22878	0.00656
9	-74887.0000	0.25000	0.22966	0.02034
10	-56341.0000	0.27778	0.27499	0.00278
11	-49348.0000	0.30556	0.29311	0.01244
12	-39911.0000	0.33333	0.31842	0.01491
13	-39237.0000	0.36111	0.32028	0.04083
14	-23379.0000	0.38889	0.36481	0.02408
15	-10011.0000	0.41667	0.40389	0.01278
16	-7186.00000	0.44444	0.41222	0.03222
17	-2603.00000	0.47222	0.42600	0.04622
18	6298.00000	0.50000	0.45278	0.04722
19	6911.00000	0.52778	0.45466	0.07312
20	7170.00000	0.55556	0.45545	0.10011
21	9338.00000	0.58333	0.46204	0.12130
22	23234.00000	0.61111	0.50442	0.10669
23	25095.00000	0.63889	0.51012	0.12877
24	27320.00000	0.66667	0.51690	**<u>0.14976</u>**
25	43784.00000	0.69444	0.56684	0.12760
26	49562.00000	0.72222	0.58418	0.13804
27	69726.00000	0.75000	0.64313	0.10687
28	85632.00000	0.77778	0.68739	0.09039
29	90578.00000	0.80556	0.70068	0.10488
30	94553.00000	0.83333	0.71119	0.12215
31	103813.0000	0.86111	0.73493	0.12618
32	114227.0000	0.88889	0.76028	0.12860
33	131490.0000	0.91667	0.79935	0.11731
34	339524.0000	0.94444	0.99253	0.04808
35	384937.0000	0.97222	0.99729	0.02507
36	389861.0000	1.00000	0.99757	0.00243

Sample test statistic   =   0.150

α	Critical	Decision
-------	--------	--------
0.20	0.178	*Accept Ho*
0.15	0.190	*Accept Ho*
0.10	0.203	*Accept Ho*
0.05	0.227	*Accept Ho*
0.01	0.272	*Accept Ho*

.

Table D3. *Kolmogorov-Smirnov One Sample Test on the Normality of the Residuals in Case of Water Flow through Heterogeneous Soil – Soil Moisture Data (data from Table 4.2).*

CELL	X	Sample probability	Expected probability	Absolute Difference
1	-80.00000	0.01538	0.02821	0.01283
2	-70.00000	0.03077	0.04546	0.01469
3	-55.00000	0.04615	0.08628	0.04012
4	-53.00000	0.06154	0.09335	0.03181
5	-50.00000	0.07692	0.10469	0.02777
6	-44.00000	0.09231	0.13043	0.03812
7	-41.00000	0.10769	0.14481	0.03712
8	-39.00000	0.12308	0.15492	0.03185
9	-37.00000	0.13846	0.16550	0.02704
10	-35.00000	0.15385	0.17660	0.02275
11	-34.00000	0.16923	0.18229	0.01306
12	-32.00000	0.18462	0.19405	0.00944
13	-29.00000	0.20000	0.21253	0.01253
14	-28.00000	0.21538	0.21884	0.00346
15	-27.00000	0.23077	0.22531	0.00546
16	-26.00000	0.24615	0.23192	0.01423
17	-26.00000	0.26154	0.23192	0.02962
18	-25.00000	0.27692	0.23867	0.03825
19	-25.00000	0.29231	0.23867	0.05364
20	-24.00000	0.30769	0.24543	0.06226
21	-24.00000	0.32308	0.24543	0.07765
22	-22.00000	0.33846	0.25931	0.07915
23	-21.00000	0.35385	0.26639	0.08745
24	-18.00000	0.36923	0.28828	0.08095
25	-16.00000	0.38462	0.30332	0.08130
26	-15.00000	0.40000	0.31101	0.08899
27	-10.00000	0.41538	0.35045	0.06493
28	-10.00000	0.43077	0.35045	0.08032
29	-10.00000	0.44615	0.35045	**0.09570**
30	-4.00000	0.46154	0.39992	0.06162
31	-3.00000	0.47692	0.40832	0.06860
32	-1.00000	0.49231	0.42539	0.06692
33	2.00000	0.50769	0.45106	0.05663
34	3.00000	0.52308	0.45974	0.06334
35	5.00000	0.53846	0.47706	0.06141
36	8.00000	0.55385	0.50308	0.05076
37	12.00000	0.56923	0.53777	0.03146
38	13.00000	0.58462	0.54642	0.03819

CELL	X	Sample probability	Expected probability	Absolute Difference
39	14.00000	0.60000	0.55503	0.04497
40	14.00000	0.61538	0.55503	0.06035
41	20.00000	0.63077	01.60600	0.02476
42	24.00000	0.64615	0.63910	0.00706
43	25.00000	0.66154	0.64719	0.01435
44	26.00000	0.67692	0.65525	0.02168
45	26.00000	0.69231	0.65525	0.03706
46	26.00000	0.70769	0.65525	0.05245
47	29.00000	0.72308	0.67896	0.04411
48	30.00000	0.73846	0.68673	0.05173
49	36.00000	0.75385	0.73151	0.02234
50	37.00000	0.76923	0.73860	0.03063
51	37.00000	0.78462	0.73860	0.04601
52	49.00000	0.80000	0.81599	0.01599
53	54.00000	0.81538	0.84360	0.02821
54	54.00000	0.83077	0.84360	0.01283
55	56.00000	0.84615	0.85373	0.00757
56	59.00000	0.86154	0.86819	0.00665
57	63.00000	0.87692	0.88592	0.00900
58	64.00000	0.89231	0.89011	0.00220
59	65.00000	0.90769	0.89415	0.01355
60	65.00000	0.92308	0.89415	0.02893
61	67.00000	0.93846	0.90188	0.03659
62	67.00000	0.95385	0.90188	0.05197
63	89.00000	0.96923	0.96171	0.00753
64	144.00000	0.98462	0.99850	0.01388
65	148.00000	1.0000	0.99890	0.00110

Sample test statistic =   0.096

α	Critical	Decision
0.20	0.133	*Accept Ho*
0.15	0.141	*Accept Ho*
0.10	0.151	*Accept Ho*
0.05	0.169	*Accept Ho*
0.01	0.202	*Accept Ho*

Appendix E

Computer Programs

Files **Page**

```matlab
% FINAL_FRAP_CODE   identifies biomolecule transport parameters

% This code optimizes biomolecular transport and binding rate parameters.
% The code uses 1) the Osborne-More adapted version of the Levenberg-
% Marquardt optimization algorithm, 2)an adaptive strategy to build the
% Jacobian matrix, and 3) a mixed termination criterion.
% The code calls the m-file frap_inverse_func which solves the forward
% problem (a system of three coupled nonlinear partial differential
% equations).
%
% Inputs consist of: an experimental data set obtained by FRAP technique
% and initial guesses for parameters to be optimized.
%
% Copyright 2006 Kouroush Sadegh Zadeh
% Bioengineering Department, University of Maryland at College Park, MD


%================================================================
%                        Insert Experimental data (data from McNally, personal
%                        communication)
%================================================================
tout = [0.009 0.049 0.088 0.128 0.167 0.206 0.246 0.285 0.325 0.364 0.403 ...
    0.443 0.482 0.522 0.561 0.60 0.64 0.679 0.719 0.758 1.546 2.335 3.123 ...
    3.911 4.699 5.487 6.275 7.064 7.852 8.64 9.428 10.216 11.005 11.793 ...
    12.581 13.369 14.157 14.946 15.734 16.522 17.31 18.098 18.887];
y = [0.0574 0.2231 0.2988 0.4216 0.4536 0.4970 0.4989 0.53 0.5978 0.6850...
    0.5796 0.6828 0.6568 0.6715 0.7315 0.7438 0.6946 0.7363 0.7056 0.775...
    0.8423 0.8989 0.9226 0.9365 0.9471 0.9347 0.946 0.9526 0.9538 0.9546...
    0.9724 0.9748 0.9845 0.9696 0.9799 0.9804 0.9802 0.9907 0.9635 0.98...
    0.9843 0.9768 0.9878];
%================================================================
%                        Set the initial guess for parameters
%================================================================
parms_vec = [56 10 1.24 0.001 0.001];
w = 1.1;                              % Micro-meter/sec
Df = parms_vec(1);                    % Micro-meter^2/sec
kon = parms_vec(2);                   % 1/sec
koff = parms_vec(3);                  % 1/sec
Ds = parms_vec(4);                    % Micro-meter/sec
Dc = parms_vec(5);                    % Micro-meter/sec
Ceq = kon/(kon + koff);
Feq = koff/(kon + koff);
N = length(y);
tmax = tout(end);
maxerror = 1e-3;
deltaobjfunc = 2*maxerror;
obj_func = 1000;
grad = 100*[1 1 1 1 1];
lambda = 1;
p = 5;%length(parms_vec);
D = zeros(p);
parms_vec_new = parms_vec';
%================================================================
                        Start Optimization
%================================================================
while (abs(grad)>maxerror*[1 1 1 1 1]) & (deltaobjfunc>1e-4)
    parms_vec = parms_vec_new;
```

```
frap = frap_inverse_func(tout,Df,kon,koff,Ds,Dc,Feq,Ceq,w);
r = y - frap;
dDf = 0.01*Df;
dkon = 0.01*kon;
dkoff = 0.01*koff;
dDc = 0.01*Dc;
dDs = 0.01*Ds;
v1 = -(frap_inverse_func(tout,Df+dDf,kon,koff,Ds,Dc,Feq,Ceq,w) - frap)/dDf;
v2 = -(frap_inverse_func(tout,Df,kon+dkon,koff,Ds,Dc,Feq,Ceq,w) - frap)/dkon;
v3 = -(frap_inverse_func(tout,Df,kon,koff+dkoff,Ds,Dc,Feq,Ceq,w) - frap)/dkoff;
v4 = -(frap_inverse_func(tout,Df,kon,koff,Ds,Dc+dDc,Feq,Ceq,w) - frap)/dDc;
v5 = -(frap_inverse_func(tout,Df,kon,koff,Ds+dDs,Dc,Feq,Ceq,w) - frap)/dDs;
j = [v1' v2' v3' v4' v5'];
grad = r*j;
for i=1:p;
    D(i,i) = max(norm(j(:,i)),D(i,i));
end
oldobj_func = obj_func;
obj_func =  r*r';
deltaobjfunc = abs(obj_func - oldobj_func);
if obj_func > oldobj_func
    parms_vec = parms_vec;
    lambda = 1.5*lambda;
else
    lambda = 0.25*lambda;
end
B = [j ; sqrt(lambda)*D];
q = [-r' ; zeros(5,1)];
deltap = B\q;
parms_vec_new = parms_vec + deltap;
[parms_vec_new' r*r' lambda]
grad
minparms = [0.01 1e-4 1e-5 1e-5 1e-5];
maxparms = [20 3e3 1e2 1e1 1e1];
parms_vec_new = max(min(real(parms_vec_new),maxparms'),minparms');
Df = parms_vec_new(1);
kon = parms_vec_new(2);
koff = parms_vec_new(3);
Dc = parms_vec_new(4);
Ds = parms_vec_new(5);
end
while (abs(grad) > (0.1*maxerror*[1 1 1 1 1])) & (deltaobjfunc > 1e-6)
    parms_vec = parms_vec_new;
    frap = frap_inverse_func(tout,Df,kon,koff,Ds,Dc,Feq,Ceq,w);;
    r = y - frap;
    dDf = 0.01*Df;
    dkon = 0.01*kon;
    dkoff = 0.01*koff;
    dDc = 0.01*Dc;
    dDs = 0.01*Ds;
    v1=-(frap_inverse_func(tout,Df+dDf,kon,koff,Ds,Dc,Feq,Ceq,w)-frap_inverse_func(tout,Df-
dDf,kon,koff,Ds,Dc,Feq,Ceq,w))/(2*dDf);
    v2= -(frap_inverse_func(tout,Df,kon+dkon,koff,Ds,Dc,Feq,Ceq,w) - frap_inverse_func(tout,Df,kon-
dkon,koff,Ds,Dc,Feq,Ceq,w))/(2*dkon);
    v3=-(frap_inverse_func(tout,Df,kon,koff+dkoff,Ds,Dc,Feq,Ceq,w)-
frap_inverse_func(tout,Df,kon,koff-dkoff,Ds,Dc,Feq,Ceq,w))/(2*dkoff);
```

286

```
    v4=-(frap_inverse_func(tout,Df,kon,koff,Ds,Dc+dDc,Feq,Ceq,w)-
frap_inverse_func(tout,Df,kon,koff,Ds,Dc-dDc,Feq,Ceq,w))/(2*dDc);
    v5=-(frap_inverse_func(tout,Df,kon,koff,Ds+dDs,Dc,Feq,Ceq,w)-
frap_inverse_func(tout,Df,kon,koff,Ds-dDs,Dc,Feq,Ceq,w) )/(2*dDs);
   j = [v1' v2' v3' v4' v5'];
   grad = r*j;
   for i=1:p;
      D(i,i) = max(norm(j(:,i)),D(i,i));
   end
   oldobj_func = obj_func;
   obj_func =  r*r';
   deltaobjfunc = abs(obj_func - oldobj_func);
   if obj_func > oldobj_func
      parms_vec = parms_vec;
      lambda = 1.5*lambda;
   else
      lambda = 0.5*lambda;
   end
   B = [j ; sqrt(lambda)*D];
   q = [-r' ; zeros(5,1)];
   deltap = B\q;
   parms_vec_new = parms_vec + deltap;
   [parms_vec_new' r*r' lambda]
   grad
   minparms = [0.01 1e-3 1e-5 1e-5 1e-5];
   maxparms = [20 3e2 1e2 1e1 1e1];
   parms_vec_new = max(min(real(parms_vec_new),maxparms'),minparms');
   Df = parms_vec_new(1);
   kon = parms_vec_new(2);
   koff = parms_vec_new(3);
   Dc = parms_vec_new(4);
   Ds = parms_vec_new(5);
end
Df = parms_vec_new(1);
kon = parms_vec_new(2);
koff = parms_vec_new(3);
Dc = parms_vec_new(4);
Ds = parms_vec_new(5);
phi = r'*r/norm(j'*j);
H = j'*j + lambda*(D'*D)
j'*j
display(['gradient:'])
grad
norm(grad)
display(['Eigenvalues of Hessian:'])
eig(H)
display(['Eigenvalues of JJ:'])
eig(j'*j)
Se = r*r'/(N-p);
% Parameter Covariance Matrix(C).
COV_P = Se*inv(j'*j);
% Parameter Correlation Matrix:
for i = 1:p;
   for k = 1:p;
      COR_P(i,k) = COV_P(i,k)/((sqrt(COV_P(i,i)))*sqrt(COV_P(k,k)));
   end
```

```
end
%95 confidence region around the optimized parameters
prob95 = 0.05;
df = N - 1;
for ii = 1:p
    conf_95(ii,ii) = (tinv(1-prob95/2,df))*sqrt(COV_P(ii,ii));
end


%=================================================================
%                           Summary of statistics
%=================================================================
RMSE = sqrt(r*r'/(N-p))
R_Square = 1-var(r)/var(y)
mean_resdual = mean(r)
std_res = std(r)
full(COV_P)
full(COR_P)
display(['%95 confidence intervals on optimized parameters: Df, kon, koff'])
[Df-conf_95(1,1) Df+conf_95(1,1)]
[kon-conf_95(2,2) kon+conf_95(2,2)]
[koff-conf_95(3,3) koff+conf_95(3,3)]
[Dc-conf_95(4,4) Dc+conf_95(4,4)]
[Ds-conf_95(5,5) Ds+conf_95(5,5)]


%=================================================================
%                           Plot the results
%=================================================================
figure(1)
plot(tout,y,'.')
hold on
plot(tout,frap,'r')
xlabel('time, (seconds)')
ylabel('Normalized Laser Beam Recovery, (-)')
legend('Exp','model')
axis([-0.5 20 0 1.05])

figure(2)
plot(frap,r,'+')
ylabel('residuals, (-)')
xlabel('FRAP Recovery, (-)')
axis([0 1 -0.1 0.1])

figure(3)
hist(r)
xlabel('residuals, (-)')
ylabel('Frequency, (-)')
axis([-0.1 0.1 0 20])

figure(4)
res = normplot(r);
xlabel('residuals, (-)')
```

```
% frap_inverse_func solves theforward problem in FRAP
%
% This function solves the system of three coupled nonlinear partial
% differential equations governing macro-molecule transport and reaction
% inside living cells. The solver uses the fully implicit finite difference
% scheme to form the matrix equations and the Picard iteration method to
% solve the system of nonlinear algebraic equations.
%
% Inputs are observation time series on FRAP (tout), diffusion coefficients
% of free macro-molecule (Df ), bound complex (Dc ), vacant binding sites ( Ds),
% bleach spot radius (w ), and rate parameters (kon and koff ) .
% The user should insert the bleach spot radius, time series, and initial
% guesses for model parameters.
%
% Outputs are a matrix whose rows are the concentrations of free macro-
% molecule, vacant binding sites, and bound biomolecules inside cell.
% The columns are the observation times (tout).

% Copyright 2006 Kouroush Sadegh Zadeh
% Bioengineering Department, University of Maryland at College Park, MD


function r = frap_inverse_func(tout,Df,kon,koff,Ds,Dc,Feq,Ceq,w)

tmax = tout(end);
dt = 1e-3;                                  % seconds
R = 11;
nr = 111;
dr = R/(nr+1);
r = linspace(0,R,nr);
r(1) = 1e-6;
error_tol = 1e-7;
% I.C.
bleach_spot = find(r<=w);
F0 = Feq*ones(nr,1);
F0(bleach_spot) = 0;
S0 = ones(nr,1);
C0 = Ceq*ones(nr,1);
C0(bleach_spot) = 0;
sol_vec = [F0 S0 C0];
sol_vec = sol_vec';
sol_vec = sol_vec(:);
F = [];
S = [];
C = [];
the_times = 0;
thetout = [];
tout = [tout 100*tmax];
kout = 1;
while the_times < tmax
   old_sol_vec = sol_vec;
   max_error = 1e4;
   picard_iter_counter = 0;
   while max_error > error_tol
      s_star = sol_vec(2:3:end);
      a1 = -Df*dt/dr^2 + Df*dt./(2*r*dr);
```

```matlab
        a2 = -Ds*dt/dr^2 + Ds*dt./(2*r*dr);
        a3 = -Dc*dt/dr^2 + Dc*dt./(2*r*dr);
        b1 = 1 + 2*Df*dt/dr^2 + kon*dt*s_star;
        b2 = (ones(nr,1) + 2*Ds*dt/dr^2);
        b3 = (ones(nr,1) + 2*Dc*dt/dr^2 + koff*dt);
        g1 = -Df*dt/dr^2 - Df*dt./(2*r*dr);
        g2 = -Ds*dt/dr^2 - Ds*dt./(2*r*dr);
        g3 = -Dc*dt/dr^2 - Dc*dt./(2*r*dr);
        aa = [a1; a2; a3];
        aa =aa(:);
        bb = [b1 b2 b3]';
        bb = bb(:);
        gg = [g1; g2; g3];
        gg = gg(:);
        mat1 = [zeros(nr,1) zeros(nr,1) -kon*dt*s_star];
        mat1 = mat1';
        mat1 = mat1(:);
        mat2 = [zeros(nr,1) kon*dt*s_star zeros(nr,1)];
        mat2 = mat2';
        mat2 = mat2(:);
        mat3 = [zeros(nr,1) -koff*dt*ones(nr,1) zeros(nr,1)];
        mat3 = mat3';
        mat3 = mat3(:);
        mat4 = [-koff*dt*ones(nr,1) zeros(nr,1) zeros(nr,1)];
        mat4 = mat4';
        mat4 = mat4(:);
        LHS = spdiags([gg mat4 mat3 bb mat2 mat1 aa],-3:3, 3*nr, 3*nr)';
        % B.C. at r=0
        LHS(1,4) = -2*Df*dt/dr^2;
        LHS(2,5) = -2*Ds*dt/dr^2;
        LHS(3,6) = -2*Dc*dt/dr^2;
        % DB.C. at r = R
        LHS(end-2,:) = 0;
        LHS(end-2,end-2) = 1;
        LHS(end-1,:) = 0;
        LHS(end-1,end-1) = 1;
        LHS(end,:) = 0;
        LHS(end,end) = 1;
        new_sol_vec = LHS\old_sol_vec;
        max_error = max(abs((new_sol_vec - sol_vec)));
        sol_vec = new_sol_vec;
        picard_iter_counter = picard_iter_counter + 1;
    end
    the_times = the_times + dt;
    if picard_iter_counter < 4
        dt = 1.05*dt;
    elseif picard_iter_counter < 8
        dt = dt;
    else
        dt = 0.98*dt;
    end
    if dt < 1e-3
        dt = 1e-3;
    elseif dt > 0.5
        dt = 0.5;
    end
```

```
    if the_times >= tout(kout)
        kout = kout + 1;
        thetout = [thetout the_times];
        F = [F sol_vec(1:3:end)];
        S = [S sol_vec(2:3:end)];
        C = [C sol_vec(3:3:end)];
    end
end
r_node = r(bleach_spot);
f_node = F(bleach_spot,:);
c_node = C(bleach_spot,:);
int_cylinder = r_node*(f_node + c_node)*2*dr/w^2;
r = int_cylinder;
```

```
% Mult_Obj_inv   identifies hydraulic parameters of porous media
%
% This code estimates the hydraulic parameters of partially saturated
% porous media using a Multi-objective optimization approach. The code uses
% 1) the Osborne-More adapted version of the Levenberg-Marquardt
% optimization  algorithm, 2) an adaptive strategy to build the Jacobian
% matrix, and 3) a mixed termination criterion. It calls the m-file
% forward_func which solves the mixed form Richards' equation.
%
% Inputs consist of: 1) experimental time/space series of fluid content of a
% porous medium, 2) fluid pressure head profiles, 3) the spatio-temporal
% domain, and 4) initial guesses for parameters to be optimized.
%
% Copyright 2006 Kouroush Sadegh Zadeh
% Bioengineering Department, University of Maryland at College Park, MD


close all
clear all
clc


%========================================================
%      Insert Experimental data (Data from Abeel (1984), Table-3, pp:11)
%========================================================
tout = [1 4 10 20 40 100];                          % day
theta_exp = [ 0.29345  0.31176  0.31889  0.33100  0.33100  0.33100
   0.24628  0.26198  0.26691  0.28739  0.33100  0.33100
   0.21935  0.23352  0.23730  0.25538  0.25538  0.29250
   0.20095  0.21407  0.21710  0.23356  0.23932  0.25580
   0.18409  0.19623  0.19862  0.21360  0.22427  0.23491
   0.16396  0.17492  0.17659  0.18981  0.20583  0.21368];
h_exp = 100*[0.27 0.25  0.17  0  0  0
   0.91  0.79  0.64  0.44  0.00  0.00
   1.40  1.19  0.99  0.85  0.66  0.62
   1.89  1.60  1.35  1.26  1.05  0.92
   2.37  2.00  1.70  1.66  1.45  1.22
   3.15  2.65  2.30  2.30  1.95  1.51];
theta_exp = theta_exp(:);
h_exp = h_exp(:);
N1 = length(theta_exp);
N2 = length(h_exp);
N = N1 + N2;
%========================================================
%                Start optimization
%========================================================
% parms_vec = [Ks a n tr b]
parms_vec = [16.32  0.0297  1.5781  0.098  -2];
ks = parms_vec(1);                    % Saturated Hydraulic Conductivity (cm/day)
a = parms_vec(2);                     % a in van Genuchten's model (1/cm)
n = parms_vec(3);                     % n in van Genuchten's model
tr = parms_vec(4);                     % Residual water content
b = parms_vec(5);                     % Pore connectivity index in Mualem's model
ts = 0.3310;                          % Saturated water content (measured)
maxerror = 1e-4;
deltaRMSE = maxerror;
RMSE = 1000;
```

```
phi = 1000;
grad = 100*[1 1 1 1 1];
lambda = 1;
p = 5;                              % Number of parameters to be optimized
D = zeros(p);                       % D: positive definite scaling matrix
parms_vec_new = parms_vec';
while deltaRMSE>1e-4
   parms_vec = parms_vec_new;
   h = Abeel_rich1d_mixed_Imp_func(tout,ks,ts,tr,a,n,b);
   theta = VGTHETA(h,ts,tr,a,n);
   r = (theta_exp - theta)/mean(theta_exp) + 0.5*(h_exp - h)/mean(h_exp);
   dks = 0.01*ks;
   da = 0.01*a;
   dn = 0.01*n;
   dtr = 0.01*tr;
   db = 0.01*b;
   v1 = -(Abeel_rich1d_mixed_Imp_func(tout,ks+dks,ts,tr,a,n,b) - h)/dks;
   v2 = -(Abeel_rich1d_mixed_Imp_func(tout,ks,ts,tr,a+da,n,b) - h)/da;
   v3 = -(Abeel_rich1d_mixed_Imp_func(tout,ks,ts,tr,a,n+dn,b) - h)/dn;
   v4 = -(Abeel_rich1d_mixed_Imp_func(tout,ks,ts,tr+dtr,a,n,b) - h)/dtr;
   v5 = -(Abeel_rich1d_mixed_Imp_func(tout,ks,ts,tr,a,n,b+db) - h)/db;
   j = [v1 v2 v3 v4 v5];
   grad = (j'*r)';
   for i=1:p;
      D(i,i) = max(norm(j(:,i)),D(i,i));
   end
   oldRMSE = RMSE;
   RMSE =  sqrt(r'*r/(N-p));
   deltaRMSE = abs(RMSE - oldRMSE);
   if RMSE > oldRMSE
      parms_vec = parms_vec;
      lambda = 1.25*lambda;
   else
      lambda = 0.2*lambda;
   end
   B = [j ; sqrt(lambda)*D];
   q = [-r ; zeros(5,1)];
   deltap = B\q;
   parms_vec_new = parms_vec + deltap;
   [parms_vec_new' RMSE lambda]
   minparms = [1.1 1e-4 1.002 1e-4 -25];
   maxparms = [500 0.8 150 0.75*ts 25];
   parms_vec_new = max(min(real(parms_vec_new),maxparms'),minparms');
   ks = parms_vec_new(1);
   a = parms_vec_new(2);
   n = parms_vec_new(3);
   tr = parms_vec_new(4);
   b = parms_vec_new(5);
end
while (abs(grad) > (0.01*maxerror*[1 1 1 1 1])) & (deltaRMSE > 1e-6)
   parms_vec = parms_vec_new;
   h = Abeel_rich1d_mixed_Imp_func(tout,ks,ts,tr,a,n,b);
   theta = VGTHETA(h,ts,tr,a,n);
   r = (theta_exp - theta)/mean(theta_exp) + 0.5*(h_exp - h)/mean(h_exp);
   var1 = -(Abeel_rich1d_mixed_Imp_func(tout,ks+dks,ts,tr,a,n,b)-Abeel_rich1d_mixed_Imp_func(tout,ks-dks,ts,tr,a,n,b))/(2*dks);
```

```
     var2 = -(Abeel_rich1d_mixed_Imp_func(tout,ks,ts,tr,a+da,n,b)-
Abeel_rich1d_mixed_Imp_func(tout,ks,ts,tr,a-da,n,b))/(2*da);
     var3 = -(Abeel_rich1d_mixed_Imp_func(tout,ks,ts,tr,a,n+dn,b)-
Abeel_rich1d_mixed_Imp_func(tout,ks,ts,tr,a,n-dn,b))/(2*dn);
     var4 = -(Abeel_rich1d_mixed_Imp_func(tout,ks,ts,tr+dtr,a,n,b)-
Abeel_rich1d_mixed_Imp_func(tout,ks,ts,tr-dtr,a,n,b))/(2*tr);
     var5 = -(Abeel_rich1d_mixed_Imp_func(tout,ks,ts,tr,a,n,b+db)-
Abeel_rich1d_mixed_Imp_func(tout,ks,ts,tr,a,n,b-db))/(2*db);
    j = [var1 var2 var3 var4 var5];
    for i=1:p;
       D(i,i) = max(norm(j(:,i)), D(i,i));
    end
    oldRMSE = RMSE;
    RMSE = sqrt(r'*r/(N-p));
    deltaRMSE = abs(RMSE - oldRMSE);
    if RMSE > oldRMSE
       parms_vec = parms_vec;
       lambda = 1.25*lambda;
    else
       lambda = 0.7*lambda;
    end
    B = [j ; sqrt(lambda)*D];
    q = [-r ; zeros(5,1)];
    deltap = B\q;
    parms_vec_new = parms_vec + deltap;
    minparms = [1.5 1e-5 1.02 1e-4 -35];
    maxparms = [500 0.5 6 0.8*ts 35];
    parms_vec_new = max(min(real(parms_vec_new),maxparms'),minparms');
    ks = parms_vec_new(1);
    a = parms_vec_new(2);
    n = parms_vec_new(3);
    tr = parms_vec_new(4);
    b = parms_vec_new(5);
    grad = (j'*r)'
    [parms_vec_new RMSE lambda]
end
ks = parms_vec_new(1)
a = parms_vec_new(2)
n = parms_vec_new(3)
tr = parms_vec_new(4)
b = parms_vec_new(5)
H = j'*j + lambda*(D'*D)
j'*j
display(['gradient:'])
grad
norm(grad)
display(['Eigenvalues of Hessian:'])
eig(H)
display(['Eigenvalues of JJ:'])
eig(j'*j)
%========================================
%                Goodness_of_fit indices:
%========================================
depth = [0.4 1.16 1.91 2.71 3.47 4.23];            % meter
tout = [1 4 10 20 40 100];                         % day
theta = reshape(theta,length(tout),length(depth));
```

```matlab
theta_exp = reshape(theta_exp,length(tout),length(depth));
h_reshaped = reshape(h,length(tout),length(depth));
h_exp = reshape(h_exp,length(tout),length(depth));
Se = r'*r/(N-p);
for i = 1:length(depth)
   R(i) = 1 - Se/var(theta(:,i));
end
Coef_det_overal = 1-Se/(mean(var(theta_exp(:))));
C1 = Se*inv(j'*j);
for i = 1:p;
   for k = 1:p;
      A1(i,k) = C1(i,k)/((sqrt(C1(i,i)))*sqrt(C1(k,k)));
   end
end
prob95 = 0.05;
prob99 = 0.01;
df = N - 1;
for ii = 1:p
   conf_95(ii,ii) = (tinv(1-prob95/2,df))*sqrt(C1(ii,ii));
   conf_99(ii,ii) = (tinv(1-prob99/2,df))*sqrt(C1(ii,ii));
end
%=======================================
%         Summary of goodness-of-fit indices
%=======================================
residusl_mean = mean(r)
residual_variance = var(r)
display(['Coefficients of determination for different days'])
[R]
display(['Overall Coefficient of determination'])
[Coef_det_overal]
display(['Parameter Covariance Matrix'])
C1
display(['Parameter Correlation Matrix'])
A1
display(['variance of optimized parameters: ks,a,n,tr,b'])
[diag(C1(1,1)) diag(C1(2,2)) diag(C1(3,3)) diag(C1(4,4)) diag(C1(5,5))]
display(['%95 confidence intervals on optimized parameters: ks,a,n,tr,b'])
[ks - conf_95(1,1) ks + conf_95(1,1)]
[a - conf_95(2,2) a + conf_95(2,2)]
[n - conf_95(3,3) n + conf_95(3,3)]
[tr - conf_95(4,4) tr + conf_95(4,4)]
[b - conf_95(5,5) b + conf_95(5,5)]
display(['%99 confidence intervals on optimized parameters: ks,a,n,tr,b'])
[ks - conf_99(1,1) ks + conf_99(1,1)]
[a - conf_99(2,2) a + conf_99(2,2)]
[n - conf_99(3,3) n + conf_99(3,3)]
[tr - conf_99(4,4) tr + conf_99(4,4)]
[b - conf_99(5,5) b + conf_99(5,5)]


%=======================================
%                 Plot the results
%=======================================
hh=ts*ones(6,1);
t_exp = [theta_exp(:); hh];
t_exp = reshape(t_exp,length(tout),length(depth));
theta = reshape(theta,length(tout),length(depth));
```

```
r = theta - t_exp;

figure(1)
for i= 1:length(depth)
    plot(t_exp(i,:),-depth,'*k')
    hold on
    plot(theta(i,:),-depth,'r')
    ylabel('Depth(m)')
    ylabel('Soil Depth, (meter)')
    xlabel('Volumetric Soil Moisture Content, (cm^3/cm^3)')
    axis([0.15 0.35 -6.05 0])
end

figure(2)
plot(t_exp(1,:),-depth,'o')
hold on
plot(t_exp(3,:),-depth,'p')
plot(t_exp(4,:),-depth,'v')
plot(t_exp(5,:),-depth,'s')
plot(t_exp(6,:),-depth,'d')
plot(theta(1,:),-depth,'r')
plot(theta(3,:),-depth,'r')
plot(theta(4,:),-depth,'r')
plot(theta(5,:),-depth,'r')
plot(theta(6,:),-depth,'r')
ylabel('Soil Depth, (meter)')
xlabel('Volumetric Soil Moisture Content, (cm^3/cm^3)')
legend('day 1','day 4','day 10','day 40','day 100','model')
axis([0.0 0.35 -6.05 0])

figure(3)
plot(theta(:),r(:),'+')
ylabel('residuals, (cm^3/cm^3)')
xlabel('Volumetric Soil Moisture Content(\theta), (cm^3/cm^3)')

hold off
```

```
% forward_func  solves the mixed form Richards' equation
%
% This function solves the mixed form Richards' equation by mass lumped,
% Galerkin based, linear finite element approximation, and the Picard iteration
% method
%
% Inputs are values of hydraulic parameters in the Mualem-
% van genuchten formula, and time and space domains.
%
% Outputs are profiles of fluid content of a porous medium at discret times (tout) and
% selected depths

% Copyright 2006 Kouroush Sadegh Zadeh
% Bioengineering Department, University of Maryland at College Park, MD

function r = forward_func(tout,ks,ts,tr,a,n,b)

x = 600;                    % cm
nx = 601;
dx = x/(nx - 1);            % cm
tmax = tout(end);
max_iter = 50;
err_tolerance = 1e-5;
m = 1- 1/n;
dt = 1e-2;
% I.C.
h = -ones(nx,1);
theta = VGTHETA(h,ts,tr,a,n);
h_new = h;
theta_new = theta;
thetime = 0;
thetout = 0;
wc = [];
tout = [tout 2*tmax];
kout = 1;
while thetime < tmax
    max_error = 1e5;
    picard_iter_counter = 0;
    h_old = h_new;
    theta_old = theta_new;
    while ((max_error > err_tolerance) & (picard_iter_counter < max_iter))
        k = VGK(h_new,ks,a,n,b);
        c = VGC(h_new,ts,tr,a,n);
        cmean = (VGC(h_new,ts,tr,a,n)+VGC(h_old,ts,tr,a,n))/2;
        AA_vec = (k(1:end-1)+ k(2:end))/(2*dx);
        AAr = [AA_vec; 0];
        AAl = [0; AA_vec];
        AAc = AAr + AAl;
        AA_mat = spdiags([-AAr AAc -AAl], -1:1, nx,nx)';
        BBc = cmean*dx;
        BBc(1) = cmean(1)*dx/2;
        BBc(end) = cmean(end)*dx/2;
        BB_mat = spdiags(BBc,0, nx,nx);
        thet_vec_old = (theta_old(1:end-1)+ theta_old(2:end))*dx/6;
        thet_vec_old_r = [thet_vec_old; 0];
        thet_vec_old_l = [0; thet_vec_old];
```

```matlab
    thet_vec_old_c = thet_vec_old_r + thet_vec_old_l + 2*theta_old*dx/6;
    thet_vec_old_c(1) = (2*theta_old(1) + theta_old(2))*dx/6;
    thet_vec_old_c(end) = (2*theta_old(end) + theta_old(end-1))*dx/6;
    thet_vec_new = (theta_new(1:end-1)+ theta_new(2:end))*dx/6;
    thet_vec_new_r = [thet_vec_new; 0];
    thet_vec_new_l = [0; thet_vec_new];
    thet_vec_new_c = thet_vec_new_r + thet_vec_new_l + 2*theta_new*dx/6;
    thet_vec_new_c(1) = (2*theta_new(1) + theta_new(2))*dx/6;
    thet_vec_new_c(end) = (2*theta_new(end) + theta_new(end-1))*dx/6;
    Driving_force_vec = gradient(k);
    LHS = AA_mat + BB_mat/dt;
    RHS = BB_mat/dt;
    % B.C. at the upper boundary
    q_top = 0;
    Driving_force_vec(1) = (k(2)+k(1))/2 + q_top;
    % BC at the lower boundary
    LHS(end,:) = 0;
    LHS(end,end) = 1;
    RHS(end,:) = 0;
    RHS(end,end) = 1;
    Driving_force_vec(end) = 0;
    thet_vec_old_c(end) = 0;
    thet_vec_new_c(end) = 0;
    h_new_c = LHS\(RHS*h_new - Driving_force_vec + (thet_vec_old_c - thet_vec_new_c)/dt);
    max_error = max(abs(h_new_c - h_new));
    h_new = h_new_c;
    theta_new = VGTHETA(h_new,ts,tr,a,n);
    picard_iter_counter = picard_iter_counter + 1;
  end
  % Adaptive time step
  thetime = thetime + dt;
  if picard_iter_counter < 5
    dt = 1.05*dt;
  elseif picard_iter_counter < 10
    dt = dt;
  else
    dt = 0.99*dt;
  end
  if thetime >= tout(kout)
    kout = kout + 1;
    thetout = [thetout thetime];
    wc = [wc theta_new];
  end
end
r1 = wc(40,:)';
r2 = wc(116,:)';
r3 = wc(191,:)';
r4 = wc(271,:)';
r5 = wc(347,:)';
r6 = wc(423,:)';
r = [r1 r2 r3 r4 r5 r6];
r = r(:);
```

```
% Single_Obj_inv   identifies hydraulic parameters of porous media
%
% This code estimates the hydraulic parameters of partially saturated
% porous media using a single-objective optimization approach. The code uses
% 1) the Osborne-More adapted version of the Levenberg-Marquardt
% optimization  algorithm, 2) an adaptive strategy to build the Jacobian
% matrix, and 3) a mixed termination criterion. The code calls the m-file
% forward_func which solves the mixed form Richards' equation.
%
% Inputs consist of: experimental time/space series of fluid content of a
% porous medium and initial guesses for parameters to be optimized.

% Outputs are the optimized values of the Mualem-van genuchten hydraulic
% parameters

% Copyright 2006 Kouroush Sadegh Zadeh
% Bioengineering Department, University of Maryland at College Park, MD




close all
clear all
clc
%====================================================
%      Insert Experimental data (Data from Abeel(1984), Table-3, pp:11)
%====================================================
tout = [1 4 10 20 40 100];                            % day
theta_exp = [ 0.29345  0.31176  0.31889  0.33100  0.33100  0.33100
   0.24628  0.26198  0.26691  0.28739  0.33100  0.33100
   0.21935  0.23352  0.23730  0.25538  0.25538  0.29250
   0.20095  0.21407  0.21710  0.23356  0.23932  0.25580
   0.18409  0.19623  0.19862  0.21360  0.22427  0.23491
   0.16396  0.17492  0.17659  0.18981  0.20583  0.21368];
h_exp = 100*[0.27 0.25  0.17  0  0  0
   0.91  0.79  0.64  0.44  0.00  0.00
   1.40  1.19  0.99  0.85  0.66  0.62
   1.89  1.60  1.35  1.26  1.05  0.92
   2.37  2.00  1.70  1.66  1.45  1.22
   3.15  2.65  2.30  2.30  1.95  1.51];                % cm
theta_exp = theta_exp(:);
h_exp = h_exp(:);
N1 = length(theta_exp);
N2 = length(h_exp);
N = N1 + N2;
%====================================================
%                Start optimization
%====================================================
% parms_vec = [Ks a n tr b]
parms_vec = [16.32  0.0297  1.5781  0.098  -2];
ks = parms_vec(1);                   % Saturated Hydraulic Conductivity (cm/day)
a = parms_vec(2);                    % a in van Genuchten's model (1/cm)
n = parms_vec(3);                    % n in van Genuchten's model
tr = parms_vec(4);                   % Residual water content
b = parms_vec(5);                    % Pore connectivity index in Mualem's model
ts = 0.3310;                         % Saturated water content (measured)
maxerror = 1e-3;
```

```
deltaRMSE = 100*maxerror;
RMSE = 1000;
grad = 100*[1 1 1 1 1];
lambda = 1;
p = 5;                              % Number of parameters to be optimized
D = zeros(p);                       % D: positive definite scaling matrix
parms_vec_new = parms_vec';
while (abs(grad) > (0.01*maxerror*[1 1 1 1 1])) & (deltaRMSE > 1e-4)
    parms_vec = parms_vec_new;
    theta = forward_func(tout,ks,ts,tr,a,n,b);
    r = theta_exp - theta;
    dks = 0.01*ks;
    da = 0.01*a;
    dn = 0.01*n;
    dtr = 0.01*tr;
    db = 0.01*b;
    v1 = -(forward_func(tout,ks+dks,ts,tr,a+da,n,b) - theta)/dks;
    v2 = -(forward_func(tout,ks,ts,tr,a+da,n,b) - theta)/da;
    v3 = -(forward_func(tout,ks,ts,tr,a,n+dn,b) - theta)/dn;
    v4 = -(forward_func(tout,ks,ts,tr+dtr,a,n,b) - theta)/dtr;
    v5 = -(forward_func(tout,ks,ts,tr,a,n,b+db) - theta)/db;
    j = [v1 v2 v3 v4 v5];
    grad = (j'*r)';
    for i=1:p;
        D(i,i) = max(norm(j(:,i)),D(i,i));
    end
    oldRMSE = RMSE;
    RMSE =  sqrt(r'*r/(N-p));
    deltaRMSE = abs(RMSE - oldRMSE);
    if RMSE > oldRMSE
        parms_vec = parms_vec;
        lambda = 1.25*lambda;
    else
        lambda = 0.2*lambda;
    end
    B = [j ; sqrt(lambda)*D];
    q = [-r ; zeros(5,1)];
    deltap = B\q;
    parms_vec_new = parms_vec + deltap;
    [parms_vec_new' RMSE lambda]
    minparms = [1.1 1e-4 1.002 1e-4 -25];
    maxparms = [500 0.8 150 0.75*ts 25];
    parms_vec_new = max(min(real(parms_vec_new),maxparms'),minparms');
    ks = parms_vec_new(1);
    a = parms_vec_new(2);
    n = parms_vec_new(3);
    tr = parms_vec_new(4);
    b = parms_vec_new(5);
end
while (abs(grad) > (1e-3*maxerror*[1 1 1 1 1])) & (deltaRMSE > 1e-6)
    parms_vec = parms_vec_new;
    theta = forward_func(tout,ks,ts,tr,a,n,b);
    r = (theta_exp - theta);
    var1 = -(forward_func(tout,ks+dks,ts,tr,a,n,b)...
        -forward_func(tout,ks-dks,ts,tr,a,n,b))/(2*dks);
    var2 = -(forward_func(tout,ks,ts,tr,a+da,n,b)...
```

```matlab
                -forward_func(tout,ks,ts,tr,a-da,n,b))/(2*da);
        var3 = -(forward_func(tout,ks,ts,tr,a,n+dn,b)...
                -forward_func(tout,ks,ts,tr,a,n-dn,b))/(2*dn);
        var4 = -(forward_func(tout,ks,ts,tr+dtr,a,n,b)...
                -forward_func(tout,ks,ts,tr-dtr,a,n,b))/(2*tr);
        var5 = -(forward_func(tout,ks,ts,tr,a,n,b+db)...
                -forward_func(tout,ks,ts,tr,a,n,b-db))/(2*db);
        j = [var1 var2 var3 var4 var5];
        for i=1:p;
            D(i,i) = max(norm(j(:,i)), D(i,i));
        end
        oldRMSE = RMSE;
        RMSE = sqrt(r'*r/(N-p));
        deltaRMSE = abs(RMSE - oldRMSE);
        if RMSE > oldRMSE
            parms_vec = parms_vec;
            lambda = 1.25*lambda;
        else
            lambda = 0.7*lambda;
        end
        B = [j ; sqrt(lambda)*D];
        q = [-r ; zeros(5,1)];
        deltap = B\q;
        parms_vec_new = parms_vec + deltap;
        minparms = [1.5 1e-5 1.02 1e-4 -35];
        maxparms = [500 0.5 6 0.8*ts 35];
        parms_vec_new = max(min(real(parms_vec_new),maxparms'),minparms');
        ks = parms_vec_new(1);
        a = parms_vec_new(2);
        n = parms_vec_new(3);
        tr = parms_vec_new(4);
        b = parms_vec_new(5);
        grad = (j'*r)'
        [parms_vec_new' RMSE lambda]
    end
    ks = parms_vec_new(1)
    a = parms_vec_new(2)
    n = parms_vec_new(3)
    tr = parms_vec_new(4)
    b = parms_vec_new(5)
    H = j'*j + lambda*(D'*D)
    display(['gradient:'])
    grad
    norm(grad)
    display(['Eigenvalues of Hessian:'])
    eig(H)
    display(['Eigenvalues of JJ:'])
    eig(j'*j)
%====================================================
%                Goodness_of_fit indices:
%====================================================
depth = [0.4 1.16 1.91 2.71 3.47 4.23];                % meter
tout = [1 4 10 20 40 100];                             % day
h = VG_h_theta(theta,ts,tr,a,n)
theta = reshape(theta,length(tout),length(depth));
t_exp = reshape(theta_exp,length(tout),length(depth));
```

```
head = reshape(h,length(tout),length(depth));
h_exp = reshape(h_exp,length(tout),length(depth));
r1 = theta - t_exp;
r2 = head - h_exp;
Se = r'*r/(N-p);
for i = 1:length(depth)
   R(i) = 1 - Se/var(theta(:,i));
end
Coef_det_overal = 1-Se/(mean(var(theta_exp(:))));
C1 = Se*inv(j'*j);
for i = 1:p;
   for k = 1:p;
      A1(i,k) = C1(i,k)/((sqrt(C1(i,i)))*sqrt(C1(k,k)));
   end
end
prob95 = 0.05;
prob99 = 0.01;
df = N - 1;
for ii = 1:p
   conf_95(ii,ii) = (tinv(1-prob95/2,df))*sqrt(C1(ii,ii));
   conf_99(ii,ii) = (tinv(1-prob99/2,df))*sqrt(C1(ii,ii));
end
%====================================================
%          Summary of goodness-of-fit indices
%====================================================
residusl_mean = mean(r)
residual_variance = var(r)
display(['Coefficients of determination for different days'])
[R]
display(['Overall Coefficient of determination'])
[Coef_det_overal]
display(['Parameter Covariance Matrix'])
C1
display(['Parameter Correlation Matrix'])
A1
display(['variance of optimized parameters: ks,a,n,tr,b'])
[diag(C1(1,1)) diag(C1(2,2)) diag(C1(3,3)) diag(C1(4,4)) diag(C1(5,5))]
display(['%95 confidence intervals on optimized parameters: ks,a,n,tr,b'])
[ks - conf_95(1,1) ks + conf_95(1,1)]
[a - conf_95(2,2) a + conf_95(2,2)]
[n - conf_95(3,3) n + conf_95(3,3)]
[tr - conf_95(4,4) tr + conf_95(4,4)]
[b - conf_95(5,5) b + conf_95(5,5)]
display(['%99 confidence intervals on optimized parameters: ks,a,n,tr,b'])
[ks - conf_99(1,1) ks + conf_99(1,1)]
[a - conf_99(2,2) a + conf_99(2,2)]
[n - conf_99(3,3) n + conf_99(3,3)]
[tr - conf_99(4,4) tr + conf_99(4,4)]
[b - conf_99(5,5) b + conf_99(5,5)]


%====================================================
%                    Plot the results
%====================================================
figure(1)
plot(t_exp(1,:),-depth,'*k')
hold on
```

```
plot(t_exp(2,:),-depth,'ok')
plot(t_exp(3,:),-depth,'pk')
plot(t_exp(4,:),-depth,'vk')
plot(t_exp(5,:),-depth,'sk')
plot(t_exp(6,:),-depth,'dk')
plot(theta(1,:),-depth,'r')
plot(theta(2,:),-depth,'r')
plot(theta(3,:),-depth,'r')
plot(theta(4,:),-depth,'r')
plot(theta(5,:),-depth,'r')
plot(theta(6,:),-depth,'r')
ylabel('Soil Depth, (meter)')
xlabel('Volumetric Soil Moisture Content, (cm^3cm^-^3)')
legend('day 1','day 4','day 10','day 20','day 40','day 100','model')
axis([0.05 ts+0.02 -4.5 0])

figure(2)
plot(-h_exp(1,:)/100,-depth,'*k')
hold on
plot(-h_exp(2,:)/100,-depth,'ok')
plot(-h_exp(3,:)/100,-depth,'pk')
plot(-h_exp(4,:)/100,-depth,'vk')
plot(-h_exp(5,:)/100,-depth,'sk')
plot(-h_exp(6,:)/100,-depth,'dk')
plot(-head(1,:)/100,-depth,'r')
plot(-head(2,:)/100,-depth,'r')
plot(-head(3,:)/100,-depth,'r')
plot(-head(4,:)/100,-depth,'r')
plot(-head(5,:)/100,-depth,'r')
plot(-head(6,:)/100,-depth,'r')
ylabel('Soil Depth, (meter)')
xlabel('Soil Water Pressure Head, (meter)')
legend('day 1','day 4','day 10','day 20','day 40','day 100','model')
axis([-4.5 0.15 -4.5 0])

figure(3)
plot(theta(:),r1(:),'+')
ylabel('Residuals, (cm^3/cm^3)')
xlabel('Volumetric Soil Moisture Content(\theta), (cm^3/cm^3)')

figure(4)
plot(head(:),r2(:),'+')
ylabel('Residuals, (m)')
xlabel('Soil Water Matric Potential Head, (m)')

hold off
```

% VGK(h,ks,a,n,b) -- unsaturated hydraulic conductivity function
% from the Mualem-van Genuchten's relationship.

```
function rr = VGK(h,ks,a,n,b)
m = 1 - 1 ./ n;
ah = abs(a.*h);
nu = 1 - ah.^(n-1) ./ (1 + ah.^n).^m;
rr = ks .* nu.^2 ./ (1+ah.^n).^(m/2);
```

% VGC(h,ts,tr,a,n)—Soil water capacitance function
% from the van Genuchten's relationship.

```
function r1 = VGC(h,ts,tr,a,n)
h(find (h>-1e-4)) = -1e-4;
m = 1 - 1 ./ n;
ah = abs (a.*h);
nu = ah.^ (n-1) ./ (1 + ah.^n).^(m+1);
r1 = (n-1).*a.*(ts-tr).*nu;
```

% VG_h_theta(theta,ts,tr,a,n) -- Soil water matric potential head from the van Genuchten's relationship.

```
function r = VG_h_theta(theta,ts,tr,a,n)
m = 1 - 1/ n;
find (theta <=tr) = tr + 1e-4;
se = (theta-tr)/(ts-tr);
r = ((se.^(-1/m) - 1).^1/n)/a;
```

% VGTHETA(h,ts,tr,a,n) -- Soil water contentfrom the van Genuchten's relationship.

```
function r = VGTHETA(h,ts,tr,a,n)
m = 1 - 1 ./ n;
ah = abs(a.*h);
r = (ts-tr)./(1 + ah.^n).^m + tr;
```

9. Bibliography

Ababou, R. 1988. Three-dimensional flow in random porous media. PhD. Thesis, Dept. Civil. Eng., *Massachusetts Institute of Technology*. Cambridge. MA.

Abbaspour, K., M. Th. van Genuchten, R. Schulin and E. Schlappi.1997. A sequential uncertainty domain inverse procedure for estimating subsurface flow and transport parameters. *Water Resour. Res*. 33: 1879 – 1892.

Abbaspour, K., M. A. Sonnleitner and R. Schulin.1999. Uncertainty in estimation of soil hydraulic properties by inverse modeling: example lysimeter experiments. *Soil Sci. Soc. Am. J.* 63: 501 - 509.

Abbaspour, K., R. Kasteel, and R. Schulin. 2000. Inverse parameter estimation in a layered unsaturated field soil. *Soil Sci.* 165(2): 109-123.

Abeele, W. V. 1984. Hydraulic testing of crushed bandelier Tuff. Rep. No. LA-10037-MS, Los Alamos National Laboratory. Los Alamos, New Mexico. 21pp.

Abramovitch, M. and I. A. Stegun. 1965. Handbook of Mathematical Functions. Fourth Printing. Applied Math. Ser. 55, U. S. Government Printing Office, Washington DC.

Allen, M. B. and C. Murphy. 1986. A finite element collocation method for variably saturated flow in two dimensions. *Water Resour. Res*. 22: 1537-1542.

Alley, W. M., R. W. Healy, J. W. LaBaugh, T. E. Reilly. 2002. Flow and storage in groundwater systems. *Science.* 296(5575): 1985-1990.

Axelrod, D., D. E. Koppel, J. Schlessinger, E. Elson, and W. W. Webb. 1976. Mobility measurement by fluorescence photobleaching recovery kinetics. *Biophys. J.* 16:1055-1069.

Badurraga, T. M., and G. S. Bodvarsson.1999. Calibrating hydrogeologic parameters for the 3-D site-scale unsaturated zone model of Yucca Mountain, Nevada. *J. Contam. Hydrol.*38:25-46.

Bard, Y. 1974. Nonlinear Parameter Estimation. Academic Press, New York.

Bear, J. 1972. Dynamics of Fluids in Porous Media. American Elsevier, New York.

Bear, J. 1979. Hydraulics of Groundwater. McGraw Hill, New York.

Beaudouin J, F. Mora-Bermudez, T. Klee, N. Daigle, J. Ellenberg. 2006. Dissecting the contribution of diffusion and interaction to the mobility of nuclear proteins. *Biophys. J.*, 90:1878-1894.

Beck, J. V., and K.J. Arnold. 1977. Parameter Estimation in Science and Engineering. John Wiley, New York.

Berg, O. G. 1986. Effective diffusion rate through a polymer network: influence of nonspecific binding and inter-segment transfer. *Biopolymers.* 25:811-821.

Berk, D. A., F. Yuan, M. Leunig, and R. K. Jain. 1997. Direct in vivo measurement of targeted binding in human tumor xenograft. *Proc. Natl. Acad. Sci. USA.* 99:12813-12818.

Bitterlich, S., and P. Knabner. 2002. An efficient method for solving an inverse problem for the Richards' equation. *J. Comput. Appl. Math.* 147:153-173.

Bohne, K., and W. Salzmann. 2002. Inverse simulation of non-steady state evaporation using non-equilibrium water retention data. *Geoderma* 110:49-62.

Bouloutas, 1989. Improved numerical approximations for flow and transport in the unsaturated zone. PhD. Thesis, Dept. Civil Eng., *Massachusetts Institute of Technology.* Cambridge.

Bouwer, H., and R. D. Jackson. 1974. Determining soil properties. In: J. van Schilfgaarde (ed.). Drainage for agriculture. Am. Soc. Agron., Madison, Wisc. Monogr., 17:611-672.

Bretscher, M. S., and M. C. Rafe. 1975. Mammalian plasma membrane. *Nature.* 258:43.

Broadbridge, P. and I. White. 1988. Constant rate rainfall infiltration: a versatile nonlinear model, 1. analytical solutions. *Water Resour. Res.* 7(1): 145 - 154.

Broyden, C. G. 1970. The convergence of a class of double-rank minimization algorithms. *J. Inst. Math. Applic.,* 6: 76-90.

Bruch, J.C. and Zyvolovski, G., 1974, Transient two-dimensional Heat Conduction Problems Solved by the Finite Element Method, *Int. J. Numer. Methods Eng.,* 8: 481-494.

Buckingham, E. 1907. Studies on the movement of soil moisture. USDA Bureau of Soils, Bulletin No.38, pp61.

Bullinski, J. C., D. J. Howell, E. D. Salmon, and C. M. Waterman-Storer. 2001. Rapid dynamics of the microtubule binding of ensconsin in vivo. *J. Cell Sci.* 114:3885-3897.

Carrera, J. 1984. Estimation of aquifer parameters under transient and steay state conditions. PhD Dissertation, Dep. Hydrol. Water Resour., Univ. of Arizona, Tucson, AZ, 257pp.

Carrera, J. and S. P. Neuman. 1986a. Estimation of aquifer parameters under transient and steady state conditions: 1. Maximum likelihood method incorporating prior information. *Water Resour. Res.* 22: 199 - 210.

Carrera, J. and S. P. Neuman. 1986b. Estimation of aquifer parameters under transient and steady state conditions: 2. Uniqueness, stability and solution algorithm. *Water Resour. Res.* 22: 211-227.

Carrera, J. and S. P. Neuman. 1986c. Estimation of aquifer parameters under transient and steady state conditions: 3. Application to synthetic and field data. *Water Resour. Res.* 22: 228-242.

Carrera, J., 1987. State of the art of the inverse problem applied to the flow and solute transport equation, in analytical and numerical groundwater flow and quality modeling. In: Custodio, E., *et al.* (Eds.), NATO-ARW Series C: Mathematical and Physical Sciences, vol. 224. Reidel, Norwell, Mass, pp. 549–583.

Carrero, G., D. McDonald, E. Crawford, G. de Vries, and M. J. Hendzel. 2003. Using FRAP and mathematical modeling to determine the in vivo kinetics of nuclear proteins. *Methods.* 29:14-28.

Carsel, R. F. and R. S. Parrish. 1988. Developing joint probability distributions of soil water characteristics. *Water Resour. Res.* 24: 755-769.

Carslaw, H. S., and J. C. Jaeger. 1959. Conduction of Heat in Solids. Oxford University Press, New York.

Celia, M. A., L. R. Ahuja, G. F. Pinder. 1987. Orthogonal collocation and alternating-direction procedures for unsaturated flow problems. *Adv. Water Resour.* 10: 178-187.

Celia, M. A., E. T. Bouloutas, R. L. Zarba. 1990. A general mass conservative numerical solution for unsaturated flow equation. *Water Resour. Res.* 26: 1483-1496.

Celia, M. A., P. Binning. 1992. A mass-conservative numerical solution for two-phase flow in porous media with application to porous media. *Water Resour. Res.* 28: 2819-2828.

Chavent, C. 1991. On the theory and practice of the non-linear least squares. *Adv. Water Resour.* 14:55-63

Chen, J., J. W. Hopmans, and M. E. Grismer. 1999. Parameter estimation of two-fluid capillary pressure-saturation and permeability functions. *Adv. Water Resour.* 22:479-493.

Clement, T. P., W. R. Wise., F. J. Molz. 1994. A physically based, two-dimensional, finite-difference algorithm for modeling variably saturated flow. *J. Hydrol.* 161:71-90.

Clifton, P. M. and S. P. Neuman. 1982. Effect of kriging and inverse modeling on conditional simulation of the Avra Valley aquifer in southern Arizona. *Water Resour. Res.* 18: 1225 - 1234.

Cooley, R. L. 1971. A finite difference method for unsteady flow in variably saturated porous media: application to a single pumping well. *Water Resour. Res.* 7: 1607-1625.

Cooley, R. L. 1982. Incorporation of prior information on parameters into nonlinear regression groundwater flow models. 1. Theory. *Water Resour. Res.* 18: 965- 967.

Cooley, R. L. 1983. Incorporation of prior information on parameters into nonlinear regression groundwater flow models. 2. Applications. *Water Resour. Res.* 19: 662- 676.

Cooley, R. L. 1983. Some new procedures for numerical solution of variably saturated flow problems. *Water Resour. Res.* 19: 1271-1285.

Coscoy, S., F. Waharte, A. Gautreau, M. Martin, D. Louvard, P. Mangeat, M. Arpin, and F. Amblard. 2002. Molecular analysis of microscopic ezrin dynamics by two photon FRAP. *Proc. Natl. Acad. Sci. USA*. 99:12813-12818.

Courant, R. 1943. Variational methods for the solution of problems of equilibrium and vibration. *Bull. Ams.* 49:1-23.

Dagan, G. 1985. Stochastic modeling of groundwater flow by unconditional and conditional probabilities: The inverse problem. *Water Resour. Res.* 21: 65- 72.

Dane, J. H. and S. Hruska. 1983. In-situ determination of soil hydraulic properties during drainage. *Soil Sci. Soc. Am. J.*, 47:619-624.

Daniel, C., and F. S. Wood. 1971. Fitting equations to data. Wiley-Interscience, New York.

Darcy, H. 1856. Les fontaines publiques de la ville de Dijon. In: Hubert, M. K., 1969. The theory of groundwater and related papers. Hafner Pub. Co. N.Y.

Davidon, W. C. 1959. Variable metric method for minimization. A.E.C. Research and Development Report, ANL-5990.

Dennis, J. E., Jr., and J. More. 1977. Quasi-Newton methods: motivation and theory. *SIAM Rev.* 19: 46-89.

Dennis, J. E., Jr., D. M. Gay, and R. E. Welsch. 1981a. An adaptive nonlinear least-squares algorithm. *ACM Trans. Math. Software.* 7: 348-368.

Diersch, H. J. G., and P. Perrochet. 1999. On the primary variable switching technique for simulating saturated-unsaturated flows. *Adv. Water Resour. Res.* 23:271-301.

Dixon, L. C. W and G. P. Szegö (eds.). 1975. Toward Global Optimization, Vol. 1. North-Holland Publishing Company, Amsterdam.

Dixon, L. C. W and G. P. Szegö (eds.). 1978. Toward Global Optimization, Vol. 2. North-Holland Publishing Company, Amsterdam.

Doherty, J. 1994. PEST: Model-independent parameter estimation. Available at www.sspa.com/pest (verified 1st July, 2006). Water-mark Numerical Computing, Brisbane, Australia.

Donaldson, J. R., and R. B. Schnabel. 1987. Computational experience with confidence regions and confidence intervals for nonlinear least squares. *Technometrics.* 29:67-82.

Duguid, J. O., and M. Reeves. 1976. Material transport through porous media: A finite element Galerkin model. ORNL-4928. Oak Ridge National Laboratory, Oak Ridge TN.

Dunder, M., U. Hoffmann-Rohrer, Q. Hu, I. Grummt, L. I. Rothblum, R. D. Phair, and T. Misteli. 2002. A kinetic framework for a mammalian RNA polymerase in vivo. *Science.* 298:1623-1626.

Durner, W., B. Schultze, and T. Zurmuhl. 1997. State-of-the-art in inverse modeling of inflow/outflow experiments. P. 661-681. *In*: M. Th. van Genuchten et al (ed.) Proceedings of the international Workshop on Characterization and Measurement of the Hydraulic Properties of Unsaturated Porous Media, Riverside, CA. 22-24 Oct. 1997. University of California, Riverside.

Eching, S. O. and J. W. Hopmans. 1993. Optimization of hydraulic functions from transient outflow and soil water pressure head data. *Soil Sci. Soc. Am. J.,* 57: 1167-11785.

Eching, S. O., J. W. Hopmans and W. W. Wallender. 1994. Estimation of in situ unsaturated soil hydraulic functions from scaled cumulative drainage data. *Water Resour. Res.* 30: 2387- 2394.

Ediden, M., Y. Zagyansky, and T. J. Lardner. 1976. Measurement of membrane protein lateral diffusion in single cells. *Science.* 191:466-468.

Engelhardt, I., S. Finsterle, and C. Hofstee. 2003. Experimental and numerical investigation of flow phenomena in nonisothermal, variably saturated bentonite-crushed roch mixtures. *Vadose Zone J.* 2:239-246.

Ewing, R. E., and T. Lin. 1991. A class of parameter optimization techniques for fluid flow in porous media. *Adv. Water Resour.* 14:89-97.

Finsterle, S., and K. Pruess. 1995. Solving the estimation-identification problem in two-phase flow modeling. *Water Resour. Res. 31:913-924.*

Finsterle, S. and J. Najita. 1998. Robust estimation of hydrological model parameters. *Water Resour. Res.* 34: 2939-2947.

Finsterle, S., C. F. Ahlers, R. C. Trautz, and P. J. Cook. 2003. Inverse and predictive modeling of seepage into underground openings. *J. Contam. Hydrol.* 62-63:89-109.

Finsterle, E. 2004. Multiphase inverse modeling: Review and iTOUGH2 applications. *Vadose Zone J.*, 3:747-762.

Fletcher, R. 1970. A new approach to variable metric algorithms. Comp. J. 13: 317-322.

Fletcher, R. and M.J.D. Powell.1963. A rapidly convergent descent method for minimization. *Computer Journal,* 6:163-168.

Forsyth, P. A., Y. S. Wu, and K. Pruess. 1995. Robust numerical methods for saturated unsaturated flow with dry initial conditions in heterogeneous media. *Adv. Water Resour.* 20:1-14.

Freeze, R. A. 1969. The mechanism of natural groundwater recharge and discharge. 1. One-dimensional, vertical, unsteady, unsaturated flow above a recharging and discharging groundwater flow system. *Water Resour. Res.* 5: 153-171.

Freeze, R. A. 1971a. Three-dimensional transient, saturated-unsaturated flow in a groundwater basin. *Water Resour. Res.* 7: 347-366.

Freeze, R. A. 1971a. Influence of the unsaturated flow domain on seepage through earth dams. *Water Resour. Res.* 7: 929-941.

Gardner, W. R. 1958. Some steady-state solutions of the unsaturated flow moisture flow equation with application to evaporation from a water Table. *Soil Sci.* 85: 228-232.

Gariner, P., M. Riu, P. Boivin, M. Vauclin, P. Baveyeve. 1997. Determining the hydraulic properties of swelling soil from a transient evaporation experiment. *Soil Sci. Soc. Am. J.* 62:874-880

Ghezzehei, T. A., R. C. Trautz, S. Finsterle, P. J. Cook, and C. F. Ahlers. 2004. Modeling coupled evaporation and seepage in ventilated tunnels. *Vadose Zone J.*, 3:806-818.

Gill, P. and W. Murray. 1978. Algorithms for the solution of the nonlinear least squares problems. *SIAM J. Num. Analys.* 15(5): 977-992.

Goldfarb, D. 1970. A family of variable metric updates derived by variational means. *Math. Comput.* 24: 23-26.

Golub, G. H., and C. F. van Loan. 1983. Matrix Computations. Johns Hopkins University Press. Baltimore, MD.

Green, R.E., L.R. Ahuja, and S.K. Chong. 1986. Hydraulic conductivity, diffusivity, and sorptivity of unsaturated soils: Field method. In: Methods of Soil Analysis, Part 1. A. Klute (ed.). ASA, Madison, WI, 9:771-789.

Gribb, M. M. 1996. Parameter estimation for determining hydraulic properties of a fine sand from transient flow measurements. *Water Resour. Res.* 32: 196-1974.

Gui, S., R. Zhang, J. P. Turner, X. Xue. 2000. Probabilistic slope stability analysis with stochastic soil hydraulic conductivity. *J. Geotech. Eng., ASCE,* 126:1-8.

Hanks, R. J. and S. M. Bowers. 1962. Numerical solution of the moisture flow equation for infiltration into layered soils. *Soil Sci. Soc. Am. Proc.* 26: 530-534.

Hao, X., R. Zheng, and A. Kravchenko. 2005. A mass-conservative switching method for simulating saturated-unsaturated flow. *J. Hydrol.* 311: 254-265.

Haverkamp, R., M. Vauclin, J. Touma, P. G. Wierenga and G. Vachaud. 1977. A comparison of numerical solution models for one-dimensional infiltration. *Soil Sci. Soc. Am. J.* 41: 285-294.

Haverkamp, R., M. Vauclin. 1981. A comparative study of three forms of the Richards equation used for predicting one-dimensional infiltration in unsaturated soil. *Soil Sci. Soc. Am. J.* 45(1): 13-20.

Hills, R. G., I. Porro, D. B. Hudson, and P. J. Wierenga. 1989. Modeling one-dimensional infiltration into very dry soils. 1. Model development and evaluation. *Water Resour. Res.* 25: 1259 - 1269.

Hills, R. G., K. A. Fisher, M. R. Kirkland, and P. J. Wierenga. 1994. Application of flux-corrected transport to the Las Cruces Trench. *Water Resour. Res.* 30(8): 2377-2385.

Hoeksma, R. J. and P. K. Kitanidis. 1984. An application of the geostatistical approach to the inverse problem in two-dimensional groundwater modeling. *Water Resour. Res.* 20: 1003 - 1020.

Hofmann, J. R., and P. A. Hofmann. 1992. Darcy's law and structural explanation in hydrology. *Proceedings of the Biennial Meeting of the Philosophy of Science Association.* 1: 23-35.

Hollenbeck, K. J. 1998. invlap.m: A MATLAB function for numerical inversion of Laplace transform by the de Hoog algorithm.
http://www.isva.dtu.dk/staff/karl/invlap.html.

Hopmans, J. W., J. Simunek, N. Romano, and W. Durner. 2002. Simultaneous determination of water transmission and retention properties. Inverse methods. P. 963-1008. In: H. H. Dane and G. C. Topp(ed.) Methods of soil analysis. Part 4. SSSA Book Ser. 5. SSSA Madison, WI.

Hornberger, G. M. and I. Remson. 1969. Numerical studies of a composite soil moisture groundwater system. *Water Resour. Res.* 5(4): 797-802.

Hromadka, T. V., and G. L. Guymon. 1980. Numerical mass balance for soil moisture transport problems. *Adv. Water Resour.* 3: 107-114.

Hudson, D. B., P. J. Wierenga, and R. G. Hills. 1996. Unsaturated hydraulic properties from upward flow into soil cores. *Soil Sci. Soc. Am. J.* 60: 388-396.

Hughson, D. L., and T. C. J. Yeh. 2000. An inverse model for three-dimensional flow in variably saturated porous media. *Water Resour. Res.* 36: 829- 840.

Huyakorn, P. S., and G. F. Pinder. 1983. Computational Methods in Subsurface Flow. San Diego. Academic Press.

Huyakorn, P. S., S. D. Thomas and B. M. Thompson. 1984. Techniques for making finite element competitive in modeling flow in variably saturated media. *Water Resour. Res.* 20: 1099-1115.

Huyakorn, P. S., E. P. Springer V. Guvanasen and T. D. Wasworth. 1986. A three-dimensional finite element model for simulating water flow in variably saturated porous media. *Water Resour. Res*. 22: 1790-1808.

Hwang, S. I., and S. E. Powers. 2002. Estimating unique soil hydraulic properties for sandy media from multi-step outflow experiments. *Adv. Water Resour*. 26: 445-456.

Javandel, I., and P. A. Whiterspoon. 1968. Applications of the finite element method to transient flow in porous media. *Soc. Pet. Eng. J.* 3:241-252.

Javandel, I., and P. A. Whiterspoon. 1969. A method of analyzing transient fluid flow in multilayered aquifers. *Water Resour. Res.* 5: 856-869.

Jhorar, R. K., W. G. M. Bastiaanssen, R. A. Feddes and J. C. van Dam. 2002. Inversely estimating soil hydraulic functions using evapotranspiration fluxes. *J. Hydrol.* 258: 198 – 213.

Kaufman, E., and R. K. Jain.1990. Quantification of transport and binding parameters using fluorescence recovery after photobleaching. Potential for in vivo applications. *Biophys. J.* 58:873-885.

Kelleners, T. J., R. W. O. Soppe, J. E. Ayars, J. Simunek, and T. H. Skaggs. 2005. Inverse analysis of upward water flow in a groundwater Table lysimeter. *Vadose Zone J.* 4: 558-572.

Kimura, H., K. Sogaya, and P. R. Cook. 2002. The transcription cycle of RNA polymerase II in living cells. *J. Cell Biol.* 159:777-782.

Kirkland, M. R., R. G. Hills and P. J. Wierenga. 1992. Algorithms for solving Richards' equation for variably saturated soils. *Water Resour. Res.* 28: 2049-2058.

Kitanidis, P.K. 1995. Quasi-linear geostatistical theory for inversing. *Water Resour. Res.* 31: 2411- 2419.

Kitanidis, P.K. and E.G. Vomvoris. 1983. A geostatistical approach to the inverse problem in groundwater modeling (steady state) and one-dimensional simulations. *Water Resour. Res.* 19: 677- 690.

Klute, A., and C. Dirksen. 1986. Hydraulic conductivity and diffusivity: Laboratory methods. In: Methods of Soil Analysis, Part 1. A. Klute (ed.). ASA, Madison, WI, 9:687-734.

Knowles, I., T. Le, and A. Yan. 2004. On the recovery of multiple flow parameters from transient head data. *J. Comput. Appl. Math.* 169: 1-15.

Knowles, I., and A. Yan. 2004. On the recovery of transport parameters in groundwater modeling. *J. Comput. Appl. Math.* 171: 277-290.

Kool, J. B., J. C. Parker and M. Th. van Genuchten. 1985. Determining soil hydraulic properties from one-step outflow experiments by parameter estimation. 1. Theory and numerical studies. *Soil Sci. Soc. Am. J.*, 49: 1348 - 1354.

Kool, J. B., J. C. Parker and M. Th. van Genuchten. 1987. Parameter estimation for unsaturated flow and transport models- A review. *J. Hydrol.* 91: 255 - 293.

Kool, J. B. and J. C. Parker. 1988. Analyses of the inverse problem for transient unsaturated flow. *Water Resour. Res.* 24: 817- 830.

Kowalsky, M, S. Finsterle, and Y. Rubin. 2004. Estimating flow parameter distributions using ground-penetrating radar and hydrological measurements during transient flow in the vadose zone. *Adv. Water Resour.* 27:583-599.

Kreft, A. and A. Zuber. 1978. On the physical meaning of the dispersion equation and its solution for different initial and boundary conditions. *Chem. Eng. Sci.* 33: 1471–1480.

Kuiper, L. K. 1987. A comparison of iterative methods as applied to the solution of nonlinear three-dimensional groundwater flow equation. *SIAM J. Scientific and Statistical Computing.* 8(4)521-528.

Lehmann, F., and P. Ackerer. 1997. Determining soil hydraulic properties by inverse method in one-dimensional unsaturated flow. *J. Environ. Qual.* 26: 76-81.

Lehmann, F., and P. Ackerer. 1998. Comparison of iterative methods for improved solutions of the fluid flow equation in partially saturated porous media. *Transport Porous Media.* 31: 275-292.

Levenberg, K. 1944. A method for the solution of a certain non-linear problems in least squares. *Q. Appl. Math.* 2: 164-168.

Levene, H. (1960). Essays in honor of Harold Hotelling. In: Contributions to Probability and Statistics. Olkin et al. (eds.). Stanford University Press, pp. 278-292.

Liakopoulous, A. C. 1966. Theoretical prediction of evaporation losses from the groundwater. *Water Resour. Res.* 2: 227-240.

Liebman, P. A., and G. Entine. 1974. Lateral diffusion of visual pigment in photoreceptor disk membrane. *Science.* 185:457-459.

Lomen, D. O. and A. W. Warrick. 1974. Time dependent linearized infiltration: 2. Line sources. *Soil Sci. Soc. Am. Proc.*, 38: 68-72.

Malengier, B. 2004. Parameter identification in stationary groundwater flow problems in drainage basins. *J. Comput. Appl. Math.* 168: 299-307.

Marquardt, D. W. 1963. An algorithm for least squares estimation of nonlinear parameters. *SIAM J. Appl. Math*. 11: 431 – 441.

Mathworks, 2006. Optimization toolbox. User's guide. Available at: http://www.mathworks.com/access/helpdesk/help/toolbox/optim/ (Verified Aug. 08, 2006).

McLaughlin, D., and L. R. Townly. 1996. A reassessment of the groundwater inverse problem. *Water Resour Res*. 32:1131-1161.

McNally, J. G., W. G. Muller, D. Walker, R. Wolford, and G. L. Hager. 2000. The glucocorticoid receptor: rapid exchange with regulatory sites in living cells. *Science*. 287:1262-1265.

McCuen, R. H. 1985. Statistical Methods for Engineers. Prentice Hall. Upper Saddle River. NJ.

McCuen, R. H. 2003. Modeling Hydrologic Change: Statistical Methods. Lewis publishers.

Milly, P. C. D. 1985. A mass conservative procedure for time stepping in models of unsaturated flow. *Adv. Water Resour.* 8:32-36.

Mishra, S. and J.C. Parker. 1989. Parameter estimation for coupled unsaturated flow and transport. *Water Resour. Res.* 25: 385- 396.

Molz, F. J. and I. Remson. 1970. Extraction term models of soil moisture use by transpiring plants. *Water Resour. Res.* 6: 1346-1356.

Moré, J. J. 1977. The Levenberg-Marquardt algorithm: Implementation and theory. numerical analysis, ed. G. A. Watson, Lecture Notes in Mathematics 630, Springer Verlag, pp. 105-116.

Moré, J. J., and S. J. Wright. 1993. Optimization software guide. *Frontiers Appl. Math. 15*. Available at: http://www-fp.mcs.anl.gov/otc/Guide/SoftwareGuide/index.html (Verified 1 July, 2006). *SIAM*, Philadelphia, PA.

Mualem, Y. 1976. A new model for predicting hydraulic conductivity of unsaturated porous media. *Water Resour. Res.* 12: 513-522.

Nazareth, L. 1980. Some recent approaches to solving large residual nonlinear least squares problems. *SIAM Review.* 22(1): 1-11.

Neuman, S. P. 1973. Saturated-unsaturated seepage by finite element. *ASCE J. Hydraulic Div.,* 99(HY12): 2233-2250.

Neuman, S. P. 1975. Galerkin approach to saturated-unsaturated flow in porous media. In: R. H. Gallagher *et al.* (eds.): Finite element in fluids, 1, J. Wiley, New York.

Olyphant, G. A., 2003. Temporal and spatial (down profile) variability of unsaturated soil hydraulic properties determined from a combination of repeated field experiments and inverse modeling. *J. Hydrol.* 281:23-35.

Oreskes, N., K. Shrader-Frechette, K. Belitz. 1994. Verification, validation, and confirmation of numerical models in the earth science. *Science.* 263(5147): 641-646.

Osborne, M. R. 1976. Nonlinear least squares-the Levenberg-Marquardt revisited. *J. Aus. Math. Soc., Ser. B19*, 343-357.

Pan, L., and P. J. Wierenga. 1995. A transformed head-based approach to solve Richards' equation fro variably saturated soils. *Water Resour. Res.* 31: 925–931.

Pan, L., P. J. Wierenga., and A. W. Warrick. 1996. Finite element methods for modeling water flow in variably saturated porous media: Numerical oscillation and mass-distributed schemes. *Water Resour. Res.* 32: 1883–1889.

Pan, L., and L. Wu. 1998. A hybrid global optimization method for inverse estimation hydraulic parameters: Annealing-simplex method. *Water Resour. Res.* 34:2261-2269.

Paniconi, C., A. A. Aldama, and E. F. Wood. 1991. Numerical evaluation of iterative and noniterative methods for the solution of the nonlinear Richards equation. *Water Resour. Res.* 27(6): 1147–1163.

Paniconi, C., and M. Putti. 1994. A comparison of Picard Newton and iteration in the numerical solution multidimensional variably saturated flow problems. *Water Resour. Res.* 30: 3357-3374.

Parker, J.C. 1984. Analysis of pollutant transport in column tracer studies. *Soil Sci. Soc. Am. J.*, 48: 719 - 724.

Parker, J.C., J. B. Kool and M. Th. van Genuchten. 1985. Determining soil hydraulic properties from one-step outflow experiments by parameter estimation: Experimental studies. *Soil Sci. Soc. Am. J.*, 49: 1354 - 1360.

Parlange, J.Y., R., Haverkamp and J. Touma. 1985. Infiltration under ponded condition. 2. Optimal analytical solution and comparison with experimental observations. *Soil Sci.* 139: 305-311.

Phair, R. D., and T. Misteli. 2000. High mobility of proteins in the mammalian cell nucleus. *Nature.* 404:604-609.

Philip, J.R. 1957a. The theory of infiltration: 1. The infiltration equation and its solution. *Soil Sci.* 83: 345-357.

Philip, J.R. 1957b. The theory of infiltration: 4. Sorptivity and algebraic infiltration equations. *Soil Sci*. 84: 329-339.

Philip, J.R. 1969. Theory of infiltration. *Adv. Hydrosc*. 5: 215-305. Academic press, New York.

Philip, J.R. 1987. The infiltration joining problem. *Water Resour. Res.* 23: 2239-2245.

Philip, J. R. 1992. Exact solutions for redistribution by nonlinear convection-diffusion. *J. Aus. Math. Soc. Ser. B*. 33: 363-383.

Pinder, G. F. and W. G. Gray. 1977. Finite Element Simulation in Surface and Subsurface Hydrology. Academic Press, New York.

Poeter, E. P., and M. C. Hill. 1998. Documentation of UCODE, a computer code for universal inverse modeling. USGS Water-Resources Invest. Rep. 98-1080. Available at www.water.usgs.gov/software/ucode.html (verified 1st, July 2006). USGS and International Ground Water Modeling Center, Colorado School of Mines, Golden, CO.

Polisetty, P. K., E. O. Voit, and E. P. Gatzke. 2006. Identification of metabolic system parameters using global optimization methods. *J. Theor. Biol. Med. Mod.*

Poo, M., and R. A. Cone. 1974. Lateral diffusion of rhodopsin in the photoreceptor membrane. *Nature.* 247:438-441.

Rathfelder, K., and L. M. Abriola. 1994. Mass conservative numerical solutions of the head-based Richards' equation. *Water Resour. Res.* 30(9): 2579-2586.

Remson, I., G. M. Hornberger, and F. J. Molz. 1971. Numerical Methods in Subsurface Hydrology. Wiley-Interscience. New York. 389p.

Richards, L. A. 1931. Capillary conduction of liquids in porous media. *Physics*, 1:318-333.

Ritter, A., F. Hupet, R. Munoz-Carpena, S. Lambot, and M. Vanclooster. 2003. Using inverse methods for estimating soil hydraulic properties from field data as an alternative to direct methods. *Agric. Water Management*. 59: 77-96.

Ritter, A., R. Munoz-Carpena, C. M. Regalado, M. Javaux, and M. Vanclooster. 2005. Using TDR and inverse methods to characterize solute transport in a layered agricultural volcanic soil. *Vadose Zone J.* 59: 77-96.

Rogers, J. S. 1994. Capacities and initial time step effects on numerical solution of Richards' equation. *Trans. ASAE*. 37:807-813.

Rubin, J. 1968. Theoretical analysis of two-dimensional, transient flow of water in unsaturated and saturated soils. *Soil Sci. Soc. Am. Proc.*, 32: 607 – 615.

Rucker, D. F., and T. P. A. Ferre. 2004. Parameter estimation for soil hydraulic properties using zero-offset borehole radar: Analytical method. *Soil Sci. Soc. Am. J.* 68: 1560-1567.

Russo, D., E. Bresler, U. Shani, J.C. Parker. 1991. Analyses of infiltration events in relation to determining soil hydraulic properties by inverse modeling methodology. *Water Resour. Res*. 27: 1361-1373.

Russo, D. 1997. On the estimation of parameters of log-unsaturated conductivity covariance from solute transport data. *Adv. Water Resour.* 20(4):191-205.

Sabatier, P. 2000. Past and future of inverse problem. *J. Math. Phys*. 41(6): 4082-4124.

Sander, G. C., J. Y. Parlange, V. Kühnel, W. L. Hogarth, D. Lockington, and J. P. J., O'Kane. 1988. Exact nonlinear solution for constant flux infiltration. *J. Hydrol*., 97: 341-346

Schlessinger, J., D. E. Kopple, D. Axelrod, K. Jacobson, W. W. Webb, and E. Elson. 1976. Lateral transport on cell membranes: mobility of cancanavalin A receptors on myoblasts. *Proc. Natl. Acad. Sci. USA*. 73:2409-2413.

Schmied, B., K. Abbaspour, and R. Schulin. 2000. Inverse estimation of parameters in a nitrogen model using field data. *Soil Sci. Soc. Am. J.* 64:533-542.

Seber, G. A. F., and C. J. Wild, 2004. Nonlinear Regression. John Wiley and sons. New York, 768 pp.

Shanno, D. F. 1970. Conditioning of quasi-Newton methods for function minimization. *Mathematics of Computation.* 24: 647-656.

Shirazi, M.A., and L. Boersma. 1984. A unifying quantitative analysis of soil texture. *Soil Sci. Soc. Am. J.* 48:142–147.

Shirazi, M.A., L. Boersma, and J.W. Hart. 1988. A unifying quantitative analysis of soil texture: Improvement of precision and extension of scale. Soil *Sci. Soc. Am. J.* 52:181–190.

Shouse, P.J., J.B. Sisson, T.R. Ellsworth and J.A. Jobes. 1992. Estimating in situ unsaturated hydraulic properties of vertical heterogeneous soils. *Soil Sci. Soc. Am. J.,* 56: 1673 – 1679.

Simunek, J. and M. Th. van Genuchten. 1996. Estimating unsaturated soil hydraulic properties from tension disc infiltrometer data by numerical inversion. *Water Resour. Res.* 32: 2683 – 2696.

Simunek, J. and M. Th. van Genuchten, and M. Sejna. 2005. The HYDRUS-1D software package for simulating the movement of water, heat, and multiple solutes in variably saturated media, Version 3.0, HYDRUS Software Series 1, Department of Environmental Sciences, University of California Riverside, Riverside, California, USA, 270 pp.

Smith, R. E. and J. Y. Parlange. 1978. A parameter-efficient hydrologic infiltration model. *Water Resour. Res.* 14: 533-538.

Snedecor, G. W. and W. G. Cochran. 1989. Statistical methods. Eighth Edition, Iowa State University Press.

Sorooshian, S., V. K. Gupta, and J. L. Fulton. 1983. Evaluation of maximum likelihood parameter estimation techniques for conceptual rainfall-run off models: Influence of calibration data variability and length on model credibility. *Water Resour. Res.* 14: 533-538.

Sorooshian, S., and V. K. Gupta. 1983. Automatic calibration of conceptual rainfall-run off models: the question of parameter observability and uniqueness. *Water Resour. Res.* 19(1): 260-.

Sprague *et al.,* 2004. Analysis of binding reactions by fluorescence recovery after photobleaching. *Biophys. J.* 86:3473-3495.

Sun, N.-Z. 1994. Inverse Problem in Groundwater Modeling. Kluwer Academic Publishers, Dordrecht, The Netherlands.

Sun, N.-Z. and W.G. Yeh. 1990. Coupled inverse problems in groundwater modeling, 1.Sensitivity analysis and parameter identification. *Water Resour. Res.* 26: 2507 – 2525.

Tardy, Y., J. L. McGrath, J. H. Hartwig, and C. F. Deway. 1995. Interpreting photoactivated fluorescence microscopy measurements of steady-state actin dynamics. *Biophys. J.* 69:1674-1682.

Thompson, N. L., T. P. Burghardt, and D. Axelrod. 1981. Measuring surface dynamics of biomolecules by total internal reflection fluorescence with photobleaching recovery or correlation spectroscopy. *Biophys. J.* 33:435-454.

Toorman, A. F., P. J. Wierenga, R. G. Hills. Parameter estimation of hydraulic properties from one-step outflow data. *Water Resour. Res.* 28: 3021–3028.

Toride, Nobuo, F. J. Leij and M. Th. van Genuchten. 1993. A comprehensive set of analytical solutions for nonequilibrium solute transport with first-order decay and zero-order production. *Water Resour. Res.* 29: 2167 – 2182.

Truskey, G. A., F. Yuan, and D. F. Katz. 2004. Transport Phenomena in Biological Systems. Prentice Hall. N.J.

Turner, M. J., R. W. Clough, H. C. Martin, and L. J. Topp. 1956. Stiffness and deflection analysis of complex structures. *J. Aeronautical Sci.* 23:805-823.

Tyn Myint-u. 1980. Partial Differential Equations of Mathematical Physics. Elsevier science publishing company Inc. New York.

van Dam, J. C., J. N. M. Stricker and P. Droogers. 1994. Inverse method to determine soil hydraulic functions from multi-step outflow experiment. *Soil Sci. Soc. Am. J.*, 58: 647 - 652.

van Genuchten, M. Th.. 1978. Numerical solutions of the one-dimensional saturated-unsaturated flow equation. *Research Report 78-WR-9*. Water Resources Program. Dept. Civil Eng. Princeton University.

van Genuchten, M. Th. 1980. A closed form equation for predicting the hydraulic conductivity of unsaturated soils. *Soil Sci. Soc. Am. J.*, 44: 892-898.

van Genuchten, M. Th. 1982. A comparison of numerical solutions of the one-dimensional unsaturated flow and mass transport equations. *Adv. Water. Resour.* 5: 47-55.

van Genuchten, M.T., F.J. Leij, and S.R. Yates. 1991. The RETC code for quantifying the hydraulic functions of unsaturated soils. U.S. EPA, Robert S. Kerr Environmental Research Laboratory, EPA/600/S2-91/065.

Vasco, D. W., and A. Datta-Gupta. 1997. Integrating multiphase production history in stochastic reservoir characterization. *SPEFE* 9:149-156.

Wang, W., S. P. Neuman, T. Yao, and P. J. Wierenga. 2003. Simulation of large scale infiltration experiments using hierarchy of models based in public, generic, and site data. *Vadose Zone J.* 2:297-312.

Warren, J. E., and P. J. Root. 1963. The behavior of naturally fractured reservoirs. *Soc. Pet. Eng. J. Trans. AIME,* 228: 245-255.

Warrick, A. W. 1975. Analytical solutions to the one-dimensional linearized moisture flow equation for arbitrary input. *Soil Sci.* 120: 79-84.

Warrick. A. W. 1976. Time-dependent linearized infiltration: III. Strip and disk sources. *Soil Sci. Soc. Am. J.*, 40: 639-643.

Whisler, F. D. and A. Klute. 1965. The numerical analysis of infiltration considering hysteresis into a vertical soil column at equilibrium under gravity. *Soil Sci. Soc. Am. Proc.*, 29: 489-494.

Wise, W. R., 1991. Discussion of "On the relation between saturated conductivity and capillary retention characteristics", by S. Mishra and J. C. Parker, September-October 1990 issue, 28(5): 775-777. *Ground Water,* 29(2):272-273.

Wu, Z., A. C. Teynolds, and D. S. Oliver. 1999. Conditioning geostatical models to two-phase flow production data. *SPE J.* 4:140-155.

Yeh, G. T., and D. S. Ward, 1980. FEMWATER: A finite element model of water flow through saturated-unsaturated porous media. ORNL-5567, Oak Ridge National Laboratory, Oak Ridge, TN.

Yeh, W. G. and Y.S. Yoon. 1981. Aquifer parameter identifiability with optimum dimension in parameterization. *Water Resour. Res.* 17: 664 – 672.

Yeh, W. G. 1986. Review of parameter estimation procedures in groundwater hydrology: The inverse problem. *Water Resour. Res.* 22: 95 – 108.

Yeh, T. C. J., and J. Zhang . 1996. A geostatistical inverse method for variably saturated flow in the vadose zone. *Water Resour. Res.* 32: 2757-2766.

Youngs, E. G. 1957. Moisture profiles during vertical infiltration. *Soil Sci.*84: 283-290.

Zachmann, D.W., P.C. Duchateau and A. Klute. 1981. The calibration of the Richards flow equation for a draining column by parameter identification. *Soil Sci. Soc. Am. J.*, 45: 1012 - 1015.

Zachmann, D.W., P.C. Duchateau and A. Klute. 1982. Simultaneous estimation of water capacity and soil hydraulic conductivity by parameter identification. *Soil Sci. Soc. Am. J.*, 134: 157 - 163.

Zarba, R. L. 1988. A numerical investigation of unsaturated flow. M. S. thesis. Dept. of Civ. Eng., *Massachusetts Institute of Technology.* Cambridge.

Zhang, J. and T. C. J. Yeh. 1997. An iterative geostatistical inverse method for steady flow in the vadose zone. *Water Resour. Res.* 33: 63-71.

Zhang, X. 2002. Efficient methods for solving water flow in variably saturated soils under prescribed flux infiltration. *J. Hydrol.* 260:75-87.

Zienkiewicz, O. C., P. Mayer, Y. K. Cheung. 1966. Solution of anisotropic seepage problems by finite elements. *ASCE Proc. Engr. Mech. Div*. 92:111-120.

Zienkiewicz, O. C. 1967. Finite Element Methods in Structural and Continuum Mechanics. London, McGraw-Hill.

Zijlstra, J., and J. H. Dane. 1996. Identification of hydraulic parameters in layered soils based on a quasi-Newton method. *J. Hydrol.* (Amsterdam). 181:233-250

Zimmerman, D.A., De Marsily, G., Gotway, C.A., Marietta, M.G., Axness, C.L., Beauheim, R.L., Bras, R.L., Carrera, J., Dagan, G., Davies, P.B., Gallegos, D.P., Galli, A., Gomez-Hernandez, J., Grindrod, P., Gutjahr, A.L., Kitanidis, P.K., Lavenue, A.M., Mclaughlin, D., Neuman, S.P., Ramarao, B.S., Ravenne, C., Rubin, Y. 1998. A comparison of seven geostatistically based inverse approaches to estimate transmissivities for modeling advective transport by groundwater flow. *Water Resour. Res*. 34: 1373 – 1413.

Zurmuhl, T., and W. Durner. 1998. Determination of parameters for bimodal hydraulic functions by inverse modeling. *Soil Sci. Soc. Am. J.* 62:874-880.

The Revelations of Devout and learn'd
Who rose before us, and as Prophet burn'd
Are all but stories, which, awoke from Sleep
They told their comrades and to sleep return'd

Khayyam

Curriculum Vitae

KOUROUSH SADEGH ZADEH
Fischell Department of Bioengineering
0501 ANS Bldg. (Bldg. 142)
University of Maryland,
College Park, MD, 20742
Phone: (301) 405-0109
Fax: (301) 314- 9023
E-mail: kouroush@eng.umd.edu

Education

2001-2006: Ph.D., Biological Engineering
University of Maryland at College Park,
College Park, Maryland, 20742, U.S.A.
Thesis: Multi-Scale Inverse Modeling in Biological Mass Transport
Processes.

1995 -1997: M.Sc., Agricultural Engineering
Tarbiat Modarres University,
Tehran, Iran.
Thesis: Mathematical Modeling of Transient Flow in Partially
Saturated Porous Media.

1190- 1994: B. Sc., Agricultural Engineering
University of Azarabadegan
Tabriz, Iran.
Senior Project: Comparison of Methods for Measuring Cation
Exchange Capacity of Colloids.

Work Experience

01/2001 – 9/2006:   Graduate Research Assistant
Fischell Department of Bioengineering
University of Maryland
College Park, Maryland
Responsibilities: Conducting research, developing numerical models
and optimization algorithms for different in vivo transport problems,
teaching graduate and undergraduate courses when faculty are at
national and international conferences.

11/1995 – 1/2001:   Research Scientist
                    Iranian Agricultural Engineering Research Institute (IAERI)
                    Karaj, Iran.
                    Responsibilities: Writing research proposal, securing government funding,
                    conducting projects, developing mathematical models for fluid flow and
                    material transport in different engineering systems, analyzing the results,
                    and writing publications to appropriate outlets.

Publications in Refereed Journals:

1. **Sadegh Zadeh, K.,** H. J. Montas, and A. Shirmohammadi. 2006. Identification of biomolecule mass transport and binding rate parameters in living cells by inverse modeling. *Journal of Theoretical Biology and Medical Modeling* (published online. Available at: http://www.tbiomed.com, doi: 10.1186/1742-4682-3-36).

2. **Sadegh Zadeh, K.,** H. J. Montas, A. Shirmohammadi, and P. R. Gudla. 2006. A Diagnosis-Prescription system for nitrogen management in environment. *Journal of Environmental Science and Health* (in press).

3. **Sadegh Zadeh, K.**, and H. J. Montas. 2006. An exact solution for macro-molecule bicontinuum reaction- diffusion equations in living cells. *SIAM Journal on Applied Mathematics* (in review).

4. **Sadegh Zadeh, K.,** H. J. Montas, and A. Shirmohammadi. 2006. Dynamic modeling of in vivo biomolecule transport. *Journal of Computational Biology* (in review).

5. **Sadegh Zadeh, K.,** H. J. Montas, and A. Shirmohammadi. 2006. Multi-objective optimization in variably saturated fluid flow. *Journal of Computational and Applied Mathematics* (in review).

6. **Sadegh Zadeh, K.,** H. J. Montas, A. Shirmohammadi, and H. Elman. 2006. Quantification of hydraulic parameters in fluid flow through heterogeneous variably saturated porous media with realistic initial condition. *Journal of Computational and Applied Mathematics* (in review).

7. **Sadegh Zadeh, K.,** H. J. Montas, and A. Shirmohammadi. 2006. How reliable Fluorescence Recovery after Photobleaching is? *Science.* (In preparation).

8. **Sadegh Zadeh, K.,** H. J. Montas, and A. Shirmohammadi. 2006. A robust and efficient algorithm for solving inverse problem in biological systems (In preparation-to be submitted to the *Journal of Mathematics of Computation*).

9. **Sadegh Zadeh, K.,** H. J. Montas, and A. Shirmohammadi. 2006. A mass conservative and switching algorithm for solving flow equation in variably

saturated porous materials. (In preparation-to be submitted to the *International Journal for Numerical Methods in Engineering*).

10. **Sadegh Zadeh K**. 2000. Deficit irrigation: Mathematical framework and economic appraisal. *Journal of the Iranian Agricultural Engineering Research Institute. Vol. 15* (in Persian).

11. **Sadegh Zadeh K**. 2000. One-dimensional and non-steady state drainage in a homogeneous soil column. *Journal of the Iranian Agricultural Engineering Research Institute. Vol.13* (in Persian with English abstract).

12. **Sadegh Zadeh K**., M. M. Shooshtari, and S. K. Mirnia. 1998. Non-steady State and one-dimensional drainage flow modeling. *Journal of the Iranian Soil and Water Research Institute. Vol.12* (in Persian with English abstract).

13. **Sadegh Zadeh K**., M. R. Neishaburi, and Z. Meghnatisi. 1998. Evaluation of various methods in determining cation exchange capacity of soils. *Journal of the Iranian Agricultural Engineering Research Institute. Vol. 11* (in Persian with English abstract).

14. **Sadegh Zadeh K**. 1998. Water use efficiency and some strategies for optimizing it in farm levels. *Journal of the Iranian Agricultural Engineering Research Institute. Vol.10* (in Persian with English abstract).

15. **Sadegh Zadeh K**. and F. Abbasi. 1998. The use of RETC code for describing and quantifying the soil hydraulic functions and water retention curves. *Journal of the Iranian Agricultural Engineering Research Institute. Vol. 9* (in Persian with English abstract).

Conference Papers and Proceedings

1. **Sadegh Zadeh, K.,** H. J. Montas, and A. Shirmohammadi. 2006. A Mass Conservative Algorithm for Simulating Saturated-Unsaturated Flow in Porous Media**.** ASABE annual international meeting. Paper # 063053, Jul. 9-14, 2006. Portland, OR. (This paper won the 2006 *Information & Electrical Technology* (IET) Best Paper award in Portland, OR).

2. **Sadegh Zadeh, K.,** H. J. Montas, A. Shirmohammadi, and A. Sadeghi. 2003. Automated Spatial Allocation of Best Management Practices (BMPs) for Watershed Scale Nitrogen Management**.** ASAE annual international meeting. Paper # 033036, Las Vegas, Nevada, Jul. 20-23, 2003.

3. **Sadegh Zadeh K**., A. Shirmohammadi, H. J. Montas, and A. Sadeghi. 2003. Applicability of Philip's Three-Parameter Type Infiltration Equation in Layered

Soils. ASAE annual international meeting. Paper # 033037, Las Vegas, Nevada. Jul. 20 – 23, 2003.

4. **Sadegh Zadeh K**., H. J. Montas and A. Shirmohammadi. 2002. Determination of unsaturated hydraulic functions by inverse modeling of flow processes. ASAE annual international meeting (oral presentation). Chicago, Illinois. Jul. 29 – 30, 2002.

5. Keshavarz A., and **K., Sadegh Zadeh**. 2000. Agricultural water management in IRAN: Current situation, future perspective and some strategies for its optimization. Proceedings of the 10th *Iranian National Irrigation and Drainage Committee* Conference, pp: 377-398. Tehran, Iran (In Persian with English abstract).

6. Pazira, E. and **K. Sadegh Zadeh.** 1999. Sustainable Soil and Water Use in Agricultural Sector of Iran. Proceedings of the 99 International Conference on Agricultural Engineering, Beijing, China. Dec. 1999. pp: II-25 – II-32.

7. Pazira, E. and **K. Sadegh Zadeh.** 1999. Optimizing soil and water use in Iran. *In*: N. van Duivenbooden, M. Pala. C. Studer and C. L. Bidders (Eds.). Efficient soil water use: the key to sustainable crop production in dry areas of West Asia and North and Sub-Saharan Africa. Proceedings of the workshops organized by the Optimizing Soil Water Use Consortium. Niamey, Niger, April 26 - 30, 1998.

8. **Sadegh Zadeh K**., A. Keshavarz, and S. K. Mirnia. 1998. An analytical solution of Richards' equation for one-dimensional, non-steady state and vertical drainage problem. Proceedings of the international agricultural engineering conference. Asian Institute of Technology. Bangkok, Thailand. Dec.7 - 10, 1998.

9. Pazira E. and **K**. **Sadegh Zadeh**. 1998. Soil desalinization and land reclamation in Iran: A case study: Khuzistan province. Proceedings of the international symposium on: New Technologies to combat desertification. pp: 80-88. Tehran, Iran. Oct.12-15, 1998.

Invited talks and Guest Lectures

1. Dynamic Modeling of in-Vivo Protein Transport. Presented at the National Cancer Institute (NCI), Fredrick, Maryland. August 23, 2006.

2. Transport Parameter Identification in Fluorescence Recovery after Photobleaching by Inverse Modeling. Presented at the Molecular and Functional Optical Imaging Lab at the NIH, Bethesda, Maryland. January 18, 2006.

3. Lectures on *Advanced Biotransport Processes, Water Resources Engineering,* and *Flow through Porous Media* for graduate and undergraduate students at the Biological Resources Engineering Department in the University of Maryland at College Park.

Courses Taught

1. **Mathematics (3):** Analytical geometry, derivatives, line, surface, and volume integrations, linear algebra, and ordinary differential equations.
   School of Agricultural Engineering, Karaj, Iran. 4 Semesters, Undergraduate level.

2. **Statistics (3):** Discrete and continuous variables, probability density function, mass function, Bayesian theorem, uniform, normal, and Poison distributions, hypothesis tests, correlation and linear regression, goodness-of-fit indices analysis.
   School of Agricultural Engineering, Karaj, Iran. 4 Semesters, Undergraduate level.

3. **Applied Drainage (3):** Soil survey for drainage network design and installation, principles of surface and subsurface drainage engineering, drain spacing formulas, drain envelopes and filters, soil desalinization and leaching, system design and layout.
   School of Agricultural Engineering, Karaj, Iran. 4 Semesters, Undergraduate level.

4. **Design of Irrigation Systems (3)**: Estimation of evapotranspiration, the concept of water use efficiency, design and layout of different irrigation systems such as furrow, border, and subsurface irrigation.
   School of Agricultural Engineering, Karaj, Iran. 4 Semesters, Undergraduate level.

Honors and Awards

1. Recipient of the 2006 Information & Electrical Technology (IET) Best Paper award for authorship of a research paper from the American Society of Biological and Agricultural Engineers.

2. First ranking student in M.Sc. course in field of Agricultural Engineering at the College of Agriculture, Tarbiat Modarres University, Tehran, Iran (1997).

Additional Expertise

1. Finite element simulation of Biological systems.
2. Finite difference simulation of Biological systems.
3. Optimization algorithms, time series analysis, principal component analysis.
4. Expert Systems, Decision Support System.